Stability Concepts of Networked Infrastructure Networks

DISSERTATION

zur Erlangung des akademischen Grades

doctor rerum naturalium

(Dr. rer. nat.)

im Fach Physik

Spezialisierung: Theoretische Physik

eingereicht an der
Mathematisch-Naturwissenschaftlichen Fakultät
Humboldt-Universität zu Berlin

von

M.Sc. Paul Schultz

Präsidentin der Humboldt-Universität zu Berlin:
Prof. Dr.-Ing. Dr. Sabine Kunst

Dekan der Mathematisch-Naturwissenschaftlichen Fakultät:
Prof. Dr. Elmar Kulke

Gutachter/innen:
1. Prof. Dr. Dr. h.c. mult. Jürgen Kurths
2. Prof. Dr. Joachim Peinke
3. Asst. Prof. Dr.-Ing. Johannes Schiffer

Tag der mündlichen Prüfung: 27.03.2018

To T&E

Abstract

The power system is currently undergoing a major transition, where coal-fired and nuclear power plants are being replaced by renewable energy producers and storage facilities. This transformation is enabled by appropriate modifications of the power grid's underlying structure. This network constitutes the complex interaction of numerous producers and consumers. Due to the intermittent nature of renewable production, the power grid is additionally subject to a distribution of disturbances that also includes large deviations.

In conjunction, these aspects prompt methodological problems for (future) power grids in particular and complex systems in general. How can the stability of different operating points or scenarios be compared? What are the critical components of the network? To which extent is the stability of an operating point determined by the network structure?

This dissertation considers questions of this sort from the perspective of nonlinear dynamics and network theory. Here, the focus is on the emergent phenomenon of synchronisation in networks of coupled oscillators. In the context of power grids, this corresponds to all units working at the same rhythm – the rated grid frequency. The probability that a random perturbation strongly destroys this rhythm is given by basin stability, which is an example for so-called probabilistic stability measures that offer different approaches to quantify stability.

On the one hand, the following pages contain methodological advances to probabilistic stability measures, assessing important limitations but also developing novel approaches. In particular, the new measures consider sequences of repeated perturbations as well as operational bounds on transient deviations.

On the other hand, the influence of small network structures, so-called motifs, on the stability of synchronisation is investigated. For this purpose, the probabilistic stability measures are paired with network characteristics, using statistical approaches. To create a sufficient ensemble of diverse network topologies, a network model is created to provide synthetic power grids. On this basis, it turns out that while the abundance of special motifs enhances stability, others typically diminish it.

In conclusion, the development of analysis methods and their comparison with network characteristics uncovers relationships between network motifs and the stability of synchronisation. These results are general to a large class of complex systems and build a foundation to future research in this direction. In addition to that, the novel probabilistic stability measures extend the range of methods in nonlinear dynamics by important aspects, especially for high-dimensional complex systems.

Zusammenfassung

Aktuell unterliegt unsere Stromversorgung einer grundlegenden Transformation durch den allmählichen Austausch von fossilen und Kernkraftwerken mit erneuerbaren Energiequellen und Speichertechniken. Diese Transformation muss letzten Endes auch durch die Bereitstellung einer entsprechenden Infrastruktur ermöglicht werden, also durch Änderungen der Struktur des Stromnetzes. Letzteres ist ein hochkomplexes System welches unzählige Erzeuger und Verbraucher verbindet die dadurch miteinander in Wechselwirkung treten. Dieses System unterliegt wegen der intermittenten Natur erneuerbarer Erzeugung einem Störungsprofil das auch große Abweichungen beinhaltet.

Dies führt zu einigen grundlegenden methodischen Fragen, die daraus (nicht nur) für zukünftige Stromnetze abgeleitet werden können. Wie kann die Stabilität verschiedener Betriebszustände oder Szenarien miteinander verglichen werdem? Welches sind die neuralgischen Punkte eines Stromnetzes? Zu welchem Grad bestimmt die Netzwerkstruktur die Systemstabilität?

Fragen dieser Art sind die Grundlage der vorliegenden Dissertation, welche hierzu Methoden der nichtlinearen Dynamik und der Theorie komplexer Netzwerke zusammenführt. Im Zentrum steht dabei das emergente Phänomen der Synchronisation in Oszillatornetzwerken sowie dessen Stabilität. Im Bezug auf Stromnetze ist die Synchronisation dadurch gekennzeichnet, dass alle Erzeuger und Verbraucher mit der Netzfrequenz im Takt schwingen. Die Wahrscheinlichkeit, dass zufällige Störungen das Stromnetz aus diesem Takt bringen wird durch die Bassin-Stabilität angegeben. Sie ist ein Beispiel für sogenannte probabilistische Stabilitätsmaße, mit denen sich die Systemstabilität auf verschiedene Art und Weise quantifizieren lässt.

Zum Einen widmen sich die folgenden Seiten der Untersuchung möglicher Beschränkungen der Bassin-Stabilität sowie der Entwicklung zweier neuer probabilistischer Stabilitätsmaße. Dabei werden vorherige Ansätze insbesondere durch eine Untersuchung der Auswirkungen wiederholt auftretender Störungen sowie die Einbeziehung von Betriebsgrenzen in die Stabilitätsanalyse entscheidend erweitert.

Zum Anderen geht es darum, den Einfluss kleiner Netzwerkstrukturen, sogenannter Motive, auf die Stabilität der Synchronisation herauszuarbeiten. Hierzu werden die probabilistischen Stabilitätsmaße in statistischen Verfahren mit charakteristischen Größen aus der Netzwerktheorie verknüpft. Damit eine ausreichende Menge an verschiedenen Netzwerken untersucht werden kann, wird außerdem ein Modell zur Erzeugung synthetischer Stromnetztopologien vorgeschlagen. Es zeigt sich dann, dass das Auftreten spezieller Motive die Systemstabilität erhöht, wohingegen andere diese herabsetzen.

Diese Zusammenhänge zwischen Netzwerkmotiven und Stabilität der Synchronisation erweitern die Kenntnisse über Zusammenhänge zwischen Struktur und Stabilität komplexer Systeme. Darüber hinaus erweitern die neu entwickelten probabilistischen Stabilitätsmaße das Methodenspektrum der nichtlinearen Dynamik zur Stabilitätsanalyse, insbesondere für Systeme auf komplexen Netzwerken mit vielen Freiheitsgraden.

Journal Articles

I contributed to the following selection of peer-reviewed journal articles.

References to articles directly related to this dissertation appear with a prefix *P* in the text, e.g. the first entry is cited as *P1*. When a section is mainly devoted to ideas presented in one of these articles, this is highlighted separately following the section title. Further publications without a dedicated section analogously appear with a prefix *F*.

Discussed in this Dissertation

[1] Schultz, P., J. Heitzig, and J. Kurths (2014b). „Detours around basin stability in power networks“. In: *New J. Phys.* 16.12, p. 125001. DOI: 10.1088/1367-2630/16/12/125001 (cit. on pp. 120, 122–125, 147, 151).

[2] Hellmann, F., P. Schultz, C. Grabow, J. Heitzig, and J. Kurths (2016). „Survivability of Deterministic Dynamical Systems“. In: *Nat. Sci. Reports* 6.1, p. 29654. DOI: 10.1038/srep29654 (cit. on pp. x, 101 sqq., 105, 107 sqq., 147, 150).

[3] Schultz, P., F. Hellmann, J. Heitzig, and J. Kurths (2016). „A Network of Networks Approach to Interconnected Power Grids“. In: *arXiv:1701.06968* (cit. on pp. 50, 74, 134 sqq., 145, 149, 155).

[4] Schultz, P., T. K. D. Peron, D. Eroglu, T. Stemler, G. M. Ramírez Ávila, F. A. Rodrigues, and J. Kurths (2016). „Tweaking synchronization by connectivity modifications“. In: *Phys. Rev. E* 93.6, p. 062211. DOI: 10.1103/PhysRevE.93.062211 (cit. on pp. 25, 133, 148, 151).

[5] Nitzbon, J., P. Schultz, J. Heitzig, J. Kurths, and F. Hellmann (2017). „Deciphering the imprint of topology on nonlinear dynamical network stability“. In: *New J. Phys.* 19.3, p. 033029. DOI: 10.1088/1367-2630/aa6321 (cit. on pp. x, 71, 126, 128–131, 148 sq., 151, 157).

[6] Schultz, P., F. Hellmann, K. N. Webster, and J. Kurths (2017). „Bounding the first exit from the basin: Independence Times and Finite-Time Basin Stability“. In: *subm. to Chaos An Interdiscip. J. Nonlinear Sci.* Pp. 1–9 (cit. on pp. 90, 92, 95, 97, 100, 146, 150).

[7] Schultz, P., P. J. Menck, J. Heitzig, and J. Kurths (2017). „Potentials and limits to basin stability estimation“. In: *New J. Phys.* 19.2, p. 023005. DOI: 10.1088/1367-2630/aa5a7b (cit. on pp. 33, 85, 87 sq., 146, 150).

Further Publications

[1] Elagin, M., P. Schulz, M. Elagin, M. Semtsiv, H. Kirmse, A. Mogilatenko, and W. Masselink (2013). „Highly strained photovoltaic dual-channel intersubband photodetectors grown by gas-source MBE“. In: *J. Cryst. Growth* 378, pp. 607–610. DOI: 10.1016/j.jcrysgro.2012.12.123.

[2] Schultz, P. (2014). „Stability Analysis of Power Grid Networks“. Master Thesis. Humboldt-Universität zu Berlin, p. 95 (cit. on pp. 38, 46, 50, 135).

[3] Schultz, P., J. Heitzig, and J. Kurths (2014a). „A random growth model for power grids and other spatially embedded infrastructure networks“. In: *Eur. Phys. J. Spec. Top.* 223.12, pp. 2593–2610. DOI: 10.1140/epjst/e2014-02279-6 (cit. on pp. 50–53, 70, 72 sq., 119, 149).

[4] Auer, S., K. Kleis, P. Schultz, J. Kurths, and F. Hellmann (2016). „The impact of model detail on power grid resilience measures“. In: *Eur. Phys. J. Spec. Top.* 225.3, pp. 609–625. DOI: 10.1140/epjst/e2015-50265-9 (cit. on pp. 61 sq., 65).

[5] Plietzsch, A., P. Schultz, J. Heitzig, and J. Kurths (2016). „Local vs. global redundancy – trade-offs between resilience against cascading failures and frequency stability“. In: *Eur. Phys. J. Spec. Top.* 225.3, pp. 551–568. DOI: 10.1140/epjst/e2015-50137-4 (cit. on pp. x, 84, 119).

[6] Goswami, B., P. Schultz, B. Heinze, B. Bodirsky, H. Lotze-Campen, and J. Kurths. „Inferring interdependencies from short time series“. In: *accpt. Pramana J. Phys.* (Cit. on p. x).

Comments: In [P2] and [F6], I share the leading authorship with Frank Hellmann respectively Bedartha Goswami. Two articles, [P5] and [F5], arose from my co-supervision of the students Jan Nitzbon and Anton Plietzsch.

Contents

List of Figures

List of Tables

Nomenclature

$\|\cdot\|$	norm of a vector, Euclidean norm if not stated otherwise
$\lvert\cdot\rvert$	modulus of a real or complex number
$\cdot^\top$	transpose of a vector or matrix
x, t	state variable, time
$\dot{x}$	time derivative of x
$\imath$	imaginary unit
$\mathbf{A}$	binary adjacency matrix associated to a network $\mathcal{G}$, $\mathbf{A} = \{A_{ij}\}_{ij}$
$\mathbf{L}$	Laplacian matrix associated to a network $\mathcal{G}$, $\mathbf{L} = \{\delta_{ij}\sum_k A_{ik} - A_{ij}\}_{ij}$
$\mathbf{Y}$	nodal admittance matrix associated to a network $\mathcal{G}$, $\mathbf{Y} = \{Y_{ij}\}_{ij}$
$\mathcal{E}$	set of all edges in $\mathcal{G}$
$\mathcal{G}$	graph or network
$\mathcal{V}$	set of all nodes/vertices in $\mathcal{G}$
G_{ij}/B_{ij}	conductance/susceptance of a link ij, $G_{ij} = \mathfrak{Re}Y_{ij}$ and $B_{ij} = \mathfrak{Im}Y_{ij}$
w	function that assigns weights to all edges in $\mathcal{G}$
z^*	complex conjugate of a complex number z
$\mathcal{A}$	attractor of a dynamical system
$\mathcal{B}(\mathcal{A})$	basin of attraction of an attractor $\mathcal{A}$
μ	probability measure in a probability space $(X, \mathcal{F}, \mu)$ with sample space X and events $\mathcal{F}$
$\mu_{\mathcal{B}}$	basin stability of an attractor $\mathcal{A}$ with basin of attraction $\mathcal{B}$
X	phase space of a dynamical system
b_i, b_i^w	shortest-path/current-flow betweenness of node i
C_i, C_i^w	un-/weighted local clustering coefficient of node i
c_i, c_i^w	un-/weighted closeness centrality of node i

d_i, s_i	degree/strength of node i
Ω	rated frequency of a power grid
ϕ_k, ω_k	phase and frequency of an oscillator in a reference frame co-rotating with frequency Ω, $\omega_k = \dot{\phi}_k$
θ_k, ν_k	phase and frequency of an oscillator in a static reference frame, $\nu_k = \dot{\theta}_k$
$\delta(\cdot)$	the delta distribution
δ_{jk}	the Kronecker symbol, $\delta_{jk} = 1$ for $i = j$ and $\delta_{jk} = 0$ otherwise
$\Theta(\cdot)$	the Heaviside step function, $\Theta(x) = 0$ for $x < 0$ and $\Theta(x) = 1$ otherwise

1. Introduction

Contents of this Chapter

1.1. Motivation

The emergence of long-distance power transmission has been a major force in the Great Transformation of societies in the industrial revolution (German Advisory Council On Global Change 2011). The production facilities required electrical energy, which had to be transported over increasing distances. The first DC transmission line ran from the town of Miesbach to Munich in 1881 (Arrillaga 1998) but has already been superseded within a decade by the world-first three-phase AC transmission line between Lauffen and Frankfurt/Main (Steen 1991) for the International Electrotechnical Exhibition 1891. These developments did not only help to establish AC over DC long-distance power transmission, but also allowed for the spatial separation of large power plants and industrial production.

By now, in the face of climate change, we are right in the middle of the next transformation. Though there has apparently been an early awareness of the problems brought about by the industrialisation, they have been underestimated for a long time:

> "The furnaces of the world are now burning 2,000,000,000 tons of coal a year. [...] The effect may be considerable in a few centuries." („Coal Consumption Affecting Climate" 1912)

The modern transformation from fossil and nuclear to renewable energy sources – widely known as "Energiewende" – crucially affects the electricity sector among others. It inevitably changes the way how electricity is produced as well as transmitted in a yet undetermined way, both locally and globally. Consequently, it is necessary to compare different variants in a reasonable way by means of simulations. The aim of this thesis is, to further develop methods for comparing power grids with respect to their stability as well as to complement established notions of stability with new variants. This research is done in the light of the following topics.

Renewables challenge the established transmission system. Firstly, spatial separation of supply and demand increasingly becomes a complex and time-varying factor. Renewable energy sources (RES) are not generally constructed in proximity to load centres but rather where environmental conditions are optimal. In Germany, for instance, a dominant wind-infeed in the North-East causes non-local stresses in the whole network due to high North-to-South power flows, revealing bottlenecks in the grid infrastructure. This problem is tackled by the national Network Development Plan (Pesch et al. 2014; Netzentwicklungsplan 2017), proposing several thousand kilometres of grid extensions and updates.

Secondly, the RES production renders the power supply more and more distributed. Consequently, *prosumers*[1] emerge on the lower grid levels, leading to a more local, distributed production of small- and medium-sized RES. Also the massive appearance of inverter-connected RES causes a heterogeneous (time-dependent) distribution of inertia, which is a quantity important for stabilising power grids.

[1] *Prosumer* is a portmanteau of 'producer' and 'consumer' referring to households with RES installed, acting as power producers at least for a certain time.

Low-inertia devices give rise to weakly-damped frequency oscillations, i.e. frequency instabilities are amplified if the primary control reserve is not sufficient or fast enough (Ulbig et al. 2013). This problem is addressed by so-called grid-forming inverters, providing virtual inertia (Schiffer, Zonetti, et al. 2016).

The complexity of the transformation requires holistic scientific approaches. The traditional planning and operation practice has so far been very successful in maintaining the power system without the necessity of considering complex dynamical effects. Nonlinear characteristics, however, are becoming more and more important (Hill et al. 2006). This fact is amplified by the exploding number of electricity producers which are small, have varying availability and a different dynamic behaviour. With an increasing share of RES, like wind, solar, geothermal or hydro power, the requirements for the design and topology of transmission systems change alike, especially in the distribution grid (Dena 2012). This interaction of structural and dynamical transformations shapes a future power grid as one of the most "complex" complex systems. The necessity of gaining a deeper understanding about this process is given by the potential consequences of power blackouts on the functioning of our society. To put it straight:

> "[...], humanity has come close to building a machine that is so intricate that it can't be comprehended." (Marris 2008)

An interconnected power system is a trade-off between risks and benefits. When 13.500 Potsdamers where sitting in the dark on August 1st, 2017, the reason was a blackout in the low-voltage grid following a short-circuit in the next-higher layer (Klotz 2017).[2]

On the one hand, this shows the systemic risks in an interconnected power system. On the other hand, the earlier construction of a redundant high-voltage cable (passing by Telegraphenberg) enabled the quick reconnection of the network after just 14 minutes, showing also the benefits of interconnection. Besides such local intermezzos, large and severe blackouts (UFE 2003; U.S.-Canada Power System Outage Task Force 2004; Maas et al. 2007) – are, however, rather rare. This is an indication of the apparent robustness of power systems.

Such robustness is only characteristic for conventional highly-developed power systems. Rural areas in the Global South face very different transformative challenges in the course of primary electrification. Here, the development happens towards a distributed energy supply, for instance based on bottom-up DC microgrids (Strenge et al. 2017). Microgrids operate as (electric) islands which might in the future be connected to a national transmission system. In turn, this approach could serve as a blueprint for microgrids (Schiffer et al. 2014b) in the Global North, with the potential to operate in an uncoupled island mode in case of major disturbances.

[2] Sometimes an animal's tragic fate is the reason for blackouts, be it squirrels (Hofmann 2015) or even monkeys: "When a monkey fell on a transformer at a Kenyan hydroelectric dam, the entire nation lost its electrical power." (Guarino 2016).

1.2. Methods and Approaches

The ambitions of this thesis are twofold and might be framed in two central questions:

> *What can be appropriate concepts of power grid stability?*

and

> *What are the essential structural features of power grids, determining their stability?*

I attempt to find answers by following a transdisciplinary approach that combines *network science* with the toolbox of *dynamical system's theory*. Instead of studying the microscopic dynamics of every single machine in exhaustive detail, I focus on the collective, macroscopic behaviour of the overall power system. I base my analysis on a dynamic power grid model of intermediate complexity in a way that features the main characteristics of the actual dynamics. In popular words, this thesis provides a "macroscope" on the power grid, in a trade-off between "over-simplification" and "over-sophistication" (Schellnhuber 1999).

Power system research ranges from fast self-organised respectively automatic processes to slower, actively-controlled processes determined by e.g. energy balancing markets. In the following, I will focus on the self-organised *emergence of synchronisation* as one of the fastest processes on short time scales in AC power systems. This way, the modelling approach also includes automated decentral control as part of the intrinsic dynamics of power grids.[3] I do not focus on optimising decentral controllers but assume them to exhibit a dynamical behaviour compatible with or even resembling the physics of conventional generators.

After this little disclaimer, let me go into further detail on the emergent phenomenon in the centre of interest. Power grids are characterised by an operating state where all units move in synchrony, referred to as the *phase synchronisation of coupled oscillators*. I will explain how this aspect of the dynamical behaviour of power grids is resembled by a basic model of so-called inert phase oscillators, i.e. the renowned *Kuramoto model with inertia*. It is essential to gaining an understanding of the stability of synchronisation. Established approaches, like master stability functions, are based on linearisation or Lyapunov functions and mainly yield a qualitative understanding – stable or not. There is no a priori notion for comparing the stability of different settings. Moreover, these approaches consider only small (infinitesimal) perturbations or are difficult to apply to high-dimensional systems. A recent method to quantify stability with respect to large (finite) perturbations is given by the concept of basin stability. It is an example of what I will refer to as *probabilistic stability measures* and corresponds to the probability that a perturbed system returns to an attractor. The extension and development of probabilistic stability measures, as well as their interplay with the structure of complex networks, is the main theme of this thesis.

[3] The term *decentral control* here and in the following refers to programmed devices using primarily only local input without an additional communication infrastructure. The closed-loop formulation of a system with decentral control is discussed in Sec. 4.2.2 in more detail.

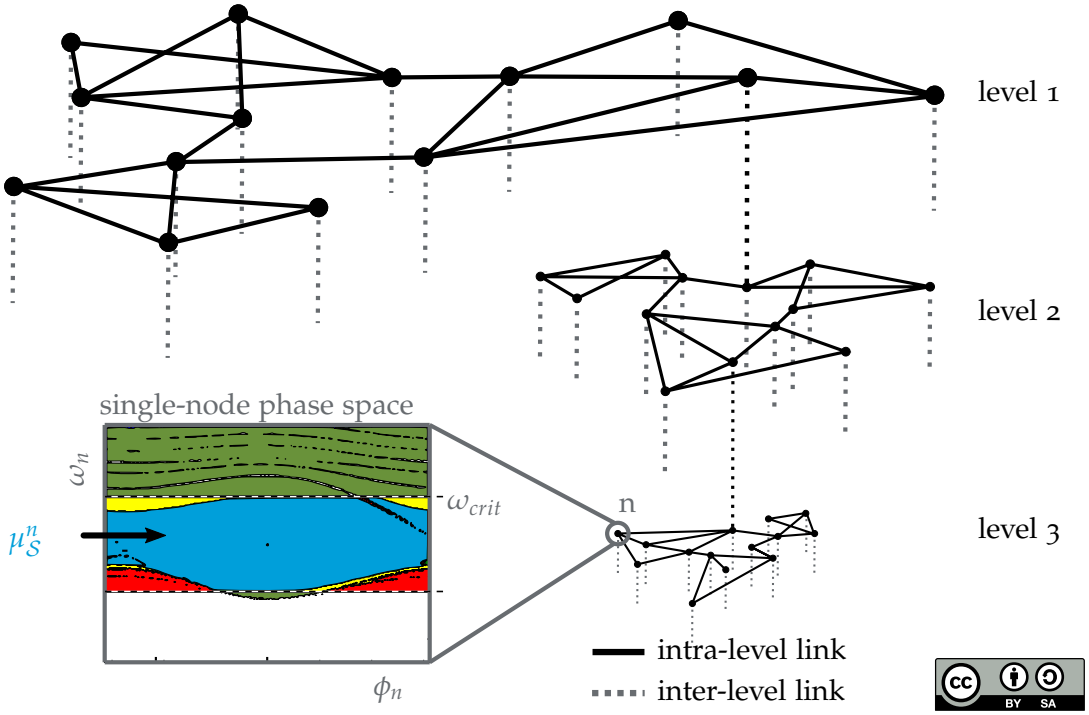

Figure 1.1. – **Network-local probabilistic stability analysis**: Scheme of a high-dimensional dynamical system of networked interactions, possibly with multiple levels (top three are shown), i.e. a network of networks. Solid lines indicate edges within the same sub-network, while dashed lines indicate edges between different sub-networks. Each node is characterised by two variables, its state, consisting of a phase ϕ_n and frequency ω_n. The inset schematically indicates the stability classification of initial states at a single node as outlined in the text.

My methodological approach to power grid stability is summarised in Fig. 1.1, which visualises different aspects[4]. Firstly, a developed power grid is not a monolithic network but consists of multiple interconnected networks on different spatial scales and voltage levels. The dashed vertical lines indicate these interconnections, realised by transformers. Nodes carry dynamical units which are coupled via transmission lines with a limited capacity. All together, this setup represents a high-dimensional, multistable dynamical system of synchronising phase oscillators. Using probabilistic stability measures, the grid's weak points as well as its resilience towards large perturbations shall be characterised. To achieve this, consider the consequences of a localised perturbation at a single node n. Being initially synchronised, a random large perturbation has some chance to trigger the transition of the power grid towards undesired stable regimes. The inset illustrates a classification of the perturbations at node n regarding different notions of stability for the power system, which will be detailed in the course of this thesis. In general, these methods might be referred to as *network-local probabilistic stability measures*. A naturally appearing question is whether the system returns to synchronisation. Furthermore, it can be of practical interest to assess the likelihood for the power grid to remain within certain dynamical bounds $\omega_{crit.}$ (at least for a finite time) and how much time should pass at least between disturbances such that they do not build up a severe displacement. I approach these problems by complementing existing probabilistic stability measures with novel variants.

Congruously, research in the context of power grids repeatedly lead to new insights in *network theory*. To name a few highlights: The first algorithm to construct minimum spanning trees, for instance, has been developed for the design of the Moravian network in 1926 (Borůvka 1926a,b). Resistance distance is a network metric inspired by networks of resistors (Klein and Randić 1993). Current-flow betweenness is based on Kirchhoff's current law (Newman 2005).

The other way around, the theory of complex networks is also influencing power grid research and this thesis in particular. On the one hand, I will rely on network theory for a *statistical analysis* of power grids as complex networks. In this framework, nodes correspond to power producers, consumers or substations and edges are transmission lines or transformers. Nodes (and edges) can be classified in distinct groups based on their various network characteristics. On the other hand, I am going to apply concepts from network theory, e.g. the minimum spanning trees, to develop a *growth model* for spatially-embedded networks of networks. This model is then used to create ensembles of synthetic power grid topologies for analysing the relationship between node characteristics and localised probabilistic stability measures.

[4] **Expert comment to Fig. 1.1**: The inset shows a single-node phase space, i.e. a slice of the phase space corresponding to the states (ϕ_n, ω_n) of a single node n, in the third level. The blue region indicates the set of initial states from which the system never violates the constraint ω_{crit}, i.e. the basin of survival. Its volume determines the single-node survivability μ^n_S, a novel probabilistic stability measure introduced in Sec. 5. The union of the blue, yellow and green region corresponds to the set of initial states from which the system synchronises. Its volume determines the single-node basin stability (cf. Sec. 2.4.2).

1.3. Contents and Arrangement of this Thesis

As a quick orientation, three parts constitute this thesis. They comprise (i) an introduction of the underlying theory (Chap. 2 and 3), (ii) the derivation of a power grid model (Chap. 4) and (iii) a discussion of methodological advances (Chap. 5) as well as applications of the theory to the model (Chap. 6).

The first part recapitulates concepts from dynamical systems and complex networks theory, respectively.

In particular, Chap. 2 introduces the basics of nonlinear dynamics. It begins in Sec. 2.2 with the definition of continuous-time dynamical systems and the discussion of appropriate notions of attractors. Furthermore, I briefly introduce the emergent phenomenon of phase synchronisation that is inherent to power grids. The established characterisation of stability, obtained from linearisations of a dynamical system, follows in Sec. 2.3. It features fundamental bifurcations in two-dimensional systems, which are revisited in later chapters, and the concept of master stability functions, suited to dynamical systems with a complex network structure. Complementary, Sec. 2.4 discusses methods for assessing stability given large perturbations. After introducing a direct method given by Lyapunov functions, I focus on basin stability as a probabilistic stability measure. Consequently, a discussion of basins of attractions and their potentially complex geometries concludes the chapter, a topic taken up again in Sec. 5.3.

Chap. 3 is devoted to complex networks. It commences with their definition and mathematical description in Sec. 3.2. Based on that, Sec. 3.3 introduces various characteristics for nodes in a network. Depending on the amount of information they rely on, local, mesoscale and global characteristics are distinguished. Sec. 3.4.1 then discusses existing frameworks to model networks of networks. I present a novel approach, termed "neonet", in order to capture properties of interconnected power grids. In particular, Sec. 3.4.3 contributes a novel network growth model for spatially-embedded neonets.

After introducing the theoretical foundation, the second part formulates a consistent model of the power grid dynamics and topology in Chap. 4

This chapter might serve also as a compendium of the details respective background of the modelling strategy. The final model is briefly summarised in Sec. 4.4. It is modular in the sense that it merges the dynamics taking place at the nodes with a model for the network structure. Sec. 4.2 discusses the node dynamics in great detail, focusing on established models for synchronous machines and inverters. Both might (under certain assumptions) be described as Kuramoto oscillators with inertia. The transmission network topology is discussed in Sec. 4.3, summarising empirical facts about real-world network topologies. The complex network perspective concludes the chapter by setting up the neonet model from Sec. 3.4.3 for power grids.

The third and last part contains two chapters, addressing probabilistic stability measures and their relation to the network structure. Each section relates to research published in one of the publications listed in the very beginning of this thesis.

Chap. 5 focuses on methodological advances with regard to probabilistic stability approaches in general and for power grid stability in particular. Basin stabil-

ity, as a particular probabilistic measure, is increasingly applied to various systems. Consequently, Sec. 5.3 investigates limitations to a basin stability estimation. It turns out, that an estimation using Monte Carlo sampling is difficult in systems with fractal basin boundaries or riddled basins of attraction. Sec. 5.4 investigates how rare disturbances have to be such that they do not build up, leading to the concept of a dynamical system's independence time. In this context, I define a novel probabilistic measure termed finite-time basin stability. It is the probability for a system to return close to an attractor within a certain finite time, given a large perturbation. Furthermore, I derive an efficient lower bound on the probability to remain in a basin of attraction, depending on the frequency of repeated perturbations. Sec. 5.5 adopts a different viewpoint, shifting the focus from asymptotic sets to transient dynamics of deterministic dynamical systems. I present a novel probabilistic stability measure termed survivability that is related to the probability that a system remains in a pre-defined desirable regime up until a finite time, given a random perturbation. The description includes a derivation of analytic survivability bounds and their numerical assessment.

Finally, Chap. 6 discusses structural properties determining power grid stability. It focuses mainly on the central role of certain network motifs, i.e. small subgraphs of a network.

In Sec. 6.3, I identify stabilising motifs with respect to basin stability. Together with previous results on the detrimental effect of tree-shaped network appendices, they provide the basis for a statistical prediction of critical nodes, solely incorporating network characteristics. Complementary, Sec. 6.4 presents a novel, more fine-grained classification scheme for such tree-shaped appendices together with a particularly insightful visualisation of basin stability and survivability outcomes, respectively. I highlight how this approach, termed a "stability map", is not only able to distinguish various node classes in terms of stability, but also how it reveals so-called exotic solitary states induced only by perturbations at specific nodes. This is followed by new results on the role of hubs with respect to survivability. The chapter is concluded by Sec. 6.5, discussing results on the asymptotic stability of cyclic motifs. They imply that four-cycles, created for instance by adding a new transmission line, potentially have strong effects on the synchronisability of a system.

The thesis is concluded in Chap. 7, discussing the contributions of my research presented in this thesis. It follows an outlook on how the research might be extended in the future.

2. Nonlinear Dynamics

Contents of this Chapter

2.1. In a Nutshell

In this section, I briefly introduce basic concepts from dynamical systems theory in anticipation of the research results presented in the proceeding chapters.

An introduction to autonomous dynamical systems and their asymptotic behaviour sets the stage for a phenomenon in the centre of this thesis – phase synchronisation of coupled oscillators. Synchronisation is essential for a proper functioning of AC power grids, a connection further advanced in Sec. 4.2.

An established framework to assess the stability of asymptotic states given small perturbations is the linear stability approach. I introduce the essential ideas dating back to Lyapunov and Poincaré. Furthermore, I discuss a selection of commonly-observed bifurcations – i.e. general scenarios for the loss or gain of stability under parameter variation – in view of appearances in later chapters (e.g. Sec. 4.2.3). In conjunction with complex networks (cf. Chap. 3) an asymptotic stability analysis with master stability functions is particularly insightful. I refer to this method in Sec. 6.5, where it is used to uncover the impact of particular network structures on the stability of synchronisation.

Finally, as the results in Chap. 5 and Chap. 6 are mainly concerned with a system's response to large perturbations, I here review established methods using Lyapunov functions and recent approaches like basin stability. Furthermore, I discuss complex basin geometries, in view of the discussion about potentials for and limits to basin stability estimation in Sec. 5.3.

2.2. Nonlinear Dynamics and Synchronisation

Abstract This section defines dynamical systems, discusses attractors and introduces the concept of phase synchronisation.

2.2.1. Autonomous Dynamical Systems and their Flows

Let us consider a dynamical system[1] as the time evolution of a set of variables in the context of a given model. A set of values associated to these variables uniquely defines the system's *state*. Assume that the time evolution is determined by a (system of) first-order nonlinear differential equation(s) with a dynamics given by a smooth function $f : X \to X$:

$$\dot{x}(t) = f(x(t)) \;, \quad x \in X \subseteq \mathbb{R}^D \;, \quad x(0) = x_0 \;. \tag{2.1}$$

We call X the *phase space* (state space)[2] of the dynamical system and each x at time $t \in \mathbb{R}$ is a point in X. Typically, a real D-dimensional phase space $X \subseteq \mathbb{R}^D$ is considered in physical applications.

[1] I mainly follow the notation of Guckenheimer et al. (2002).

[2] Historically, the state of a dynamical system is referred to as its *phase*, not to confuse with the phase of an oscillator.

The right hand side f does not explicitly depend on time t, hence the differential equation is called *autonomous* as it is usually the case in the absence of external drivers, control or stochastic terms. Furthermore, it is *deterministic* in the sense that the time evolution always yields the same output for identical input. Consequently, the evolution only depends on the initial state and the evolution laws do not change over time.

To a large extent, the analysis of dynamical systems is concerned with extracting qualitative information from a system without actually solving it. Nevertheless, for the sake of the following definitions, the existence and uniqueness of solutions – or more general of a so-called *flow* – is essential. Eqn. 2.1 generates a smooth flow $\varphi_t : U \subseteq X \to X$ parametrised by a real number t which I call *time* from here on, i.e. a set of solution curves $x(t) = \varphi_t(x_0)$ each based at a specific initial condition $x_0 \in U$. Solution curves $\varphi_{[0;t]}(x_0)$ are also referred to as a *trajectory*.

The instantaneous flow for $t = 0$ equals the identity $\varphi_0(u) = u$ such that states do not change spontaneously. Furthermore, the flow obeys the group action $\varphi_a(\varphi_b(v)) = \varphi_{a+b}(v)$, as the system is autonomous. Now, it is easy to see that the flow fulfils Eqn. 2.1:

$$\frac{d}{dt}\varphi_t(x)\,|_{t=\tau} = \frac{d}{ds}\varphi_{s+\tau}(x)\,|_{s=0} = \frac{d}{ds}\varphi_s(\varphi_\tau(x))\,|_{s=0} = f(\varphi_\tau(x)) \ . \tag{2.2}$$

The questions, however, whether a flow exists, at least locally, and if it is unique, are addressed by the following fundamental theorem (Guckenheimer et al. 2002, Theorem 1.0.1).

Theorem 1 (Local existence and uniqueness)**.** *Given an $x_0 \in U$ with U open and connected as well as an open interval $I \subseteq \mathbb{R}$ symmetric around 0. The local existence and uniqueness of solutions is given when f is continuously differentiable (C^1) on U w.r.t. x. In particular, the solution to Eqn. 2.1 is unique and exists at least locally for $t \in I$ and a corresponding neighbourhood of x_0.*

Still, flows are often globally defined, especially if U is a compact set (i.e. a flow on a sphere/torus) or if the dynamics given by Eqn. 2.1 is linear. If not stated otherwise, all following examples consider globally defined flows with $U = X$.

The important consequences of the existence and uniqueness theorem are that:

(i) It is not possible for two trajectories to intersect or to be tangential in any point.

(ii) A trajectory cannot intersect itself, except for cycles.

(iii) Fixed points cannot be reached by a trajectory in finite time.

Here, two important concepts were introduced en passant. Firstly, *fixed points* $x^\star$ are singular points of the flow such that

$$\forall_t : \ \varphi_t(x^\star) = x^\star \quad \text{respectively} \quad f(x^\star) = 0 \ , \tag{2.3}$$

i.e. physically any motion eventually comes to a hold approaching $x^\star$. Secondly, closed trajectories, so-called *cycles* γ might exist in U. Such trajectories correspond

to periodic dynamics with a minimal *period* $T > 0$ such that $\varphi_{t+T}(x) = \varphi_t(x)$ for all $x \in \gamma$. In the following section, the diverse asymptotic behaviour of dynamical systems and their flows are further investigated.

2.2.2. Asymptotic Behaviour of Flows

The asymptotic behaviour of dynamical systems is determined by properties of their flow. In a *dissipative system*[3] that dissipates energy (e.g. friction, Joule heating, inelastic collisions, ...), one observes distinct dynamical features in the time-asymptotic behaviour. The flow might be attracted to – or repelled from – so-called *fixed* or *equilibrium points*, for instance the equilibrium position of a pendulum. In the presence of externally-supplied energy, a self-sustained *periodic* (oscillatory) or even *chaotic motion* is common. The former appears, for instance, when a motor applies a constant force on the pendulum, while the latter can be caused by certain periodic driving forces.

The simple example of a pendulum already serves to demonstrate a complex asymptotic structure. These asymptotic solutions correspond to the existence of invariant sets of the flow. Those which are limit sets of many solution curves are termed *attractors* $\mathcal{A}$ of a dynamical system[4].

Up to now, there is no general definition of an *attractor* and there might never be one. The two main directions go along the lines represented by Milnor (1985) and Hurley (1982), both of which showing a different intuition about the characteristics of attractors.

As a preparation to define an attractor, two notions are useful. Firstly, note that there is an invariant set of points, the *non-wandering set* $\Omega(f)$ of the flow. It is defined for all $t > 0$ such that for all $x \in \Omega(f)$ there is $\exists_{t' \geq t} : \ \varphi_{t'}(U(x)) \cap U(x) \neq \emptyset$, where $U(x)$ is a neighbourhood of x. An attractor $\mathcal{A}$ should be a subset of $\Omega(f)$, i.e. attractors should be invariant objects. In general, trajectories pertaining from all initial states in a dissipative system asymptotically converge to the non-wandering set. Secondly, for each state x_0, the accumulation points of the flow $\varphi_t(x_0)$ form the invariant so-called *omega-limit set* $\omega(x_0)$. A *basin of attraction* is defined as the set $\mathcal{B}(\mathcal{A})$ of states x_0 whose omega-limit set $\omega(x_0) \subset \mathcal{A}$ is contained in $\mathcal{A}$.

Hurley's definition of an attractor $\mathcal{A}$ emphasises the existence of an open neighbourhood $U \supset \mathcal{A}$ in the basin of attraction such that $\bigcap_{t \geq 0} \varphi_t(U) = \mathcal{A}$. It encodes the notion that a set is attracting if the system returns from any small enough deviation.

Milnor, on the contrary, notes that such definitions exclude many (physical) examples where such an open neighbourhood does not exist. His notion of an attractor is that of an asymptotic set which is predominantly reached (with high probability) from a certain part of X.

Definition 1 (Measure attractor)**.** *Given the above definition of a basin of attraction, a* measure attractor $\mathcal{A}$ *is defined by:*

[3] Contrarily, *conservative* (incl. Hamiltonian) systems conserve the total amount of energy and have a distinguished spectrum of time-asymptotic behaviour. For an overview see Iooss et al. (1990).

[4] There might also be divergence but by compactification we can regard this as an attractor at infinity.

1. *There is a minimal compact invariant set $\mathcal{A} \subset X$ whose basin of attraction $\mathcal{B}(\mathcal{A})$ has positive Lebesgue measure.*

2. *There is no strictly smaller set $\mathcal{A}'$ whose basin of attraction coincides with that of $\mathcal{A}$ up to a zero-measure set. (Minimality)*

While Hurley's definition fails for example in the case of riddled basins of attraction (cf. Sec. 2.4.3) containing no open neighbourhood at all, Milnor's definition covers unintuitive cases of linearly unstable attractors (cf. Sec. 2.3).

If not otherwise stated, I will refer to a *measure attractor* in the sense of Milnor (1985) throughout this thesis.[5]

As indicated above, there are different categories of attractors appearing in dynamical systems. The essential parameter here is the system dimension. In $D = 1$ dimension, e.g. if X is a subset of the real line, only fixed points $x^\star$ exist as attracting invariant sets because f changes only monotonically (a direction-reversal would violate uniqueness)[6]. In general, it takes at least $D = 2$ dimensions for periodic motion to be observed in continuous dynamical systems. Periodic attractors are referred to as *limit cycles*, as they are closed orbits in X.

It is known for several decades by now (Lorenz 1963; Li and Yorke 1975; Rössler 1976), that in higher dimensions ($D \geq 3$)[7] a more complex phenomenon arises, namely a deterministic, oscillatory but non-periodic motion termed *chaos* in a seminal paper by Li and Yorke (1975). Chaos is associated with the combination of a *sensitive dependence* on initial conditions, i.e. trajectories from arbitrarily close-by initial states quickly diverge, and a *strange attractor*, i.e. a compact invariant set with fractal dimension. The precise definition, however, varies between authors and recently, a more general entropy-based definition has been developed (Hunt et al. 2015). The discovery of chaos triggered many research directions like chaos control (Ott, Grebogi, et al. 1990; Romeiras et al. 1992) or transient chaos (Tél 1990, 1991). This is indicated, for instance, by several scientific journals whose name contains the word 'chaos'.

2.2.3. Phase Synchronisation of Coupled Oscillators

Concerning the asymptotic behaviour of flows, a particularly interesting special case is that of the synchronisation of self-sustained oscillators.[8] This macroscopic phenomenon appears in a multitude of natural or engineered systems, with power grids being a prime example of oscillators coupled in a complex network.

Oscillators are physical systems that perform a periodic or chaotic oscillatory motion which can be characterised by an amplitude, frequency and phase variable.

[5] Note also that *repellers* can then be defined as attractors of the flow under time-reversal.

[6] An exception to the rule is the circle $X = \mathrm{S}^1$, i.e. if x is a periodic variable like the angular phase of a pendulum. Then, a circular flow corresponding to an oscillation might appear.

[7] This restriction does not transfer to discrete systems like the logistic map, where chaos emerges already in one dimension.

[8] There are various books (Pikovsky et al. 2001; Osipov et al. 2009; Strogatz 2012) and review articles (Glass et al. 1988; Winfree 2001; Boccaletti, Kurths, et al. 2002; Arenas, Díaz-Guilera, et al. 2008) on synchronisation of dynamical systems, for periodic as well as chaotic oscillators.

Generally, a phase can be defined for all oscillatory systems with a neutral direction and this notion can be extended to chaotic oscillators as well (Pikovsky et al. 2001). Oscillators are called self-sustained if there is an internal source of energy to maintain a steady oscillatory motion against dissipative forces. The *amplitude* is the maximal deviation from a central value (often an equilibrium), while the *phase* characterises the position of the oscillator at a given time. The *frequency* is the corresponding phase velocity and determines the oscillation speed. Usually, the frequency of an isolated oscillator is referred to as its *natural frequency*. Examples for oscillators are pendulum clocks, flashing fireflies or synchronous machines in power grids, which are treated later in great detail (cf. Sec. 4.2.1).

Such oscillators might adjust their rhythms when they interact through a weak coupling, i.e. *synchronisation* translates to *common movement in time* (ibid.). In particular, *phase synchronisation* is characterised by two phenomena: *phase locking* and *frequency entrainment*[9]. Consider, for instance, an oscillator with a stable *limit cycle*. As we will see in the next section, this means that transverse to the cycle, (most) points are attracted. Hence, the amplitude is typically forced back to its stable value. Small perturbations of the motion along a limit cycle, however, are neutral in the sense that the dynamics is invariant under phase shifts, i.e. a constant change in the phase remains and the phase is considered a free variable.

Phase synchronisation then appears via an adjustment of phases of coupled oscillators irrespective of their amplitude dynamics. In particular, the coupling force balances the separating effect of different natural frequencies (so-called frequency detuning) at a certain constant value of phase differences, i.e. phases become locked. When the frequency detuning is small enough, the oscillators synchronise to a common frequency. It is generally different from their natural frequencies, an effect which is referred to as frequency entrainment.

An instructive and widely-used model for synchronisation, which can easily be applied also to complex networks, has been introduced by Kuramoto[10] (Kuramoto 1975, 1984; Sakaguchi et al. 1986; Strogatz 2000; Acebrón et al. 2005):

$$\dot{\theta}_k = \nu_k - \epsilon \sum_{j=1}^{n} A_{kj} \sin\left(\theta_k - \theta_j\right) \ , \tag{2.4}$$

i.e. the oscillators are slowed down when their phases θ_k advance and are sped up when their phases are behind. Here, ν_k are the natural frequencies, ϵ is a constant quantifying the coupling strength and the matrix $\mathbf{A}$ encodes the coupling topology (cf. Sec. 3.2). In the all-to-all coupled thermodynamic limit, analytic solutions exist (Ott and Antonsen 2008) and were already suggested by Kuramoto. There also is an extensive literature on the application of this model to complex networks, considering delayed coupling, phase lags, natural frequency distributions or inertia (Rodrigues et al. 2016). We will see in Sec. 4.2.3 that the power grid model falls

[9] If not otherwise specified, I always refer to synchronisation in the meaning of phase synchronisation. For other approaches, i.e. explosive or generalised synchronisation, see e.g. Ji, Peron, et al. (2013) or Abarbanel et al. (1996).

[10] "I didn't have a slightest idea that my simple model could ever find any example in real physical systems." Y. Kuramoto in a letter to S. Strogatz (Strogatz 2012)

into the class of Kuramoto oscillators with inertia, usually with a bi-modal distribution of natural frequencies (Martens, Barreto, et al. 2009).

To observe phase synchronisation in applications, a so-called *order parameter* can be evaluated, measuring the degree of phase locking between mutually coupled oscillators. A recent approach (Schröder, Timme, et al. 2017) to define an order parameter is given by:

$$r = \frac{1}{\sum_{i,j=1}^{n} A_{ij}} \sum_{i,j=1}^{n} A_{ij} \langle \cos\left(\theta_i - \theta_j\right) \rangle_t \,. \tag{2.5}$$

The reasoning behind this is, that the time average of the cosine of the phase differences is close to one when the phases are locked and close-by. Hence, one observes $r \to 1$ for high values of the coupling constant. It becomes exactly one for vanishing frequency detuning. Oppositely, $r \to 0$ for a random distribution of phases in the absence of synchronisation. Recently, also the coexistence of synchronised and incoherent ($r \approx 0$) oscillator groups in a network has been discovered and the phenomenon is referred to as *Chimera* (Kuramoto and Battogtokh 2002; Abrams et al. 2004; Wolfrum et al. 2011; Panaggio et al. 2015; Kemeth et al. 2016) or *solitary states* (Maistrenko et al. 2017).

2.3. Stability of Linear Systems

Abstract This section reviews traditional approaches to stability regarding infinitesimal perturbations, gives examples for important bifurcations and introduces the powerful tool of master stability functions.

2.3.1. Linear Stability Framework

Going back to the pioneering ideas of Aleksandr Michajlovič Lyapunov, attractors of dynamical systems are considered to be stable if small perturbations to the initial conditions lead to small reactions of the system, i.e. small perturbations cannot substantially alter the system's asymptotic behaviour. In the following, the discussion is based on this notion of stability also known as Lyapunov's first method.

To quantify what 'small' means in this context, let us define a distance measure between a point x and an arbitrary set $C \subset X$ as

$$d\left(x, C\right) := \inf\{\|x - y\| \mid y \in C\} \,, \tag{2.6}$$

where $\|\cdot\|$ is a suitable norm. In this section, two cases for the set C are considered, namely fixed points $x^\star$ and limit cycles γ. For fixed points, $d\left(\cdot, x^\star\right)$ is just the regular distance according to the norm, while for limit cycles it reduces to the minimal distance to a point on γ.

Now, Lyapunov's first method can be formalised in the following three definitions.

Definition 2 (Locally attracting)**.** *A set C is said to be* locally attracting *if there exists a*

neighbourhood

$$U_\epsilon = \{x_0 \in X |\ d(x_0, C) < \epsilon\}$$

with $\epsilon > 0$ *for which*

$$\lim_{t\to\infty} d(\varphi_t(x_0), C) = 0\ ,$$

i.e. all trajectories from U_ϵ *converge to* C*.*

Definition 3 (Lyapunov stable)**.** *Consider a* $\delta > 0$*,* $\delta < \epsilon$ *defining a set*

$$U_\delta = \{x_0 \in X |\ d(x_0, C) < \delta\}\ .$$

A set C *is said to be* Lyapunov stable *if for each neighbourhood* U_ϵ *as above there exists a* U_δ *such that for all* $x_0 \in U_\delta$

$$\forall_{t\geq 0} :\ \varphi_t(x_0) \in U_\epsilon\ .$$

Trajectories starting sufficiently close to C *remain bounded in a finite neighbourhood.*

Definition 4 (Asymptotically stable)**.** *When a set is both locally attracting and Lyapunov stable – i.e. small deviations asymptotically converge back to the set and are bounded –* C *is said to be* asymptotically stable[11]*.*

For limit cycles, this property is better known as *(asymptotic) orbital stability*, because, due to our choice of d above, trajectories can approach each other as a whole although single points on them do not.

Whether a set C is locally attracting or asymptotically stable is determined by its (local) stable respectively unstable manifolds W^s and W^u:

$$\begin{aligned} W^s &= \{x \in U_\epsilon |\ \lim_{t\to\infty} d(\varphi_t(x), C) = 0 \wedge \forall_{t\geq 0} : \varphi_t(x) \in U_\epsilon\} \\ W^u &= \{x \in U_\epsilon |\ \lim_{t\to-\infty} d(\varphi_t(x), C) = 0 \wedge \forall_{t\leq 0} : \varphi_t(x) \in U_\epsilon\}\ , \end{aligned} \tag{2.7}$$

defined at least locally in a neighbourhood U_ϵ of the set C.

An asymptotically stable fixed point has no unstable manifold and vice versa. *Saddle points* are a special class of fixed points which have both stable and unstable manifolds. In general, finding analytic expressions for W^s and W^u is not feasible. However, as they are locally defined and as only small (infinitesimal) perturbations are considered, it is possible to write Eqn. 2.1 in coordinates $\xi = x - x^\star$, $\|\xi\| \ll 1$ such that[12]

$$\dot{\xi} \simeq \underbrace{f(x^\star)}_{=0} + \mathbf{J}(x^\star)\,\xi + \mathcal{O}\left(\|\xi\|^2\right)\ . \tag{2.8}$$

In this equation, $\mathbf{J}(x^\star)$ is the *Jacobian matrix* of f at $x^\star$ with the entries given by $\mathbf{J}_{ij}(x^\star) = \frac{\partial f_i(x)}{\partial x_j}|_{x^\star}$. This linearisation at $x^\star$ is essential to assessing the stability of

[11] Note that measure attractors don't need to be asymptotically stable, as the existence of a locally attracting neighbourhood is not required. Examples are semi-stable or even unstable attractors (Timme et al. 2002).

[12] Here, and in the following, the relation $\simeq$ indicates an asymptotic equality up to an error of quadratic order.

fixed points. Eqn. 2.8 captures the dynamics of the nonlinear system in a neighbourhood of the fixed point sufficiently well if certain conditions are met.

If the real parts of all eigenvalues λ_i of $\mathbf{J}(x^\star)$ are distinct from zero, the fixed point is called *hyperbolic* and the theorem of Hartman and Grobman (Guckenheimer et al. 2002, Theorem 1.3.1) guarantees the existence of a homeomorphism between the nonlinear flow $\varphi_t(x)$ with its un-/stable manifolds (W^s and W^u) and the linear flow of Eqn. 2.8. In other words, in a neighbourhood of a hyperbolic fixed point, the nonlinear flow is topologically equivalent to the flow of a linear system. Furthermore, it can be shown that W^s and W^u have the same dimension and are tangent to the corresponding un-/stable sub-spaces of the linear system spanned by the eigenvectors of the Jacobian (ibid., Theorem 1.3.2).

Theorem 2 (Stable hyperbolic fixed point)**.** *A hyperbolic fixed point $x^\star$ is asymptotically stable if all eigenvalues of the associated Jacobian $\mathbf{J}(x^\star)$ have negative real part.*

Moreover, hyperbolic fixed points are unstable if all eigenvalues have positive real part. A fixed point, where the real parts of the eigenvalues have mixed sign is called a saddle point.

Consider again Eqn. 2.8 with a fixed point $x^\star$. According to Theorem 2, the eigenvalues of $\mathbf{J}(x^\star)$ have negative real part when $x^\star$ is asymptotically stable. This means small deviations $\xi(t)$ to $x^\star$ decay exponentially. Otherwise, if there were a positive eigendirection to $\mathbf{J}(x^\star)$, small deviations grow exponentially.

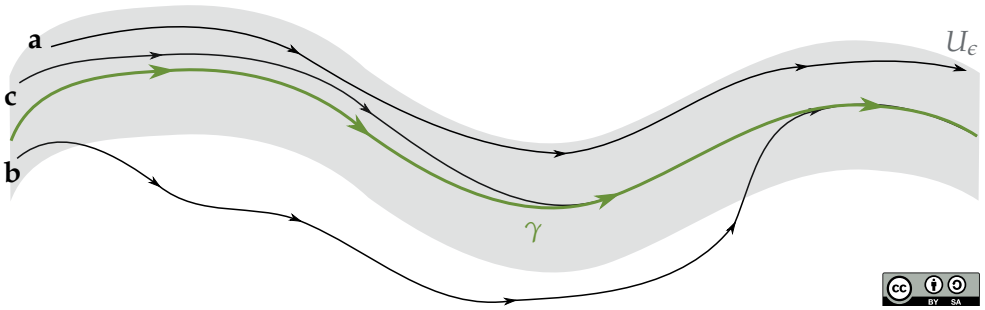

Figure 2.1. – **Stability of Limit Cycles**: The green line labelled γ represents a section of a limit cycle and the shading indicates an arbitrarily chosen open neighbourhood U_ϵ (see text). γ is **a** Lyapunov stable, **b** locally attracting and **c** asymptotically stable.

Fig. 2.1 shows a section of a limit cycle γ and three different representatives for the behaviour of close-by trajectories labelled **a**, **b** and **c**. The shaded band marks the choice of a neighbourhood U_ϵ. Firstly, if there exists a $U_\delta \subseteq U_\epsilon$ s.t. trajectories emanating from U_δ remain bounded in U_ϵ, we say γ is Lyapunov stable (**a**). Secondly, the limit cycle is locally attracting if nearby trajectories from U_ϵ converge to γ (**b**). Lastly, if the nearby trajectories are locally attracting and Lyapunov stable, γ is considered to be asymptotically stable (**c**).

Furthermore, Theorem 2 can be extended to limit cycles in a straight-forward way by considering a so-called *Poincaré section* S. This is a $D-1$-dimensional local cross-section which should intersect a limit cycle γ in a single point s, i.e. $|\gamma \cap S| = 1$.

Nearby points $x \in S$ are mapped back to S after one period T of the limit cycle by the so-called *return* or *Poincaré map* $\sigma : x \mapsto \sigma_x := \varphi_{\tau(x)}(x)$, where $\tau(x) := \min\{t > 0 : \varphi_t(x) \in S\}$. At the intersection, we clearly have $\sigma_s = \varphi_T(s) = s$.

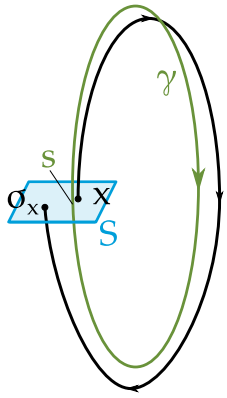

Figure 2.2. – **Illustration of a Poincaré map** σ.

Now, the following theorem (Kuznetsov 1998) can be formulated.

Theorem 3 (Stable hyperbolic limit cycle)**.** *If s is a hyperbolic fixed point of the Poincaré map σ, then the limit cycle γ is called* hyperbolic. *γ is asymptotically stable if all $D-1$ eigenvalues of the associated Jacobian $\mathbf{J}(s)$ of σ have a magnitude less then* 1.

Considering the full-dimensional system, the theorem requires that all perturbations corresponding to directions *transverse* to the limit cycle γ are contracted. Hence, the single eigenvalue *longitudinal* to γ is zero, i.e. perturbations along the orbit remain constant (ibid.). This encodes the intuitive notion that longitudinal deviations along a limit cycle should not affect its stability but only transverse deviations and the corresponding invariant manifolds.

These theorems ensure that under certain conditions, it is possible to gain information about the fixed points or limit cycles of nonlinear systems by looking at the eigenvalue spectrum of locally-defined linear approximations. This aspect is a foundation of the so-called *linear* or *asymptotic stability analysis*.

The idea of the eigenvalue analysis can be extended to the nonlinear case by defining so-called *Lyapunov exponents*, generalising the idea of exponential contraction respectively separation. Consider the difference $\zeta(t) := u(t) - v(t)$ of two trajectories u and v of Eqn. 2.1 from nearby initial conditions u_0 and v_0. Then, the Lyapunov exponents are defined as

$$\lambda(u_0, v_0) := \lim_{\zeta(0)\to 0^+} \lim_{t\to\infty} \frac{1}{t} \ln \frac{\|\zeta(t)\|}{\|\zeta(0)\|}, \tag{2.9}$$

i.e. it measures the asymptotic rate at which v and u are converging $\lambda < 0$ or diverging $\lambda > 0$. If the distance ζ between u and v does not change over time, we have $\lambda = 0$. There are at most D distinct Lyapunov exponents $\lambda(u_0, v_0)$ given that ζ can be written in an orthonormal basis of independent components in D directions. Clearly, for a linear system, the Lyapunov exponents from Eqn. 2.9 equal the real part of eigenvalues of the Jacobian. Consequently, a fixed point has all negative Lyapunov exponents. A limit cycle has a zero longitudinal Lyapunov exponent while the transverse exponents are negative. Close to a chaotic attractor, one Lyapunov exponent is positive, one is zero and the remaining are negative[13].

[13] For simplicity, this brief overview is not complete and excludes cases like quasi-periodic torii and hyperchaos (Hilborn 2000). Hyperchaos appears if there are at least two positive Lyapunov exponents (Rössler 1979).

2.3.2. One-Parameter Bifurcations of Two-Dimensional Flows

THE STABILITY of attractors changes, if one or more parameters of the system Eqn. 2.1 are slowly varied. At particular values, the number and stability of attractors changes. These values are called *bifurcation points*, in some contexts also *critical* or *tipping points*. The knowledge of bifurcation points is essential as their transgression alters the long-term behaviour of dynamical systems qualitatively and many research branches are devoted to estimating them from data as well as to define early-warning indicators. In the following I consider bifurcations of a single parameter, so-called *codimension-1 bifurcations* (Guckenheimer et al. 2002).

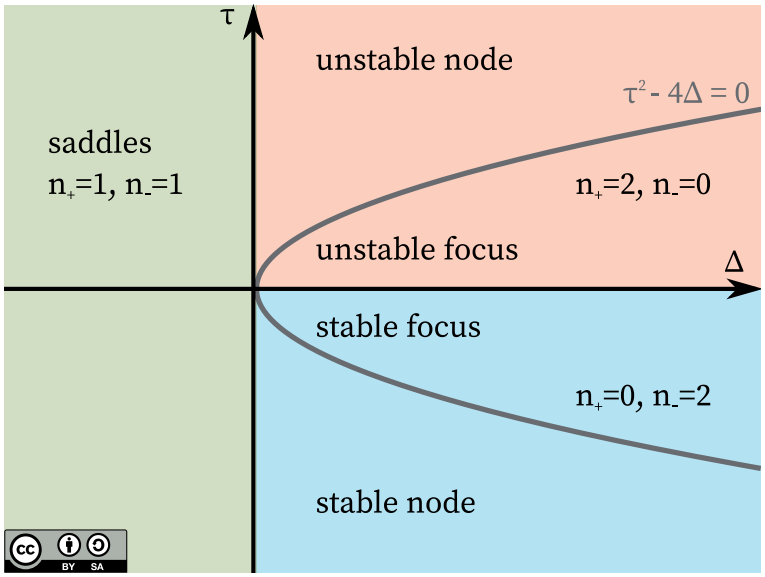

Figure 2.3. – **Classification of fixed points in two-dimensional systems**: In two-dimensional dynamical systems, based on the trace τ and determinant Δ of the Jacobian $\mathbf{J}(x^\star)$, each fixed point is mapped on a point in the (τ, Δ)-space. Here, n_+ and n_- are the number of eigenvalues with positive respectively negative real part of the Jacobian. See the text for details on the classification scheme.

In two-dimensional flows, all bifurcations can be categorised into a finite number of qualitatively distinct scenarios for fixed point as well as limit cycle attractors, which is detailed in various textbooks, e.g. Strogatz (1994) or Guckenheimer et al. (2002). Essentially, the method makes use of the fact that the real part of at least one of the Jacobian eigenvalues changes its sign at the bifurcation point. For instance, in a transcritical bifurcation, the real parts of both of the eigenvalues of the Jacobian at a fixed point $x^\star$ become positive and a former asymptotically stable fixed point $x^\star$ becomes unstable. Geometrically, it merges with an unstable fixed point.

The following relations hold for the trace and determinant of the Jacobian:

$$\tau := \mathrm{tr}\left(\mathbf{J}\left(x^\star\right)\right) = \sum_{k=1}^{D} \lambda_k \quad \Delta := \det\left(\mathbf{J}\left(x^\star\right)\right) = \prod_{k=1}^{D} \lambda_k \,, \tag{2.10}$$

for the eigenvalues λ_k of $\mathbf{J}(x^\star)$ at a fixed point $x^\star$. Fig. 2.3 illustrates the resulting cases for $D = 2$. Consider the characteristic equation of the Jacobian

$$\lambda^2 - \tau\lambda + \Delta = 0 \tag{2.11}$$

with the trace τ and determinant Δ that has solutions

$$\lambda_{1/2} = \frac{\tau}{2}\left(1 \pm \sqrt{1 - \frac{4\Delta}{\tau^2}}\right) . \tag{2.12}$$

When $\mathfrak{Re}(\lambda_1)$ and $\mathfrak{Re}(\lambda_2)$ have different signs, the determinant Δ is negative. Hence, all saddle points are located in the left half plane. When they have equal sign, the trace τ distinguishes between asymptotically stable (both negative) and unstable fixed points (both positive). In the case of a non-zero imaginary part ($\tau^2 < 4\Delta$), they are referred to as an *un-/stable focus or spiral*. Take, for instance, above example of a transcritical bifurcation. One of the fixed points $x_1^\star$ loses asymptotic stability and becomes unstable. Hence, the state of $x_1^\star$ in the (Δ, τ)-diagram moves from the negative right half plane to the positive right half plane.

Another important distinction is that between local and global bifurcations. Local bifurcations can be analysed by considering an arbitrarily small neighbourhood of an attractor. For the observation of global bifurcations, however, this is not sufficient and one needs to regard larger parts of the phase space. The bifurcations of fixed points discussed above are all local.

There are two examples of global bifurcations of limit cycles I would like to mention here, namely a *homoclinic bifurcation* and an *infinite-period bifurcation*. As a prerequisite, the following special class of trajectories is introduced.

Definition 5 (Homoclinic/Heteroclinic trajectory)**.** *A trajectory $\varphi_t(x_0)$ starting at $x_0 \in X$ is called* heteroclinic *to the fixed points $x_-^\star \neq x_+^\star$ of Eqn. 2.1 if*

$$\varphi_t(x_0) \to x_-^\star \text{ for } t \to -\infty$$

as well as

$$\varphi_t(x_0) \to x_+^\star \text{ for } t \to \infty$$

If rather $x_-^\star \equiv x_+^\star$, the trajectory is called homoclinic.

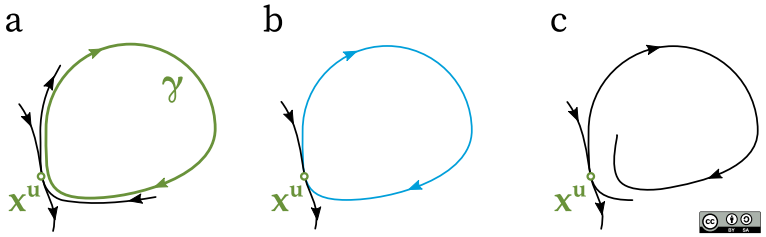

Figure 2.4. – **Homoclinic bifurcation**: **a** Before, **c** after and **b** at the bifurcation point.

In a homoclinic bifurcation (cf. Fig. 2.4), a limit cycle γ becomes the homoclinic orbit (blue colour in Fig. 2.4b) of a saddle x^u at the bifurcation point when a param-

eter of Eqn. 2.1 is varied. Homoclinic orbits to a hyperbolic fixed point are, however structurally unstable, i.e. they do not persist over an extended parameter regime. Particularly, by crossing the bifurcation point, the homoclinic orbit splits, leaving the saddle point x^u.

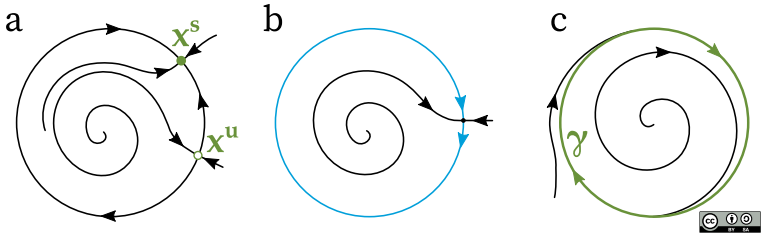

Figure 2.5. – **Infinite-period bifurcation**: **a** Before, **c** after and **b** at the bifurcation point.

An infinite-period bifurcation (Keener 1980) (cf. Fig. 2.5) differs from the previous case in the following way. Two fixed points – a saddle x^u and a stable node x^s – are connected via two heteroclinic orbits. At the bifurcation point, the fixed points merge, forming a so-called *saddle-node* with a homoclinic orbit (blue colour in Fig. 2.5b). By crossing the bifurcation point, the saddle-node vanishes and a stable limit cycle γ emerges. This bifurcation's name stems from the fact that – by approaching the bifurcation point from the right – the period of motion on the limit cycle diverges until it is infinite on the homoclinic orbit. This is a consequence of the existence and uniqueness theorem (cf. Theorem 1).

2.3.3. Master Stability Functions

Complex networks[14] form an important class of high-dimensional dynamical systems, for which an asymptotic stability analysis can be performed in a particularly insightful way. The focus here is on the dynamics *on* networks (i.e. for a fixed coupling structure), in contrast to the dynamics *of* networks themselves (Holme et al. 2012).

Consider a network of n mutually coupled oscillators, each of them has a local evolution law – i.e. in the absence of coupling – according to Eqn. 2.1 and the coupling structure is given by a connected network represented by a matrix $\mathbf{A}$[15]. As discussed in Sec. 2.2.3, the phase dynamics of coupled oscillators synchronises if the difference in natural frequencies is sufficiently small and if the coupling strength is high enough.

The key insight of master stability functions (Pecora et al. 1998) for synchronisation is that the linear stability question of complex networks (cf. Eqn. 2.8) decomposes in a part determined by the local dynamics at each node and a part solely depending on the eigenvalues spectrum of the network's coupling structure. By this, the complexity of the problem is reduced and it becomes feasible to directly infer asymptotic stability for a variety of network structures (Barahona et al. 2002; Arenas,

[14] Complex networks are introduced en detail in Sec. 3.2.
[15] A_{ij} is nonzero if there exists a connection between two nodes i and j.

Díaz-Guilera, et al. 2008; Menck, Heitzig, Marwan, et al. 2013)[P4]. Particularly, if networks are imprinted with mesoscale structures like certain multi-layer networks, additional patterns arise in the Jacobian leading to interesting insights on the relation between stability and structural organisation of complex systems (Brechtel et al. 2016; Tang et al. 2016).

The concept of master stability functions has been successfully applied to study the stability of the synchronous regime in a variety of systems, like delay-coupled oscillators (Dahms et al. 2012), multiplex (Tang et al. 2016) and multi-layer networks (Brechtel et al. 2016), stochastically coupled maps (Porfiri 2011) and slightly non-identical oscillators (Sun et al. 2009).

The dynamical system is given by n local processes at each node of dimension d with real-valued states $x \in X$. The state space $X = U^n$ is the tensor product of nodal phase spaces $U \subset \mathbb{R}^d$ and the state vector x has n d-dimensional components $x_k \in U$. Then, the system can be formulated using n equations

$$\dot{x}_k = f_k\left(x_k\right) + \sigma \sum_{j=1}^{n} A_{jk} h\left(x_k, x_j\right) \tag{2.13}$$

with the intrinsic local dynamics $f_k : U \to U$, the coupling function $h : U \to U$ – prescribing through which variables the nodes are coupled – and an overall coupling constant σ. Typically, the coupling only depends on the differences $x_k - x_j$, for instance $h\left(x_k, x_j\right) = \sin\left(x_k - x_j\right)$. This is commonly called *diffusive coupling* and will be denoted by $h\left(x_k - x_j\right)$.

A phase-locked solution $S\left(t\right) = \left(s_1(t), ..., s_n(t)\right)^\top$ evolves within the so-called *synchronisation manifold* S and is determined by the set of equations

$$\dot{s_k} \simeq f_k\left(s_k\right) + \sigma \sum_{j=1}^{n} A_{jk} h\left(s_k - s_j\right) \ . \tag{2.14}$$

Depending on the nature of $S\left(t\right)$, the manifold can have a complex structure. If the solution is a fixed point of the node dynamics, i.e. $f_k\left(s_k\right) = 0$ for all k, the n constraints on the differences define a typically lower-dimensional manifold, depending on the precise coupling structure h. In the limit of complete synchronisation, i.e. for identical oscillators $f_k\left(x_k\right) \equiv f\left(x_k\right)$, the solution of Eqn. 2.13 is contained in the diagonal manifold M[16]

$$M = \left\{x_k \in U \middle|\ x_1 = ... = x_k = ... = x_n =: s\right\} . \tag{2.15}$$

To pursue with an asymptotic stability analysis, Eqn. 2.13 is being linearised around a point on M, $\tilde{S}\left(t\right) = \left(s(t), ..., s(t)\right)^\top$, by considering the deviations $\xi_k = x_k - s$, $\left\|\xi_k\right\| \ll 1$.

[16] For stable complete synchronisation, the local dynamics need to be identical up to a mismatch that can be considered small enough (Fujiwara et al. 2009; Pereira et al. 2014).

Close to M, the coupling function can be approximated as[17]

$$h\left(x_k - x_j\right) \simeq h\left(0\right) + \mathbf{Dh}\left(s\right)\left(\xi_k - \xi_j\right) \ . \tag{2.16}$$

Furthermore, the local dynamics are approximately given by[18]

$$f\left(x_k\right) \simeq f\left(s\right) + \mathbf{Df}\left(s\right)\xi_k \ . \tag{2.17}$$

Then, using Eqn. 2.13, the deviations evolve according to[19]

$$\dot{\xi_k} \simeq \mathbf{Df}\left(s\right)\xi_k + \sigma\sum_{j=1}^{n} A_{jk}\mathbf{Dh}\left(s\right)\left(\xi_k - \xi_j\right) \ , \tag{2.18}$$

which can be written succinctly using the so-called *Laplacian matrix* $\mathbf{L}$ as[20]

$$\dot{\xi} \simeq \left(\mathbf{J}\left(s\right) - \sigma\mathbf{L}\otimes\mathbf{Dh}\left(s\right)\right)\xi \ , \tag{2.19}$$

where $\mathbf{J}\left(s\right) = \mathbb{1}_n \otimes \mathbf{Df}\left(s\right)$ and $\xi = \left(\xi_1, ..., \xi_n\right)^\top$. The Laplacian matrix is determined via the relation

$$\sum_{j=1}^{n} A_{jk}\mathbf{Dh}\left(s\right)\left(\xi_k - \xi_j\right) = -\sum_{j=1}^{n} L_{jk}\mathbf{Dh}\left(s\right)\xi_j \ . \tag{2.20}$$

It will be discussed in further detail in Sec. 3.2 as it plays an essential role in algebraic graph theory. For now, it is sufficient to know that it is symmetric when the oscillators are bidirectionally coupled and that one eigenvalue is 0 corresponding to the eigenvector $\mathbf{1}_n$ of all ones. To proceed, we have to assume that the Laplacian is diagonalisable, i.e. that it is normal, which might not be the case in general.

Let us define the diagonal matrices $\mathbf{\Lambda} = \mathbf{P}^{-1}\mathbf{L}\mathbf{P}$ and $\mathbf{\Gamma} = \mathbf{Q}^{-1}\mathbf{Df}\left(s\right)\mathbf{Q}$ with the eigenvalues λ_j of $\mathbf{L}$ and γ_j of $\mathbf{Df}\left(s\right)$ on the diagonal. Here, it is assumed that also $\mathbf{Df}\left(s\right)$ is diagonalisable. In case it is not, replace $\mathbf{\Gamma}$ by $\mathbf{Df}\left(s\right)$ and $\mathbf{Q}$ by an identity matrix $\mathbb{1}_d$ in the following.

Switching to new coordinates $y = \left(\mathbf{P}\otimes\mathbf{Q}\right)\xi$ yields[21]:

$$\begin{aligned}\dot{y} &\simeq \left(\left(\mathbf{P}^{-1}\otimes\mathbf{Q}^{-1}\right)\mathbf{J}\left(s\right)\left(\mathbf{P}\otimes\mathbf{Q}\right) - \sigma\mathbf{\Lambda}\otimes\left(\mathbf{Q}^{-1}\mathbf{Dh}\left(s\right)\mathbf{Q}\right)\right)y \\ &= \left(\mathbb{1}_n\otimes\mathbf{\Gamma} - \sigma\mathbf{\Lambda}\otimes\left(\mathbf{Q}^{-1}\mathbf{Dh}\left(s\right)\mathbf{Q}\right)\right)y\end{aligned} \tag{2.21}$$

Now there are n completely decoupled d-dimensional blocks that are identical except for the value of λ_k, yielding the local equations

[17] $\mathbf{Dh}\left(s\right)_{ab} = \frac{\partial h(x_k - x_a)}{\partial x_b}|_s$ is the Jacobian matrix of the coupling function.

[18] $\mathbf{Df}\left(s\right)_{kj} = \frac{\partial f(x_k)}{\partial x_j}|_s$ is the Jacobian matrix of the local dynamics.

[19] Note that for attractors more complicated then fixed points, i.e. limit cycles, the linearisation at a point on such an attractor yields a time-dependent linear problem.

[20] $\otimes$ is the Kronecker product.

[21] Note that $\left(\mathbf{P}\otimes\mathbf{Q}\right)^{-1} = \left(\mathbf{P}^{-1}\otimes\mathbf{Q}^{-1}\right)$.

$$\dot{y}_k = \left(\mathbf{\Gamma} + \sigma\lambda_k \mathbf{Q}^{-1}\mathbf{Dh}\left(s\right)\mathbf{Q}\right) y_k \,. \tag{2.22}$$

This defines the *master stability function* $\Lambda_{f,h}\left(\sigma\lambda_k\right)$, i.e. the maximum non-zero real part of the eigenvalues of Eqn. 2.22 as a function of $\sigma\lambda_k$, first described by Pecora et al. (1998). From the discussion in Sec. 2.3.1, we see that $\tilde{S}$ is asymptotically stable if $\Lambda_{f,h}\left(\sigma\lambda_k\right) < 0$ for all eigenvalues λ_k of the Laplacian matrix.

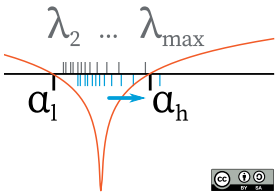

Figure 2.6. – **Schematic illustration of master stability functions:** The orange curve marks $\Lambda_{f,h}\left(\sigma\lambda_k\right)$ for a dynamical system with a stability interval $I = [\alpha_l; \alpha_h]$. The grey ticks illustrate the location of the Laplacian spectrum which can shift, for instance, due to link addition (blue ticks).

In applications, it is often of interest how $\Lambda_{f,h}\left(\sigma\lambda_k\right)$ varies with the coupling strength σ for a fixed network. Typically, there are at least four classes by which the shape of the master stability function for coupled oscillators can be categorised depending on the number of its roots (Huang et al. 2009). In the absence of coupling, $\Lambda_{f,h}\left(0\right)$ corresponds to the largest eigenvalue of the local Jacobian $\mathbf{Df}\left(s\right)$, i.e. it is positive for chaotic and zero for periodic oscillators.

Assume that $\Lambda_{f,h}\left(\sigma\lambda_k\right)$ is negative on some interval $I = [\alpha_l; \alpha_h]$. The associated dynamical system has an asymptotically stable fixed point if for all values $\sigma\lambda_k \in I$, excluding $\lambda_1 = 0$ (eigenvalues are sorted by increasing real part). Equivalently, this formulates to

$$R = \frac{\lambda_n}{\lambda_2} < \frac{\alpha_h}{\alpha_l} \,. \tag{2.23}$$

In the context of synchronisation on complex networks, the eigenratio R is known as the *synchronisability* of a network. Networks with smaller R have a narrower spectrum allowing for a wider range of coupling constants σ, hence they are said to be more synchronisable.

2.4. Stability in the Realm of Large Perturbations

Abstract This section discusses stability with respect to finite perturbations using direct methods or basin stability and introduces final state sensitivity in complex basins of attraction.

2.4.1. Direct Methods

Direct methods, comprising conceptually similar approaches such as Lyapunov functions (Lyapunov 1907; Hahn 1958; Malisoff et al. 2009; Giesl and Hafstein 2015) or non-equilibrium potentials (Graham and Tél 1984; Graham, Hamm, et al. 1991), are powerful tools for assessing the stability of attractors. They are termed direct

methods because they do not rely on an analysis of specific trajectories but are directly obtained from the dynamical equations. A main application of direct methods is approximating basins of attraction.

Lyapunov functions are potential-like functions $V(x)$ with monotonous orbital derivative, meaning they decrease along the trajectories of Eqn. 2.1. Assuming the system has a fixed point $x^\star$, by definition a Lyapunov function has a (local) minimum at $x^\star$. If $V(x)$ is strictly minimal in $x^\star$ and additionally $\dot{V}(x) < 0$ for all x in an open neighbourhood of the fixed point, $x^\star$ is asymptotically stable.

Although they are commonly thought of as energy functions, Lyapunov functions are generally not potentials in the original meaning. Here, the approach of non-equilibrium potentials forms an important subgroup. Additionally, these yield information on the transition probabilities between attractors and can even be constructed for systems with fractal basin boundaries (Graham, Hamm, et al. 1991).

Generally, the explicit construction of Lyapunov functions for a given system turns out to be a difficult problem. It is possible to resort to numerical approaches for their computation, for instance the SOS (sums of squares) method (Parrilo 2000), the CPA (continuous piece-wise affine) method (Hafstein 2004), radial basis functions (Giesl, Hamzi, et al. 2016) and the numerical solution of Zubov's equation (Camilli et al. 2001). A survey of numerical methods can be found in Giesl and Hafstein (2015).

There are, however, several disadvantages associated to direct methods. On the one hand, they are typically not efficient for high-dimensional systems, while on the other hand they yield conservative lower bounds on the attraction basin (Hsiao-Dong Chang et al. 1995; Gajduk et al. 2014). In general, this makes it difficult to determine whether a basin grows or shrinks due to a parameter change.

2.4.2. Basin Stability

In the previous section, I recapitulated how to assess stability based on local properties of the vector field in the vicinity of fixed points. Summarising, one could say, that linear stability analysis gives a qualitative picture on whether a solution asymptotically approaches an attractor, given non-local infinitesimal perturbations. In the following we encounter a complementary approach using network-local (e.g. single nodes in a network) but finite – possibly large – perturbations, which is able to *quantify* stability of an attractor in multistable systems (Shrimali et al. 2008; Pisarchik et al. 2014), introduced by Menck, Heitzig, Marwan, et al. (2013). Multistable systems are of special interest, as large perturbations can cause non-local effects like the transition to a different attractor.

Above, we learned that asymptotic stability requires an open neighbourhood from which the flow stays close – and asymptotically approaches – the attractor. However, the catchment area of an attractor, its basin of attraction (cf. Sec. 2.2), is typically much larger and a complicated geometrical object. Take for instance the basin of attraction in Fig. 2.7a which contains infinitely many branches due to the phase periodicity. Examples of more complicated basins, which are not necessarily open sets, will occur in Sec. 2.4.3.

Consider again the dynamical system Eqn. 2.1. Assume a multistable system

with an attractor $\mathcal{A}$ that has a basin of attraction $\mathcal{B}(\mathcal{A})$. Intuitively, the volume of the basin of attraction, or generally a suitable measure μ, seems to be related to the stability of the corresponding attractor $\mathcal{A}$. The measure μ is chosen to be a probability measure in the probability space $(X, \mathcal{F}, \mu)$, where $\mathcal{F}$ is a σ-algebra on X. Then, $\mu_{\mathcal{B}}$ will give the probability to hit $\mathcal{B}$ by randomly drawing an initial condition from a compact subset $R \supset \mathcal{A}$ and is henceforth referred to as *basin stability* (Menck and Kurths 2012; Menck, Heitzig, Marwan, et al. 2013; Menck 2014; Menck, Heitzig, Kurths, et al. 2014)

$$\begin{aligned} \mu_{\mathcal{B}} &:= \mu(\mathcal{B}(\mathcal{A})) = \int\limits_{R \subseteq X} \mathbf{I}_{\mathcal{B}(\mathcal{A})} \, d\mu = \int\limits_{R \subseteq X} \mathbf{I}_{\mathcal{B}(\mathcal{A})}(x) \, \rho(x) \, dx^D \,, \\ \mu_{\mathcal{B}} &\in [0,1] \,, \end{aligned} \tag{2.24}$$

where $\mathbf{I}_{\mathcal{B}(\mathcal{A})}(x)$ is the indicator function of $\mathcal{B}$ yielding 1 if $x \in \mathcal{B}$ and 0 otherwise. The probability measure μ is specified by choosing a probability density ρ that has the interpretation of encoding the frequency of relevant perturbations to $\mathcal{A}$. If not otherwise stated, ρ is chosen as a uniform probability density. In this case, μ is proportional to the volume measure.

The domain R of the integral Eqn. 2.24 typically is high-dimensional, especially if the underlying structure of the dynamical system is given by a network (cf. Sec. 3.2). Despite that, such integrals can be efficiently estimated by using a *simple Monte Carlo sampling* (Von Neumann 1951; Evans et al. 2000). Given, that for each initial condition one can numerically integrate the system with sufficient precision to decide to which attractor it converges (or whether it diverges), the $\mu_{\mathcal{B}}$ estimation procedure is:

1. If X is not compact, select a compact subset $R \supset \mathcal{A}$. Otherwise, choose $R = X$.
2. Specify the probability measure μ.
3. Draw a sample of $N > 0$ initial conditions independently according to μ.
4. By numerical integration, assess to which attractor the system converges (if at all).
5. Count the number N_A of times the system has converged to $\mathcal{A}$.
6. Use the fraction $\hat{\mu}_{\mathcal{B}} = \frac{N_A}{N}$ as an estimator for $\mu_{\mathcal{B}}$.

This procedure resembles a N-times repeated Bernoulli experiment with success probability $\mu_{\mathcal{B}}$. The absolute standard error of its estimate $\hat{\mu}_{\mathcal{B}}$ is independent of the dimension of X and given by[22]

$$e_{std.} = \sqrt{\frac{\hat{\mu}_{\mathcal{B}}(1 - \hat{\mu}_{\mathcal{B}})}{N}} \,. \tag{2.25}$$

[22] If $\hat{\mu}_{\mathcal{B}} \approx 1$ or $\hat{\mu}_{\mathcal{B}} \approx 0$, more robust estimators are available (Agresti and Coull 1998).

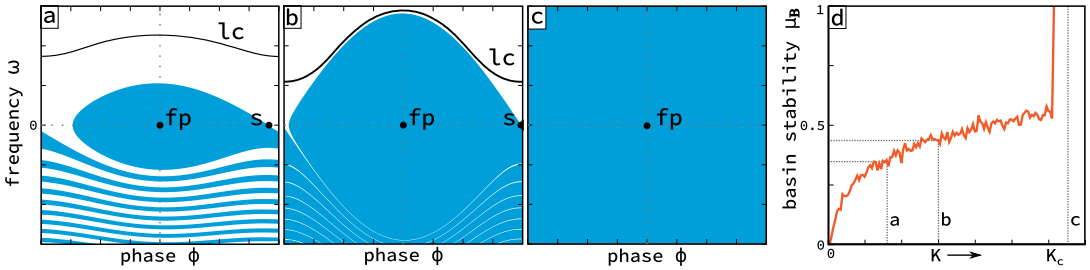

Figure 2.7. – **Tracing bifurcations with basin stability:** Shown is a schematic illustration of the phase space of a damped-driven pendulum. The blue colour indicates the basin of attraction of the fixed point `fp` which is located in the centre. The figures **a**, **b** and **c** picture snapshots of the basin at three different values of K, i.e. **a** $K \ll K_c$, **b** $K < K_c$ and **c** $K > K_c$. `s` denotes a saddle point and `lc` limit cycle. In **d** the dependence of the fixed point's basin stability $\hat{\mu}_{\mathcal{B}}$ on K is plotted.
Adapted from Menck and Kurths (2012).

Hence, it is not necessary to increase the sample size N with the dimension D to achieve a certain error. This effect might be counter-intuitive at first but is clearly due to the fact that basin stability measures the basin volume w.r.t. μ regardless of the specific geometry. However, the time for assessing convergence by means of numerical integration typically increases with D.

Basin stability of a fixed point in a dynamical system is further illustrated in Fig. 2.7. The system has a parameter K that is slowly increased until the system undergoes a homoclinic bifurcation (cf. Sec. 2.3.2) at a critical value K_c. Here the system loses multistability and the stable fixed point, formerly coexisting with a stable limit cycle becomes a global attractor. Consequently, the estimation procedure gives $\hat{\mu}_{\mathcal{B}} = 1$ beyond the bifurcation point. Clearly, this is not sufficient to infer global stability but a necessary condition. The main advantage of basin stability over common linear approaches is that it also yields a quantitative information about *how stable* an attractor is w.r.t. the extent of its basin. In Fig. 2.7d we observe that the values indeed change in a monotonous way, indicating transformations of the basin way before the bifurcation point. Under certain conditions, this fact might be exploited to design early-warning schemes for dynamical systems approaching a tipping point (Menck, Heitzig, Marwan, et al. 2013).

So far, the distribution ρ of perturbations considered for $\mu_{\mathcal{B}}$ is global in the sense that it corresponds to perturbations with components associated to all dimensions. In many applications, i.e. for complex networks (cf. Sec. 3.2), the phase space can be written as the tensor product of subspaces associated to each of the n nodes in a network $X = \bigotimes_{k=1}^{n} X^k$. Then we can define a particularly interesting class of local perturbations at single nodes in a network and consequently a *single-node basin stability*

$$\mu_{\mathcal{B}}^k = \mu|_{X^k}\left(\mathcal{B}\left(\mathcal{A}\right) \cap X^k\right) , \tag{2.26}$$

where $\mu|_{X^k}$ is the measure μ restricted to X^k. The estimation procedure of $\hat{\mu}_{\mathcal{B}}^k$ is

analogous[23] to that of $\hat{\mu}_{\mathcal{B}}$ with setting $R \subseteq X^k$.

Basin stability[24] has recently been applied in a variety of contexts, e.g. power grids (Menck, Heitzig, Kurths, et al. 2014; Schmietendorf, Peinke, Friedrich, et al. 2014; Schäfer, Matthiae, Timme, et al. 2015; Kim et al. 2016; Rodrigues et al. 2016), chimera states (Martens, Bick, et al. 2016) and explosive synchronisation (Zou et al. 2014) in oscillator networks, delayed dynamics (Leng et al. 2016) and integrated in resilience measures (Mitra, Kurths, et al. 2015). It genuinely complements stability analyses based on linear approaches and yields a fundamentally different kind of information. This has been demonstrated, for instance, by Menck, Heitzig, Marwan, et al. (2013) who identify a trade-off between synchronisability and basin stability. While the synchronisability of small-world networks is optimal for random networks, the average single-node basin stability tends to be optimal in the small-world regime lying inbetween regular and random networks.

Basin stability has to be distinguished from alternative concepts in complex socio-ecological systems defining a *resilience* (Holling 1973; Scheffer 2009) based on the width of the basin in a particular direction. It is not only inherently difficult to find the single-most important direction to characterise a system, but the interpretation of resilience is essentially different from stability although these words are sometimes used interchangeably. Resilience of a system, as the ability to recover from a perturbation, is deeply intertwined with the ability of adaptation. The evolution laws of a resilient system change over time, adapting to repeated perturbations in some kind of deterministic or non-deterministic feedback loop.

Reverse History of Basin Stability In the spirit of the reverse history of chaos synchronisation (Pecora et al. 2015), I want to highlight earlier research partly anticipating but also inspiring the concept of basin stability. Basin stability has been introduced by Menck, Heitzig, Marwan, et al. (2013) on a broad conceptual foundation, while the idea of ranking an attractor's stability by it's basin size has already some history, for instance in power grid stability (Kundur et al. 2003; Hill et al. 2006).

Lundström and Aidanpää (2007) studied vibrations in hydro power generators due unbalanced motion caused by shape deformations of the rotor. For various shapes, the authors numerically estimate the basin for certain attractors without impacts between the rotor and stator from a uniform grid of initial conditions. The two key observables in this experiment are the number of converging initial conditions (corresponding to $\mu_{\mathcal{B}}$) and the radius of the largest sphere fitting into the basin.

Wiley et al. (2006) sampled the basin size distribution for different kinds of fixed points in the Kuramoto model on a regular ring network, based on a random sampling of initial conditions. They find that the synchronous fixed point dominates as it is more likely to obtain and conjecture that this is due to a larger extent of the corresponding basin of attraction. From their numerical experiments, the authors

[23] Note, however, that in general $\mu_{\mathcal{B}}$ is *not* related to $\prod_{k=1}^{n} \mu_{\mathcal{B}}^k$!

[24] Recently, the basin stability approach has been validated experimentally (Brzeski, Wojewoda, et al. 2017). In practice, it is especially advantageous compared to linear stability when parameter values are not exactly known.

conjecture that the "sync basin's" size – as a measure for the relevance of the attractor – depends on the network topology and system parameters in a complicated manner, i.e. there is no a priori relation between synchronisability of a network and the size of the sync basin.

The idea of estimating a basin of attraction's extent also appeared in earlier work, e.g. on the changing smoothness of basin boundaries (basin erosion) under parameter variation termed global dynamic integrity measure G_τ by Soliman et al. (1989)(and later Soliman et al. (1990) and Rega et al. (2005)). Taking a regular grid of initial conditions, this measure is defined as the fraction that *doesn't approach* an attractor within a given time τ up to a given tolerance. In the limit, G_τ is related to the above definition of $\mu_\mathcal{B}$ via $G_\infty = 1 - \hat{\mu}_\mathcal{B}$, where $\hat{\mu}_\mathcal{B}$ is the estimator of $\mu_\mathcal{B}$ for a uniform ρ. Besides that, Soliman et al. (1989) further introduced the minimum distance between boundary and attractor as well as the largest impulse that could be sustained as complementary stability measures. This closes the circle to recent developments to incorporate even more information about a basin of attraction into integrated measures (Mitra, Kurths, et al. 2015).

2.4.3. Fractal Basin Geometries

Basins of attraction are not necessarily open sets (Milnor 1985) and the basin boundary is not necessarily smooth. Consider, for instance, the damped pendulum with a time-dependent periodic driving force (Battelino et al. 1988; Kennedy et al. 1991):

$$\begin{aligned} \dot{\phi} &= \omega \\ \dot{\omega} &= p\cos(t) - \nu\omega - \sin(\phi) \ . \end{aligned} \tag{2.27}$$

For $p = 7/4$ and $\nu = 1/5$ there are four attracting limit cycles with period 2π, two librations (orange/yellow) and two rotations (black/red), see in Fig. 2.8a. Their corresponding basins of attraction are pictured in Fig. 2.8b for $t = 0$. It becomes immediately visible that, while some regions appear to be uniformly coloured (i.e. all points belong to the same basin), others seem to be sprinkled with dots belonging to different basins. Hence, the boundaries between the basins are not discernible, even after increasing the resolution in certain regions. This is a prime example for a system with *fractal basin boundaries*. The appearance of fractal boundaries is common in physical systems as well as e.g. complex root-finding with the Newton-Raphson method (Daza, Wagemakers, Sanjuán, et al. 2015).

For distinguishing different types of fractal boundaries, it is common to associate a fractal dimension to them. Taking a ball of radius ε around an initial condition in one basin, let $f(\varepsilon)$ denote the relative number of points inside the ball from which trajectories approach the corresponding attractor. This quantity is known as the *uncertainty fraction* (Grebogi et al. 1983; McDonald et al. 1985). It estimates the probability that a perturbation of magnitude ε or less leads to a different basin. Far away from the boundary, f is expected to be 1, regardless of ε. Positioning the ball sufficiently close to the boundary, however, the interior contains points from another

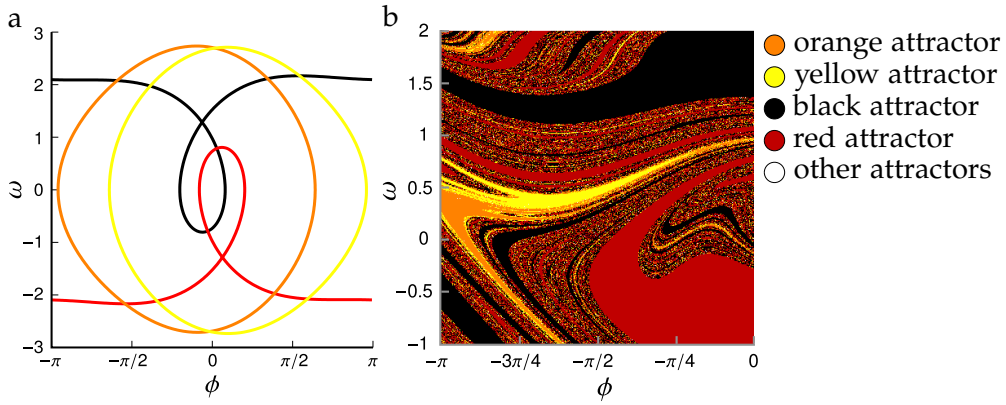

Figure 2.8. – **Fractal basin boundaries in the Wada pendulum. a** The four limit cycle attractors of the damped-driven pendulum according to Eqn. 2.27, where the time dimension is perpendicular to the page. The red and black limit cycles are over-turning rotations of the pendulum, while the orange and yellow limit cycles are librations. **b** Phase space of the system Eqn. 2.27 at time $t = 0$. The colour indicates the basins of attraction of the corresponding limit cycles. The figure has been previously published in [P7].

basin. Generally, in the second case, one observes $f(\varepsilon) \propto \varepsilon^{\alpha}$ for some positive real exponent α. If D denotes the phase space dimension, the *uncertainty dimension* d of a basin boundary (Pelikan 1985; Grebogi et al. 1987; Grebogi, Nusse, et al. 1988) is defined as:

$$d = D - \lim_{\varepsilon \to 0} \frac{\ln f(\varepsilon)}{\ln \varepsilon} = D - \alpha \,. \tag{2.28}$$

For a smooth basin boundary, f is usually proportional to ε and $d = D - 1$ (or $\alpha = 1$ holds in the limit (McDonald et al. 1985)). Contrarily, $0 < \alpha < 1$ indicates a fractal basin boundary and implies that decreasing f (i.e. the uncertainty of a numerical experiment) by an order of magnitude needs a substantially larger decrease in ε (i.e. the numerical precision). This fact is known as *final state sensitivity* (Grebogi et al. 1983), similar to the sensitive dependence on initial conditions in chaotic systems[25]. Recently, the "spatial" distribution of uncertainty exponents across the phase space has been used to develop a probabilistic approach termed basin entropy (Daza, Wagemakers, Georgeot, et al. 2016) which combines the final state uncertainty due to fractal boundaries with the distribution of relative basin volumes.

For above example Eqn. 2.27, it is further known that the basin boundaries are not only fractal but also that the black basin, the red basin and the union of the orange and yellow basins possess the so-called *Wada property* (Kennedy et al. 1991; Nusse et al. 1996, 2003), i.e. any point on the boundary of one subset is also on the boundary of the others. Hence, for a small perturbation sufficiently close to the boundary,

[25]Note that the uncertainty dimension can vary along a basin boundary and a number of smooth and fractal sections can be mixed (Grebogi, Kostelich, et al. 1986), related to basic sets, i.e. sets of boundary points with the same asymptotic behaviour (Battelino et al. 1988; Grebogi, Nusse, et al. 1988).

the trajectory could in principle converge to any of the four attractors. It has been named after Takeo Wada who first gave an explicit construction of a system having this property, later referred to as the "lakes of Wada" (Daza, Wagemakers, Sanjuán, et al. 2015).

A more subtle situation appears with so-called *riddled basins of attraction* (Lai and Tél 2011). Such basins are not open but rather have an empty interior, as their complement intersects every ε-ball in a set of positive measure (Alexander et al. 1992; Ott, Alexander, et al. 1994; Lai and Grebogi 1996b; Lai, Grebogi, et al. 1996). In other words, all points in a riddled basin have sections of another attractor's basin arbitrarily closely nearby (Ott, Alexander, et al. 1994) and there always is a positive probability that a small perturbation leads to the other basin. For practical purposes, such systems are effectively non-deterministic (Sommerer et al. 1993). Consequently, attractor definitions based on locally attracting open neighbourhoods are not applicable to invariant sets with riddled basins, but they are measure attractors and unstable in the sense of Lyapunov.

Similar to the Wada property for fractal basin boundaries, riddled basins can be *intermingled*, i.e. any open set intersecting one basin in a set of positive measure also intersects all other basins in a set of positive measure (Kan 1994; Lai and Grebogi 1995).

Riddled/intermingled basins are not a mere academic example but appear in a variety of applications. They have been observed numerically in coupled time-delayed systems (Jiang 2000; Ashwin et al. 2005; Chaudhuri et al. 2014), for a damped periodically-driven point particle moving in a two-dimensional potential (Sommerer et al. 1993) and can be induced by the addition of noise (Lai and Grebogi 1996a). Experimental observations further indicate a riddled phase space structure for laser-cooled ions in a Paul trap (Shen et al. 1996).

3. Complex Networks (of Networks)

Contents of this Chapter

3.1. In a Nutshell

The intricate structure of large-scale power grids can be represented using a complex network in a straight-forward way and I discuss a particular implementation in Chap. 4. Prior to that, I first introduce important concepts from network science in the following.

The foundation is given by the definition of a weighted network and its algebraic representation using an adjacency or Laplacian matrix. Here, I chose a mathematical formulation that is particularly suitable for the general power grid model in Sec. 4.4. In particular, I focus on weighted undirected connected networks to represent the underlying structure of power grids.

Networks are characterised by (statistical) observables from local to global scales, concerning the necessary amount of input. Although such characteristics can be defined for edges alike, I focus on node characteristics to compare them with network-local probabilistic stability measures in Chap. 6.

A recent generalisation of the network approach are so-called multilayer networks or networks of networks. The central idea is to partition a network into interacting sub-networks in a particular meaningful way, depending on the nature of an underlying complex system or associated research questions. I define "neonets" as a generalisation of multilayer networks in view of their application to power grids, which are hierarchically organised across several voltage layers (Sec. 4.3).

Furthermore, I present a novel growth model to create synthetic neonet topologies. It is suited to model a wide range of spatially-embedded infrastructure networks. Here, I use it to provide synthetic power grid ensembles for gaining insights on the interaction between structure and dynamics of power grids in Chap. 6.

3.2. Complex Networks

When Stanley Milgram sent out his letters to reach a set of target persons via randomly chosen contacts in 1967, it came to a surprise that people tend to be connected via four to six circles of acquaintances[1], giving experimental evidence of the so-called *small-world effect* (Milgram 1967; Travers et al. 1969). Milgram's experiment is a pioneering observation of a complex network and might be regarded as one of the founding elements of modern network science. Thirty years later, Watts et al. (1998) provided a mathematical model for small-world networks that is widely used and serves well to interpret Milgram's experimental results.

Complex networks are mathematically described as graphs, i.e. they are constituted by entities called *nodes* which are interconnected by relations called *edges*. They are neither regular nor purely random graphs but occupy a space inbetween, where the topology cannot be simply described by one or two numbers[2], i.e. they are heterogeneous. Complex networks are characterised in terms of distributions of node

[1] These famous *six degrees of separation* actually vary across experiments and highly depend on social structures.

[2] In random graph theory (Erdős et al. 1960) this would be the probability whether two nodes are connected or not, while regular graphs are solely determined by their connectivity (i.e. every node has the same number of neighbours).

and edge characteristics and a multitude of different statistical measures. Hence, they can indeed by regarded as *complex* in the sense of Kolmogorov (Kolmogorov 1998) (or other attempts to define complexity). Complex networks cannot be algorithmically determined in a "compressed" way by specifying only a few numbers, i.e. information about almost all nodes and edges is typically needed. In particular, complex networks are commonly structured on different scales, from very local via mesoscale to global structures, which I discuss in the following (Sec. 3.3).

Conceptually, there are at least two distinct types of complex networks, namely *structural* and *functional networks*. Structural networks model the actual connectivity of a system. Examples are, for instance, the connections of neurons in the brain, power grids, highway and other infrastructure networks, extended river basins or the physical layer of the internet. The networks considered in this thesis are all of this sort.

Functional networks, in contrast, represent (observed) interactions in functionality and can deviate strongly from structural interrelations (if present). Illuminating examples are the functional neural networks determined from EEG data, recurrence networks from time series of observations or the world wide web created by websites linking to each other. For more examples and detailed references, I refer the reader to the growing amount of articles on complex networks (Newman 2003; Barrat et al. 2004; Boccaletti, Latora, et al. 2006; Costa et al. 2007; Newman 2008; Barthélemy 2011; Strano, Zanin, et al. 2013) and applications, e.g. in climate (Tsonis et al. 2004; Donges, Petrova, et al. 2015; Molkenthin, Rehfeld, et al. 2015), world trade (Kaluza et al. 2010; Maluck et al. 2017) or neural networks (Bullmore et al. 2009).

In the following, complex networks and their mathematical representation are formally introduced.

Definition 6 (Network)**.** *Given a node set $\mathcal{V}$ and an edge set $\mathcal{E} \subset \mathcal{V}^2$, a* network *is defined as the pair $\mathcal{G} = (\mathcal{V}, \mathcal{E})$. It has $n = |\mathcal{V}|$ nodes and $m = |\mathcal{E}|$ edges.*

Here, all edges $e \in \mathcal{E}$ of $\mathcal{G}$ are binary relationships between two nodes, denoted by $e = ij$ where i and j are the head and tail nodes, respectively[3]. When both $ij \in \mathcal{E}$ and $ji \in \mathcal{E}$ for all edges connecting nodes i and j, the network is said to be *undirected* and the – formally different – pairs ij and ji are considered the same edge.

Definition 7 (Weighted network)**.** *Given a function $w : \mathcal{E} \to \mathbb{R}_+ \setminus \{0\}$ that assigns positive weights $w(U) = \sum_{e \in U} w(e)$ to each subset $U \subset \mathcal{E}$. Then, a* weighted network[4] *is defined as the triple $\mathcal{G} = (\mathcal{V}, \mathcal{E}, w)$.*

If w assigns unit weight to all edges, we retrieve an *unweighted network*. If not otherwise stated, the weight function is specified as $w^Y : ij \mapsto |Y_{ij}|$ for all $ij \in \mathcal{E}$, where $\mathbf{Y}$ is the admittance matrix of a power grid (cf. Sec. 4.2.1).

[3] Edges can also be relationships between elements of $P(\mathcal{V})$ with higher cardinality, leading to the concept of *hypernetworks* (Johnson 2016). Here, $P(\mathcal{V}) \supset \mathcal{V}^2$ denotes the power set of $\mathcal{V}$, i.e. the set of all subsets of $\mathcal{V}$.

[4] The case of complex-valued edge weights has been discussed in [F2].

Definition 8 (Path, Path length, Cycle). *A* path $\pi(j,k)$ *in a network* $\mathcal{G} = (\mathcal{V}, \mathcal{E}, w)$ *is defined as an alternating sequence of nodes and edges – starting at node* $j \in \mathcal{V}$ *and ending with a node* $k \in \mathcal{V}$ *– such that no node is traversed more than once and no edge appears more than once in the sequence*[5]*. The* path length ℓ_{jk} *is given by the number of contained edges. Generally, there is a set* $\Pi(j,k)$ *of multiple paths between any pair of nodes. Then, the* shortest-path length *is defined as*

$$\ell_{jk}^{s} = \min_{\pi(j,k)\in\Pi(j,k)} \ell_{jk} \, .$$

A path $\pi(j,j)$ *for which start and end node coincide is called a* cycle.

Hence, a network is said to be *connected* if there exists a path of finite length between any pair of nodes. Otherwise, $\mathcal{G}$ consists of at least two *connected components*.

Hereafter, I use weighted undirected connected networks to represent the underlying structure of power grids.

Networks are usually represented algebraically using the so-called adjacency matrix $\mathbf{A}$ which I define here as

$$A_{ij} = \begin{cases} w(ij) \text{ if } ij \in \mathcal{E} \\ 0 \text{ otherwise} \end{cases} \, . \tag{3.1}$$

For unweighted networks, $\mathbf{A}$ becomes a binary matrix. In the absence of directed links, $\mathbf{A}$ further is symmetric. Entries on the diagonal correspond to self-links, so-called *loops*, which are not considered here. Additionally, it is convenient to further define the *Laplacian matrix* $\mathbf{L}$ of $\mathcal{G}$ as

$$L_{ij} = \begin{cases} \sum\limits_{k\neq i, k=1}^{n} A_{ik} \text{ if } i = j \\ -A_{ij} \text{ otherwise} \end{cases} \, . \tag{3.2}$$

The Laplacian matrix encodes essential information to describe dynamical processes on networks, for instance particle diffusion or random walks (Kriener et al. 2012), and can be regarded as a discrete analogue to a Laplace operator. $\mathbf{L}$ has the following important properties:

- $\mathbf{L}$ is symmetric if $\mathcal{G}$ is undirected.
- $\mathbf{L}$ is a singular matrix, since each row sum $\sum\limits_{k=1}^{n} \mathbf{L}_{ik}$ vanishes.
- $\mathbf{L}$ is positive-semidefinite and the number of zero eigenvalues $\lambda_k = 0$ equals the number of connected components of $\mathcal{G}$.

Since $\mathbf{L}$ is singular, it cannot be inverted. Instead, one commonly uses a generalised or pseudoinverse $\mathbf{R} = \mathbf{L}^{+}$. A convenient definition (Klein and Randić 1993) is

$$\mathbf{R} = (\mathbf{L} + \mathbf{J})^{-1} - \frac{1}{n^2}\mathbf{J} \, , \tag{3.3}$$

[5] This is also called a *simple* or *cycle-free walk*.

where $\mathbf{J}$ is the unit matrix such that all $\mathbf{J}_{ij} \equiv 1$. As the row and column sum of $\mathbf{L}$ vanish, we have $\mathbf{LJ} = 0$ respectively $\mathbf{JL} = 0$ and the same holds for $\mathbf{R}$. Then, using $\mathbf{J}^2 = n\mathbf{J}$ and the fact that $\mathbf{LR} = \mathbb{1}_n - \frac{1}{n}\mathbf{J}$, one can check that $\mathbf{R}$ fulfils the pseudoinverse relations:

$$\mathbf{LRL} = \mathbf{L}, \quad \mathbf{RLR} = \mathbf{R}, \quad (\mathbf{RL})^\top = \mathbf{RL}, \quad (\mathbf{LR})^\top = \mathbf{LR}\,. \tag{3.4}$$

3.3. Node Characteristics by Scale

Abstract In the following, I discuss a selection of network characteristics ordered by their scale, i.e. whether they can be evaluated locally or rely on information about distant parts of the network. Usually, they exist in a weighted as well as unweighted flavour, depending on the choice of w.

Node distance As many network characteristics are based on distances, I briefly mention two relevant distance metrics. Above I introduced the path length ℓ_{ij} as the number of edges on a path between two nodes i and j. This is not unique as there are many choices for the path between a pair of nodes. Typically, the *shortest path length* ℓ^s_{ij} is taken, which is the minimum number of edges needed to traverse from i to j.

In networks where the flow/coupling/exchange of information is not related to shortest paths – especially in electrical networks – an alternative metric has been established. The *effective resistance* (Klein and Randić 1993; Gurvich 2010; Spielman et al. 2011) between two nodes i and j is

$$r_{ij} = (\chi_i - \chi_j)^\top \mathbf{R}\,(\chi_i - \chi_j) = R_{ii} + R_{jj} - R_{ij} - R_{ji}\,, \tag{3.5}$$

where $(\chi_i)_j = \delta_{ij}$. Here, $\mathbf{R}$ is the pseudo-inverse of the Laplacian matrix. Effective resistances are strictly positive for different nodes, finite for a connected network, symmetric and fulfil the triangle inequality, i.e. forming a metric (Gurvich 2010). They gain a physical meaning as the equivalent (total) resistance r_{ij} of a resistor network between nodes i and j when choosing the weight function to be w^Y as defined in Sec. 3.2. It is straightforward to then define new network characteristics by replacing shortest path lengths with the respective effective resistances.

Recent research also investigated node-weighted networks (Heitzig, Donges, et al. 2012; Wiedermann, Donges, Heitzig, et al. 2013), where a weight is assigned to nodes corresponding to their relevance to a specific research question. For instance, the surface area represented by a measurement station can be taken as a node weight when constructing functional networks of climate observations. Consequently, appropriate node-splitting invariant statistical measures can be defined to remove a potential bias from ignoring node weights.

3.3.1. Global Characteristics

Networks can be categorised in various ways depending on the research question and scientific community. A very basic distinction is that between *trees* and networks

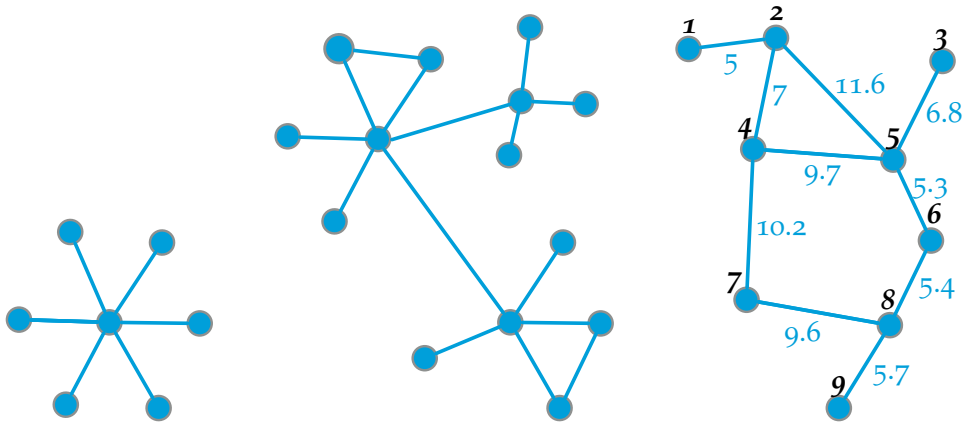

Figure 3.1. – **Global characterisation of network topologies**: A useful characterisation of spatially-embedded networks is that into centralised, decentralised and distributed topologies. Black number at nodes correspond to their index, blue numbers next to edges state their weights.

containing *cycles*. Trees are the most *sparse* connected networks as they contain the minimal number of edges $m = n - 1$ to be connected. Every tree but not every network with cycles is *planar* in the sense that they can be embedded in a two-dimensional plane without edge-crossings.

In the context of spatially-embedded networks, a global classification based on the spatial distribution of nodes adds intuitive insights on the overall organisation of complex systems. In Fig. 3.1 I depict three especially relevant cases. In a *centralised* network, a node typically serves as a central communicator hub of flows, i.e. almost all paths between the leaf nodes have to pass through the central node. A paradigmatic example here is the French TGV network (Perl et al. 2014). Somehow the opposite are *distributed* networks which are not trees but rather meshed and apparently show no spatial clustering of nodes. They apply to a situation where no group of nodes functions in a unique role but rather all nodes are equally important, e.g. in a power grid (Pagani et al. 2013). *Decentralised* networks occupy a space inbetween in the sense that there is no unique hub but there might still be local centres. Such a network might, for instance, represent commuting flows in a polycentric urban area with municipal hubs (De Montis et al. 2005; Roth et al. 2011).

Most of these distinctions can be captured in statistical characteristics which are commonly either of scalar nature or distributions. Examples of the first kind are the *graph density* $\rho = \frac{2m}{n(n-1)}$ related to the sparsity of networks, the *algebraic connectivity*

λ_2[6] which is proportional to the minimal cut-set of a network or the *transitivity*

$$T = \frac{\sum_{i,j,k\in\mathcal{V}} \Theta\left(A_{ij}\right)\Theta(A_{jk})\Theta\left(A_{ki}\right)}{\sum_{i,j,k\in\mathcal{V};j\neq k} \Theta\left(A_{ij}\right)\Theta\left(A_{ik}\right)} , \quad T \in [0;1] , \tag{3.6}$$

counting the global density of triangles in a network. $\Theta(\cdot)$ is the Heaviside step function[7].

Furthermore, distributions of local characteristics across nodes or edges and their moments are often used to characterise networks, especially the degree distribution (see below). Other examples are the *characteristic path length* $\langle \ell_{ij}^s \rangle_{i,j}$ or *average effective resistance* $\langle r_{ij} \rangle_{i,j}$, averaged over all pairs of nodes. They are global characteristics that give an intuition about the presence of long-range interconnections or short-cuts in complex networks.

3.3.2. Mesoscale Characteristics

Complex networks are characterised on the mesoscale by *communities* (Newman 2006; Fortunato 2010; MacMahon et al. 2015), i.e. groups of nodes with a high internal link density and only few connections to outside. Communities are immanent in various spatial scales, typically reflecting underlying organisational structures (Schaub, Delvenne, et al. 2012; Schaub, Lambiotte, et al. 2012). Even smaller building blocks are so-called *motifs*, induced subgraphs of only a few nodes (Milo et al. 2002; Shen-Orr et al. 2002; Wegner 2014). These can be triangles, 4-cycles or small tree-shaped appendices (cf. Sec. 6). Transitivity, as defined above, is the frequency of the triangle motif in a network.

There are frequently used network characteristics for single nodes that depend on information about the whole network, hence I attribute them to the group of mesoscale characteristics. Two of them are *closeness centrality* and *betweenness*.

Betweenness An established importance measure is the so-called *shortest-path betweenness* b_i (Freeman 1977) defined as

$$b_i = \frac{2}{(n-1)(n-2)} \sum_{s\neq t,\, i\neq s,t} \frac{g^{st}(i)}{g^{st}} , \quad b_i \in [0;1] , \tag{3.7}$$

where g^{st} is the number of shortest paths from s to t and $g^{st}(i)$ the number of those containing node i. That is, the node's participation in the geodesic information flow on a network is averaged over all pairs of source s and target nodes t. See e.g. Brandes (2001) for an efficient betweenness algorithm.

While b_i appeared to be a meaningful network characteristic in many applications, its essential limitation lies in the fact that it only considers the flow along shortest paths. Consider, for instance, the case illustrated in Fig. 3.2, where a small group of nodes joins two densely connected communities of a network. Opposed to nodes A

[6] λ_2 is the smallest nonzero eigenvalue of the graph Laplacian.

[7] It is possible to extend the concept of transitivity to the number of arbitrary k-clique motifs, i.e. fully-connected subgraphs of k nodes (Donges 2012).

and B, node C has a very low shortest-path betweenness as it does not lie on any shortest-path between the two groups. Still, node C can play an important role for a flow on that network, especially when the capacity of edge AB is small compared to AC and CB. Motivated by resistor networks, Newman (2005) introduced an alternative betweenness measure, taking care of this effect. In the following I generalise Newman's derivation to include edge weights.

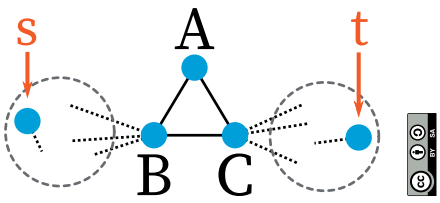

Figure 3.2. – **Current-flow betweenness**: Schematic illustration of the concept.

To start with, consider again a network with the physical weight function w^Y, i.e. using admittance-weighted edges. Given a current $\hat{I}$ injected at node s and extracted at node t as in Fig. 3.2, Kirchhoff's current law can be formulated as

$$\mathbf{L}v = \hat{I}\left(\chi_s - \chi_t\right) , \tag{3.8}$$

where $(\chi_i)_j = \delta_{ij}$, i.e. the in- and out-going currents at all nodes $i \neq s,t$ cancel out. The solutions to this linear equation are given up to a constant vector c by

$$v = \hat{I}\mathbf{R}(\chi_s - \chi_t) + c . \tag{3.9}$$

We can use this result to determine the current between adjacent nodes i and j and the through-current at node i to be

$$c^{st}_{i\to j} = A_{ij}\left(v_i - v_j\right) = A_{ij}\left(\chi_i - \chi_j\right)^\top v = \hat{I}A_{ij}\left(\chi_i - \chi_j\right)^\top \mathbf{R}(\chi_s - \chi_t) . \tag{3.10}$$

The share of the current between s and t that goes via node $i \neq s,t$, i.e. the through-current c^{st}_i, is

$$c^{st}_i = \frac{1}{2}\sum_{j=1}^{n}|c^{st}_{i\to j}| = \frac{\hat{I}}{2}\sum_{j=1}^{n}|A_{ij}\left(R_{is} + R_{jt} - R_{it} - R_{js}\right)| , \tag{3.11}$$

with $c^{st}_s = \hat{I}$ and $c^{st}_t = -\hat{I}$. Then, the *current-flow betweenness* (ibid.) b^w_i associated to a node i is defined as c^{st}_i averaged over all pairs s/t of source/target nodes:

$$b^w_i = \frac{2}{(n-1)(n-2)}\sum_{s<t}c^{st}_i = \frac{\hat{I}}{(n-1)(n-2)}\sum_{s<t}\sum_{j=1}^{n}|A_{ij}\left(R_{is} + R_{jt} - R_{it} - R_{js}\right)| ,$$
$$b^w_i \in [0;\hat{I}] . \tag{3.12}$$

Choosing $\hat{I} = 1$ yields a measure normalised to the unit interval. Likewise, $c^{st}_{i\to j}$ can be used to define an *edge current-flow betweenness* as

$$b^w_{ij} = \frac{2}{(n-1)(n-2)}\sum_{s<t}|c^{st}_{i\to j}| . \tag{3.13}$$

Alternatively to a derivation using Kirchhoff's rule for a resistor network, one can define an absorbing random walk on the network starting at s and stopping at t. Then, it can be shown that the current-flow betweenness equals the expected net number[8] of times such random walk passes through a node averaged over all sources and targets (Newman 2005). Hence, this centrality measure is also known as *random-walk betweenness*[9].

Closeness centrality An important category of network measures is formed by characteristics based on the concept of *node centrality*. It is related to the dominance of single nodes in a way that "a network is central to the degree that a single point can control its communication" (Freeman 1977), where the term communication, in a broader sense, can refer to the flow of some quantity on a network.

To which extent a node is close to all other nodes, i.e. in a sense the compactness of a network (Freeman 1978), is measured by *closeness centrality*. It is defined as the inverse sum of shortest path lengths from a node i to the rest as

$$c_i = \frac{n-1}{\sum\limits_{j\neq i, j=1}^{n} \ell_{ij}^{s}} \,. \tag{3.14}$$

Using effective resistance distances instead, a weighted closeness centrality (Stephenson et al. 1989) – also referred to as *current-flow closeness* – can be analogously defined as

$$\begin{aligned} c_i^w = \frac{n}{\sum\limits_{j=1}^{n} r_{ij}} &= \left(R_{ii} + \frac{1}{n} \left(\operatorname{tr} R - \sum_{j=1}^{n} \left(R_{ij} + R_{ji} \right) \right) \right)^{-1} \\ &= \left(R_{ii} + \frac{\operatorname{tr} R}{n} \right)^{-1} \,. \end{aligned} \tag{3.15}$$

As in the case of current-flow betweenness, all possible paths between two nodes are accounted for[10].

Alternatively, random walk processes can be used to define closeness, for instance the random-walk centrality (Noh et al. 2004) which has a close relation to the mean first passage time.

Example network As an illustration of the betweenness and closeness characteristics, Tab. 3.1 summarises their nodal distribution for the small example network in Fig. 3.1 presented earlier in this section. Notably, both b_i and b_i^w strongly separate the leaf nodes 1, 3 and 9, i.e. as terminal nodes they have vanishing betweenness centrality. Another interesting point is node 6 which interchanges its rank with 7

[8] Backward passages are counted negatively.

[9] An alternative definition of random-walk betweenness counts each individual visit at a node equally instead of considering the net flow (Arenas, Cabrales, et al. 2003).

[10] Note that both definitions are just the harmonic mean of the inverse distances.

when comparing $b_{6/7}$ and $b^w_{6/7}$, as the links adjacent to 7 have a rather high weight. A similar observation holds for the closeness $c_{6/7}$ and $c^w_{6/7}$ of the two nodes. All mesoscale characteristics identify node 5 to be the most central, all other nodes can be reached within at most 3 steps.

node	b_i	b^w_i	c_i	c^w_i
1	0	0	0.35	0.35^-
2	0.25	0.35	0.5	0.7
3	0	0	0.4	0.43
4	0.21	0.41	0.57	0.76
5	0.43^+	0.54^+	0.62^+	0.78^+
6	0.21	0.21	0.53	0.58
7	0.14	0.32	0.5	0.67
8	0.29	0.39	0.47	0.63
9	0	0	0.33^-	0.36
∅	0.17	0.25	0.47	0.58

Table 3.1. – **Mesoscale characteristics of an example network**: A collection of and mesoscale characteristics evaluated for the distributed network topology in Fig. 3.1. The superscripts $^+$ and $^-$ denote a unique maximum respectively minimum.

In summary, opposed to betweenness characteristics, closeness is able to also distinguish the leaf nodes in their properties. The current-flow closeness c^w_i discriminates the nodes in two significantly different groups of leaf and non-leaf nodes even more. b_i and b^w_i, however, put a stronger emphasis on distinguishing the most central node with a score about twice as large as the mean of the distribution.

3.3.3. Local Characteristics

THE SMALLEST SCALE is given by a single node and its direct neighbourhood, local network characteristics can be evaluated without information on the remaining network.

Degree The probably most intuitive network characteristic is given by the *degree* of a node. It simply counts the number of neighbours. It can be systematically calculated by summing up the non-zero entries in the respective row of the adjacency matrix[11]:

$$d_i = \sum_{j=1}^{n} \Theta\left(A_{ij}\right) \ , \quad d_i \in \mathbb{N} \ . \tag{3.16}$$

The degree of a node in a weighted network is referred to as its *strength* or *intensity* and evaluated analogously as[12]

$$s_i = \sum_{j=1}^{n} A_{ij} \ , \quad s_i \in \mathbb{R}_+ \ . \tag{3.17}$$

In some applications, the ratio s_i/d_i might be more revealing about underlying structural properties then the strength itself as it factors out the neighbourhood size.

[11] In directed networks, which are not symmetric, one rather defines the in- and out-degree as the row respectively column sum of adjacent nodes.
[12] Note that $d_i = s_i = 0$ only for disconnected nodes.

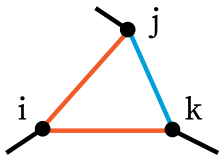

Figure 3.3. – **Clustering coefficient**: Neighbourhood connectivity of node i.

Clustering coefficient Besides the mere number of neighbours, the neighbourhood connectivity also holds important local information. The *clustering coefficient* (Watts et al. 1998) evaluates how many pairs of neighbouring nodes are themselves connected. Effectively, it counts the frequency of connected triangles (cf. Fig. 3.3) in the neighbourhood

$$C_i = \frac{\sum_{j,k,j\neq k} \Theta\left(A_{ij}\right) \Theta\left(A_{ik}\right) \Theta(A_{jk})}{d_i\left(d_i - 1\right)} \;, \quad C_i \in [0;1] \;. \tag{3.18}$$

For nodes i with $d_i = 1$, the clustering coefficient is set to $C_i = 0$, for unconnected nodes it is generally not defined. In case of weighted networks, it is possible to define a *weighted local clustering coefficient* [F2] as

$$C_i^w = \frac{\sum_{j,k,j\neq k} \min\left(A_{ij}, A_{jk}\right) \min\left(A_{ik}, A_{jk}\right)}{s_i^2 - \sum_k A_{ik}^2} \;, \quad C_i^w \in [0;1] \;. \tag{3.19}$$

node	d_i	s_i	s_i/d_i	C_i	C_i^w
1	1	5^-	5^-	0	0
2	3	23.6	7.87	0.33	0.39^+
3	1	6.8	6.8	0	0
4	3	26.9	8.97	0.33	0.29
5	4^+	33.4^+	8.35	0.17	0.12
6	2	10.7	5.35	0	0
7	2	19.8	9.9^+	0	0
8	3	20.7	6.9	0	0
9	1	5.7	5.7	0	0
∅	2.2	16.96	7.2	0.09	0.09

Table 3.2. – **Local characteristics of an example network**: A collection of local characteristics evaluated for the distributed network topology in Fig. 3.1. The superscripts $^+$ and $^-$ denote a unique maximum respectively minimum.

This definition ensures a normalisation to the unit interval, however, it also penalises large edge weights in the denominator. Hence, for some applications, different implementations of weighted clustering coefficients are more suitable. A common approach is to weigh each contribution with the arithmetic (Barrat et al. 2004) or other (Opsahl et al. 2009) means of the weights ij and ik (blue lines in Fig. 3.3). Note, however, that these definitions are insensitive to changes in the weight of the edge jk.

It is important to note that the average local clustering coefficient $\langle C_i \rangle_i$ is typically strongly correlated but not identical with the transitivity T (cf. Eqn. 3.6), it rather puts more weight on the contributions from low degree nodes.

Example network Consider again our example network Fig. 3.1. In Tab. 3.2, the distributions of degree, strength and the clustering coefficients are summarised. There are only three nodes with a positive clustering coefficient, namely the nodes 2, 4 and 5 on the edges of the triangle. Node 5 has a lower value of C_i due to its larger degree ($d_5 = 4$ instead of $d_{2,4} = 3$), i.e. only one out of $4 \cdot 3/2 = 6$ edges is present in the neighbourhood. The weighted version

C_i^w further distinguishes the seemingly similar nodes 2 and 4 such that $C_2^w > C_4^w$. This is because the edges adjacent to node 4 tend to have a higher weight (hence $s_4 > s_2$) going into the denominator of Eqn. 3.19.

While degree and strength are highly correlated, the normalised strength s_i/d_i reveals a different kind of information. Both degree and the mesoscale characteristics select node 5 as the most important in the network. The degree-normalised strength, however, ranks node 7 the highest, i.e. after factoring out the degree, node 7 is connected to the remaining network with the highest weight on average.

3.4. Networks of Networks

Abstract In this section I introduce the concept of a networks of networks – or neonet in short – and contribute a novel neonet growth model.

3.4.1. The Neonet Framework

Interconnected networks are a research direction attracting an increasing attention in recent times. It has been realised that an underlying monolithic network in many complex systems possesses an additional structure, i.e. a certain interaction structure or hierarchy of subnetworks (Gale et al. 2014; Kenett et al. 2015; De Domenico, Granell, et al. 2016; Garas 2016). This can be networks of qualitatively different complex systems which are interacting or interdependent, for instance there exists a complex coupling structure between a power grid and communication networks. Communication networks rely on stable power supply and are in turn used to perform control tasks (U.S.-Canada Power System Outage Task Force 2004; Rosato et al. 2008; Buldyrev et al. 2010; Brummitt et al. 2012). Other examples are the modular organisation of corticocortical networks in the brain (Zhou, Motter, et al. 2006; Zhou, Zemanová, et al. 2007; Zamora-López et al. 2010), infrastructure networks (Dueñas-Osorio et al. 2004; Vespignani 2010), coupled climate networks (Donges, Schultz, et al. 2011) or synchronisation of coupled oscillators (Gambuzza et al. 2015; Sonnenschein et al. 2015). All these are examples for so-called *networks of networks*, or *neonet* in short.

Typically there is a naturally appearing *partition* $\mathcal{P}$ of a network, subdividing the node set. Such a partition is guided by a specific research interest and overlays a network with an additional structure. A more objective method is to derive a partition from the output of community detection algorithms (Fortunato 2010; Mucha et al. 2010; MacMahon et al. 2015) that yield partitions already contained within the edge structure. These algorithms optimise various metrics like the popular *modularity* measure (Newman 2006) to identify communities. The notion of a community is, however, not clearly defined. Often, communities are regarded as subnetworks with their internal edge density being high compared to the density of edges to other communities (Fortunato 2010). Communities might in general overlap (fuzzy partition), however, in the following only crisp partitions $\mathcal{P}$ that yield disjoint communities are considered[13].

[13] Note also that a partition will not be required to be "optimal" in some sense.

A plethora of concepts related to neonets emerged during the last decade[14]. An early idea is that of *layered* (Kurant et al. 2006) or *multiplex networks* (Carroll 2006; Mucha et al. 2010; Nicosia et al. 2013). These are not constituted by an interaction structure of different subnetworks, but rather there is a fixed set of nodes with multiple types of edges attributed to different layers. For instance, the nodes of a multiplex network might correspond to locations and different modes of transportation (layers) or they might correspond to persons interacting in different social networks. Here, interlayer connections exist only between nodes and their counterparts in another layer. An example of a multiplex network with three layers is given in the left panel of Fig. 3.4.

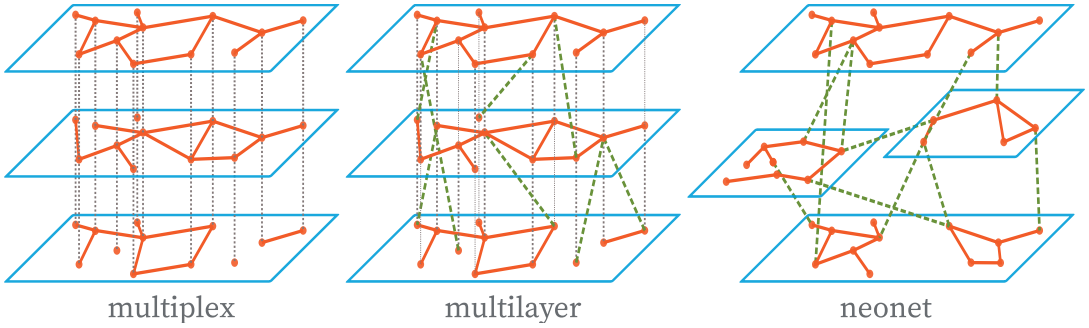

Figure 3.4. – **Networks of networks**: Schematic comparison of multiplex/multilayer networks and the neonet concept used in this thesis.

Multiplex networks are generalised in the approach of *multilayer networks* (Criado et al. 2012; De Domenico, Solé-Ribalta, et al. 2013; Boccaletti, Bianconi, et al. 2014; Kivelä et al. 2014) in two ways: (i) it includes interlayer connections between nodes which are not identified with each other and (ii) a node does not necessarily have connections to all its counterparts in other layers. There might also be different sets of layers, so-called *aspects*, i.e. modelling interactions on the one hand and a time evolution on the other. Although multilayer networks are a less restrictive concept, a layered structure is still assumed, especially that an entity is present as a node in (almost) all layers. While it is principally possible to frame a every neonet as a multilayer network, this approach is rather artificial and provides no further insight for a neonet that is not equipped with a layered structure but rather consists of arbitrary, loosely connected networks. Compare also the central and right panel of Fig. 3.4. In the next section I give a mathematical definition of neonets, closer to the definition of interacting networks in Donges, Schultz, et al. (2011) and suited to the use case of power grids.

Note that network characteristics can be extended to neonets, where they reveal interesting structural information (Donges, Schultz, et al. 2011; De Domenico, Solé-Ribalta, et al. 2013; Wiedermann, Donges, Heitzig, et al. 2013; Cozzo et al. 2015). A simple example is to separate the degree of a node into its *intralayer* and *interlayer degree*. However, it is not a priori clear how to include the layer information and there are typically different possibilities. A precise definition should always be

[14] See Kivelä et al. (2014) for an extensive overview.

chosen in a way to assist the respective research question.

3.4.2. Neonet Definition

The structure of a network of networks is determined by a partition.

Definition 9 (Partition)**.** *A* partition $\mathcal{P}$ *of the node set* $\mathcal{V}$ *of a network* $\mathcal{G}$ *is a subset of the power set of* $\mathcal{V}$ *whose elements* $\mathcal{V}^\ell$ *are nonempty, pairwise disjoint subsets of* $\mathcal{V}$ *covering the whole node set*[15]*.* $|\mathcal{P}|$ *denotes the number of elements in* $\mathcal{P}$ *which are commonly called* blocks*.*

Typically, $1 < |\mathcal{P}| \ll |\mathcal{V}|$, i.e. the node set is partitioned into a small number of subsets but the partition is not trivial. There are two things to note here. Firstly, a partition is a special form of a graph labelling where each node is labelled by the name of the block it is a member of. Secondly, a partition determines induced subnetworks $\mathcal{G}^\ell\left[\mathcal{V}^\ell\right] = \mathcal{G}^\ell = \left(\mathcal{V}^\ell, \mathcal{E}^\ell, w\right)$ where the edge sets are defined as

$$\mathcal{E}^\ell := \{uv \in \mathcal{E} \,:\, u \in \mathcal{V}^\ell \wedge v \in \mathcal{V}^\ell\}\,. \tag{3.20}$$

Definition 10 (Neonet, patch)**.** *A* network of networks *– or* neonet *in short – is the tuple* $\mathcal{G}|_\mathcal{P} := (\mathcal{G}, \mathcal{P})$ *of a graph* $\mathcal{G} = (\mathcal{V}, \mathcal{E}, w)$ *and a partition* $\mathcal{P}$ *of the node set, such that* $\mathcal{G}$ *is the supergraph of a family* $\{\mathcal{G}^\ell\}_{\ell=1}^{|\mathcal{P}|}$ *of disjoint induced subgraphs which are called* patches[16]*.*

The elements of the edge sets $\mathcal{E}^\ell$ of $\mathcal{G}^\ell$ are termed *intra-patch edges*. The set $\mathcal{E}_{seam}$ is called the *seam* of a neonet and defined as the union of all edge sets

$$\mathcal{E}_{seam} := \bigcup_{k\neq\ell} \mathcal{E}^{k\ell}\,, \quad \mathcal{E}^{k\ell} := \{uv \in \mathcal{E} \,:\, u \in \mathcal{V}^k \wedge v \in \mathcal{V}^\ell\}\,, \tag{3.21}$$

that contain the *inter-patch edges* between the patches labelled k and ℓ.

This naming convention is chosen on the one hand to stress that no layered structure is assumed, but on the other hand to clearly distinguish the neonet definition here from the frameworks of multilayer or multiplex networks.

In Sec. 4.3.3, the important special case of a spatially-embedded neonet appears, where the seam only contains edges that connect nodes at identical positions. In this case, it is useful to define the following projected neonet.

Definition 11 (Spatial projection network)**.** *A* spatial projection network $\tilde{\mathcal{G}}|_\mathcal{P}$ *of a neonet* $\mathcal{G}|_\mathcal{P}$ *is defined as the neonet resulting from a consecutive contraction of all edges in* $\mathcal{E}_{seam}$ *and the identification of the corresponding head and tail nodes at the same spatial position.*

Fig. 4.5 in Sec. 4.3.3 illustrates an example of a spatial projection network.

---

[15] $\mathcal{V}$ is the disjoint union of the elements in $\mathcal{P}$, i.e. $\mathcal{V} = \bigsqcup_{\ell=1}^{|\mathcal{P}|} \mathcal{V}^\ell$

[16] Note that, depending on the choice of partition, the patches $\mathcal{G}^\ell$ do not need to be connected. In Sec. 4.3 this appears in the case of power grids.

3.4.3. Concurrent Growth Model for Spatial Neonets

This section is related to research originally published in [P3].

While the modelling of power grids as neonets will be discussed further in Sec. 4.3, the aim of this section is to establish synthetic neonets $\mathcal{G}|_{\mathcal{P}}$ for modelling spatially-embedded infrastructure networks in general (including power grids, of course).

The algorithmic implementation is located in Appendix A.1.

There have been diverse attempts to model spatially-embedded infrastructure networks (Barthélemy 2011), for instance communication networks (Dorogovtsev et al. 2001), urban road systems (Rosvall et al. 2005), railway networks (Sen et al. 2003) or power grids (Zhifang Wang et al. 2010; Halappanavar et al. 2015; Soltan et al. 2016)[F2; F3]. Especially power grids can be seen as neonets (cf. Sec. 3.4.1) with an additional hierarchical organisation such that different patches serve different purposes, i.e. distribution grids are meant to distribute electricity locally while transmission grids balance production and consumption over long distances.

Alternatively, data sets of actual power grids might be used for research. There are various networks available, e.g. the SciGRID database (Medjroubi et al. 2017) for power grids. Often, however, network ensembles are needed to test statistical hypothesis. Hence, a method to create synthetic topologies is needed. Approaches to create randomised *surrogate networks* from real-world data sets (Wiedermann, Donges, Kurths, et al. 2016) can be useful as well, but in contrast to constructive models they do not reveal the underlying mechanisms shaping a network.

Here, the approach is *not* to specify network characteristics extracted from data *a priori* (e.g. a degree distribution) but rather to define simple heuristic rules for the placement of nodes and addition of lines.

Given that it is commonly a problem to estimate whether the degree distribution follows a power law or is otherwise heavy-tailed from a sample of only a few hundred of nodes (Clauset et al. 2009; Stumpf et al. 2012), it is a strength of the proposed model that the degree distribution does not need to be specified, in contrast to e.g. a configuration model (Boccaletti, Latora, et al. 2006).

Intuitively, there are at least two different possibilities to create a neonet topology. On the one hand, a neonet could be statically constructed, i.e. by combining isolated subnetworks in a bottom-up or top-down approach [P3]. This can be the preferred choice if existing subnetworks are to be included. In some scenarios it might be interesting to combine existing transmission systems with randomly chosen distribution networks (e.g. created using the approach described in [F3]). On the other hand, neonets could result from a *concurrent growth process*, where the several subnetworks develop at the same time.

The neonet model is going to be a concurrent-growth network generation algorithm that is rather conceptual but still flexible enough to generate synthetic infrastructure networks in which nodes and edges may reside on any number of subnetworks. The algorithm forms an undirected neonet $\mathcal{G}|_{\mathcal{P}}$ along with node locations. Edge weights are not specified and need to be added separately.

Nodes are added during the growth process and connected according to a pref-

erential attachment rule (Barabási 1999). Hence, the random process splits into two central questions: *What is the probability to place a node at a certain position?* and *What is the probability for a new edge to be created?*

Both ingredients, placing nodes in a growth process and the preferential attachment mechanism are detailed below. Notably, these ingredients already seem to be sufficient to cause the emergence of scale-invariant degree distributions (ibid.), indicating a hierarchical organisation of the network. It will be the approach of the presented model to embed this idea into the neonet framework.

Existing growth models for neonets consider preferential attachment as well (Criado et al. 2012; Nicosia et al. 2013; Wang et al. 2013; Momeni et al. 2015), however they are only considering multiplex networks (cf. Sec. 3.4.1). These are no suitable models for hierarchical infrastructures as they only consider an identical set of nodes in each layer and one-to-one connections between them. Another approach takes supply and demand ratings of nodes into account as well as their distance, to define linkage probabilities in a multilayer network (Dueñas-Osorio et al. 2004).

The model presented here results in a neonet consisting of a certain number $L = |\mathcal{P}|$ of patches, assuming that they can be ordered from 'high' to 'low', 'top' to 'bottom', 'first' to 'last' or similar. This determines the order in which patches appear over time in the growth model and is not meant to impose a layered structure. The partition $\mathcal{P}$ is not specified beyond the desired number of elements, but rather will be a result of the algorithm. The central assumption is that above structure grows in sequential *phases* ϕ. Starting from the 'lowest', patches appear one after the other in consecutive phases. Hence, the total number of phases is given by L.

This procedure is inspired by the historical development of infrastructure networks. Road networks, for instance, typically start from isolated networks of local streets that are later connected with national roads and in an even later phase overlayed with highways. Still, all patches continue to develop simultaneously. Very similar arguments hold also for power grids. The advantage is that the construction of each patch is independent of the 'lower' levels. This can be particularly useful when L is varied. In this case, the topology of the 'highest' patch stays fairly similar, no matter how many 'lower' patches are considered.

Each phase is divided into two steps, following a heuristic similar to the growth of isolated networks [F3]. In the *initialisation step*, an initial number of nodes $n_0^\ell \geq 1$ is added to $\mathcal{G}^\ell$ and connected using a minimum spanning tree that minimises the overall edge length. Furthermore, a small number of[17]

$$m^\ell = \lfloor n_0^\ell (1 - s^\ell)(p^\ell + q^\ell) \rfloor \,, \tag{3.22}$$

additional edges uv are added to $\mathcal{E}^\ell$ that maximise a *trade-off function* $f^\ell(u, v)$.

In the second part of the phase ϕ, the so-called *growth step*, a given number of nodes n_ϕ^ℓ is consecutively added to the neonet $\mathcal{G}|_\mathcal{P}$. This is done using an attachment rule which can be adjusted by three patch-specific parameters p^ℓ, q^ℓ and s^ℓ.

With a probability s^ℓ, an edge $uv \in \mathcal{E}^\ell$ is randomly selected and split in two by

[17] For small values of n_0^ℓ, m^ℓ can be larger than the maximal number of possible edges and we set $m^\ell = \left(n_0^\ell - 1\right)\left(n_0^\ell/2 - 1\right)$.

addition of a new node v'. The edge uv is removed from $\mathcal{E}^\ell$ and two edges uv' and $v'v$ are added.

Otherwise, the new node v' is randomly placed and connected to the closest other node in the same patch $\mathcal{G}^\ell$. Then, an expected number of $0 < p^\ell, q^\ell < 1$ additional edges are added that maximise f^ℓ. Opposed to the original model for isolated networks [F3], the actual number of edges is drawn from geometric distributions with means p^ℓ and q^ℓ. Note, that this slight variation allows for more than one edge to be occasionally added with a low probability. Also, added edges are allowed to connect nodes from different patches.

Now, before the trade-off function $f^\ell(u, v)$ is introduced, the following is defined for convenience.

Definition 12 (Cumulative subgraph). *$\mathcal{G}_c^\ell = (\mathcal{V}_c^\ell, \mathcal{E}_c^\ell, w)$ is defined as the* cumulative subgraph, *i.e. $\mathcal{V}_c^\ell = \bigcup_{k\geq\ell} \mathcal{V}^k$ and $\mathcal{E}_c^\ell = \bigcup_{k\geq\ell} \mathcal{E}^k$. We denote by $d_{G_c^\ell}(v, v')$ the minimum weighted length of of any path from v to v' in $\mathcal{G}_c^\ell$. The length of an edge uu' is given by the Euclidean distance $d_2(u, u')$ between the coordinates of the nodes u and u'.*

Definition 13 (Node density). *The* node density *of a node $v \in \mathcal{V}^\ell$ is defined by*

$$d(v) = \sum_{v' \in \mathcal{V}_c^\ell \setminus \{v\}} d_2(v, v')^{-2} , \tag{3.23}$$

where $d_2(v, v')$ is the Euclidean distance between the coordinates of the nodes v and v'. It measures the spatial clustering of nodes in the cumulative subgraph.

With these definitions, the trade-off function can be formulated as follows.

Definition 14 (Trade-off function). *For each patch $\mathcal{G}^\ell$, define a heuristic* trade-off function

$$f^\ell(v, v') = \frac{\left(d_{G_c^\ell}(v, v') + d_2(v, v')\right)^{r^\ell} d(v')^{u^\ell}}{d_2(v, v')} \tag{3.24}$$

where $r^\ell, u^\ell \geq 0$ are given parameters.

While the cost of a new edge vv' between two nodes at positions $x(v)$ and $x(v')$ is assumed to be determined by its length $d_2(v, v')$, there are two types of heuristic benefits whose importance is controlled by the parameters r^ℓ and u^ℓ. Firstly, a benefit might arise when a new edge creates a redundant cycle valued by its length $d_{G_c^\ell}(v, v') + d_2(v, v')$. Secondly, connecting to a densely populated area with a high node density $d(v')$ improves the access to the remaining network. Both benefits are combined in $f^\ell(v, v')$ into a Cobb-Douglas type utility assessment computed per unit cost (Cobb et al. 1928). Considering the node density at this point is inspired by a similar use of an average nearest-neighbour distance in the preferential attachment rule of a power grid model (Soltan et al. 2016). It indicates that nodes are rather placed in areas with a high node density, typically related to population density (Gastner et al. 2006).

The placement of a new node v is determined by the following placement procedure. Assume the neonet is embedded in a space R, i.e. use the square $R = [-1, 1]^2$.

Firstly, a position y is drawn uniformly at random from R. Secondly, a node v' is picked uniformly at random from the cumulative subgraph $V_c^\ell \setminus \{v\}$. Then, the position $x(v)$ of the new node is determined as

$$\begin{aligned} x(v) &= \alpha^\ell y + (1-\alpha^\ell) x(v') \quad \text{with probability } \gamma^\ell \,, \\ x(v) &= \beta^\ell y + (1-\beta^\ell) x(v') \quad \text{with probability } 1-\gamma^\ell \,, \end{aligned} \tag{3.25}$$

where the parameters $\alpha^\ell, \beta^\ell, \gamma^\ell \in [0,1]$ determine the amount of spatial clustering of nodes. Choosing $\alpha^\ell = 1$ and $\gamma^\ell = 1$ corresponds to positioning nodes uniformly at random in R. The parameter γ^ℓ can serve as a random switch between two modes of placement, i.e. clustered and uniform positions. At this point, much more complex rules can be chosen, possibly incorporating location data or the spatial boundaries of regions.

In summary, to perform the algorithm, the following parameters need to be specified:

- $L \geq 1$: Number of patches.
- $n_0^\ell = \mathcal{V}^\ell \geq 1$: Number of initial nodes of level ℓ at its introduction.
- $n_\phi^\ell \geq 0$: Number of additional nodes of level ℓ grown in phase $\phi \geq \ell$.
- $\alpha^\ell, \beta^\ell, \gamma^\ell$: Node location distribution parameters governing the amount of spatial clustering. Alternative choices, e.g. uniform distributions, are possible as well.
- p^ℓ: Expected number of redundant edges each new node gets immediately.
- q^ℓ: Expected number of additional redundant edges added to random nodes at each growth step.
- $r^\ell, u^\ell \geq 0$: Importance of redundant edge benefits.
- s^ℓ: Probability of edge splittings.

Although the model aims at producing neonet topologies, the isolated network model [F3] can easily be recovered by setting $L = 1$, yielding a single phase ϕ that consists of a single initialisation as well as growth part. Then, the set of parameters only consists of n_0, n_ϕ, s, p, q, r, u and the node placement rule. Considering the node density in the trade-off function is a novel feature of the present model but also an interesting extension to the case of isolated networks. To recover the growth model for single networks [F3], however, $u = 0$ can be fixed.

4. A Power Grid Model

Contents of this Chapter

4.1. In a Nutshell

In this chapter, I develop the components of a model that is suitable to study essential aspects of phase synchronisation in power grids, in particular the stability of synchronisation (Chap. 5) and its relation to the network topology (Chap. 6).

A dynamical model necessarily consists of two building blocks, the dynamic behaviour of single nodes[1] and the network topology through which they interact.

Firstly, I review established models for synchronous generators as well as inverter-connected power sources. While synchronous generators appear mainly in conventional power generation and provide inertia to the power system, renewable energy sources connect to the grid via programmable devices, converting their DC voltage to an AC signal. In connection with local storage, such inverters can be designed to provide so-called virtual inertia.

Under certain assumptions, the mathematical description of specific inverters and synchronous machines is equivalent to that of Kuramoto oscillators with inertia. Consequently, I choose this level of detail to model the short-term power grid dynamics conveniently in a straight-forward and consistent way. Discussing inert Kuramoto oscillators in general, I recapitulate basic properties of synchronous and limit cycle solutions.

Secondly, I develop a network model for the underlying structure that connects dynamical units in a power grid. Building upon empiric details of real-world power grid topologies, I discuss previous approaches to model them as complex networks and show how the neonet approach from Sec. 3.4.1 captures essential properties of hierarchically organised power grids.

The chapter is concluded by brief a summary of the dynamic and network model components in a joined consistent model, which I refer to as the SCONE (SeCond Order NEonet) model.

[1] The nodes of a network are often referred to as a *bus* in the context of power systems.

4.2. Node Dynamics

Abstract I present the dynamics of synchronous machines, show that inverters might be modelled similarly and discuss the overarching framework of Kuramoto oscillators with inertia.

Note that I restrict the scope of this thesis to nodes with constant power rating as an assumption to the dynamics on short time scales. This significantly reduces the model complexity and especially allows for applying the established framework of inert Kuramoto oscillators, as outlined below. In general, however, the load in power grids always fluctuates because the microscopic consumer behaviour is not deterministic. More importantly, wind and solar plants induce intermittent[2] power fluctuations (Anvari, Lohmann, et al. 2016; Anvari, Tabar, et al. 2016; Schmietendorf, Peinke, and Kamps 2016) due to the (different) turbulent character of wind and solar irradiance (Milan et al. 2013; Tabar et al. 2014). The stochastic infeed generates fat-tailed fluctuations, such that large fluctuations on short time scales are likely to occur. Apparent long-distance spatial correlations can further inhibit an often expected smoothing of the fluctuations (Nagata et al. 2017). It is an interesting direction for future research to extent the neonet model to stochastic processes.

Stochastic input has strong implications on power grid stability (Schmietendorf, Peinke, and Kamps 2016; Auer, Hellmann, et al. 2017; Schäfer, Matthiae, Zhang, et al. 2017), especially in terms of so-called power quality, i.e. exceedances of grid frequency and voltage safety ranges. Recent approaches apply a dynamic response theory to quantify a system's response to specific fluctuation spectra (Zhang et al. 2016; Schäfer, Matthiae, Zhang, et al. 2017). As a countermeasure, it has been suggested that transient uncoupling may suppress noise-induced desynchronisation (Schröder, Chakraborty, et al. 2016; Tandon et al. 2016).

4.2.1. Synchronous Machine

Synchronous machines (Anderson et al. 1979; Sauer et al. 1998; Machowski et al. 2011) consist of a moving rotor and it's surrounding, the stator (see Fig. 4.1). A field excitation coil supplied with a DC voltage E^f (reference voltage at which a generator is operated) is mounted on the rotor, creating an electro-magnetic field aligned with the rotor axis. This field induces an AC voltage in the three phase reference points a, b and c on the stator whose frequency is determined by the angular speed of the rotor. Hence the name "synchronous machine". This setup is symmetric between the use as a generator, where the rotor is driven by a (steam) turbine, and the use as a motor, where a voltage applied to the stator induces the rotor movement. The focus of this thesis are, however synchronous generators.

The generators are mutually coupled in an electrical network of n nodes. At a node k, where the turbine's mechanical energy is converted to electrical energy, holds a local power balance

[2] Intermittency here means that not only the fluctuations but also the increments, i.e. the differences between the time series at a fixed time lag, follow a fat-tailed distribution.

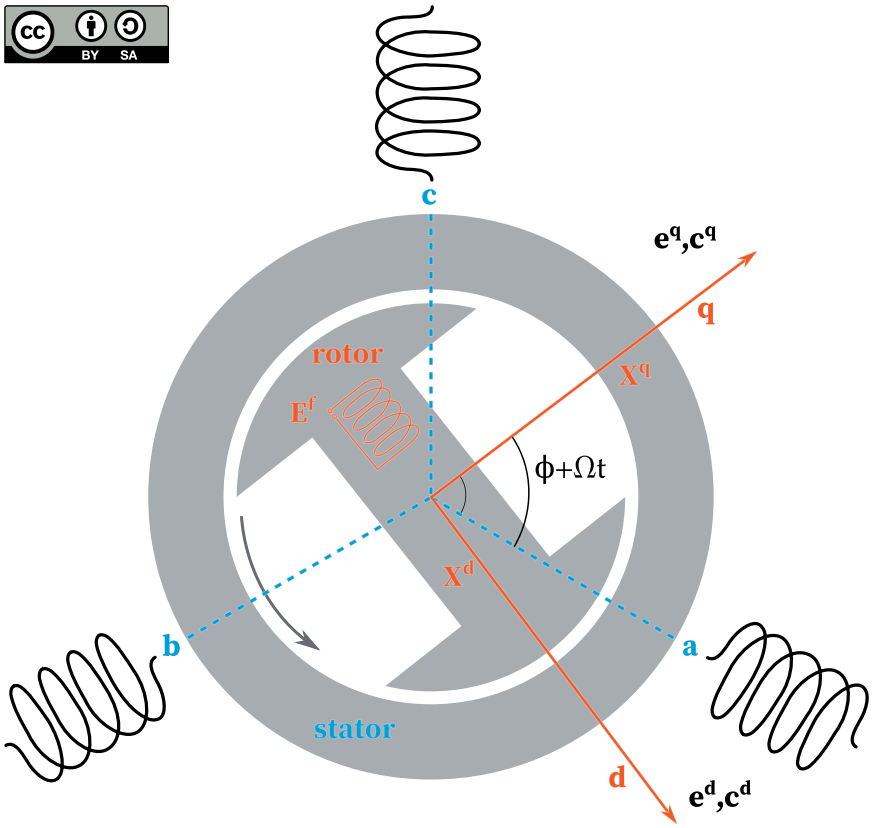

Figure 4.1. – **Sketch of a synchronous machine** The coordinate system co-rotates with the rotor at the rated frequency Ω (d,q), the rotor angle to the stator is then given by $\theta = \phi + \Omega t$. The stator has three axes (dashed; a,b,c), i.e. reference points for the voltage, one for each electrical phase. The static abc- and co-rotating dq-frame are related via the Park transformation (Anderson et al. 1979).

$$P_k^M - P_k^D - P_k^A = P_k^T \,. \tag{4.1}$$

The equation states the energy conservation at the synchronous machine. On the left hand side of the power balance, we have the mechanical input power P_k^M, damping contributions P_k^D from rotor damper windings and the power P_k^A in the rotation of the turbine. These equal the real power transmitted to or received from other nodes P_k^T. Synchronous generators are usually equipped with an additional so-called droop control. It is a governor adjusting P_k^M proportionally to an externally measured grid frequency and has the form of an additional damping term, hence I am going to omit it for brevity and assume that it is contained in P_k^D.

P_k^D and P_k^A are determined by the relations

$$\begin{aligned} P_k^D &= \kappa_k \dot{\theta_k}^2 \,, \\ P_k^A &= J_k \ddot{\theta}_k \dot{\theta}_k \,, \end{aligned} \tag{4.2}$$

where κ_k and J_k are damping and inertia constants and θ_k are the rotor angles of the turbine. Due to the symmetry of the problem, I concentrate on one of the three voltage phases that are measured at three points on the stator spaced 120° apart each (a,b,c in Fig. 4.1). The law of induction relates the frequency of the induced voltage to the generator's revolutions per time n by an integer multiple, i.e. the number of magnetic poles p, as $\dot{\theta}_k = (p/2)\, n$. Without loss of generation, I assume $p = 2$ poles in the following derivation. Furthermore

The inertia provided by synchronous machines is important for the stability of power grids. Essentially, J_k determines how much kinetic energy can be provided by the rotation in response to disturbances. A lack of inertia in RES-dominated power grids needs to be compensated for. A promising approach is to use inverters that are designed to mimic the effect of inertia. This is discussed further in the subsequent section.

It is convenient to describe the dynamics in a reference frame co-rotating with the steady-state frequency Ω, also known as the grid's rated frequency:

$$\phi_k := \theta_k - \Omega t \,, \quad \omega_k := \dot{\phi}_k = \dot{\theta}_k - \Omega \,, \quad \dot{\omega}_k = \ddot{\phi}_k = \ddot{\theta}_k \,. \tag{4.3}$$

In the approximation of small deviations from the rated frequency, i.e. $|\omega_k| \ll \Omega$, Eqn. 4.1 becomes

$$P_k^M - \kappa_k \Omega^2 - 2\kappa_k \Omega \omega_k - J_k \Omega \dot{\omega}_k = P_k^T \,. \tag{4.4}$$

The right hand side of this relation, the transmitted real power P_k^T, is essentially determined by the complex admittance matrix $\tilde{Y}_{jk}$ describing the electrical connectivity of a power grid. If the network contains passive nodes (i.e. constant impedance loads that are not synchronous machines), a Kron-reduction of $\tilde{Y}_{jk}$ has to be applied first (Nishikawa and Motter 2015). Using Kirchhoff's first law, it is convenient to define the total complex current at k as[3]

$$c_k = c_k^q + \imath c_k^d = \sum_{j \neq k, j=1}^{n} \tilde{Y}_{jk} \left(v_k - v_j \right) = \sum_{j=1}^{n} Y_{jk} v_j \,, \tag{4.5}$$

where the matrix $Y_{jk} = |Y_{jk}| \mathrm{e}^{\imath \left(\pi/2 - \alpha_{jk} \right)}$ is the so-called *nodal admittance matrix* with elements

$$Y_{jk} = \delta_{jk} \sum_{l \neq j} \tilde{Y}_{jl} - \tilde{Y}_{jk} \,. \tag{4.6}$$

Note that $\alpha_{jk} = \arctan\left(\mathfrak{Re} Y_{jk} / \mathfrak{Im} Y_{jk} \right)$ (sic!) is not the argument of Y_{jk} but its

[3] By convention, all time-dependent (AC) electrical quantities (i.e. c_k, v_k, e_k) are given in small letters while capital letters are reserved for static (DC) quantities or parameters.

difference to $\pi/2$. This definition is chosen solely for convenience in the following derivation. The parameter α_{jk} is referred to as the *phase lag*.

The voltages at the nodes are defined as (Sauer et al. 1998)[F4]

$$v_k = e_k \mathrm{e}^{\imath\phi_k} = \left(e_k^q + \imath e_k^d\right) \mathrm{e}^{\imath\phi_k} \,. \tag{4.7}$$

This relation in the co-rotating reference frame states that the stator voltage v_k as seen by the power grid is not directly linked but dynamically coupled to the rotor voltage e_k. This non-linearity in the system is due to the fact that a current induced in the stator by the rotating electro-magnetic field of the rotor, in turn induces a back-reaction of the rotor voltages e_k^q and e_k^d.

To obtain the power P_k^T transmitted between node k and all neighbours, note that in an AC circuit this is the real part of the apparent power[4] $S_k = v_k c_k^*$ and hence called the *active power transfer*.

$$\begin{aligned} v_k c_k^* &= \sum_{j=1}^{n} |Y_{jk}| \left(e_j^q e_k^q + e_j^d e_k^d + \imath \left(e_j^q e_k^d - e_j^d e_k^q\right)\right) \mathrm{e}^{\imath\left(\phi_k - \phi_j - \alpha_{jk}\right)} \\ P_k^T &= \mathfrak{Re}\left(v_k c_k^*\right) \end{aligned} \tag{4.8}$$

I omit the further derivation of the dynamics of e_k^q and e_k^d from higher-order processes for brevity and refer to the specialised literature (e.g. Sauer et al. 1998). Inserting Eqn. 4.8 into Eqn. 4.4 then yields the so-called *two-axis* (Anderson et al. 1979; Sauer et al. 1998; Machowski et al. 2011; Weckesser et al. 2013) or *fourth-order* [F4] *model*:

$$\begin{aligned} \dot{\phi}_k &= \omega_k \\ \tau_k^\omega \dot{\omega}_k &= -\omega_k + \gamma_k \left(P_k - \mathfrak{Re}\left(v_k c_k^*\right)\right) \\ \tau_k^d \dot{e_k^q} &= -e_k^q + X_k^d c_k^d + E_k^f \\ \tau_k^q \dot{e_k^d} &= -e_k^d + X_k^q c_k^q \,, \end{aligned} \tag{4.9}$$

with $\tau_k^\omega = J_k/(2\kappa_k)$, $P_k = P_k^M - \kappa_k \Omega^2$ and $\gamma_k = 1/(2\kappa_k \Omega)$. The new parameters[5] have the following physical interpretation: The time constants τ_k^d, τ_k^q parametrise the relaxation time of the voltage dynamics in the d- and q-axis, the transient rotor-reactance deviations from the steady state X_k^d, X_k^q parametrise the back-reaction of the currents in the stator on the rotor voltage and E_k^f is the voltage at the field excitation coils on the q-axis. Note that with the algebraic relation Eqn. 4.5, it is possible to eliminate the currents $c_k = c_k\left(e_1^q, ..., e_n^q, e_1^d, ..., e_n^d, \phi_1, ..., \phi_n\right)$:

[4] The imaginary part is referred to as *reactive power* and averages out over time.

[5] See also Fig. 4.1.

$$
\begin{aligned}
\dot{\phi}_k =& \omega_k \\
\tau_k^\omega \dot{\omega}_k =& -\omega_k + \gamma_k P_k \\
& - \gamma_k \sum_{j=1}^{n} |Y_{jk}| \left(e_j^q e_k^q + e_j^d e_k^d \right) \sin\left(\phi_k - \phi_j + \alpha_{jk}\right) \\
& + \gamma_k \sum_{j=1}^{n} |Y_{jk}| \left(e_j^q e_k^d - e_j^d e_k^q \right) \cos\left(\phi_k - \phi_j + \alpha_{jk}\right) \\
\tau_k^d \dot{e_k^q} =& -e_k^q + E_k^f \\
& - X_k^d \sum_{j=1}^{n} |Y_{jk}| \left(e_j^q \sin\left(\phi_j - \alpha_{jk}\right) + e_j^d \cos\left(\phi_j - \alpha_{jk}\right) \right) \\
\tau_k^q \dot{e_k^d} =& -e_k^d \\
& - X_k^q \sum_{j=1}^{n} |Y_{jk}| \left(e_j^d \sin\left(\phi_j - \alpha_{jk}\right) - e_j^q \cos\left(\phi_j - \alpha_{jk}\right) \right) .
\end{aligned}
\tag{4.10}
$$

The two-axis model is already subject to a number of simplifying assumptions, especially by neglecting the sub-transient reactance deviations in the rotor (Sauer et al. 1998; Machowski et al. 2011), that reduce the number of variables to four per node. We can perform a further separation of time scales as the voltage dynamics is typically slower then the phase dynamics, i.e. $\tau_k^q \gg \tau_k^\omega$ and $\tau_k^d \gg \tau_k^\omega$. This limit is provided by $X_k^{d/q}/\tau_k^{d/q} \to 0$ and setting $e_k^q = E_k^f$ and $e_k^d = 0$. It yields the so-called *classical model* (Anderson et al. 1979; Sauer et al. 1998; Machowski et al. 2011; Nishikawa and Motter 2015) also known as *second-order Kuramoto model* (Filatrella et al. 2008; Rodrigues et al. 2016) or *swing equation* (Aylett 1958):

$$
\begin{aligned}
\dot{\phi}_k &= \omega_k \\
\frac{\tau_k^\omega}{\gamma_k} \dot{\omega}_k &= P_k - \frac{1}{\gamma_k} \omega_k - \sum_{j=1}^{n} |Y_{jk}| E_j^f E_k^f \sin\left(\phi_k - \phi_j + \alpha_{jk}\right) .
\end{aligned}
\tag{4.11}
$$

In the swing equation, generators are represented as constant power, constant voltage sources, i.e. with constant voltage magnitude $e_k = E_k^f$. It models the transient of the grid frequency after a disturbance in the time period of the first swing – which is usually one second or less (Anderson et al. 1979) – and may not correctly reproduce the long-term asymptotic behaviour of a synchronous machine. For this, the two-axis model should be applied (Weckesser et al. 2013; Auer, Kleis, et al. 2016).

An alternative approximation is obtained be noticing, that typically τ_k^q is smaller than τ_k^d. Hence, the time scale of the d-axis dynamics separates and replacing $e_k^d = 0$ in Eqn. 4.9 yields the *third-order model* (Schmietendorf 2012; Schmietendorf, Peinke, Friedrich, et al. 2014)

$$\begin{aligned}\dot{\phi}_k =& \omega_k \\ \tau_k^\omega \dot{\omega}_k =& -\omega_k + \gamma_k P_k - \gamma_k \sum_{j=1}^{n} |Y_{jk}| e_j^q e_k^q \sin\left(\phi_k - \phi_j + \alpha_{jk}\right) \\ \tau_k^d \dot{e_k^q} =& -e_k^q + E_k^f - X_k^d \sum_{j=1}^{n} |Y_{jk}| e_j^q \sin\left(\phi_j - \alpha_{jk}\right) \ .\end{aligned} \tag{4.12}$$

In many cases, power transmission lines are assumed to be lossless and Ohmic resistances are disregarded. Then, the admittance matrix is approximately $Y_{jk} = G_{jk} + \imath B_{jk} \approx \imath B_{jk}$, i.e. $\alpha_{jk} = 0$, and the swing equation Eqn. 4.11 reduces to the *lossless swing equation*[6]:

$$\begin{aligned}\dot{\phi}_k &= \omega_k \\ \frac{\tau_k^\omega}{\gamma_k} \dot{\omega}_k &= P_k - \frac{1}{\gamma_k}\omega_k - \sum_{j=1}^{n} |Y_{jk}| E_j^f E_k^f \sin\left(\phi_k - \phi_j\right) \ .\end{aligned} \tag{4.13}$$

The overdamped limit $\tau_k^\omega \to 0$ finally yields the *Kuramoto model* Eqn. 2.4.

4.2.2. Grid-Forming Inverter

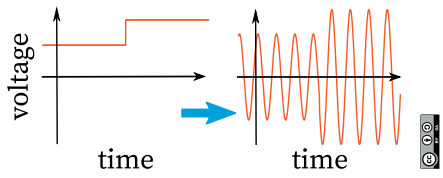

Figure 4.2. – **An inverter converts a DC voltage signal to AC.**

Renewable energy sources are commonly connected to the grid via inverters[7]. These devices transform the DC output of a renewable generation site to an AC voltage, as schematically pictured in Fig. 4.2.

Inverters do not have an inherent physical relation between active power generation and voltage phase/frequency as synchronous machines do. Contrarily, they are so-called power-electronic devices which can be programmed to exhibit a wide range of dynamical behaviour. There are two common modes of operation (Schiffer, Zonetti, et al. 2016).

So-called *grid-feeding* or *grid-following inverters* provide a given amount of (re-)active power and adjust the voltage phase and magnitude accordingly via a power controller. For this, they rely on a measurement of the frequency deviation as an input signal, which needs time and hence causes time delays. It has been found that delays increase the likelihood of instabilities when they coincide with a resonance frequency of the system (Schäfer, Matthiae, Timme, et al. 2015; Schäfer, Grabow, et al. 2016). Furthermore, grid-following inverters do not contribute to maintaining

[6] Regarding the parametrisation of synchronous generator models, sources are (Machowski et al. 2011; Glover et al. 2012; Weckesser et al. 2013). Typically, inertia and damping are also correlated with the power rating (Nishikawa and Motter 2015).

[7] Devices operating in the opposite direction, converting AC to DC, are referred to as rectifiers.

the grid frequency at its rated value and lack a substitute for the stabilising effect of the synchronous machines' physical inertia.

Both problems are addressed by so-called *grid-forming inverters*, which actively control their output phase/frequency, using a proportional (alias droop) control based on measuring the output power. Power mismatches, especially in RES, have to be covered by a fast-reacting storage, e.g. a flywheel or a battery. This way, grid-forming inverters stabilise the synchronous operating point by imitating the behaviour of synchronous generators with respect to the relation between frequency and active power (and possibly between voltage magnitude and reactive power). In the remaining, I reproduce the argument that these devices provide a "virtual" form of inertia (Schiffer, Goldin, et al. 2013).

In essence, the difference between inverter types is determined by the control design. The control input of grid-feeding inverters is the measured frequency deviation and the output is a prespecified (re-)active power, i.e. they act as power sources. Grid-forming inverters are voltage sources, i.e. they take the connected power as an input measurement and output a voltage signal with phase (and magnitude) suited to maintain the stable operating point. If not otherwise stated, "inverter" here refers to grid-forming inverters.

Inverters operate with an active power set point P_k. If the measured active power P_k^m differs from P_k, the frequency deviation ω_k is adopted proportional to a constant called droop gain g_k (Schiffer, Goldin, et al. 2013; Schiffer et al. 2014a):

$$\omega_k = \nu_k - \Omega = -g_k \left(P_k^m - P_k\right) \ , \tag{4.14}$$

where ν_k is the absolute frequency and Ω the rated frequency, e.g. 50Hz. The active power deviation serves as the input signal to the control and determines the adjustment of the inverter's instantaneous phase. The power measurement is typically subject to signals with high-frequency components. Therefore these components are filtered out firstly by a low-pass filter with a time constant τ_k such that (Coelho et al. 2002; Schiffer, Goldin, et al. 2013)

$$\tau_k \dot{P}_k^m = P_k^T - P_k^m \ , \tag{4.15}$$

exponentially relaxes to the transmitted power P_k^T, exchanged with the network defined as in Eqn. 4.8. The combination of the two equations Eqns. 4.14 and 4.15 yields a closed-loop relation that formally resembles the swing equation Eqn. 4.11 of a synchronous machine

$$\begin{aligned} \tau_k \dot{\omega}_k &= -\omega_k + g_k \left(P_k - P_k^T\right) \\ &= -\omega_k + g_k \left(P_k - \mathfrak{Re}\left(v_k c_k^*\right)\right) \ . \end{aligned} \tag{4.16}$$

In analogy to synchronous machines, an inertia constant $M_k = \tau_k / g_k$ can be defined, pointing out the ability of droop-controlled inverters with low-pass filters to provide so-called *virtual inertia* (Schiffer, Goldin, et al. 2013). Hence, such devices are representatives of so-called "virtual synchronous machines". The voltage mag-

nitude v_k is subject to further control. The resulting dynamical behaviour might deviate completely from that of a synchronous machine in general. Here, I assume a constant voltage magnitude $e_k^{inv} = const.$ with $v_k = e_k^{inv} e^{\imath\varphi_k}$. An alternative choice would be a voltage droop control with the measured reactive power as the input signal (Coelho et al. 2002)[8].

4.2.3. Kuramoto Oscillators with Inertia

Synchronous machine and inverter models come in various flavours (Sauer et al. 1998; Weckesser et al. 2013; Schmietendorf, Peinke, Friedrich, et al. 2014; Schiffer, Zonetti, et al. 2016), where the least complex is the Kuramoto model with inertia given by Eqn. 4.11 or Eqn. 4.16. Generally, which model detail is chosen depends on the modelled machine (synchronous generator or inverter) as well as on the specific research question. By including transient reactance, the fourth-order model more accurately resembles a synchronous machine's asymptotic behaviour while in turn the second-order model commonly suffices to capture the transient behaviour (i.e the first swing) (Weckesser et al. 2013). This has been further corroborated by comparing probabilistic stability measures at different model detail [F4]. It is the transient regime where nonlinear effects are most pronounced, leading to a wide range of interesting dynamic phenomena, going hand in hand with the high dimensionality of power grid models. Hence, it is worthwhile to discuss the second-order model in more detail.

Both Eqn. 4.11 for synchronous machines and Eqn. 4.16 fall into the same model class of *damped-driven oscillators with inertia*. While the following arguments are applied to the swing equation, the treatment for inverters with virtual inertia is analogous.

The rich dynamic behaviour of networks of inert Kuramoto oscillators ranges from synchronised motion (corresponding to fixed point solutions) or inter-area oscillations to chaos[9].

To better understand these dynamics, it is instructive to first look at single oscillators in the so-called infinite-busbar model. It is an approximation of the dynamics at a single node in the network interacting with a mean field, i.e. the single node couples to an infinitely inert bus whose phase is constant and chosen as a reference point.

Inserting this assumption into Eqn. 4.11 and dropping the node indices then gives the infinite-busbar dynamics[10]

$$\begin{aligned} \dot{\phi} &= \omega \\ \dot{\omega} &= \alpha - \beta\omega - \sin(\phi) \ , \end{aligned} \tag{4.17}$$

[8] Inverters with voltage droop control are sometimes referred to as grid-supporting inverters, especially if they provide further ancillary services to the power grid.

[9] See Rodrigues et al. (2016) for a recent overview article.

[10] A detailed discussion of the infinite-busbar model corresponding to the fourth-order dynamics recently appeared in (Barabanov et al. 2017).

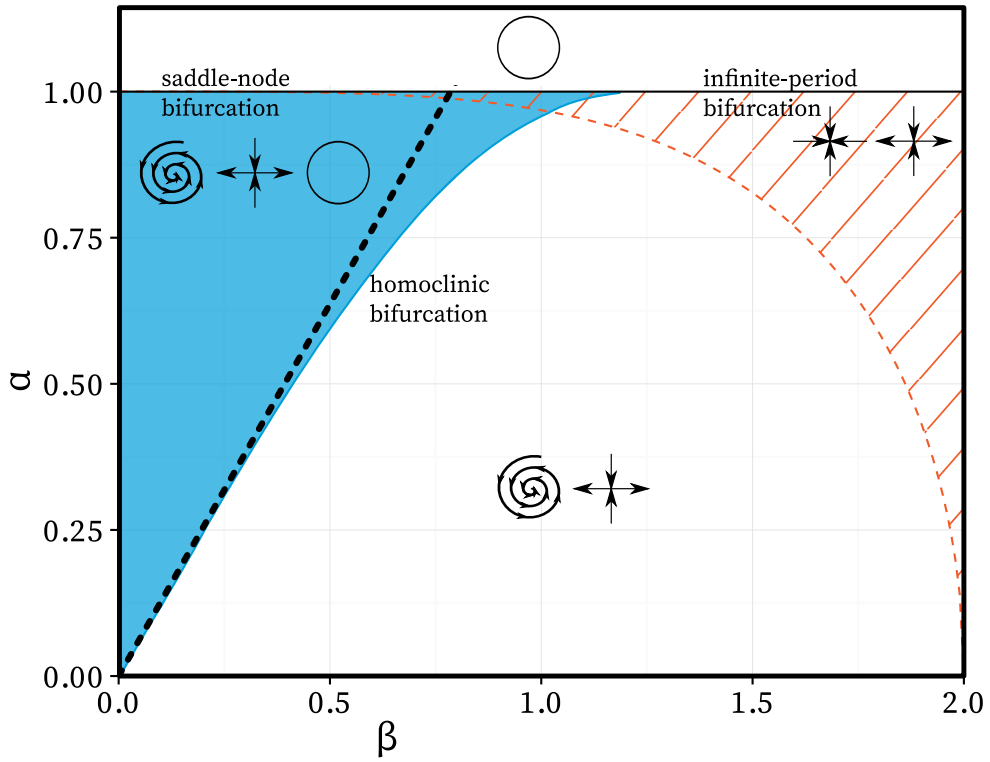

Figure 4.3. – **Parameter space of the Kuramoto model with inertia**: The blue-shaded area marks the bistable regime. The dashed black line shows the analytic approximation for the homoclinic bifurcation (data kindly provided by Ji, Peron, et al. (2013)). The orange-hatched area marks the regime of a stable node and a saddle. The symbols indicate the existence of a stable limit cycle (circle), focus/node (inward spiral/cross) and a saddle.

with the parameters $\alpha = P/K$, $\beta = 1/\sqrt{\gamma K \tau^{\omega}}$ and $K = |Y|E^f E^f$. Essentially, this is the equation for a damped pendulum with constant forcing (Coullet et al. 2005). Fig. 4.3 shows the distinct parameter regimes. The blue-shaded area marks the bistable regime, constrained by $\alpha = 1$ and a homoclinic bifurcation line (cf. Sec. 2.3.2). Approximately (dashed line), this region is given by $4\beta/\pi < \alpha < 1$ (Ji, Peron, et al. 2013; Manik, Witthaut, et al. 2014). In this regime, two attractors coexist, namely a stable focus

$$\omega = 0 \quad \phi = \arcsin(\alpha) + 2\pi k \,, k \in \mathbb{Z} \,, \tag{4.18}$$

and a limit cycle oscillating around the natural frequency α/β. For a pendulum, they correspond to an equilibrium at a constant angle respectively a periodically overturning solution. In a power grid setting, the fixed point is a synchronised state without frequency deviation, while the limit cycle corresponds to a stable oscillating frequency deviation. For $\alpha > 1$, the stability of the fixed point is lost in a saddle-node bifurcation. Otherwise, for $4\beta/\pi > \alpha$, the limit cycle merges with a saddle point in an homoclinic bifurcation. In this regime, the stable focus is globally

stable[11].

For large β, the regimes of globally stable fixed point and limit cycle directly border each other. Across this line, an infinite-period bifurcation takes place (Strogatz 1994), i.e. coming from $\alpha > 1$, the oscillation period diverges until a stable fixed point and saddle emerge on the limit cycle.

The seemingly simple model Eqn. 4.17 already offers a range of non-trivial dynamical behaviour. Particularly, the system exhibits hysteresis in the bistable regime (Ji, Peron, et al. 2013). In the following, the analysis is extended to complex networks and we will see which effects are retained.

Fixed Points A fixed point $s = (\phi^\star, \omega^\star)$ to Eqn. 4.11 is determined as the solution of the following set of nonlinear algebraic equations

$$\begin{aligned} P_k &= \sum_{j=1}^{n} |Y_{jk}| E_j^f E_k^f \sin\left(\phi_k^\star - \phi_j^\star + \alpha_{jk}\right) \\ \omega_k^\star &= 0 \,. \end{aligned} \tag{4.19}$$

Such fixed points correspond to the synchronous operating point of a power grid and are counted up to a constant global shift of all phases. In the absence of line losses α_{jk}, Eqn. 4.19 implies a power balance $\sum_k P_k = 0$ in the system. Otherwise, one finds that that total production needs to equal the sum of consumption and losses for a fixed point at $\omega_k^\star = 0$ to exist. The line losses, in turn, depend on the steady-state flows. Consequently, the problem is highly nonlinear such that the existence (and uniqueness) of solutions is generally not known, opposed to the infinite-busbar case above. In the lossless case, however, algebraic upper and lower bounds on the number of stable fixed points are known (Manik, Timme, et al. 2016; Delabays et al. 2017). A sufficient condition for a stable fixed point is that the phase differences are bounded, i.e. $|\phi_k^\star - \phi_j^\star| \leq \pi/2$ (Manik, Timme, et al. 2016). Different fixed points differ by loop flows, consequently, trees have a unique stable solution (Coletta, Delabays, et al. 2016; Manik, Timme, et al. 2016).

How does a fixed point change when a finite power imbalance occurs at one or more nodes? To get a first idea, consider the lossless Eqn. 4.13 and take the average over all nodes. The average frequency should be constant for a fixed point[12], i.e., it vanishes when the system is balanced (see above). By assuming that all γ_k are identical and noting that the coupling is antisymmetric, one obtains[13]

$$\langle \omega_k \rangle_k = \frac{\langle P_k \rangle_k}{\gamma_k^{-1}} \,. \tag{4.20}$$

Hence, when the P_k change such that the system becomes unbalanced, a new

[11] For $4\sqrt{1-\alpha^2}/\beta^2 \leq 1$, the Jacobian has real eigenvalues and the focus becomes a node (orange-shaded area in Fig. 4.3).

[12] They don't necessarily vanish, as the swing equation is in a co-rotating reference frame.

[13] Here, and in the following, $\langle \cdot \rangle_k$ denotes an ensemble average of a quantity over all nodes in a network.

stable fixed point – if existing – shifts the mean frequency from zero to a number that is determined by the ratio of power mismatch and damping in the system (Dörfler, Simpson-Porco, et al. 2016). Generally, in the presence of line losses, I will show that power imbalances cause a constant uniform frequency deviation $\Delta\omega_{global}$ to the "standard" fixed point. A finite power imbalance ΔP_k generally leads to finite phase and frequency deviations $\Delta\phi_k = \phi_k - \phi_k^\star$ respectively $\Delta\omega_k = \omega_k - \omega_k^\star$. Then, using $\omega_k^\star = 0$, Eqn. 4.11 yields

$$\begin{aligned}\Delta\dot{\phi}_k &= \Delta\omega_k \\ \frac{\tau_k^\omega}{\gamma_k}\Delta\dot{\omega}_k &= P_k + \Delta P_k - \\ &\quad - \frac{1}{\gamma_k}\Delta\omega_k - \sum_{j=1}^{n} |Y_{jk}| E_j^f E_k^f \sin\left(\phi_k^\star - \phi_j^\star + \alpha_{jk} + \Delta\phi_k - \Delta\phi_j\right) .\end{aligned}$$

For a new fixed point under power imbalance, the fixed point condition is relaxed and $\Delta\omega_k$ can be any constant with $\Delta\dot{\omega}_k = 0$. By adjusting the co-rotating frequency, it can then be assured that $\Delta\dot{\phi}_k = 0$. The first equation can be integrated to obtain $\Delta\phi_k(t) = \Delta\omega_k t + \Delta\phi_k^0$. The frequency deviations $\Delta\omega_k$ are then determined implicitly by the following equation

$$\begin{aligned}\frac{1}{\gamma_k}\Delta\omega_k &= P_k + \Delta P_k - \\ &\quad - \sum_{j=1}^{n} |Y_{jk}| E_j^f E_k^f \sin\left(\phi_k^\star - \phi_j^\star + \alpha_{jk} + \Delta\phi_k^0 - \Delta\phi_j^0 + \left(\Delta\omega_k - \Delta\omega_j\right) t\right) .\end{aligned}$$

This condition is required to hold for all time t, especially also for small t. By Taylor-expanding the sine function around $t = 0$, the condition becomes

$$\frac{1}{\gamma_k}\Delta\omega_k \simeq P_k + \Delta P_k - \sum_{j=1}^{n} S_{jk} + t\sum_{j=1}^{n} B_{jk}\Delta\omega_j + \mathcal{O}\left(|t|^2\right) , \tag{4.21}$$

where I defined the following short-hands

$$\begin{aligned}S_{jk} &= |Y_{jk}| E_j^f E_k^f \sin\left(\phi_k^\star - \phi_j^\star + \alpha_{jk} + \Delta\phi_k^0 - \Delta\phi_j^0\right) , \\ C_{jk} &= |Y_{jk}| E_j^f E_k^f \cos\left(\phi_k^\star - \phi_j^\star + \alpha_{jk} + \Delta\phi_k^0 - \Delta\phi_j^0\right) , \\ B_{jk} &= \delta_{jk}\sum_i C_{ik} - C_{jk} .\end{aligned}$$

The time-dependent linear term vanishes if the frequency deviations are uniformly constant across all nodes $\Delta\omega_k = \Delta\omega_{global}$ because the row-sum of B_{jk} vanishes. From this, we also find that the $\Delta\omega_k$ need to be constant independently for

each connected component of a network, i.e. the matrix $\mathbf{B}$ is a weighted Laplacian matrix (cf. Sec. 3.2). Hence, Eqn. 4.21 becomes

$$\frac{1}{\gamma_k}\Delta\omega_{global} = P_k + \Delta P_k - \sum_{j=1}^{n} S_{jk} \,. \tag{4.22}$$

As $\sum_k P_k = 0$, the global frequency deviation $\Delta\omega_{global}$ is then determined by the relation[14]

$$\Delta\omega_{global} \simeq \frac{\langle \Delta P_k \rangle_k}{\langle \gamma_k^{-1} \rangle_k} - \frac{\langle \sum_j S_{jk} \rangle_k}{\langle \gamma_k^{-1} \rangle_k} \,, \tag{4.23}$$

where the first term is the quotient of the amount of the power balance and the total system damping as suspected. The second term is a correction due to the nonlinearity induced by the line losses. By further assuming $|\Delta\phi_k^0| \ll 1$ and going to the lossless limit $\alpha_{jk} = 0$ the addend can be Taylor-expanded to get

$$\sum_{j=1}^{n} S_{jk} \simeq \sum_{j=1}^{n} |Y_{jk}| E_j^f E_k^f \left(\sin\left(\phi_k^\star - \phi_j^\star\right) + \cos\left(\phi_k^\star - \phi_j^\star\right) \left(\Delta\phi_k^0 - \Delta\phi_j^0\right) \right) \,. \tag{4.24}$$

As this expression is antisymmetric, averaging over all nodes k of the network finally yields

$$\Delta\omega_{global} \simeq \frac{\langle \Delta P_k \rangle_k}{\langle \gamma_k^{-1} \rangle_k} \,. \tag{4.25}$$

Such a permanent frequency deviation due to a power imbalance is visualised in Fig. 4.4. In the left panel, the power grid is balanced and the nodes resynchronise after a perturbation. In the right panel, a sudden consumption increase of 5% (i.e. $P_k \mapsto 1.05 P_k$ at consumer nodes) induces a transition to the new stable fixed point characterised by $\Delta\omega_{global} = -0.25$.

Limit Cycles In the uncoupling limit, all nodes oscillate independently at their natural frequency given by

$$\omega_k(t) = \gamma_k P_k + \mathrm{e}^{-t/\tau_k^\omega} \omega_k(0) \sim \gamma_k P_k \,. \tag{4.26}$$

From this limit, one can make an ansatz to see which solutions might arise for limit cycles in a network:

$$\begin{aligned} \omega_k(t) &= \gamma_k P_k + f_k(t) \\ \phi_k(t) &= \gamma_k P_k t + \int_0^t f_k(t') \; dt' \,, \end{aligned} \tag{4.27}$$

[14] This result does not assume any quantity to be small as the linearisation has been performed w.r.t. time.

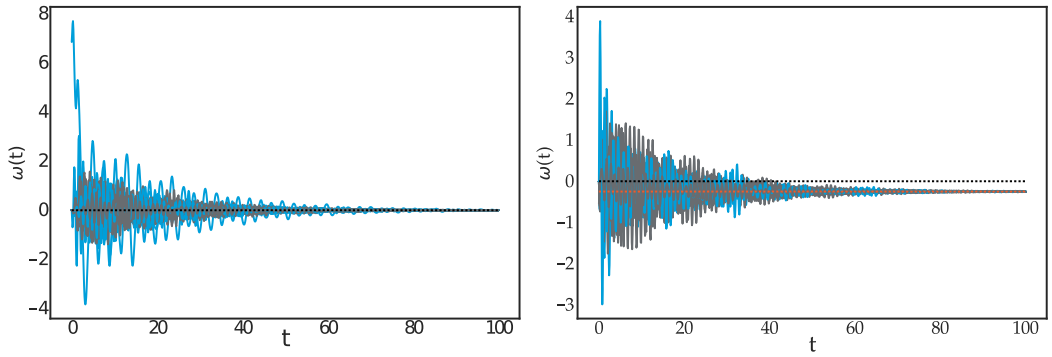

Figure 4.4. – **Permanent frequency deviation induced by a power imbalance**: Simulation of a synthetic power grid ([F3]) with 100 nodes using Eqn. 4.13 with $\tau_k^\omega = \gamma_k = 10$, $|Y_{jk}|E_j^f E_k^f = 6$ and randomly assigned $P_k = \pm 1$. **left**: The grid resynchronises to $\Delta\omega_{global} = 0$ after a random perturbation hitting node 42. **right**: Assuming a uniformly distributed load increase of 5%, the system adjusts towards a new under-frequency fixed point. The blue trajectories correspond to node 42 and the dashed orange line marks the theoretical value of $\Delta\omega_{global}$ Eqn. 4.23.

with a function $f_k(t)$ encoding a periodic time dependence. Inserting this into Eqn. 4.11 yields the following integro-differential equation

$$\begin{aligned}\frac{\tau_k^\omega}{\gamma_k}\dot{f}_k(t) = -\frac{1}{\gamma_k}f_k(t) - \sum_{j=1}^{n}|Y_{jk}|E_j^f E_k^f \cdot \\ \cdot \sin\left(\left(P_k - P_j\right)t + \alpha_{jk} + \int_0^t \left(f_k(t') - f_j(t')\right)\,dt'\right)\,.\end{aligned} \tag{4.28}$$

Without the integral, i.e. assuming the integrated pairwise differences are sufficiently small, a solution can be found. It consists of a homogeneous solution for $\omega_k(t)$ that decays exponentially to P_k and an inhomogeneous solution given by $f_k(t) = C_k(t)\,\mathrm{e}^{-t/\tau_k^\omega}$:

$$\begin{aligned}C_k(t) &= -\frac{\gamma_k}{\tau_k^\omega}\int_0^t dt'\;\mathrm{e}^{t'/\tau_k^\omega}\sum_{j=1}^{n}|Y_{jk}|E_j^f E_k^f \sin\left(\left(P_k - P_j\right)t' + \alpha_{jk}\right) \\ &= -\frac{\gamma_k}{\tau_k^\omega}\sum_{j=1}^{n}|Y_{jk}|E_j^f E_k^f \int_0^t dt'\;\mathrm{e}^{t'/\tau_k^\omega}\sin\left(\left(P_k - P_j\right)t' + \alpha_{jk}\right)\,.\end{aligned} \tag{4.29}$$

Solving the integral and neglecting exponentially decaying terms yields asymp-

totically

$$\omega_k(t) \sim \gamma_k P_k - \frac{\gamma_k}{\tau_k^\omega} \sum_{j=1}^{n} \frac{|Y_{jk}| E_j^f E_k^f}{\left(P_k - P_j\right)^2 + \left(\tau_k^\omega\right)^{-2}} \cdot \\ \cdot \left(\frac{1}{\tau_k^\omega} \sin\left(\left(P_k - P_j\right) t + \alpha_{jk}\right) + \left(P_k - P_j\right) \cos\left(\left(P_k - P_j\right) t + \alpha_{jk}\right) \right) ,$$

which is a periodic function with average $\gamma_k P_k$. Note, however, that ignoring the integral in Eqn. 4.28 is a strong assumption, especially when the dependence is nonlinear in time. Consequently, the study of limit cycles in networks of Kuramoto models with inertia still is an active field of research, e.g. recent findings reveal limit cycles located not at the natural frequencies but at fractional values (Nitzbon et al. 2017). These so-called exotic solitary states are induced by the network structure and do not exist in the infinite-busbar model. A particular example of this occurs in Sec. 6.4.

Chaotic Motion The infinite-busbar model does not have sufficient degrees of freedom to exhibit chaos (cf. Sec. 2.2), however, it has been shown that a network of swing equations exhibits chaotic motion in certain cases (Kopell et al. 1982). Particularly, the time evolution in the three-oscillator setup of Kopell et al. (ibid.) – where a node with low inertia is weakly coupled to two nodes with higher inertia – is chaotic in the undamped limit. This is due to the fact that the dynamics can be cast into an effective two-dimensional swing equation with periodic forcing. For this case, a periodically-driven infinite-busbar model, other authors identified chaotic regimes also in the presence of damping (Kautz et al. 1985; Gitterman 2008).

4.3. Network Model

Abstract In the following, I carve out essential characteristics of real-world power grids, give a review on previous approaches to model them as complex networks and synthesise these insights in a neonet model.

4.3.1. Empirical Properties of Power Grids

A DEVELOPED POWER GRID consists of millions of individual machines that interact through a hierarchy of subnetworks at different voltage levels. Hence it incorporates spatial scales from single buildings to whole continents, making it difficult to control the system but also to fully understand its dynamics.

Each of the voltage layers serves a different purpose. Typically, there are *extra-high* (>110 kV, EHV), *high* (36-110 kV, HV), *medium* (1-36 kV, MV) and *low voltage* (≤1 kV, LV) subnetworks. They are mutually interconnected by transformer substations. The extra-high voltage levels are commonly referred to as *transmission grids* whereas the other levels are summarised as *distribution grids*.

Transmission grids (partly also HV networks) are typically built as meshed networks consisting of long-range connections with a high capacity (Lakervi et al. 1995). They have to fulfil the so-called $N-1$-criterion such that they have to withstand the failure of a single node or edge (ibid.).

Contrarily, distribution grids are (operated as) radial networks, as this configuration is easier to control then a meshed network (ibid.). They have a mean degree of about 2.02 (LV) and 2.13 (MV) (Pagani et al. 2011), confirming their tree-like structure. In urban areas, the topology usually correlates with road networks (Strano, Nicosia, et al. 2012). The higher average load density compared to rural areas also leads to different topologies of urban LV and MV grids which tend to be interconnected on the same voltage level due to their proximity (Lakervi et al. 1995).

This system hierarchy in terms of voltage magnitude reflects the historical development of power grids in industrialised regions. Power grids are designed to incorporate large electricity producers in high voltage levels, leading to top-down power flows to the consumers connecting to low-voltage levels. The power grid as is undergoes a drastic transition as the introduction of renewable energy sources to medium- and low-voltage levels reverses the typical power flows. On top of that, high-voltage DC links are introduced to balance renewable infeed across long distances, creating a new overlay grid superseding/coexisting with the EHV layer (Ergun et al. 2012).

4.3.2. Power Grids as Complex Networks

THE VAST MAJORITY of complex systems literature focuses on transmission grids. They are identified as rather *sparse networks* with an *exponential degree distribution*[15], which has a mean degree less than 3, independent of their size (Rosas-Casals et al. 2007; Zhifang Wang et al. 2010; Barthélemy 2011; Pagani et al. 2013)[F3]. The exponential tail $e^{-k/\gamma}$ decays at a rate between $\gamma \approx 1.5$ and $\gamma \approx 2$ (Solé et al. 2008; Rosas-Casals 2009; Pagani et al. 2013).

[15] cf. Local Characteristics in Sec. 3.3

Although, the degree distribution of Erdős-Rényi random graphs (Gilbert 1959; Erdős et al. 1960) also decays exponentially for high degrees, they are not sufficient to explain the sparse structure of power grids (Rosas-Casals 2009)[F3].

Other authors found indications for the small-world property (Watts et al. 1998; Pagani et al. 2013), i.e. a small characteristic path length and high average clustering coefficient compared to random graphs. Large power grids, however, are too sparse to be connected networks in Watts-Strogatz' small-world model (Zhifang Wang et al. 2010) and the characteristic path length is longer than to be expected (Rosas-Casals et al. 2007).

To capture the structure of power grids, it is in fact necessary to take the spatial constraints into account as they translate to constraints on network characteristics (Molkenthin and Timme 2016). Modified random graph models, for instance, incorporating the spatial embedding of the network, i.e. random geometric (Herrmann et al. 2003) or Waxman (Waxman 1988) networks, typically show an incorrect scaling with the system size in regard of network characteristics like the mean degree [F3].

It is also insightful to estimate the line length distribution, which typically is heavy-tailed (Zhifang Wang et al. 2010), i.e. log-normal and similar. Hence, there are long-range interconnections, i.e. shortcuts in the network, however, they apparently do not reduce the characteristic path length as much as in a small-world model.

An overview about further results from complex network analyses of power grids is contained in Pagani et al. (2013) and a discussion of further network models for power grids can be found in Schultz et al. (2014a).

4.3.3. A Neonet Model for Power Grids

The aim in the following is to represent the structure of power grids by a neonet $\mathcal{G}|_{\mathcal{P}} = ((\mathcal{V}, \mathcal{E}, w), \mathcal{P})$ as defined in Sec. 3.4.1.

In general, power grids can be mapped to networks in different ways. Power sinks, i.e. various loads like households or industries, are modelled as constant impedances to the ground, imposing algebraic constraints to the dynamics at these nodes. As an alternative to treating differential-algebraic equations, the constant loads are attributed to dynamic nodes for simplicity. As a consequence, all dynamic nodes act as net producers ($P_k > 0$) or net consumers ($P_k < 0$), depending on the local balance. This is in close analogy to the effective network approach (Nishikawa and Motter 2015). The process by which loads and substations are removed from the network is known as *Kron reduction* of passive nodes (Dörfler and Bullo 2011; Manik, Witthaut, et al. 2014). The point is that Kron reduction produces a functional network of effective interactions between dynamic nodes in contrast to the structural network given by transmission lines. The difference is negligible for the transmission grid and to some extent also for MV grids, but significant for LV grids which are load-dominated[16].

In the latter case, the Kron-reduced network is almost fully-connected. Particularly, the neighbouring nodes of a load become all-to-all connected after Kron reduction.

[16] In a future scenario, with prosumers replacing loads in LV and MV grids, the share of dynamic nodes increases and hence the reduced network rather resembles the actual coupling topology.

The difference between the types of networks needs to be taken into account in any complex network analysis. For the SCONE model and the results in the subsequent chapters, I assume the networks to be already reduced.

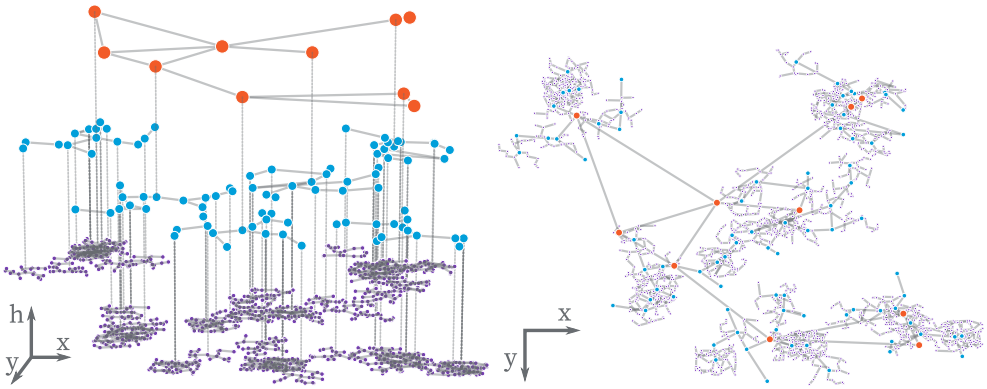

Figure 4.5. – **A neonet model for power grids**: This fictional neonet consists of three patches, indicated by node colour. The patches correspond to the voltage layer (extra-high to high to medium from top to bottom). The inter-patch edges are dashed grey lines. **left panel** Three-dimensional visualisation of the neonet, the patches are separated by a different height h according to the voltage level. **right panel** Spatial projection network $\tilde{\mathcal{G}}|_{\mathcal{P}}$ of the neonet. Adapted from [P3].

To specify $\mathcal{G}|_{\mathcal{P}}$, the single components of a network and a suitable partition are defined in the following. The nodes are partitioned according to their voltage rating, reflecting the apparent system hierarchy in terms of voltage magnitude. Each voltage layer (EHV to LV) constitutes a single patch, which generally consists of multiple connected components[17]. This is visualised in Fig. 4.5, where the nodes' colours as well as their height h indicate the subnetworks. While the EHV layer (top) is connected, this does not hold for the lower voltage layers combining local grid components.

Transmission lines only connect nodes at the same voltage rating. Hence, there are two types of edges. Firstly, the edges $\mathcal{E}^{\ell}$ in each patch represent actual transmission lines[18]. Their line admittance depends on various parameters like the material composition, cable distance or ambient temperature but mainly on the line length. Typically, it is sufficiently well approximated by taking $Y_{jk}^{-1} = (r_{jk} + \imath x_{jk}) d_2(j,k)$, where r_{jk} and x_{jk} are the specific resistance respectively reactance and $d_2(j,k)$ is the distance of the nodes j and k (Machowski et al. 2011; Glover et al. 2012). Secondly, transformers step the voltage up or down between different patches to transfer power. They are treated as an element whose admittance differs as seen from the higher or lower voltage layer by a constant factor[19]. Hence, transformers appear as entries in the admittance matrix, they can be considered as "virtual" edges which

[17] Depending on the research question, they might be divided further.

[18] Solid lines in Fig. 4.5.

[19] The ratio of the admittance ratings is given by the ratio of the winding numbers of a transformer (Glover et al. 2012). It is controlled by the tap position and can be dynamically changed to account for different operating conditions.

have no physical length, constituting the seam $\mathcal{E}_{seam}$ between patches. They are indicated by dashed vertical lines in the left panel of Fig. 4.5, connecting two nodes from different patches (different height h) at the same position (x, y). For simplicity, I consider only ideal transformers, without losses in the windings or in the core and without leakage currents. Following theses considerations, I use the admittance weight function $w^Y : ij \to |Y_{ij}|$ for assigning a positive real weight to each edge in the adjacency matrix.

As discussed above, as power sources I consider synchronous machines and inverter-connected renewables, both behaving dynamically analogous to Kuramoto oscillators with inertia and hence described by the same equation (cf. Sec. 4.2.3). These are the dynamic nodes of a power grid, i.e. the time evolution of their state variables determines the overall power grid dynamics.

4.4. Model Summary: SCONE

The following model is used in the next chapters as a representation of power grids. I refer to it as the *SCONE model*, i.e. the SeCond Order NEonet model. Here, I only summarise the essential aspects of the model as a quick reference for later chapters. The governing equations are derived and explained *en detail* in the preceding sections.

Remarks Numerical integrations of this model are performed using SciPy's linear multi-step solver `odeint` based on the Fortran library LSODA. Its default absolute and relative error tolerance is $1.49012 \cdot 10^{-8}$.

Dynamics

The dynamical system is given by the following system of differential equations for the voltage phase ϕ_k and frequency ω_k at every site k:

$$\boxed{\begin{aligned} \dot{\phi}_k &= \omega_k \\ \frac{\circ_k}{\blacktriangle_k}\dot{\omega}_k &= P_k - \frac{1}{\blacktriangle_k}\omega_k - \sum_{j=1}^{n} A_{jk} \sin\left(\phi_k - \phi_j + \alpha_{jk}\right) \end{aligned}} \tag{4.30}$$

where the coupling is given by a weighted adjacency matrix

$$A_{jk} = |Y_{jk}| E_j^f E_k^f \,, \tag{4.31}$$

and the nodal admittance matrix is defined as

$$Y_{jk} = |Y_{jk}| e^{\imath\left(\pi/2 - \alpha_{jk}\right)} \,. \tag{4.32}$$

The time constants $\circ_k$, droop constants (inverse damping) $\blacktriangle_k$ and net input powers P_k appear as parameters with comparable meaning in both synchronous machines or inverters.

parameter	$\circ_k$	$\blacktriangle_k$
sync. machine	τ_k^ω	γ_k
inverter	τ_k	g_k

Table 4.1. – **Parameter sets**: Legend

In general, however, different sets of parameter values have to be assigned. Hence, they are given with place holders in Eqn. 4.30 and should be replaced with the corresponding parameters from Tab. 4.1 as they were introduced in the preceding sections.

Network

The individual sites (nodes k) are interconnected via a power grid topology which I assume is given by a neonet (cf. Sec. 3.4.1) $\mathcal{G}|_{\mathcal{P}} = (\mathcal{G}, \mathcal{P})$ based on a partition $\mathcal{P}$ and a weighted network $\mathcal{G} = (\mathcal{V}, \mathcal{E}, w)$. Algebraically, the network is represented by an adjacency matrix $\mathbf{A}$ as given above. Given that the voltage magnitudes are stated in per-unit values[20], i.e. $E_k^f = 1p.u._V$, the weight function is w^Y such that $w^Y : ij \mapsto |Y_{ij}|$ for an edge ij. The complex phase of the admittance determines the phase lags α_{jk} via Eqn. 4.32. They correspond to the Ohmic losses on a line and are more or less specific to the voltage level. The assumption of a uniform line capacity A_{jk} in the majority of previous studies, however, can be replaced by the following consideration. In the lossless case, i.e. EHV transmission grids, the line admittance is approximated by the susceptance $|Y_{jk}| \approx B_{jk}$, which is mainly determined by the line length $d_2(i,j)$, as discussed in Sec. 4.3.3. Using the specific reactance $x' = 0.265\Omega/km$ (Machowski et al. 2011), the susceptance is $B_{jk} = (x' d_2(i,j))^{-1}$. Consequently, the $A_{jk} \propto d_2(i,j)^{-1}$ are then distributed in relation to the line length distribution.

The partition $\mathcal{P}$ separates the node set $\mathcal{V}$ such that the blocks induce patches $\mathcal{G}^{EHV}$, $\mathcal{G}^{HV}$, $\mathcal{G}^{MV}$ and $\mathcal{G}^{LV}$ corresponding to the nominal voltage magnitude (cf. Sec. 4.3.1). They are interconnected by edges jk which have no spatial extent but w^Y attributes them the equivalent admittance of a transformer between j and k. Notably, this renders the adjacency asymmetric, i.e. $Y_{jk} \neq Y_{kj}$ for a transformer, and the network representation then contains directed links.

Default Parametrisation

There is a number of basic assumptions underlying the default parametrisation that is used for the examples in Chap. 5 and Chap. 6, where the objects under study are single transmission grids. Transmission grids are here assumed to be lossless ($\alpha_{jk} = 0$), i.e. high-voltage lines have negligible Ohmic resistances. Each node in transmission grids is to some extent a representative for the surrounding area and the connected lower voltage levels. Transmission grids are up to now dominated by synchronous generation, whereas 90% of inverter-connected RES are installed in distribution grids ("Studie im Auftrag des Bundesministeriums für Wirtschaft und Energie (BMWi)" 2014). Hence, the second-order dynamics is an equivalent representation of a net producer or net consumer, depending on whether production

[20] Here, $p.u._V$ stands for per-unit voltage, a dimensionless value resulting from a suitable normalisation of voltage magnitudes by a common value (Machowski et al. 2011).

or demand dominates an area. As this is a time-varying attribution, especially in regions with a high share of RES, a pragmatic first approximation is the following. Each node is randomly assumed to be a net producer[21] ($P_k = 1\,p.u._P$) or net consumer ($P_k = -1\,p.u._P$) at the time of simulation such that the overall system is balanced, i.e. $\sum_k P_k = 0$. Characteristic parameter values for synchronous machines are chosen, as they have been used in previous studies (Rohden, Sorge, Timme, et al. 2012; Motter et al. 2013; Menck, Heitzig, Kurths, et al. 2014; Schmietendorf, Peinke, Friedrich, et al. 2014). The aim here is also to allow for a comparison with previous results. In the notation of the SCONE model, comparable parameters correspond to $\gamma_k = 10\,Hz/p.u._P$, i.e. a damping factor of $0.1\,p.u._P/Hz$, a time constant $\tau_k^\omega = 10\,s$ and $A_{jk} = 6\,p.u._P$.

In summary, this set-up is rather conceptual and serves the purpose of being a suitable test case for the methodological development of probabilistic stability measures in the context of this thesis. The numerical results cannot be seen as realistic simulations of actual power systems, still they can yield important insights on their systemic behaviour.

[21] Here, $p.u._P$ stands for per-unit power, a dimensionless value resulting from a suitable normalisation of power ratings with a common value (ibid.).

5. Probabilistic Stability Analysis

Contents of this Chapter

5.1. In a Nutshell

This chapter contains my main contributions to methodological extensions and improvements of probabilistic stability measures. Probabilistic approaches yield computationally efficient stability indicators in high-dimensional complex systems. In particular, they are able to consider network-local finite-size perturbations at single nodes in a network. The aim of this chapter is to define measures which (i) contain valuable information about stability in multistable nonlinear systems, (ii) can be obtained with reasonable computational efforts and (iii) can be translated into practical implications.

The outline is as follows. I start with a brief overview of approaches to power grid stability in Sec. 5.2, from empirical to simulation-based, linear and probabilistic methods. Given the context of this thesis and of my research, the focus is biased towards the complex systems perspective in theoretical physics. For a more in-depth review of methods from an engineering point of view, I refer to Kundur et al. (2003) and the text books by Anderson et al. (1979), Sauer et al. (1998), and Machowski et al. (2011).

Most probabilistic stability measures, especially basin stability and derived concepts, rely on a correct final-state determination. In Sec. 5.3, I explore the limitations and potentials of a Monte Carlo estimation in systems with fractal basin boundaries or riddled basins of attraction, which are often observed in applications.

Basin stability might be subject to estimation problems in fractal basin geometries, but besides that it also is based on singular perturbations. Intuitively, when the state of a system is already close to a basin boundary, a subsequent perturbation easily moves the system trajectory to an alternative basin. Hence, repeated perturbations can be destabilising even when they are small, given they appeared often enough. I discuss the consequences of such repeated perturbations in Sec. 5.4, leading to the novel concept of finite-time basin stability.

In applications, constraints on transients or fulfilling desired bounds can be more important than asymptotic stability. In general terms, the phase space might be partitioned in desirable and undesirable regimes. Hence, a novel probabilistic approach that is called survivability is introduced in Sec. 5.5. It takes the desirable regime into account for a stability assessment and hence complements probabilistic approaches focusing on asymptotics, for instance basin stability.

5.2. Review of Power Grid Stability

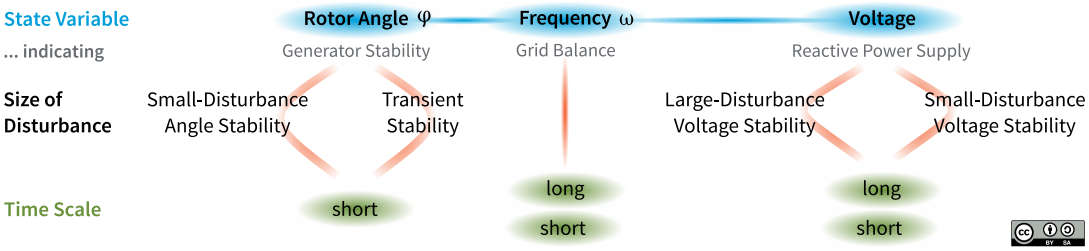

Figure 5.1. – **Classification of power system stability**. Adapted from Kundur et al. (2003)

Stability Analysis of power grids has a long-standing scientific history, especially in electrical engineering. *Power system stability* is defined as the ability of a power system to regain a desired operating point, following a disturbance (Kundur et al. 2003). This depends on the initial operating condition and state variables are required to remain bounded. The dependence on initial operating conditions refers to the inherent multistability of power systems, where the desired operating points correspond to phase-locked synchronisation of all units rotating at the grid's rated frequency of 50 or 60Hz. The condition of state variables to be bounded during the post-disturbance *transient*[1] will be one of this chapter's focus topics, leading to the concept of survivability.

We can further fine-grain the aspects of power system stability (ibid.) by distinguishing disturbances via the dominantly affected system variable as shown in Fig. 5.1. The distinction between "small" and "large" disturbances separates between perturbations small enough such that a linearisation of the system is permissible, whereas for finite perturbations the non-linear response cannot be neglected. Small-disturbance angle stability, for instance, is concerned with insufficient damping, leading to local rotor angle oscillations at single machines or even global inter-area oscillation modes. Voltage magnitude dynamics happen usually on longer time scales (cf. Sec. 4.2.1). Large voltage deviations are a common source for automated line tripping and following cascading failures, whereas small-disturbance voltage stability refers to disturbances in the form of, for instance, incremental load changes. In general, voltage stability is closely related to the provision of reactive power (Simpson-Porco et al. 2016), while frequency stability indicates a balance of active power. All system variables are of course dynamically coupled, as indicated by horizontal lines in Fig. 5.1, leading to an intertwined system response on different time scales.

Some authors (Solé et al. 2008; Rosas-Casals 2009) define power grid stability in terms of *reliability*, i.e. of electricity supply. In contrast to Fig. 5.1, reliability also includes the ability to cope with cascading failures and can be measured using macroscopic observables like the energy not supplied (per month), the total power

[1] The state of a system is called *transient*, if the system has not converged to an asymptotic state yet, for instance after changing the value of one of the variables or parameters.

loss or the restoration time after failures. Reliability is strongly related to certain features of network structure, which is discussed in Chap. 6.

Grid operators commonly perform a static power flow analysis for a set of predefined contingencies of interest. A special focus lies on the fulfilment of the so-called $N-1$ criterion (ENTSO-E 2013), meaning that the power system should be operated and designed in a way that it withstands failures of single components. Furthermore, the technical parameters are typical chosen in a way to ensure asymptotic stability of synchronisation, referred to as *small-signal stability* (Kundur et al. 2003). Hence, it is of more importance to study large perturbations in power grids.

Other stability indications are derived from time domain simulations. The rate of change of frequency (ROCOF) is directly related to the provision of kinetic energy to the grid (or absorption) (Ulbig et al. 2013) in response to a perturbation[2]. Typically, the ROCOF should remain small to limit the stress on machines and such that there is enough time for requesting the control reserve before the grid frequency deviates too far. Unfortunately, the decreasing amount of inertia, traditionally provided by synchronous generators, causes higher ROCOFs. This necessitates new concepts, like virtual inertia provided by grid-forming inverters (cf. Sec. 4.2.2), to maintain a controlled system response.

Grid-feeding inverters, however, rely on a precise measurement of the grid frequency (Quitmann et al. 2009). Hence, they could be subject to another source of instability, namely time delays. A joined linear and basin stability analysis of small-scale power grids revealed, that certain delay times render synchronisation unstable (Schäfer, Matthiae, Timme, et al. 2015; Schäfer, Grabow, et al. 2016). This problem can be solved, when the inverters do not react to an instantaneously-measured frequency but to a time-averaged signal. In particular, asymptotic stability is given for long-enough averaging times. For the case of time-varying delays, e.g. in the communication between inverters, it is also possible to derive conditions for the asymptotic stability of the synchronous state (Schiffer, Fridman, et al. 2016; Schiffer, Dörfler, et al. 2017). Complementary, other authors observed the benefit of a spatial averaging across nodes in a distributed control setup (Dörfler, Simpson-Porco, et al. 2016) for a combination of primary droop control and additional control layers.

In a different line of research, rigorous conditions for the linear stability of phase synchronisation in power grids (Dörfler and Bullo 2014), involving also droop-controlled inverters (Dörfler, Chertkov, et al. 2013), are derived. For instance, the tuning of damping, inertia and droop constants can achieve an optimised master stability function even for heterogeneously coupled oscillators (Motter et al. 2013; Nishikawa, Molnar, et al. 2015). Commonly, the synchronisation threshold (cf. Eqn. 2.4) is considered as an indicator of stability. It is the critical coupling strength, above which the macroscopic order parameter indicates the emergence of a phase-locked state. A low threshold ϵ_c is considered to support the structural stability of the synchronous state with respect to perturbations diminishing the coupling – the system is "easier" to synchronise.

Typically, network-local disturbances to the synchronous state propagate diffusively in a power grid. Under certain conditions, however, they become localised

[2] See Eqn. 4.2 for the relation between frequency and rotational power.

and decay exponentially in the network (Kettemann 2016). Another complex effect in power grids are inter-area oscillations, i.e. slow frequency modulations (less than 1Hz) between distant parts of the grid. Typically, the oscillating areas are weakly connected (Klein, Rogers, et al. 1991). Hence, it is possible that an increasing RES production amplifies small-scale inter-area oscillations in weakly-coupled distribution grids. The origin of this phenomenon, and whether the oscillations correspond to an attractor or are transient, is still under debate. There are, however, indications for this to be a linear effect due to the presence of weakly-damped oscillation modes (Wu et al. 2016).

Another important research field is to analyse the return time of perturbed trajectories. Quantifying return times to an attractor is a fundamental problem, as they can be infinite and the result depends on an arbitrary return criterion. Nevertheless, recent approaches (Kittel et al. 2017) like the regularised reaching time (relative to a reference point) or the area under distance curve (time-integral of the distance) suggest robust methods. The time it takes for a dynamical system to return after a network-local finite-size perturbation is termed single-node recovery time (Mitra, Kittel, et al. 2017) and can be used for distinguishing fast and slow nodes in a network. For the example of the UK power transmission grid, the authors discovered that about 5% of nodes return significantly slower, but correlations with topological features could not be identified.

Recently, probabilistic approaches, in particular basin stability, have been transferred to power grid research (Menck and Kurths 2012; Ji and Kurths 2014; Menck, Heitzig, Kurths, et al. 2014; Kim et al. 2015, 2016)[F5] (see also Sec. 2.4.2 on basin stability). Besides that, they are applied broadly (Maslennikov et al. 2015; Rakshit, Bera, Majhi, et al. 2017), including delayed dynamics (Leng et al. 2016) or chimera states (Martens, Panaggio, et al. 2016; Rakshit, Bera, Perc, et al. 2017), and have been extended to incorporate parameter perturbations (Brzeski, Lazarek, et al. 2016). In the latter case, probabilistic measures are a robust way to cope with parameter uncertainties in e.g. mechanical systems or control. For instance, the control parameters are optimised to ensure asymptotic stability, but in practice they can often not be adjusted precisely enough (Brzeski, Wojewoda, et al. 2017).

The original basin stability approach has been further developed in different aspects. The sensitivity to undesired transient behaviour is at the core of constrained basin stability (Kan et al. 2016), which is the joint probability of returning to an attractor and staying in a certain desirable phase space regime. Hence, it measures the subset of the basin fulfilling the constraint. As the original basin stability, however, it focuses on the asymptotic sets of a dynamical system. I present an alternative approach to include constraints in Sec. 5.5.

Single-node basin stability has been generalised to a multiple-node basin stability (Mitra, Choudhary, et al. 2017), considering perturbations localised at a subset of nodes in a network. The authors find an exponential decay of basin stability with the number of perturbed nodes in a model of the UK power grid. This gives an estimate for the number of nodes that need to be safeguarded for ensuring stability.

Furthermore, there are different approaches to combine local and global measures in a joint stability assessment (Soliman et al. 1989; Mitra, Kurths, et al. 2015; Daza, Wagemakers, Georgeot, et al. 2016; Lundström 2017). Integral stability (Mitra,

Kurths, et al. 2015), for instance, derives an integrated resilience measure from the smallest extent of the basin, basin stability and the largest local Lyapunov exponents. Close to bifurcation points, an integrated measure can yield an improved indication of a dynamical transition.

Given these recent developments of basin stability, I would like to highlight that it allows to quantify the stability of attractors given finite-size perturbations, to detect certain bifurcations in parameter studies and to be efficiently estimated in high-dimensional systems. Nevertheless, there are certain limitations to be aware of. Basin stability is

1. only meaningfully applicable to multistable systems.
2. insensitive to undesired transient behaviour.
3. dependent on a detailed knowledge about the locus (and type) of the attractor.
4. crucially dependent on correctly determining the asymptotic behaviour.
5. not applicable to systems with repeated perturbations.

The following sections are mainly devoted to addressing these issues, some of which are not specific to basin stability but inherent to various probabilistic stability measures.

5.3. Limitations of Basin Stability Under Final-State Sensitivity

This section is related to research originally published in [P7].

Abstract In this section, I discuss the influence of rounding errors in fractal basin geometries on basin stability estimations, study the effect in illustrative example systems and derive best practices.

5.3.1. Rounding Errors in Fractal Basins

Monte Carlo methods, which are applied to estimate probabilistic stability measures, generally have problems with the estimation of very small probabilities (Evans et al. 2000) within a reasonable (relative) standard error. This is especially so for rare attractors (Zakrzhevsky et al. 2010) with basin stability $\mu_{\mathcal{B}} \ll 1$.

Even if the probability to be estimated is large enough, a different contribution to the estimation error is given by a final-state sensitivity arising when the basin geometry is riddled or includes fractal boundaries[3]. As discussed in Sec. 2.4.3, a correct assessment of the specific attractor a trajectory converges to is difficult in these cases.

[3]Clearly, an attractor with a riddled basin is not asymptotically stable, as there is no attracting open neighbourhood. Still, it is a measure attractor as discussed in Sec. 2.2.2 which might be considered "basin stable". Basin stability hence is an independent notion of stability in such systems.

For instance, if transient trajectories stay close to a basin boundary for long, numerical errors will likely move the simulated trajectory across the boundary, predicting the system incorrectly to converge to another attractor. Final state identification is, however, the essence of any basin stability estimation (cf. Sec. 2.4.2). Hence, the limited numerical precision of any simulation inevitably leads to rounding errors, contributing to the overall estimation error in deterministic systems. Other error components – which are controlled by the details of the numerical procedure – are the standard error of the sampling and approximation errors in function evaluations or integration of differential equations. Fractal basin boundaries and riddled basins are examples, where rounding errors cannot be neglected and Monte Carlo methods based on numerical integration become problematic.

Especially fractal basin boundaries emerge also in the context of power grids, even in a simple two-node model (Hasegawa et al. 1999). There, the boundary might still be smooth on fine enough scales, but in practice final-state sensitivity is observed.

5.3.2. Numerical Results

To investigate the effect of rounding errors, I consider two exemplary systems that have been studied in the context of fractal basins. On the one hand, a system with fractal basin boundaries, even fulfilling the Wada property (cf. Sec. 2.4.3), is the damped-driven pendulum (Eqn. 2.27):

$$\begin{aligned} \dot{\phi} &= \omega \\ \dot{\omega} &= p\cos(t) - \nu\omega - \sin(\phi) \ , \end{aligned} \tag{5.1}$$

with $p = 7/4$ and $\nu = 1/5$. It resembles the infinite-busbar model (Eqn. 4.17) with time-dependent forcing and is hence also interesting in the context of power grids.

On the other hand, the quadratic map on the complex plane (Lopes 1992)

$$z_{t+1} = F_\lambda(z_t) = z_t^2 - (1 + \imath\lambda)z_t^* \tag{5.2}$$

is an example for a system with not only riddled but intermingled (cf. Sec. 2.4.3) basins of attraction for $\lambda = 1.02871376822$ (Alexander et al. 1992):

Let us focus on the quadratic map. A visualisation of the phase space is given in Fig. 5.2. The map has three attractors (ibid.) indicated as red/blue/purple line segments in Fig. 5.2a (not to scale). The three basins of attraction are completely intermingled at all length scales, indicated by the zoom-ins Fig. 5.2b and Fig. 5.2c.

For both systems, the behaviour of the Monte Carlo procedure is investigated by estimating basin stability $\hat{\mu}_\mathcal{B}$ at different levels of numerical precision. This is achieved by artificially discarding the significant decimal digits of 64 bit double floating point variables. Writing $\varepsilon = 10^{-p}$, where p hereafter denotes precision, double variables correspond to $p \approx 16$ while untruncated 32 bit single precision has $p \approx 7$. An integration is terminated when the trajectory is within ε-distance to an attractor in Euclidean metric.

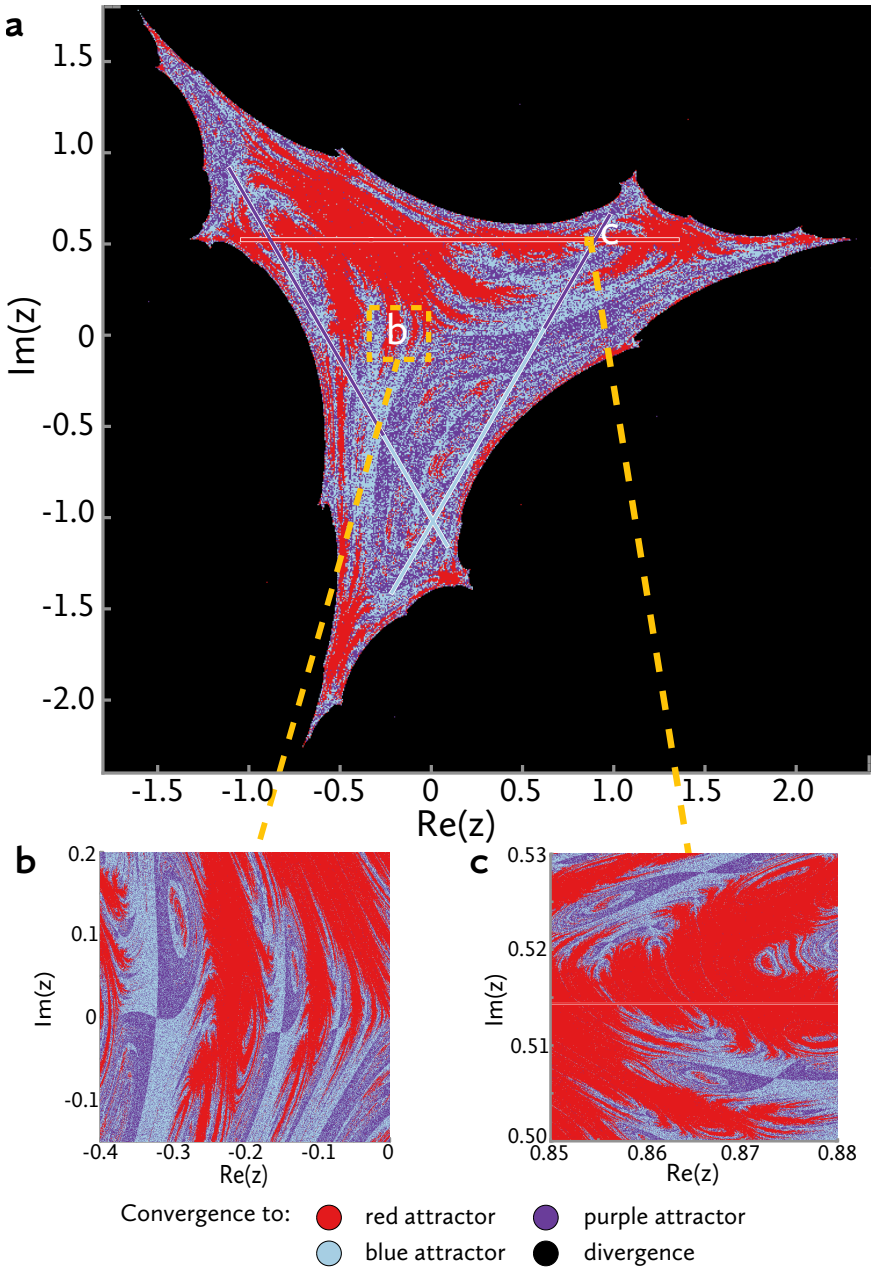

Figure 5.2. – **Intermingled basins of the quadratic map a** Phase space portrait of the three attractors (red/blue/purple line segments) of the quadratic map Eqn. 5.2 with their intermingled basins of attraction coloured alike. The black area corresponds to initial conditions for which the dynamics diverges. Below are zoom-ins of two regions, **b** and **c**. The locations of the attractors (line segments (Alexander et al. 1992)) are highlighted by red/blue/purple bars (not in scale). The figure has been previously published in [P7].

For the damped-driven pendulum, $T = 1,000$ initial conditions are drawn from ρ which is take to be a uniform density on the reference subset $R = [-\pi, \pi] \times$

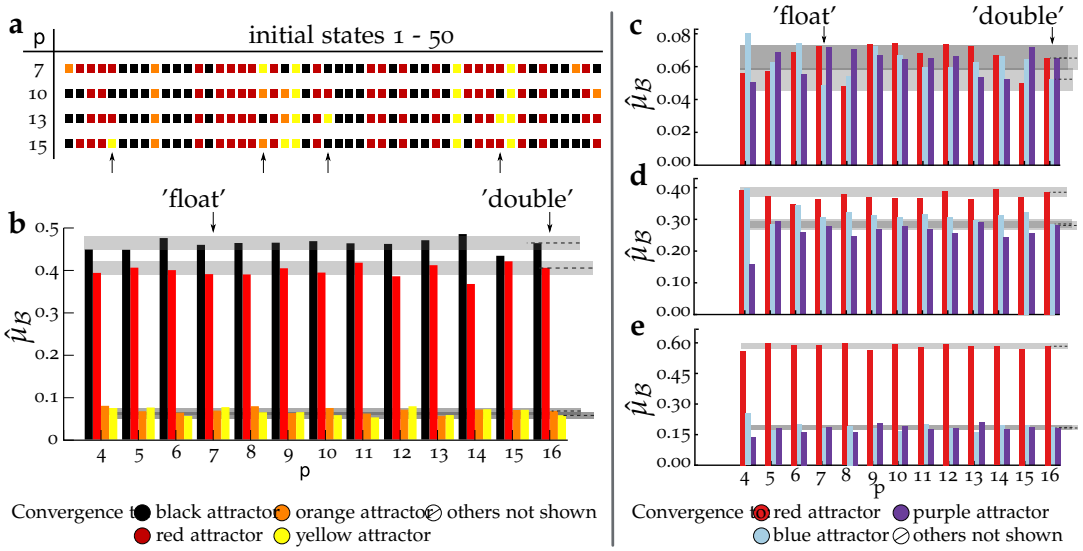

Figure 5.3. – **Basin stability estimation**: **a** Outcome of numerically integrating Eqn. 5.1 for fifty initial conditions (column) at different numerical precision p (row). **b** $\hat{\mu}_{\mathcal{B}}$ of the four attractors at different levels of p using R. For Eqn. 5.2, $\hat{\mu}_{\mathcal{B}}$ is estimated at different levels of p using **c** R_1,**d** R_2 (range of Fig. 5.2b) and **e** R_3 (range of Fig. 5.2c). In all subfigures, the shading indicates the standard error of $\hat{\mu}_{\mathcal{B}}(p = 16)$ and the bar colours indicate which attractor the system converges to. Adapted from [P7].

$[-2, 4]$. Fig. 5.3a confirms that the chosen precision can strongly influence the asymptotic outcome for single trajectories, especially for the cases highlighted by arrows. Nevertheless, for most initial conditions, increasing the precision does not influence the final-state determination. This is manifested in the humble variation of $\hat{\mu}_{\mathcal{B}}$ in Fig. 5.3b, indicating that the individual estimates $\hat{\mu}_{\mathcal{B}}(p)$ are within the standard error of the most precise estimate $\hat{\mu}_{\mathcal{B}}(16)$ for most precision values p. Furthermore, no systematic dependence on p can be identified.

These results suggest that the final-state sensitivity is inherent only close to the boundary points, leaving large parts of the interior of the basins – and hence their probability measure – almost unaffected.

In the case of the intermingled basins for the quadratic map, three different regions, the reference subset $R_1 = [-1.8, 2.4] \times [-2.4, 1.8]$ and two zoom-ins R_2/R_3 as pictured in Fig. 5.2, are chosen. While R_2 contains no points on an attractor, R_3 is centred around the red attractor on the horizontal line segment. As above, an ensemble of $T = 1,000$ initial conditions is used to estimate $\hat{\mu}_{\mathcal{B}}(p)$. Fig. 5.3c shows strong variations of $\hat{\mu}_{\mathcal{B}}$ up to 50% compared to $\hat{\mu}_{\mathcal{B}}(16)$, again with no apparent systematic dependence on p. It turns out to be similar when ρ is restricted to R_2 instead, although the variations relative to $\hat{\mu}_{\mathcal{B}}(16)$ in Fig. 5.3d are smaller. Both experiments R_1 and R_2 indicate an erratic dependence of $\hat{\mu}_{\mathcal{B}}$ on the numerical precision. The rounding errors are comparable or even larger than the standard error of the sampling, hence dominating the overall estimation error.

Contrarily, Fig. 5.3e shows a very different picture for R_3 with mostly slight varia-

tions of $\hat{\mu}_{\mathcal{B}}(p)$ within the standard error of $\hat{\mu}_{\mathcal{B}}(16)$. This somehow counter-intuitive behaviour can be explained by the foliated structure of the basins close to the attractor. In particular, it has been shown for riddled basins that the probability measure of a basin restricted to an ε-neighbourhood of the corresponding attractor approaches unit probability when $\varepsilon \to 0$ (Alexander et al. 1992). In this case, the dominance of the red basin close to its attractor would be expected. This is indeed corroborated by the relative values of $\hat{\mu}_{\mathcal{B}}(p)$ for the red attractor at each precision p in Fig. 5.3e.

5.3.3. Implications for Basin Stability

In conclusion, I demonstrated above that there are limitations to a basin stability estimation for riddled basins of attraction. Despite that, there still is potential for an estimation if only the basin boundaries are of a fractal nature. In general, it is recommended to consider the highest available numerical precision p_h, since any numerical procedure is subject to rounding errors and since intricate basin geometries are common in physical systems (cf. Sec. 2.4.3). If no a priori knowledge on the final-state sensitivity of a specific system is given, the following strategy might help:

1. Start (if possible) with a visualisation of the relevant part of the phase space (or a lower-dimensional cross-section) to get a first idea of the appearance of fractal sets.
2. Repeat the estimation of $\hat{\mu}_{\mathcal{B}}$ (sample size N) at p_h and a lower precision p_l.
3. Derive a (rough) estimate $\hat{e}_p = |\hat{\mu}_{\mathcal{B}}(p_h) - \hat{\mu}_{\mathcal{B}}(p_l)|$ of the rounding error due to the variation of $\hat{\mu}_{\mathcal{B}}$ with p.
4. Compare $\hat{e}_p$ with the standard error of the most precise sampling $\hat{s}_{p_h} = \sqrt{\hat{\mu}_{\mathcal{B}}(p_h)\,(1 - \hat{\mu}_{\mathcal{B}}(p_h))/N}$ to get an indication whether rounding has a significant impact on the overall estimation error.

Although the effect of final-state sensitivity has been presented here for two low-dimensional examples, it is expected that the inherent estimation problems – and strategies to cope with them – directly transfer to high-dimensional systems and are important to be considered in future research. In particular, for a fractal basin boundary with dimension d, the uncertainty fraction (quantifying final-state sensitivity, cf. Sec. 2.4.3) mainly depends on the difference $D - d$ where D is the phase space dimension. Note that necessarily $D - d \leq 1$ for a boundary to actually separate sets in a phase space. Hence, if present, the contribution of rounding errors is expected to vary only marginally with D. Moreover, the same holds for the overall estimation error, as the standard error of the sampling is independent of D.

5.4. Finite-Time Basin Stability: The Rate of Repeated Perturbations

This section refers to research originally published in [P6].

Abstract I discuss dynamical systems with repeated perturbations, introduce finite-time basin stability and derive a lower bound on the cumulative probability of staying within the basin of an attractor.

5.4.1. A Dynamical System Subject to Repeated Jumps

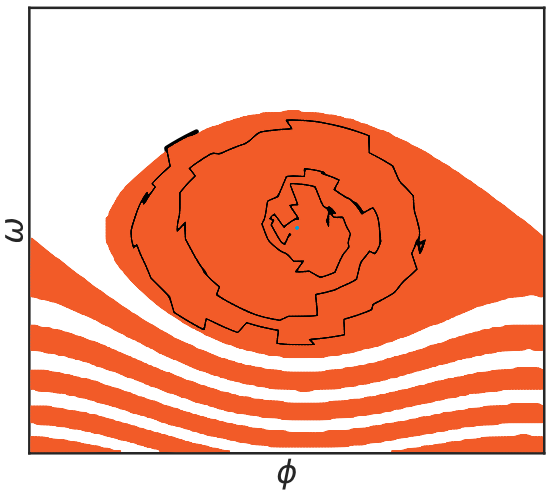

Figure 5.4. – **Example realisation**: A perturbed trajectory subjected to jumps (Eqn. 5.4) with small T for an infinite-busbar with phase ϕ and frequency ω (Eqn. 5.28). The figure has been previously published in [P6].

In the preceding discussion we encountered probabilistic stability approaches, especially basin stability (Menck, Heitzig, Marwan, et al. 2013). They are based on considering single, possibly large, finite-size perturbations. In this section, I refer to such singular perturbations as *jumps*. It is reasonable, though, to consider the effect of repeated jumps. With regard to power grids, for instance, jump sequences originate from consumer behaviour or intermittent renewables. Under such conditions, an essential question is whether the outcome of subsequent jumps is independent, meaning that they don't build up a displacement of the system's state leading to a transgression of the basin boundary.

Consider a multistable dynamical system as in Sec. 2.2.1 with an equilibrium $x^\star$ at the origin[4]

$$\dot{x} = f(x) \ . \tag{5.3}$$

The system is subjected to a possibly infinite sequence of jumps with random magnitude Δx_i at discrete times t_i, but otherwise deterministic. It is not further specified whether the jumps appear regularly or according to a stochastic process, except for the minimal interval between subsequent perturbations $T := \min_i (t_i - t_{i+1})$. Then, the time evolution is obtained from solutions to the integral equation

[4] In the following, I restrict the discussion to fixed points $x^\star$.

$$x(t) = \int_0^t dt' \, f\left(x\left(t'\right)\right) + \int_0^t dt' \sum_{i=0}^{\infty} \Delta x_i \delta\left(t' - t_i\right) \ . \tag{5.4}$$

Furthermore, the cumulative *number of jumps* $n(t)$ at a time t is

$$n(t) = \int_0^t dt' \sum_{i=0}^{\infty} \delta\left(t' - t_i\right) \ . \tag{5.5}$$

This formulation of a system consisting of a deterministic part and a jump process is very general and approximates important stochastic processes like, for instance, Levy noise in an asymptotic regime (Pavlyukevich 2007a,b). An example realisation for Eqn. 5.4 with small T is illustrated in Fig. 5.4 for the infinite-busbar model which is considered later in more detail. For now, this figure serves as an illustration on how repeated jumps build up a displacement, potentially exiting the basin of attraction. At each instance of a jump, the resulting state remains in the basin $\mathcal{B}\left(x^\star\right)$ with a certain probability. The *remain probability* P_{remain} is in general related to the *first-exit time* distribution (Redner et al. 2002) p_{fe} from the basin:

$$\begin{aligned} P_{remain}(t, x(0)) &:= P\left(\forall_{0 \le t' \le t} \, x\left(t'\right) \in B\right) \\ &= 1 - \int_0^t p_{fe}\left(t'\right) dt' \ . \end{aligned} \tag{5.6}$$

When the jumps are sufficiently rare, i.e. when T is small enough, perturbed trajectories return close enough to $x^\star$ such that the probability P_{remain} is independent of jumps at previous times and given by the basin stability $\mu_{\mathcal{B}}$ of $x^\star$. To further formalise this idea, "sufficiently rare" as well as "close enough" need to be quantified.

5.4.2. A Measure for Approximate Independence

The basin stability of a fixed point $x^\star$ of Eqn. 5.3 is determined by considering a distribution $\rho\left(x - x^\star\right)$ of initial conditions, as defined in Eqn. 2.24.

When the system's state is on the attractor $x^\star$, the probability that a jump ends up in $\mathcal{B}\left(x^\star\right)$ is exactly the basin stability $\mu_{\mathcal{B}}$. After the system evolved for some time, another jump occurs while the system is at a state y. The probability to remain in $\mathcal{B}\left(x^\star\right)$ then is given by the basin stability $\mu_{\mathcal{B}}|_y$ of the shifted probability density $\rho_y := \rho\left(x - y\right)$:

$$\mu_{\mathcal{B}}|_y := \int\limits_{R \subseteq X} \mathbf{I}_{\mathcal{B}(x^\star)}\left(x\right) \rho\left(x - y\right) \, dx \ \in [0; 1] \ . \tag{5.7}$$

Hence, the remain probability of the second jump depends on the previous out-

come (i.e. the state[5] $y = y(t_{i+1}^-)$ just before the next jump at t_{i+1}) such that they are not statistically independent. Only if the system equilibrated to $x^\star$ within T this would be the case. This motivates the definition that two jumps are considered to be *approximately independent* if the corresponding shifted probability densities differ at most by a small *tolerance* ϵ. The difference can be measured by d_ρ as

$$d_\rho(x,y) = \int_X du\, |\rho(u-x) - \rho(u-y)| \,. \tag{5.8}$$

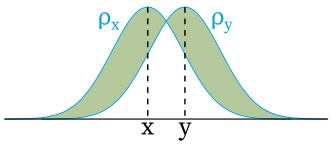

Figure 5.5. – **Schematic representation of approximate independence**: The difference between the probability density ρ_x centred at x and the shifted density ρ_y, $d_\rho(x,y)$ is given by the shaded green area. The figure has been previously published in [P6].

Fig. 5.5 schematically illustrates the concept for an exemplary one-dimensional system. The difference between the distribution at x and a shifted density ρ_y is measured by $d_\rho(x,y)$ (shaded green area) and vanishes only for $x = y$.

Now, the expectation value of a scalar observable $\chi(x)$ satisfying $|\chi(x)| \leq 1$ with respect to the two densities ρ and ρ_y differs at most by $d_\rho(x^\star, y)$:

$$\begin{aligned} &\left| \int_X \chi(u)\,\rho(u)\; du - \int_X \chi(u)\,\rho_y(u)\; du \right| \\ &\leq \int_X |\chi(u)|\,|\rho(u) - \rho_y(u)|\, du \\ &\leq \int_X |\rho(u) - \rho_y(u)|\, du \\ &= d_\rho(x^\star, y) \end{aligned} \tag{5.9}$$

This relation holds especially also for basin stability such that

$$|\mu_\mathcal{B} - \mu_\mathcal{B}|_y| \leq d_\rho(x^\star, y) \;. \tag{5.10}$$

Consequently, Eqn. 5.8 can be used to define a set U_ϵ as

$$U_\epsilon := \{y \in X \,:\, d_\rho(x^\star, y) \leq \epsilon\} \tag{5.11}$$

that comprises all states which are close enough to the equilibrium such that the outcome of repeated jumps is approximately independent within the tolerance ϵ. Moreover, for all points $u \in U_\epsilon$ the basin stability difference is bounded by $|\mu_\mathcal{B} - \mu_\mathcal{B}|_u| \leq \epsilon$.

How $d_\rho(x^\star = 0, y)$ depends on the displacement y can be directly calculated for certain densities ρ. In the following, I briefly derive $d_\rho(x^\star, y)$ for multivariate Gaussian and bounded uniform distributions.

[5] t_i^+ and t_i^- denote the right and left limit of t to the jump time t_i, respectively.

Multivariate Gaussian Suppose, there is a D-dimensional system with variables $x = (x_1, ..., x_D)^\top$ and a phase space $X \subseteq \mathbb{R}^D$. A multivariate Gaussian distribution of initial conditions centred at a fixed point $x^\star$ at the origin generally has the form

$$\rho(x) = \frac{1}{\sqrt{(2\pi)^D \det(M)}} \mathrm{e}^{-\frac{1}{2}(x-x^\star)^\top \mathbf{M}^{-1}(x-x^\star)} , \tag{5.12}$$

where $\mathbf{M}$ is the covariance matrix. By a change of variables, the covariance matrix becomes diagonal with entries $M_{kk} = \sigma_k^2$ such that $\rho(x) = \prod_{i=1}^D f_i(x_i)$ factorises and σ_k^2 is the variance of f_k. The factors f_k are given by

$$f_k(x_k) = \frac{1}{\sqrt{2\pi\sigma_k^2}} \mathrm{e}^{-\frac{1}{2}\left((x_k - x_k^\star)/\sigma_k\right)^2} \tag{5.13}$$

Without loss of generality, let us assume that $y_k > 0$ for all k. Then, Eqn. 5.8 yields[6]:

$$\begin{aligned}
d_\rho(x^\star, y) &= \prod_{k=1}^D \frac{1}{\sqrt{2\pi\sigma_k^2}} \int_{-\infty}^{\infty} \left| \mathrm{e}^{-\frac{1}{2}\left(\frac{x_k}{\sigma_k}\right)^2} - \mathrm{e}^{-\frac{1}{2}\left(\frac{x_k - y_k}{\sigma_k}\right)^2} \right| dx_k \\
&= \prod_{k=1}^D \frac{1}{\sqrt{2\pi\sigma_k^2}} \int_{-\infty}^{\infty} \left| \mathrm{e}^{-\frac{1}{2}\left(\frac{u_k + y_k/2}{\sigma_k}\right)^2} - \mathrm{e}^{-\frac{1}{2}\left(\frac{u_k - y_k/2}{\sigma_k}\right)^2} \right| du_k \\
&= \prod_{k=1}^D \frac{2}{\sqrt{2\pi\sigma_k^2}} \int_{0}^{\infty} \left(\mathrm{e}^{-\frac{1}{2}\left(\frac{u_k + y_k/2}{\sigma_k}\right)^2} - \mathrm{e}^{-\frac{1}{2}\left(\frac{u_k - y_k/2}{\sigma_k}\right)^2} \right) du_k \\
&= \prod_{k=1}^D \sqrt{\frac{2}{\pi}} \left(\int_{-y_k/(2\sigma_k)}^{\infty} \mathrm{e}^{-\frac{1}{2}v_k^2} dv_k - \int_{y_k/(2\sigma_k)}^{\infty} \mathrm{e}^{-\frac{1}{2}v_k^2} dv_k \right) \\
&= \prod_{k=1}^D 2\,\mathrm{erf}\left(\frac{1}{\sqrt{2}} \frac{y_k}{2\sigma_k} \right) .
\end{aligned} \tag{5.14}$$

Bounded uniform distributions Analogously, consider the case of a continuous uniform distribution ρ on a rectangular region of the phase space X with symmetric bounds $a_k > 0$ in every dimension.

$$\rho(x - y) = \frac{1}{C} \mathbf{I}_{R(y)}(x) , \tag{5.15}$$

where $R(y)$ is given by

$$R(y) = \{ x \in X : -a_k < x_k - y_k < a_k \text{ for } 1 \le k \le D \} . \tag{5.16}$$

[6] $\mathrm{erf}(x) := \frac{2}{\sqrt{\pi}} \int_0^x \mathrm{e}^{-t^2} dt$ is the so-called error function.

The volume $C = \prod_{k=1}^{D} 2a_k$ of $R(y)$ clearly depends only on the boundaries but not on the offset vector y. Plugging this into Eqn. 5.8 yields:

$$\begin{aligned} d_\rho(x^\star, y) &= \int_X d^D x \, |\rho(x) - \rho(x-y)| \\ &= \frac{1}{C} \int_X d^D x \, |\mathbf{I}_{R(x^\star)}(x) - \mathbf{I}_{R(y)}(x)| \\ &= \frac{1}{C} \int_X d^D x \, \mathbf{I}_{(R(x^\star) \cup R(y)) \setminus (R(x^\star) \cap R(y))}(x) \\ &= \frac{1}{C} \int_X d^D x \, \mathbf{I}_{R(x^\star)}(x) + \mathbf{I}_{R(y)}(x) - 2\mathbf{I}_{R(x^\star)}\mathbf{I}_{R(y)}(x) \\ &= 2 - \frac{2}{C} \int_X d^D x \, \mathbf{I}_{R(x^\star)}\mathbf{I}_{R(y)}(x) \\ &= 2 - \frac{2}{C} \prod_{k=1}^{D} (2a_k - |y_k|) \, \Theta(2a_k - |y_k|) \end{aligned} \tag{5.17}$$

For general choices of ρ, d_ρ can still be approximated. Typically, ϵ is required to be small such that U_ϵ (Eqn. 5.11) can be approximated as

$$U'_\epsilon \simeq \{x \in X : \|x\| \leq \epsilon C_\rho\} . \tag{5.18}$$

C_ρ is a constant determined from a linearisation of Eqn. 5.8 as

$$\begin{aligned} d_\rho(x^\star, y) &\simeq \int_X |y \cdot \nabla\rho(x')| dx' \leq \|y\| \int_X \|\nabla\rho(x')\| dx' , \\ C_\rho &:= \left(\int_X \|\nabla\rho(x')\| dx' \right)^{-1} , \end{aligned} \tag{5.19}$$

where $\nabla\rho$ denotes the gradient of ρ. Hence, close to the fixed point at the origin, the function $d_\rho(x^\star, y)$ scales linearly with the distance and C_ρ is a distribution-specific coefficient. C_ρ can be determined in two ways. On the one hand, the potentially high-dimensional integral Eqn. 5.19 can be numerically evaluated using a Monte Carlo scheme (if the derivative is bounded). On the other hand, it can again be explicitly calculated for certain classes of distributions $\rho(x)$.

In conclusion, the construction of U_ϵ yields a neighbourhood of $x^\star$ which finds its use as a *return set*. A trajectory is considered to have returned sufficiently close to $x^\star$ when it enters U_ϵ and does not leave again. This construction appears unintuitive at first but is directly related to the notion of approximate independence of consecutive jumps.

Now that a return criterion is defined, one might ask for an arbitrary initial con-

dition $u \in \mathcal{B}(x^\star)$ how long it takes to reach U_ϵ. This *return time* is finite and can be determined in a robust way, using a *time-tracking Lyapunov function* V.

Let V be a Lyapunov function as in Sec. 2.4.1 which is defined on $\mathcal{B}(x^\star)$ and chosen such that

$$\frac{d}{dt} V(x(t)) = -1 \,, \tag{5.20}$$

i.e. it strictly decreases along any trajectory $x(t)$. To see that the values of V indeed track the time, take $x(t)$ and $x(t')$ as two points on the same trajectory at times t and t'. By integrating the above equation, we get

$$V(x(t)) - V\left(x(t')\right) = t - t' \,. \tag{5.21}$$

As the time-tracking is only defined up to a reference point at t', the boundary condition $V(S) = 0$ on a transverse surface S needs to be given for fully specifying such a Lyapunov function. For a certain choice of S, the time-tracking Lyapunov function will be denoted by V_S.

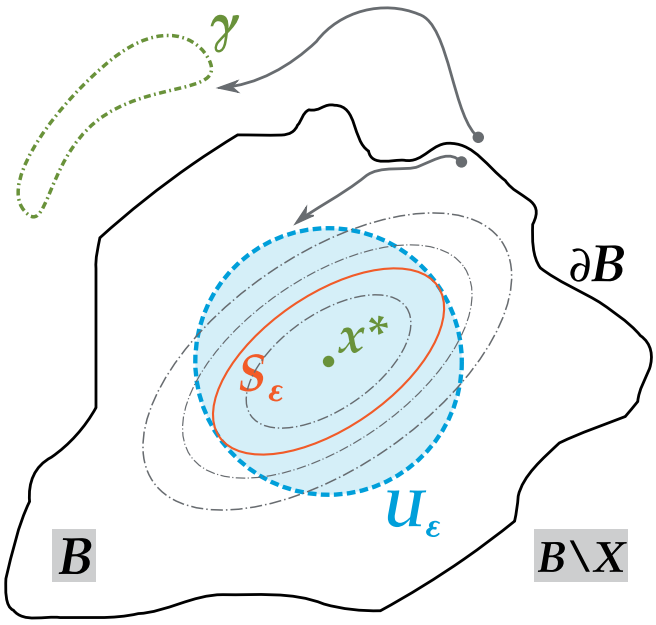

Figure 5.6. – **Schematic illustration of S_ϵ**: This figure illustrates the relation of the sets U_ϵ and the surface S_ϵ, given the basin of attraction $\mathcal{B}$ of a the fixed point $x^\star$ with boundary $\partial\mathcal{B}$ in a phase space X. The dash-dotted lines indicate level lines (transverse surfaces) of a time-tracking Lyapunov function V_S. In a multistable system, trajectories either approach the fixed point or other attractors, for instance a limit cycle γ. The figure has been previously published in [P6].

A convenient choice for S is a transverse surface S_ϵ entirely contained within U_ϵ, as illustrated in Fig. 5.6. Finding the largest S_ϵ in practice involves, however, a

geometric optimisation problem.

For small ϵ, the return set U'_ϵ is a sphere around $x^\star$ (Eqn. 5.18). Hence, one might make use of the quadratic Lyapunov function V^{lin} associated to the linearised dynamical system in U'_ϵ with Jacobian matrix $\mathbf{J}$. Then, $V^{lin}(x) := x^\top \mathbf{L} x$ is determined via the Lyapunov equation

$$\begin{aligned} \dot{V}^{lin}(x) = x^\top \left(\mathbf{J}^\top \mathbf{L} + \mathbf{L}\mathbf{J}\right) x = -x^\top \mathbf{Q} x \\ \mathbf{J}^\top \mathbf{L} + \mathbf{L}\mathbf{J} = -\mathbf{Q} \,. \end{aligned} \tag{5.22}$$

The matrix $\mathbf{Q}$ should be chosen such that the transverse surfaces of V^{lin} are as spherical as possible. Then, S_ϵ can be approximated by a transverse surface of V^{lin}. To be entirely contained within U'_ϵ, the maximal extent x_{max} of the transverse surface needs to be smaller than ϵC_ρ. As the maximal extent is given in the eigendirection of $\mathbf{L}$ corresponding to the smallest eigenvalue λ, we have:

$$S_\epsilon \simeq \{x \in X \,:\, x^\top \mathbf{L} x = \lambda \left(\epsilon C_\rho\right)^2\} \,. \tag{5.23}$$

In summary, I defined what it means to return to an equilibrium closely enough and discussed how time-tracking Lyapunov function can be applied to obtain return times. With these ingredients, the *finite-time basin stability* is finally defined as

$$\mu_{\mathcal{B}}(T) := \int_X \mathbf{I}_{\mathcal{B}(x^\star)}(x)\, \Theta\left(T - V_S(x)\right) \rho(x)\; dx \;\in [0;1] \,. \tag{5.24}$$

$\mu_{\mathcal{B}}(T)$ is the probability that a trajectory returns to within S_ϵ in a finite time T, given a distribution $\rho(x)$ of jumps. It is an extension of basin stability as defined in Sec. 2.4.2, measuring the subset of $\mathcal{B}(x^\star)$ of initial conditions from which the return time to S_ϵ is at most T. Thus, finite-time basin stability is a novel probabilistic stability measure taking a bound on the return time into account. In the following section, I discuss how $\mu_{\mathcal{B}}(T)$ induces a characteristic time scale to a dynamical system.

5.4.3. Independence Time and Remain Probability

Taking a closer look at Eqn. 5.24, one expects that the finite-time basin stability $\mu_{\mathcal{B}}(T)$ asymptotically approaches $\mu_{\mathcal{B}}$ from below as $\lim_{T\to\infty} \mu_{\mathcal{B}}(T) = \mu_{\mathcal{B}}$. Furthermore, $\mu_{\mathcal{B}}(T)$ is monotonous in T. Hence, there is a $\delta > 0$ and a critical time scale $T_{ind}(\epsilon, \delta)$ – the *independence time* of a dynamical system – such that:

$$T_{ind}(\epsilon, \delta) := \inf\{T > 0 \,:\, \mu_{\mathcal{B}} - \mu_{\mathcal{B}}(T) \leq \delta\} \,. \tag{5.25}$$

The independence time has a clear interpretation as the critical time scale for the frequency of repeated jumps. If a perturbed trajectory returns to within U_ϵ before

the next jumps, i.e. when the return time is less than $T_{ind}(\epsilon, \delta)$, the outcomes are approximately independent. In this case, the remain probability P_{remain} is approximately given by the asymptotic basin stability $\mu_{\mathcal{B}}$.

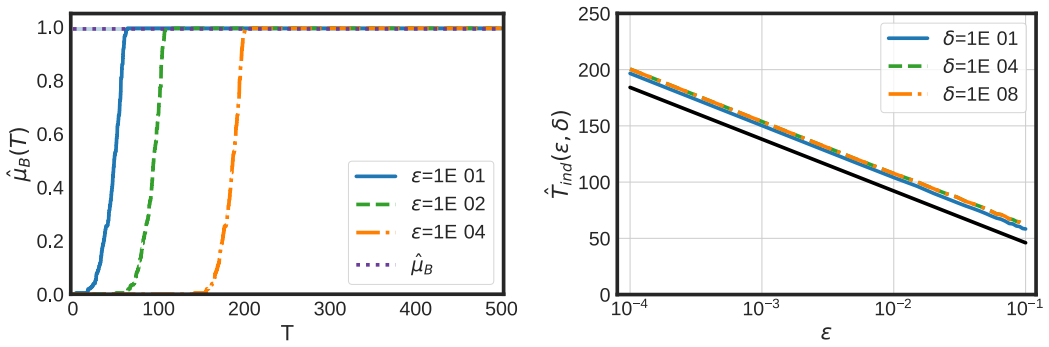

Figure 5.7. – $\mu_{\mathcal{B}}(T)$ **curves and independence times**: **a** $\hat{\mu}_{\mathcal{B}}(T)$ curves (Eqn. 5.24) for various tolerances ϵ. The dotted horizontal line is the asymptotic basin stability estimate $\hat{\mu}_{\mathcal{B}}$. **b** The estimate $\hat{T}_{ind}(\epsilon, \delta)$ for various δ as a function of ϵ. The figure has been previously published in [P6].

To obtain an estimate for $T_{ind}(\epsilon, \delta)$, it is necessary to evaluate $\mu_{\mathcal{B}}(T)$ for a series of T, i.e. a finite-time basin stability curve as pictured in Fig. 5.7a. In the following, I present an efficient numerical procedure to estimate finite-time basin stability and independence times.

As a probabilistic stability measure, finite-time basin stability is amenable to a sampling-based Monte Carlo estimation analogous to that of the original basin stability. When a Lyapunov function V_S is known, the integrand in Eqn. 5.24 can be directly evaluated. If this is not the case, the sampling can be performed as follows:

1. Fix a distribution ρ and choose a tolerance ϵ.
2. Determine S_ϵ from the linear approximation or evaluate $d_\rho(x^\star, x)$ directly in the next steps.
3. Draw N random initial conditions from ρ centred at $x^\star$[7].
4. Numerically integrate the system and record
   (i) if the trajectory returns to S_ϵ before a cut-off time T^c
   (ii) and the return time T if applicable.

From M_T, the number of trajectories returning to S_ϵ within time $T < T^c$ or less, and the total number N of trajectories sampled, an estimator $\hat{\mu}_{\mathcal{B}}(T)$ for finite-time basin stability is given by

$$\hat{\mu}_{\mathcal{B}}(T) = \frac{M_T}{N} \tag{5.26}$$

[7]Step 3 can easily be adjusted to network-local perturbations at single nodes in a network, creating a *finite-time single-node basin stability*.

As for a fixed T, trajectories either return or not, the sampling can be regarded as a Bernoulli experiment and the standard error $e_{\hat{\mu}_{\mathcal{B}}(T)}$ is given by the well-known relation (cf. Sec. 2.4.2)

$$e_{\hat{\mu}_{\mathcal{B}}(T)} = \sqrt{\frac{\hat{\mu}_{\mathcal{B}}(T)\left(1-\hat{\mu}_{\mathcal{B}}(T)\right)}{N}} \,. \tag{5.27}$$

Hence, $\mu_{\mathcal{B}}(T)$ can be efficiently estimated also for high-dimensional systems. Fig. 5.7 illustrates the finite-time basin stability curves resulting from such a numerical procedure. The system used as an example here is the infinite-busbar model (Eqn. 4.17) for a node in a power grid

$$\begin{aligned} \dot{\phi} &= \omega \\ \dot{\omega} &= P - \alpha\omega - K\sin\left(\phi + \arcsin\frac{P}{K}\right) \,, \end{aligned} \tag{5.28}$$

with the power input $P = 1$, damping $\alpha = 0.1$ and coupling $K = 8$. The reference point of the phase is shifted by $\arcsin\frac{P}{K}$ such that the fixed point $x^\star = (\phi^*, \omega^*)$ is at the origin.

The distribution $\rho(\phi, \omega)$ is chosen to be uniform on

$$R(\phi, \omega) = [\phi - \pi/3; \phi + \pi/3] \times [\omega - 5; \omega + 5]$$

and d_ρ can be directly evaluated using Eqn. 5.17. $\mu_{\mathcal{B}}(T)$ is estimated using $N = 20,000$ initial conditions such that $e_{\hat{\mu}_{\mathcal{B}}(T)}$ is at most 0.4%.

For this choice, $\hat{\mu}_{\mathcal{B}} = 0.9874 \pm 0.0008$ is close to one, i.e. the probability that the system's state remains in the basin of attraction after a single jump is very high. This set-up is chosen on purpose to demonstrate the complementary information that can be derived from $\mu_{\mathcal{B}}(T)$ even if the attractor is very stable regarding singular perturbations. In particular, Fig. 5.7a shows a steep decrease of $\hat{\mu}_{\mathcal{B}}(T)$ for small return times T. This means that when T is too small, repeated jumps quickly build up a displacement that transgresses the basin boundary.

The smallest T fulfilling the relation $|\hat{\mu}_{\mathcal{B}} - \hat{\mu}_{\mathcal{B}}(T)| < \delta$ then is an estimate $\hat{T}_{ind}(\epsilon, \delta)$ for the independence time. Due to the steep increase in the finite-time basin stability curve, $\hat{T}_{ind}$ depends only marginally on δ for this particular system as Fig. 5.7b shows. The important parameter here is the tolerance ϵ. The semi-logarithmic scale indicates an exponential scaling of $\hat{T}_{ind}(\epsilon, \delta)$ with ϵ in the norm d_ρ due to the exponential slowing down of a dynamical system in the linear regime close to an asymptotically stable fixed point like $x^\star$. The exponent is given by the real part $\nu = -\alpha/2$ of the two conjugated eigenvalues of the Jacobian $\mathbf{J}(x^\star)$ associated to Eqn. 5.28 (solid black line in Fig. 5.7b). This result corroborates the findings of Kittel et al. (2017) for the same system with similar parameters. There, the authors identify an exponential scaling with respect to the integrated distance to $x^\star$.

Lastly, it is also possible to derive the following proposition on the probability P_{remain} to remain in the basin, returning to the initial considerations of this section

in Eqn. 5.6.

Proposition 1 (Lower bound)**.** *Consider a dynamical system subject to repeated jumps as in Eqn. 5.4 with phase space X and an asymptotically stable fixed point $x^\star$ at the origin. Assume that the time T between consecutive jumps is larger than the independence time $T_{ind}(\epsilon, \delta)$.*

Let $P_{remain}(t, x(0))$ be the probability to remain within the basin of attraction $\mathcal{B}(x^\star)$ up until time t. Given that the initial condition $x(0)$ is contained in the set $\bar{S}_\epsilon$ bounded by S_ϵ near the attractor, the following lower bound holds:

$$P_{remain}(t, x(0)) \geq (\mu_{\mathcal{B}} - \delta - \epsilon)^{n(t)}$$

Proof. Consider the sequence of jumps occurring at times t_i that are drawn from $\rho\left(x - x\left(t_i^-\right)\right)$. The general bound Eqn. 5.9 implies that within $\bar{S}_\epsilon$

$$\mu_{\mathcal{B}}|_{x\left(t_i^-\right)}(t_{i+1} - t_i) \geq \mu_{\mathcal{B}}(t_{i+1} - t_i) - \epsilon \,.$$

The left-hand side, i.e. the shifted finite-time basin stability, corresponds to the probability that the system's state returns to $\bar{S}_\epsilon$ before the next jump, given it originated there as well. Hence, we can write

$$\begin{aligned} P\left(x(t_{i+1}^-) \in \bar{S}_\epsilon \,|\, x(t_i^-) \in \bar{S}_\epsilon\right) &= \mu_{\mathcal{B}}|_{x\left(t_i^-\right)}(t_{i+1} - t_i) \\ &\geq \mu_{\mathcal{B}}(t_{i+1} - t_i) - \epsilon \,. \end{aligned}$$

Now, $\min_i(t_{i+1} - t_i) = T > T_{ind}(\epsilon, \delta)$ implies that the perturbations are rare enough such that the outcomes of consecutive jumps are approximately independent and $\mu_{\mathcal{B}}(t_{i+1} - t_i) = \mu_{\mathcal{B}}(T)$. Using Eqn. 5.25, we further have

$$\mu_{\mathcal{B}}(t_{i+1} - t_i) - \epsilon \geq \mu_{\mathcal{B}} - \delta - \epsilon \,.$$

Hence, the probability P_{remain} to remain in $\mathcal{B}(x^\star)$ for at least $n(t)$ jumps spaced $T > T_{ind}(\epsilon, \delta)$ apart is bounded as

$$\begin{aligned} P_{remain}(x([0;t]) \in \mathcal{B}(x^\star)) &\geq P\left(x(t_{n(t)}^+) \in \mathcal{B}(x^\star) \,|\, x(t_{n(t)}^-) \in \bar{S}_\epsilon\right) \cdot \\ &\quad \cdot \prod_{i=1}^{n(t)-1} P\left(x(t_{i+1}^-) \in \bar{S}_\epsilon \,|\, x(t_i^-) \in \bar{S}_\epsilon\right) \\ &\geq \mu_{\mathcal{B}}|_{x(t_{n(t)}^-)} \prod_{i=1}^{n(t)-1} (\mu_{\mathcal{B}} - \delta - \epsilon) \\ &\geq (\mu_{\mathcal{B}} - \epsilon)(\mu_{\mathcal{B}} - \delta - \epsilon)^{n(t)-1} \\ &\geq (\mu_{\mathcal{B}} - \delta - \epsilon)^{n(t)} \end{aligned}$$

□

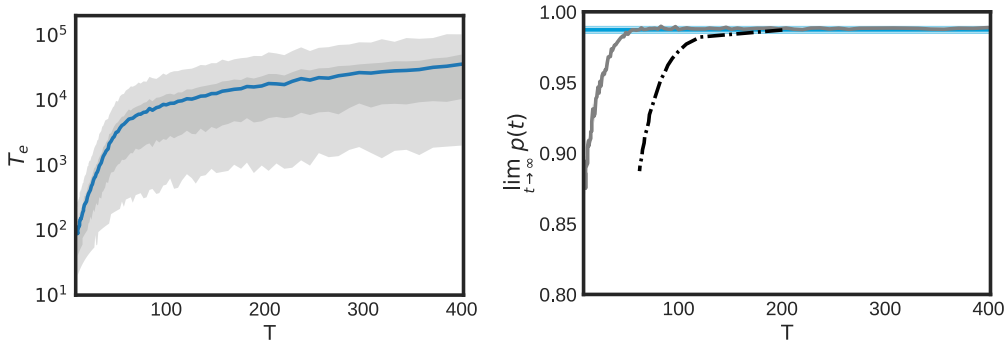

Figure 5.8. – **Asymptotic bound on the remain probability**: **a** Expected first exit time T_e from the basin vs. the perturbation interval T. The shading indicates the 5%, 25%, 75% and 95% percentiles of the distribution (bottom to top). **b** Asymptotic limit of $p(t)$ vs. T derived from 100 realisations each. The horizontal blue line indicates $\hat{\mu}_{\mathcal{B}}$ and the dash-dotted black curve corresponds to the lower bound given by Prop. 1. The figure has been previously published in [P6].

The bound is illustrated in Fig. 5.8. For 100 values of T between 10 and 400, the remain probability is estimated from 1,000 realisations of jump sequences each. At each jump time t_i, a random displacement is chosen from $\rho_{x(t_i^-)}$ centred at the current state. Then the first exit time distribution is estimated as given in Fig. 5.8a, yielding an estimate $\hat{P}_{remain}$ for each T from the cumulative of the distribution. For convenience, define $p(t) = \hat{P}_{remain}^{1/n(t)}$. The asymptotic limit of $p(t)$ is plotted in Fig. 5.8b and the lower bound is given for comparison (black, dash-dotted curve). It is determined as

$$\mu_{\mathcal{B}} - \delta - \epsilon\left(\hat{T}_{ind}\right) \ . \tag{5.29}$$

Here, $\epsilon\left(\hat{T}_{ind}\right)$ is given by inverting the logarithmic relation in Fig. 5.7b and yields the corresponding value of ϵ for which T would be the independence time. The tolerance is fixed to $\delta = 10^{-8}$.

As expected, Eqn. 5.42 provides a lower bound on the remain probability. The deviation is mainly due to the bound given in Eqn. 5.9 for the shifted (finite-time) basin stability, which is rather conservative. Furthermore, for small T there is a non-negligible contribution to the remain probability from jumps that cancel out each other.

Related studies investigated the exit time distribution for basin escapes in systems subject to Levy noise (Serdukova et al. 2016, 2017). As mentioned above the present framework (Eqn. 5.4) approximates Levy processes in an asymptotic regime as a deterministic system interspersed with jumps (Pavlyukevich 2007a,b). It remains a subject for future research to investigate whether the bound on the remain probability can be applied to quantify when this asymptotic regime is reached. In particular, the sampling-based approach suggested here should lead to an improved (computationally more efficient) way of performing the analysis in Serdukova et al. (2016).

5.5. Survivability: How to Define Stability Under Constraints?

This section refers to research originally published in [P2].

Abstract In this section, I present a novel stability measure, derive a semi-analytic lower bound and perform numerical tests with a model of the Scandinavian power grid.

5.5.1. Survivability of Deterministic Systems

I DISCUSSED ABOVE, how basin stability crucially depends on the correct identification of asymptotic behaviour. In practical applications, however, asymptotic stability is less important when there are bounds on *transient* deviations of a system. For instance, a European power grid operates at a rated frequency of $50Hz$ and deviations need to be kept within a band of $\pm 200mHz$, as a violation of these bounds leads to the activation of rescue mechanisms – a frequency outside $47.5Hz$ - $51.5Hz$ most likely causes a blackout (ENTSO-E 2016). Hence, the actual trajectory – especially on shorter time-scales – is more important than the long-term asymptotic behaviour. This motivates the concept of *survivability* $\mu_{\mathcal{S}}(t)$ of a dynamical system as a stability measure with respect to transient constraints, or generally a *desirable regime* of its phase space.

Assume that the states of a system can be divided into desirable (allowed) and undesirable regimes. Then, $\mu_{\mathcal{S}}(t)$ is the probability that the state of the system is in the desirable regime (i.e. it fulfils certain constraints) up to time t, given a distribution of initial conditions. The set of the corresponding initial conditions for which the systems remains in the desirable regime (for a finite time t) is referred to as a *(finite-time) basin of survival*. Analogous to using the (volume) measure of the basin of attraction for quantifying asymptotic stability of attractors, survivability uses the (volume) measure of the finite-time basin of survival for quantifying the ability of transients to remain within a given desirable regime.

To illustrate the concept of survivability, consider a simple thought experiment (Fig. 5.9), showing a penguin that attempts to ski down a mountain. The penguin has several different options. The goal serves as an attractor for the skiing penguin. However, for some starting positions (A), the penguin will tumble over a cliff and uncomfortably slide down the mountain. Starting from (B), the penguin reaches the goal safely but might also divert to the valley as an alternative attractor. Instead of explicitly modelling the microscopic state of the penguin, we might declare the cliffs and the valley to be outside the desirable regime. Consequently, the set of starting positions (B) from which the penguin reaches the goal is a basin of survival for all times and entirely contained within the goal's basin of attraction. This is not the case if the valley is considered to be desirable as well. In that case, all starting positions in (B) constitute a basin of survival with no direct relation to the asymptotic behaviour of the penguin. Hence, survivability complements basin stability as a closely-related concept, focusing an transient instead of asymptotic

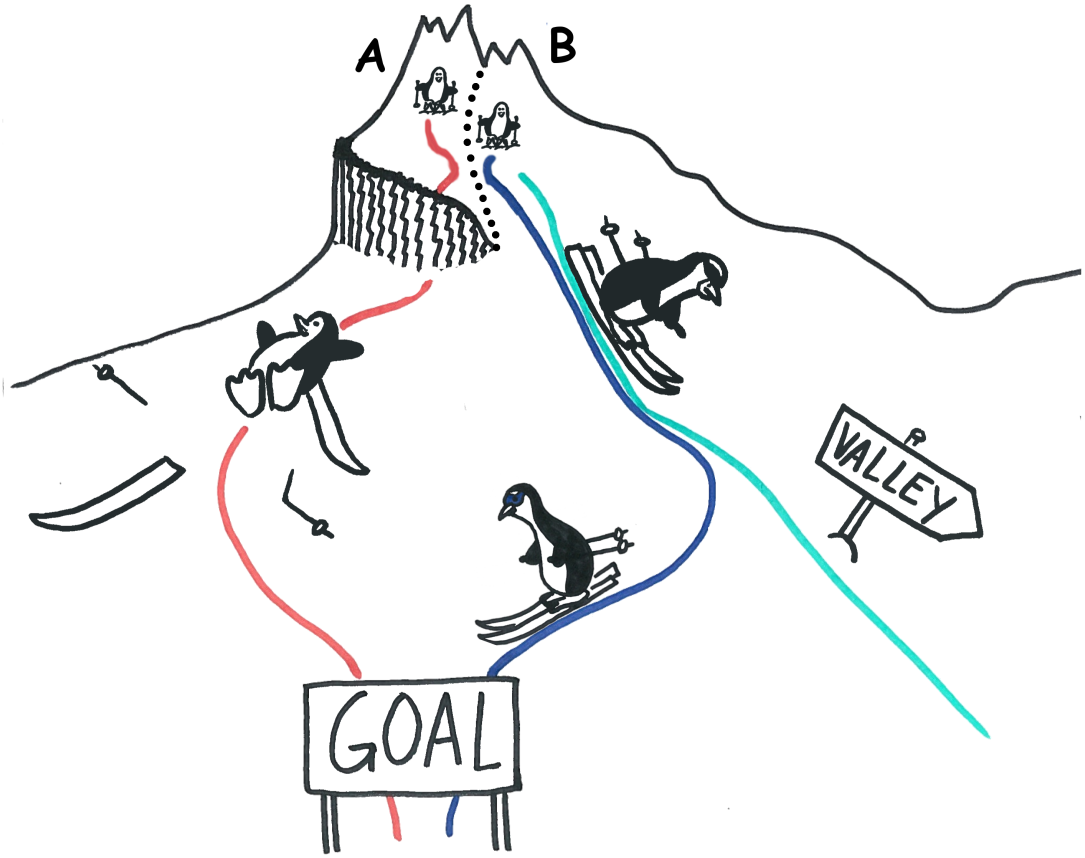

Figure 5.9. – **Survivability cartoon**: Imagine a thought experiment given by a penguin that can ski down a mountain starting from different positions. From (A), the penguin passes cliffs, i.e. an undesirable state, although asymptotically it reaches the goal. Starting from (B), the penguin reaches the goal safely or it might end up in the valley, which might or might not be desirable. The figure has been previously published in [P2].

properties of dynamical systems

An application of survivability is especially appropriate, when external interventions or controllers operate at the dynamical time scale of a system or when the desirable regime corresponds with the validity of model assumptions.

In the following, the concept of survivability is formalised. Take a deterministic dynamical system generating a flow $\varphi_t(x)$ with states x in a phase space X as in Sec. 2.2.1. Given a set of desirable states $X^+ \subset X$, define the t-time basin of survival $X_t^S \subset X^+$ as

$$\begin{aligned} X_t^S &= \{x_0 \in X : \varphi_{[0;t]}(x_0) \in X^+\} \\ &= \bigcup_{0 \le t' \le t} \varphi_{t'}^{-1}(X^+) \ . \end{aligned} \tag{5.30}$$

Now, survivability $\mu_S(t)$ is defined as the probability of hitting X_t^S by randomly drawing an initial state from X:

$$\mu_S(t) = \mu\left(X_t^S\right) = \mu\left(X_t^S | X^+\right) \mu\left(X^+\right) \ . \tag{5.31}$$

The probability measure μ is specified by choosing a probability density ρ that has the interpretation of encoding the importance of relevant perturbed initial conditions (cf. Sec. 2.4.2). An insightful choice of ρ is a uniform probability density, in which case μ is just proportional to the volume. Then, $\mu_S(t)$ directly measures the volume of the t-time basin of survival.

Typically, X^+ does not change over time and does not depend on the dynamics. Hence, $\mu(X^+)$, the probability that an initial condition is drawn from X^+, remains a constant factor. In the following, survivability is used in its definition as the conditional probability for a system to survive initial perturbations originating in the *desirable regime*

$$\mu_S(t) = \mu\left(X_t^S | X^+\right) = \frac{\mu\left(X_t^S \cap X^+\right)}{\mu\left(X^+\right)} \ . \tag{5.32}$$

The measure μ can further be restricted to a certain subset of perturbations. Of particular interest here are network-local perturbations at single nodes of a network. The subspace $X_k \subset X$, corresponding to a node k's degrees of freedom, is a low-dimensional cross-section of X called single-node phase space. Analogous to single-node basin stability, this leads to the definition of *single-node survivability*, i.e. the conditional survivability restricted to network-local perturbations from $X_k \cap X^+$ at a node k of a network is:

$$\mu_S^k(t) = \mu|_{X_k}\left(X_t^S \cap X_k | X^+ \cap X_k\right) = \frac{\mu|_{X_k}\left(X_t^S \cap X_k\right)}{\mu|_{X_k}\left(X^+ \cap X_k\right)} \ . \tag{5.33}$$

The long-term behaviour of (single-node) survivability,

$$\mu_S = \lim_{t\to\infty} \mu_S(t) \ , \tag{5.34}$$

measures the *infinite-time basin of survival* X_∞^S. It is a set of initial conditions such that emanating trajectories remain in X^+ for all times. Typically, $\mu_S^k(t)$ approaches its asymptotic value after a characteristic time scale [P2]. The limit in Eqn. 5.34 exists, as it is bounded by 0 from below and monotonically decreasing with t because each t-time basin of survival is a subset of a previous one ($X_t^s \subseteq X_{t'}^s$ for $t > t'$).

In conclusion, survivability not only inherits the advantages of basin stability, but also offers further desirable properties. In fact, it overcomes the first four points raised in Sec. 6.2 as disadvantages of basin stability. As survivability only depends on the chosen desirable regime, it applies not only to multistable but also to globally stable or unstable systems – depending on the research question. Consequently, no a priori knowledge about attractors is necessary. In the previous chapter, the effect of final-state sensitivity due to basins of a fractal nature on numerically estimating the asymptotics has been discussed. For a majority of important applications, X^+

can be chosen as an open set and the flow $\varphi_t(x) : X \to X$ is continuous or even smooth. In this case, each X_t^S is the union of open sets (the images of X^+) and itself open and therefore commonly measurable. Fortunately, this means that the problems associated to asymptotic sets like final-state sensitivity do not carry over to survivability.

5.5.2. Analytic Results for Linear Systems

For linear systems, an upper bound of the infinite-time basin of survival X_∞^S can be derived, yielding a lower bound to μ_S[8]. Consider the N-dimensional linear system

$$\dot{x}(t) = \mathbf{A}x(t) \ , \tag{5.35}$$

which has N_r real eigenvalues and N_c complex-conjugated pairs such that $N = N_r + 2N_c$. The differential equation can be solved as

$$\begin{aligned} x(t) &= \mathrm{e}^{\mathbf{A}t}x(0) \\ &= \sum_{j=1}^{N_r} c_j \mathrm{e}^{\lambda_j t} v_j + \sum_{j=N_r+1}^{N_r+N_c} \mathfrak{Re}\left(c_j \mathrm{e}^{\lambda_j t} v_j\right) \ . \end{aligned} \tag{5.36}$$

Here, the coefficients c_j are real for the real eigenvalues and complex otherwise. I denote by $\mathfrak{Re}(v_j)/\mathfrak{Im}(v_j)$ the vector of real/imaginary parts of the components of v_j. All eigenvectors are assumed to be linearly independent and all nonzero eigenvalues are assumed to have a negative real part (i.e. the system is damped).

The coefficients c_j are related to the initial conditions $x(0)$ via the equation

$$x(0) = \mathbb{V} \cdot \iota(c) \ . \tag{5.37}$$

Here, we define the real $N \times N$-matrix $\mathbb{V}$ given by the eigenvectors of $\mathbf{A}$ as

$$\mathbb{V} = \left[v_1, ..., v_{N_r}, \mathfrak{Re}(v_{N_r+1}), ..., \mathfrak{Re}(v_{N_r+N_c}), -\mathfrak{Im}(v_{N_r+1}), ..., -\mathfrak{Im}(v_{N_r+N_c})\right] . \tag{5.38}$$

Additionally, the map ι rearranges the real and complex coefficients in $c := (c_1, ..., c_{N_r+N_c})^\top$ appropriately, analogous to the sequence of eigenvectors in $\mathbb{V}$. Then, inverting Eqn. 5.37 yields

$$c = (\mathbb{V} \circ \iota)^{-1} x(0) \ . \tag{5.39}$$

To obtain a bound on X_∞^S, we still need to fix the desirable regime. In particular, take X^+ to be polyhedral as defined by m linear conditions $\hat{y}^k \cdot x(t) \leq 1$ on solutions $x(t)$. Here, the $\hat{y}^k$ are real direction vectors. The deviation of a trajectory in the

[8] The following discussion analogously applies to the single-node survivability μ_S^k

direction of $\hat{y}^k$ is then given by the inner product

$$\hat{y}^k \cdot x(t) = \sum_{j=1}^{N_r} c_j e^{\lambda_j t} \hat{y}^k \cdot v_j + \sum_{j=N_r+1}^{N_r+N_c} \mathfrak{Re}\left(c_j e^{\lambda_j t} \hat{y}^k \cdot v_j\right) . \tag{5.40}$$

Hence, the deviation is essentially determined by the overlap $\hat{y}_{kj} := \hat{y}^k \cdot v_j$ with the eigenvectors. Then, the following bound holds for all times:

$$\max_{t\in[0;\infty[} |\hat{y}^k \cdot x(t)| \leq \sum_{j=1}^{N_0} c_j \hat{y}_{kj} + \sum_{j=N_0+1}^{N_r} \max\left(0, c_j \hat{y}_{kj}\right) + \sum_{j=N_r+1}^{N_0+N_r+N_c} |c_j \hat{y}_{kj}| . \tag{5.41}$$

In this expression, each contribution is maximised individually. The N_0 null eigenvalues yield constant contributions, while the $N_r - N_0$ real eigenvalues add terms bounded by their value at $t = 0$ or by 0, depending on their sign. The third sum is over the complex eigenvalues, where the contribution of the real part is maximally given by the magnitude.

This approximation demonstrates that, opposed to asymptotic stability methods, survivability is mainly determined by the eigenvectors and not the eigenvalues of $\mathbf{A}$.

Furthermore, the m conditions defining the polyhedral desirable regime imply that

$$\sum_{j=1}^{N_0} c_j \hat{y}_{kj} + \sum_{j=N_0+1}^{N_r} \max\left(0, c_j \hat{y}_{kj}\right) + \sum_{j=N_r+1}^{N_0+N_r+N_c} |c_j \hat{y}_{kj}| \leq 1 \tag{5.42}$$

for a trajectory to survive. This defines a subspace V_c, spanned by the real and imaginary parts of the coefficients c_j. Consider the Lebesgue measure $Vol(X) = \int_X dx^D$. V_c is mapped to X_∞^S by $\mathbb{V} \circ \iota$ such that the measure Vol is pushed forward as[9]

$$\mu_S = Vol\left(X_\infty^S\right) \geq \sqrt{\det \mathbb{V}\mathbb{V}^\top} Vol\left(V_c\right) . \tag{5.43}$$

Notably, this is a lower bound on μ_S because the image of V_c is a subset of X_∞^S due to the bound Eqn. 5.41. In practice, a semi-analytic lower bound $\underline{\mu_S}$ can be numerically obtained for a sample of initial conditions[10] $x(0)$ from X^+ ,without the need of costly time-domain simulations. The bound becomes exact for systems with vanishing real parts of the eigenvalue spectrum, i.e. $\mathfrak{Re}(\lambda_k) = 0$ for all k.

5.5.3. Numerical Investigations

In the following, I present numerical results to confirm that survivability extracts complementary information from high-dimensional systems as well as to test the

[9] When a single condition $\hat{y}^k$ is dominant such that any solution $x(t)$ violating one of the m conditions also violates $\hat{y}^k \cdot x \leq 1$ and $N_0 = N_r = 0$, $Vol(V_c)$ can also be explicitly calculated [P2].

[10] Recall that the dependence is hidden in the coefficients.

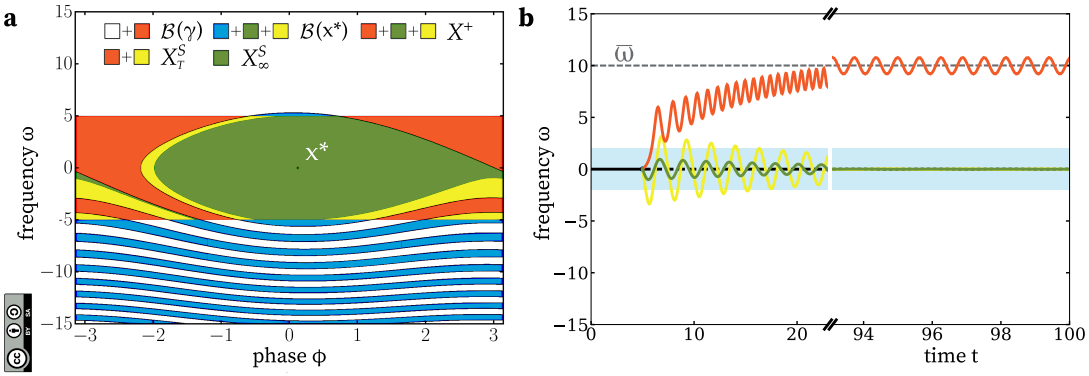

Figure 5.10. – **Survivability of the infinite-busbar approximation**: Panel **a** illustrates the phase space classification for $\omega^+ = 5$ (see text). $x^\star$ denotes the stable fixed point. Panel **b** shows three example trajectories for $\omega^+ = 2$. They correspond to initial conditions from X_∞^S (green), $X_T^S \cap \mathcal{B}(x^\star)$ (yellow) and $X_T^S \cap \mathcal{B}(\gamma)$ (orange). The natural oscillation frequency is denoted by $\bar{\omega}$. The dynamics is given by Eqn. 4.17 with $\alpha = 1/6$ and $\beta = 1/60$.

performance of above analytic bounds.

Firstly, however, consider again the infinite-busbar approximation (Eqn. 4.17) of a single node in a power grid. It has a fixed point $x^\star$ and a limit cycle γ located around the natural frequency $\overline{\omega} = \alpha/\beta$. The schematic in Fig. 5.10a illustrates the concept of a desirable regime and the resulting classification of the phase space. The two attractors have basins of attraction $\mathcal{B}(x^\star)$ and $\mathcal{B}(\gamma)$, determining their basin stability. The desirable regime X^+ is defined as

$$X^+ := \{(\phi, \omega) \in X \ : \ |\omega| \leq \omega^+ = 5\} \ . \tag{5.44}$$

X^+ comprises two sets. Firstly, there is the set X_T^S of states which survive until a respective finite time T, before they either approach the limit cycle (orange) or the fixed point (yellow). Secondly, there is the infinite-time basin of survival X_∞^S (green). As $x^\star$ is the only desirable attractor in X^+, X_∞^S is a subset of $\mathcal{B}(x^\star)$. Fig. 5.10b gives three typical frequency time series originating from phase perturbations. They are coloured alike the sets in Fig. 5.10a, e.g. the upper (orange) time series survives until $T \approx 0.75$ units before it approaches the limit cycle at $\overline{\omega}$.

As discussed above, the ability to operate a power grid within such frequency bounds is crucial. Consequently, let us now consider a power grid of n nodes. In particular, the SCONE model of inert Kuramoto oscillators (summarised in Sec. 4.4) is considered, here applied to a single, lossless transmission grid with default parameters. The line admittances are chosen to be uniform for this example, which has the benefit of disentangling dynamical effects from those mainly attributable to the spatial embedding of the network. The transmission topology is given by the Scandinavian (ultra)-high-voltage transmission grid (Menck, Heitzig, Kurths, et al. 2014), consisting of $n = 236$ nodes and $m = 320$ edges. This is a typical sparse power grid topology with a mean degree of $\bar{d} = 2.7$.

The numerical estimation procedure of (single-node) survivability using a Monte

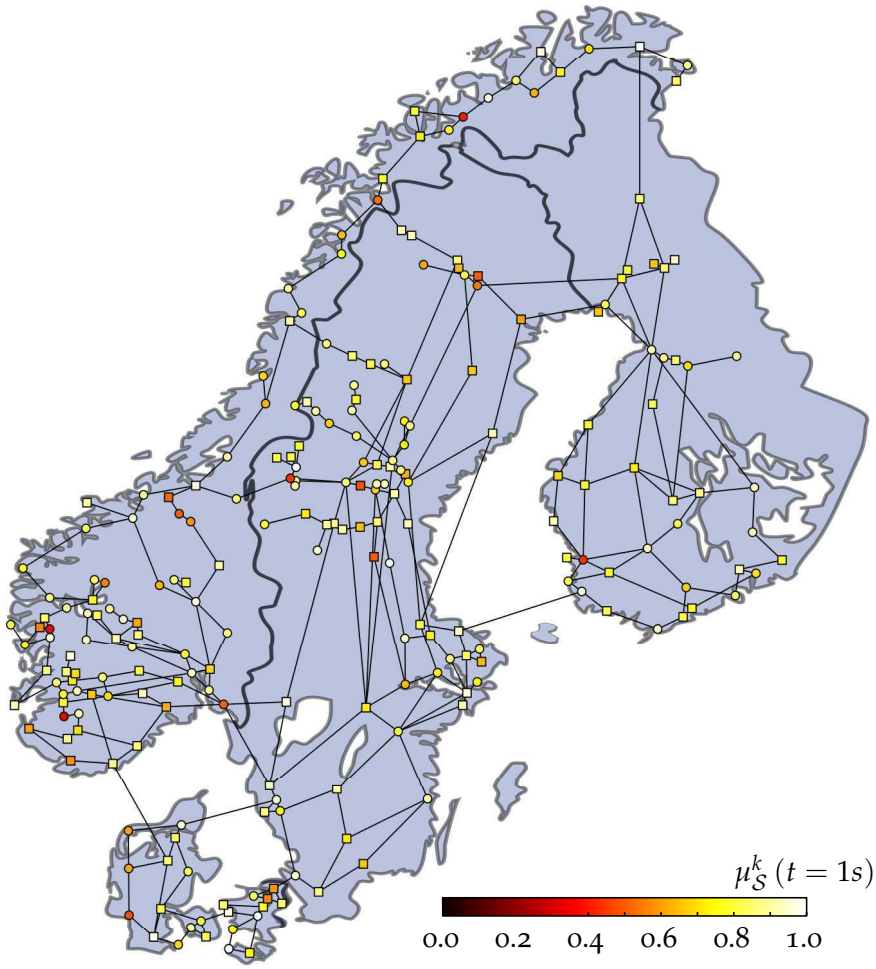

Figure 5.11. – **Single-node survivability of the Scandinavian power grid**: Visualisation of single-node survivability estimates $\hat{\mu}_{\mathcal{S}}^{k}\,(t = 1s)$ for the Scandinavian power grid with a random dispatch scenario. The frequency bound is $\omega_{+} = 10$, circular nodes are net generators and squares are net consumers. The map of Scandinavia has been modified from https://commons.wikimedia.org/wiki/File:Scandinavia.svg, which is licensed under the Attribution-Share-Alike 3.0 Unported license. The license terms can be found on the following link: https://creativecommons.org/licenses/by-sa/3.0/. The figure has been previously published in [P2].

Carlo sampling is analogous to that of basin stability described in Sec. 2.4.2. By counting the number $S\,(t)$ out of T trajectories surviving until time t, the estimate is given by

$$\hat{\mu}_{\mathcal{S}}\,(t) = \frac{S\,(t)}{T}\,, \tag{5.45}$$

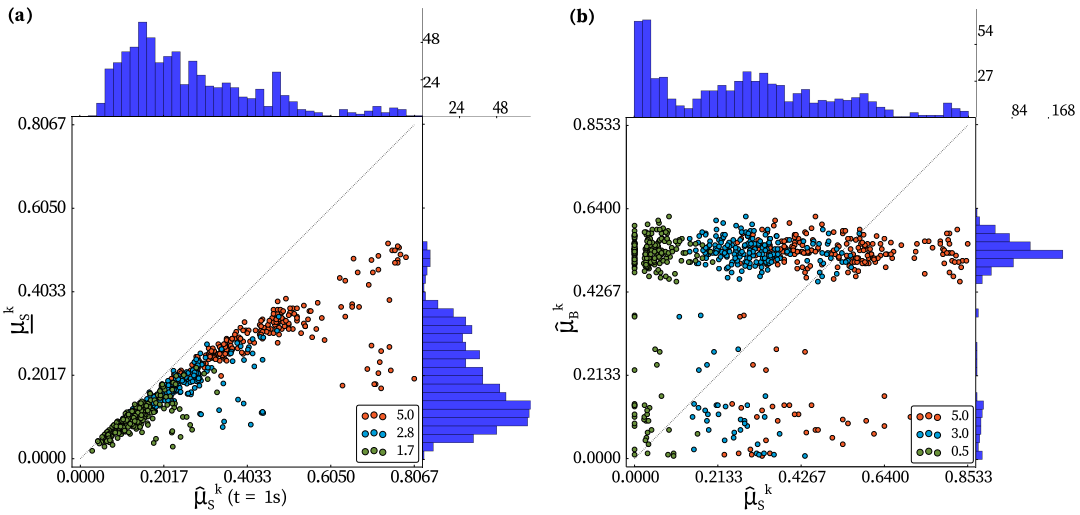

Figure 5.12. – **Semi-analytic bounds and basin stability**: For all nodes in the Scandinavian grid (Fig. 5.11), the scatter plots depict **a** the semi-analytic lower bound $\underline{\mu_{\mathcal{S}}^k}$ (Eqn. 5.42) vs. the single-node survivability estimate $\hat{\mu}_{\mathcal{S}}^k(t = 1s)$ (Eqn. 5.45), and **b** the single-node basin stability $\hat{\mu}_{\mathcal{B}}^k$ vs. the asymptotic single-node survivability estimate $\hat{\mu}_{\mathcal{S}}^k$. Note that the $\hat{\mu}_{\mathcal{B}}^k$ are estimated by drawing initial conditions from $R_k(100)$. The colours indicate the value of ω^+ given in the legend. The distributions of the points are given on the sides. The figure has been previously published in [P2].

with a standard error of

$$e_{std.}(t) = \sqrt{\frac{\hat{\mu}_{\mathcal{S}}(t)\left(1 - \hat{\mu}_{\mathcal{S}}(t)\right)}{T}} \,. \tag{5.46}$$

As above, the desirable regime is defined depending on a frequency bound ω^+:

$$X^+\left(\omega^+\right) := \{(\phi, \omega) \in X \,:\, |\omega_k| \leq \omega^+ \,\forall_k\} \,. \tag{5.47}$$

A trajectory is considered to survive, if the constraint is fulfilled at all nodes. To estimate the single-node survivability $\mu_{\mathcal{S}}^k$, initial conditions are drawn uniformly at random from

$$\begin{aligned} &R_k\left(\omega^+\right) = \\ &\{(\phi, \omega) \in X \,:\, |\phi_k| \leq \pi \wedge |\omega_k| \leq \omega^+ \wedge (\phi_i, \omega_i) = (\phi_i^*, \omega_i^*) \;\forall_{i \neq k}\} \,. \end{aligned} \tag{5.48}$$

This sampling can be done at no additional computational cost along with a basin stability estimation.

An advantage of single-node survivability is its time dependence to incorporate important system time scales and, even more, the possibility to consider network-local perturbations. Fig. 5.11 visualises an actual single-node survivability distri-

bution on the Scandinavian network. The node colour is determined by their 1s-survivability $\hat{\mu}_S^k\,(t = 1s)$. Given a desirable regime bounded by $\omega^+ = 10$, the nodes exhibit extremely different behaviour. For some nodes, network-local perturbations almost always cause violations of the frequency constraint within a second. How these diverse survivability ratings relate to the network topology is the subject of Chap. 6.

Fig. 5.12a investigates the performance of the semi-analytic bound $\underline{\mu}_S^k$ (Eqn. 5.42) for the linearisation of the dynamics close to the synchronous state $x^\star$ by comparing it with $\hat{\mu}_S^k\,(t = 1s)$ derived from numerical integration of the trajectories. Independently of the choice of ω^+, the bulk of the nodes exhibits a high linear correlation. However, the correlation decreases with larger perturbations at $\omega^+ = 5.0$ as the linear bound does not consider the multistability of the nonlinear system. What characterises the nodes far below the diagonal, for which the bound performs the worst, needs to be further investigated in the future. Nevertheless, given the error introduced by linearising the dynamics and given that Eqn. 5.42 defines just a lower bound, $\underline{\mu}_S^k$ is a promising survivability estimator for the majority of nodes in the power grid.

For comparison, the asymptotic single-node survivability estimate $\hat{\mu}_S^k$ is plotted against single-node basin stability estimates $\hat{\mu}_B^k$ of the synchronous state in Fig. 5.12b. Here, $\hat{\mu}_B^k$ is estimated by sampling the initial conditions from $R_k\,(100)$ for comparison with previous results (Menck, Heitzig, Kurths, et al. 2014). Regardless of the size of X^+, the measures of X_∞^S and $\mathcal{B}\,(x^\star)$ are uncorrelated. This result emphasises that the asymptotic behaviour of a power grid has only marginal implications on the transient.

In summary, survivability is an alternative probabilistic stability measure for complex systems. In the context of power grids, there are two main applications. On the one hand, single-node survivability identifies nodes which are critical in the sense that disturbances there likely push the system outside operating bounds even if it synchronises on the long run. On the other hand, it yields an estimate for the time left to counter-measures after a (network-local) disturbance causes a violation of these bounds. The numerical investigations in this section show that survivability indeed contains complementary information and is amenable to analytic approximations.

5.5.4. Relationship to Basin Stability and Other Concepts

Similar phase space classifications appeared, for instance, in Earth system dynamics, where desirable regimes are termed *planetary boundaries* (Rockström et al. 2009) or *sunny region* (Heitzig, Kittel, et al. 2016), while the basin of survival appears as the *safe operating space*.

In [P2], we delineate survivability from conceptually similar concepts in a variety of disciplines and discuss various similarities. For brevity, I recapitulate three key insights regarding basin stability as well as control theory and the survival analysis of stochastic systems.

Under two assumptions, the basin stability of an attractor is an upper bound on the infinite-time survivability. Basin stability $\mu_B = \mu\,(\mathcal{B}\,(\mathcal{A})\,|R)$ is defined w.r.t.

a set $R \subset X$. If, firstly, the set R coincides with the desirable regime X^+ such that both measures are commonly normalised and, secondly, if the attractor $\mathcal{A}$ is entirely contained within X^+ and the only attractor therein, we have $\forall t \geq 0 : \ \mu_{\mathcal{B}} \geq \mu_{\mathcal{S}}(t)$. In case there are multiple attractors in X^+, the relation holds for the basin stability of the union of these attractors. The difference between $\mu_{\mathcal{B}}$ and $\mu_{\mathcal{S}}$ is exactly given by those trajectories that asymptotically converge to $\mathcal{A}$ but transiently leave X^+.

In *control theory*, control schemes are often designed in a way to ensure that a system stays within bounds for a certain time at least (Amato, Ariola, and Dorato 2001; Amato, Ariola, Cosentino, et al. 2003), i.e. to find an optimal closed-loop system with $\mu_{\mathcal{S}} = 1$. There is an important branch of control theory that shares similarities on a conceptual level: the viability theory (Aubin 2001; Aubin et al. 2011) by Aubin et al. Analogous to the basin of survival, they define a so-called *viability kernel* V as the set of all initial conditions from which a system can stay within an environment K, alias desirable regime. The subtle difference lies in the word 'can', referring to a set of multiple paths of the system at each time instance due to management options or stochastic terms. In the limit of deterministic evolution paths, we retrieve the basin of survival. Though the viability kernel's volume as an indicator of the degree of viability has been proposed (Aubin et al. 2011), a numerical estimation method has not been developed yet. Rather, the focus lies on estimating the precise geometry of the viability kernel (Bonneuil 2006; Maidens et al. 2013), which is feasible only for low-dimensional systems. Whether a point belongs to the viability kernel or not in turn depends on the optimal control which might not be known. Survivability is distinguished from questions regarding the capability of controllers by measuring the ability of the uncontrolled intrinsic dynamics to withstand perturbations and remain bounded.

Besides considering deterministic systems, a survival analysis for a stochastic system is a close analogy to survivability. The main observables here are *first hit times* (or hitting times) and the *survival probability* (Redner et al. 2002; Ebeling et al. 2005; Anishchenko et al. 2006), which can be analysed, for instance, by means of quasi-potential methods (Graham and Tél 1984; Kraut et al. 2003; Freidlin et al. 2012). The first hit time τ is an expectation value for the time a system first hits the undesirable regime $X \setminus X^+$. Then, the cumulative first-hit probability $P(t' < t)$ to hit before a time t is the stochastic equivalent to $1 - \mu_{\mathcal{S}}(t)$. In the definition of survivability, however, the role of stochasticity is replaced by a probabilistic set of initial conditions. Hence, although there are close conceptual analogies and similar sampling methods, the analytic description and the interpretation in the context of stability are rather distinguishing elements.

5.6. Summary and Key Results

For every method, it is essential to explore the limitations of its applicability, both to avoid misleading results as well as to reveal where improvements might be needed. I discuss how limitations to basin stability estimation with a Monte Carlo sampling approach arise due to the problems inherent to numerical integration in *fractal basin geometries*. The key insights of Sec. 5.3 are the following. On the

one hand, the appearance of fractal basin boundaries does not seem to affect the estimation of basin stability significantly, although the correct final-state determination of single trajectories can be obstructed. On the other hand, riddled basins lead to a final-state sensitivity too high for a meaningful estimation. An exception are special cases, when the measure is restricted to an attractors neighbourhood. As a consequence, I provide a suggestion to cope with these effects in practice.

Furthermore, I present two novel probabilistic stability measures which attempt to overcome the above and further limitations of basin stability. Firstly, Sec. 5.4 is concerned with the consequences of repeated finite-size perturbations (jumps) on the probability to remain within the basin of a desirable attractor. If such jumps, arising from an arbitrary stochastic process, appear less often then a certain time period, the disturbances do not build up a serious displacement and their outcome is approximately independent. This time is introduced as the *independence time* of a dynamical system and can be estimated using *finite-time basin stability*. The latter is an extension of basin stability, corresponding to the probability that a perturbed state returns close to its equilibrium within given a finite time. The essence of this section is that a combination of these novel concepts yields an analytic lower bound on the cumulative remain probability, that is computationally efficient to determine. Furthermore, finite-time basin stability on its own is a novel and potentially interesting probabilistic stability measure with a broad applicability.

Secondly, Sec. 5.5 is related to an essential question: Given a random initial condition, is it possible to predict whether a system's state remains in a certain desirable regime, i.e. that the system survives? If not, will it do so at least for a finite time? The set of initial conditions, for which the system survives, is the (finite-time) *basin of survival* and the *survivability* is its probability measure. In particular, survivability then corresponds to the probability that a system remains within the desirable regime at least for a finite time, given a random finite-size perturbation. As it is less considered about the asymptotic behaviour but rather focuses on transient deviations, survivability extracts a complementary kind of information from dynamical systems compared to basin stability. When it comes to reacting to disturbances in e.g. a power grid, this information is often more relevant than asymptotic stability. Hence, it is an important insight of this section that it is possible to derive semi-analytic bounds on the survivability, which do not require costly time-domain simulations.

6. Motifs for Stability

Contents of this Chapter

6.1. In a Nutshell

How STRUCTURE influences dynamics is a constantly recurring theme in complex systems science, lately also with respect to power grids. In coupled oscillator networks, probabilistic stability measures reveal interrelations between topological characteristics (cf. Sec. 3.2) and the stability of synchronisation with respect to large perturbations at single nodes. The question is: Can the complexity of this interaction be boiled down to key structural influences? This chapter is devoted to identify some of them, utilising statistical relationships between different notions of stability and the structural characteristics of power grids. Particularly, the aim is to gain insights on high-dimensional network systems by considering finite-size perturbations at single nodes, using the measures outlined in Sec. 2.4.2 and Chap. 5.

Before presenting research results, in Sec. 6.2 I give a brief overview of recent developments concerning the stability of synchronisation. The literature overview reveals that various phenomena offer clues for relating stability to structure. The results for basin stability and linear methods are, however, partly converse resulting in trade-offs between different facets of power grid stability.

A particularly important factor seems to be the abundance of certain network motifs as basic building blocks of complex networks.In Sec. 6.3 I systematically study the role of small motifs using a large ensemble of synthetic power grids. Furthermore, I investigate a possibility for predicting to outcome of a single-node basin stability estimation from only topological features and network characteristics.

As discussed in the previous chapter, not only asymptotic stability but also the size of transient deviations is important in many systems, especially power grids. Hence, I accompany basin stability by survivability in Sec. 6.4 to construct a so-called stability map. Furthermore, I focus on the role of network appendices, i.e. tree-shaped substructures. These two aspects are merged in a joint analysis of the probabilistic stability measures over a synthetic power grid ensemble.

Finally, Sec. 6.5 singles out the role of cycles for the stability of synchronisation, using the framework of master stability functions. This is representative for an alternative probabilistic approach, not based on sampling initial conditions or parameter values but structural variations of the network topology.

6.2. Review of Structure vs. Stability

That "wires shape volumes" (Menck 2014), i.e. that the basin stability of power grids is deeply related to their transmission infrastructure, not only appears reasonable but further allows to draw inferences from the structure on the stability of synchronisation. An estimation of single-node basin stability for a large network ensemble identified nodes in certain tree-shaped appendices (Menck and Kurths 2012; Menck, Heitzig, Kurths, et al. 2014) to have particularly low stability[1]. Hence, such appendices contain critical nodes where a perturbation likely desynchronises the grid[2]. The stability can be improved by closing the cycle between a leaf of an appendix and another node from the remaining grid (Menck, Heitzig, Kurths, et al. 2014). The authors also discovered a general scaling of single-node basin stability with the nodes' average neighbour degree $d_i^N = d_i^{-1} \sum_{j=1}^{n} \Theta\left(A_{ij}\right) d_j$, characterising the neighbourhood connectivity. For nodes outside appendices, single-node basin stability is furthermore slightly correlated with the degree of a node, such that hubs can be expected to be more stable.

Dead ends are a particular type of motif[3] in a network. Small-scale motifs, induced by three or four nodes, have mainly been studied in directed networks with applications in biology (Milo et al. 2002). Certain motifs are even suitable to sustain synchronisation under noise (Klemm et al. 2005). Concerning consequences for stability, it has been found that a high relative abundance of certain motifs is correlated with a dynamical systems' potential to exhibit asymptotically stable fixed points (Prill et al. 2005) (in terms of permissible parameter regimes). Studying the motifs as isolated networks furthermore showed that this potential is diminished for an increase in the number of motif edges, i.e. an increase of the edge density. This suggests that motifs with a higher edge density are less likely to exhibit asymptotic stability.

Contrarily, for isolated undirected four-node networks of phase oscillators, the synchronisability derived from their Laplacian eigenvalue spectrum is found to increase with the number of edges (Moreno et al. 2004; Lodato et al. 2007). This is also indicated by the results discussed below in Sec. 6.5. In the context of power grids, the synchronisation threshold, i.e. the critical coupling value, has been analytically derived for star-like networks and regular grid motifs (Rohden, Sorge, Witthaut, et al. 2014). Apparently, it depends not only on the network structure but as well on the dispatch[4].

It has been highlighted by several authors that a decentralisation of power supply, such that generation and consumption are spatially close and distributed, implies diverse affects for power grid stability even without taking line losses into account. A minimisation of the largest negative Lyapunov exponent by optimising power generation within a dispatch leads to configurations that have more coherent

[1] The authors refer to these structures as dead ends or dead trees.
[2] A node or edge is considered *critical*, if a random perturbation at this place is likely to desynchronise the network.
[3] A *motif* is an induced subgraph of typically only a few nodes, cf. Sec. 3.3.
[4] From here on, a *dispatch* is defined as a particular assignment of power production and consumption to the nodes in a power grid.

phases (i.e. reduced power flows) and a faster convergence to the synchronous state after small perturbations (Li and Wong 2017). Intriguingly, the optimal dispatches show a decentralised pattern in the sense that producers are embedded in neighbourhoods with consumers and vice versa. This is related to the eigenvectors of the Laplacian matrix (cf. Sec. 3.2). While the eigenvector v_n, corresponding to the largest eigenvalue, has entries of rather mixed sign, the Fiedler eigenvector v_2, corresponding to the smallest non-zero eigenvalue, relates to spectral bipartitions of graphs. The latter corresponds to a separation in two rather weakly-connected components of producers respectively consumers and hence large power flows between them. Now, the optimal dispatch tends to align with the v_n whereas an alignment with v_2 is suppressed, indicating a mixed dispatch. In a similar line of research, another group of authors additionally discovered a correlation between degree and input power for large producers/consumers in the optimal dispatch (Skardal et al. 2014). Together, the results suggest that asymptotic stability of synchronisation is optimal in some sense, if the heterogeneity of the dispatch compares to the heterogeneity of the network topology.

Contrarily, an analysis of large demand perturbations indicates that decentralised power grids are prone to a reduced structural stability regarding perturbations to the dispatch (Rohden, Sorge, Timme, et al. 2012). For a fixed large perturbation, the probability that a randomly drawn dispatch supports a stable synchronous state decreases with the degree of decentralisation. This corresponds to a probabilistic approach in the parameter space (see also Brzeski, Lazarek, et al. 2016), i.e. by sampling dispatches. Here, the amount of decentralisation is controlled by successively replacing generators with high production by several generators with smaller production.

In actual load flow scenarios, some edges are typically bottlenecks, i.e. they are traversed by macroscopic flows in the network and operated close to their limit. Whether an edge is critical or not, however, cannot be predicted by looking at local quantities like the line loading alone, instead the *redundant capacity* of an edge has to be considered (Witthaut, Rohden, et al. 2016). The redundant capacity is the maximum flow between nodes u and v that can be supported by the remaining network after removing the direct link uv. Hence, it links the network topology to dynamical stability. A renormalised linear response theory further yields that the phase response mainly depends on components of the Fiedler eigenvector of the graph Laplacian, i.e. the removal of an edge between weakly-connected components is expected to have the largest effect. Critical edges can be cured using nonlocal strategies for adding transmission capacity along redundant paths (Rohden, Witthaut, et al. 2017).

In a different line of research, the linear response theory can also be used to define so-called network susceptibilities, measuring the change of a load flow solution at a node/edge in response to a network-local perturbation at a single node/edge (Manik, Rohden, et al. 2017). The different network susceptibilities share similarities with the vertex current-flow betweenness but more so they are directly related to resistance distances (cf. Sec. 3.3). Furthermore, the node-to-node network susceptibility is particularly high between nodes within the same appendix. At the same time, the sensitivity of the bulk to perturbations in an appendix is significantly smaller.

Hence, the mechanism suggested by the linear theory is that nodes in appendices mutually destabilise each other, while this disturbance stays localised. This corroborates earlier results on the detrimental effect of dead ends obtained via a single-node basin stability analysis (Menck, Heitzig, Kurths, et al. 2014).

A rather counter-intuitive interaction between structure and dynamics needs to be mentioned. Curing the detrimental effect of dead ends (ibid.) or curing critical edges (Rohden, Witthaut, et al. 2017) results in adding cycles to the network. Consider a cycle, i.e. a closed path π^c, in a network of coupled oscillators. A constraint for a fixed point of the swing equation (cf. Eqn. 4.19) to exist is that the sum of all phase differences along edges in π^c vanishes (modulo 2π) (Witthaut and Timme 2012). The addition of an edge or the increase of an edge's transmission capacity typically reduces the load of existing edges. In some cases, however, such a change violates the constraint, leading to *geometric frustration* of the phases and phase synchronisation becomes unstable. This counter-intuitive effect that an increase of transport capacities causes a collapse of existing infrastructure is known as *Braess' paradox* in various contexts (Braess 1968; Witthaut and Timme 2012). For a chain of nodes, the regime where an additional edge diminishes stability, can be calculated explicitly by considering the largest Lyapunov exponent (Coletta and Jacquod 2016). When a power grid is operated close to it's transmission capacity limit, taking a single additional line into operation might cause a cascading failure due to Braess' paradox (Witthaut and Timme 2013). Conversely, the removal of an edge can, in some cases, also improve the synchronisability (Nishikawa and Motter 2010).

In essence, the observation of Braess' paradox in power systems clarifies that non-local effects need to be taken into account. Hence, local network characteristics alone will not be sufficient for inferring stability.

As discussed in Sec. 2.4.2, basin stability detects certain bifurcations in dynamical system, for instance when the transmission capacity varies between units in a power grid[5]. In a complex network, different nodes show distinctive bifurcation profiles in a single-node basin stability analysis for uniformly increasing the capacity, i.e. the coupling strength. Kim et al. (2015) define the so-called *transition window* as the interval between the coupling for which synchronisation becomes stable, i.e. positive single-node basin stability, and the point where it reaches one at all nodes. The transition window is an estimate for the regime where stable synchronisation co-exists with other attractors. It is characterised by its width and mean. Nodes with a wide transition window remain at medium or low basin stability over a broad parameter range, hence they tend to be critical. In a case study of the Chilean power grid, it turned out that nodes with an exceptionally wide transition window are identical with the nodes for which community detection algorithms yield inconsistent results (ibid.). An analysis of all non-isomorphic connected networks of two, four or six nodes, together with all distinct dispatches (half are consumers, half producers) revealed further insights (Kim et al. 2016). The two-node pattern effectively reduces to a two-dimensional system and hence reproduces the curve of Fig. 2.7d. Now, leaf nodes show similar transitions, while other nodes can have considerably en-

[5]Compare also with Fig. 2.7d.

hanced or suppressed stability at fixed coupling strengths. In the limit of all-to-all coupling, the distinct transition windows of single nodes become identical, i.e. distinct patterns only appear in sparse networks. The functional form of the transition window, not it's width, can be predicted by the nodes' shortest-path betweenness. This is another indication for the links between structural properties and stability.

It turned out that the average single-node basin stability is to some extent influenced by global network characteristics. For coupled Rössler oscillators on Watts-Strogatz networks (Watts et al. 1998), it has been found that the optimal basin stability regime coincides with the small-world region (Menck, Heitzig, Marwan, et al. 2013). This happens to be in contrast to the linear synchronisability, which increases monotonically with the randomness of a network. This implies a trade-off between asymptotic and basin stability optimisation. Similarly, there is a trade-off between basin stability and the robustness against cascading failures in power grids [F5]. This result refers to synthetic power grid topologies [F3] varying between local and global regimes of redundancy. It can be observed that the single-node basin stability distribution becomes skewed to a higher number of uncritical nodes when the redundancy becomes more global as measured by the algebraic connectivity. This regime is also characterised by long-range interconnections appearing in the network.

In the introduction to Chap. 5, I briefly mentioned the concept of *reliability*, e.g. the ability of power grid to withstand cascading failures. A large-deviation sampling over different network classes revealed that robust networks have a higher overall graph density and a smaller diameter (Dewenter et al. 2015). Moreover, the most robust networks have a high fraction of edges connecting producers directly with consumers, indicating a decentralised dispatch. Different authors observe that networks whose degree distribution has a fast-decaying exponential tail[6] are fragile in terms of reliability while the others tends to be more robust, irrespective of system size (Solé et al. 2008; Rosas-Casals 2009). Particularly, robust networks contain more star-like motifs and triangles as well as less chains of nodes, indicating a higher local connectivity.

[6] with exponent $\gamma < 1.5$, cf. Sec. 4.3

6.3. Stability via Detours

This section refers to research originally published in [P1].

Abstract I identify motifs that are stabilising with respect to basin stability and develop a statistical prediction of critical nodes, solely incorporating network characteristics.

6.3.1. Four-Node and Detour Motifs

As the basis for a stability analysis of small network motifs serves an ensemble of 570 synthetic transmission grid topologies with realistic properties[7]. They have $n = 100$ nodes, are very sparse and the mean degree is $\bar{d} = 2.7$ on average. Furthermore, the networks feature a spatial embedding, such that the line admittances can be derived from the line lengths. This ensemble is used in conjunction with the SCONE model given by Eqn. 4.30 for synchronous machines in a lossless transmission grid. Half of the n nodes are randomly selected as net producers with $P_k = 1$ and the other half are net consumers with $P_k = -1$.

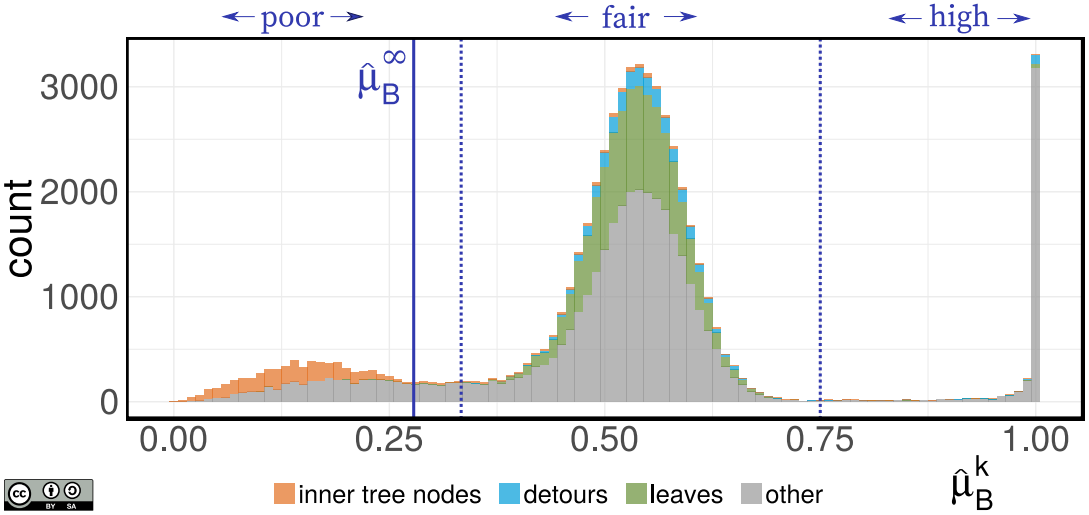

Figure 6.1. – **Single-node basin stability histogram**: Ensemble estimate of $\hat{\mu}_{\mathcal{B}}^k$ for $570 \cdot 100$ nodes. The bin colours indicate selected network motifs, of which a node k is part. Dashed vertical lines delineate the poor, fair and high basin stability classes, while the solid vertical line indicates the estimate $\hat{\mu}_{\mathcal{B}}^\infty$ for a corresponding infinite-busbar model. Adapted from [P1].

Based on this setup, the distribution of single-node basin stability $\hat{\mu}_{\mathcal{B}}^k$ is determined for all nodes k in the network ensemble by drawing $T = 100$ initial conditions uniformly at random from

$$R_k = \{(\phi, \omega) \in X \ : \ |\phi_k| \leq \pi \wedge |\omega_k| \leq 100 \wedge (\phi_i, \omega_i) = (\phi_i^*, \omega_i^*) \ \forall_{i \neq k}\} \tag{6.1}$$

[7]The model parameters are $\{n_0, s, p, q, r, u\} = \{1, 0.2, 0.3, 0.1, 1, 0\}$, cf. Sec. 3.4.3.

at every node k, where $x^\star = (\phi^*, \omega^*)$ is the synchronous operating state of the system and X its phase space. According to Eqn. 2.25 the absolute standard error of the sampling is than at most 5%. The large extent of R_k in the frequency directions is chosen here, to obtain results comparable with previous studies (Menck, Heitzig, Marwan, et al. 2013; Menck, Heitzig, Kurths, et al. 2014).

The ensemble histogram of $\hat{\mu}_{\mathcal{B}}^k$ is given in Fig. 6.1. First of all, notice that the general shape of the distribution is multi-modal and that nodes fall into one of three rather well-separated stability classes, which can be separated as

$\mathcal{V}^p$: *poor* ($\hat{\mu}_{\mathcal{B}}^k < 1/3$),

$\mathcal{V}^f$: *fair* and

$\mathcal{V}^h$: *high* ($\hat{\mu}_{\mathcal{B}}^k > 3/4$) stability.

In the ensemble, 79% of nodes exhibit a fair estimate of $\hat{\mu}_{\mathcal{B}}^k$, while 14% fall into $\mathcal{V}^p$ and the remaining 7% into $\mathcal{V}^h$. These results are in accordance with earlier studies (Menck and Kurths 2012; Menck, Heitzig, Kurths, et al. 2014) using similar parameters and the same choice of R_k but homogeneous coupling strengths $A_{jk} \equiv 8$ and a random graph model (Gilbert 1959). Hence, it is unlikely that the observed distribution of $\hat{\mu}_{\mathcal{B}}^k$ is an artefact of the specific structure of the synthetic networks $\mathcal{G}$ in the ensemble.

Consider for comparison the infinite-busbar model (cf. Sec. 4.2.3) for a single node coupled to a bulk mean field. Within the SCONE model, the parametrisation is chosen such that the average coupling is $A_{jk} = 6$ for edge lengths in the given spatial embedding. Using this value for K in Eqn. 4.17 yields an estimate for the infinite-busbar basin stability of $\hat{\mu}_{\mathcal{B}}^\infty = 0.237 \pm 0.013$[8], indicated with a solid vertical line in Fig. 6.1. While the majority of nodes exhibits a higher, i.e. fair or high, stability, most poor nodes score even lower than $\hat{\mu}_{\mathcal{B}}^\infty$. On the one hand, a perturbation drawn from R_k at a node k in $\mathcal{V}^p$ has at least a chance of about 67% to desynchronise the power grid, consequently they can be considered critical for a stable operation On the other hand, by being interconnected, the majority of nodes profits from a *positive network effect* in terms of an increased stability with regard to large perturbations. Comparing to Fig. 2.7, this might in part be due to an effective coupling strength at the nodes, increasing with their degree. This can, however, not be the full story, since single-node basin stability is generally not correlated with degree but rather with the average degree of the neighbours (Menck and Kurths 2012; Menck, Heitzig, Kurths, et al. 2014).

As a last point about Fig. 6.1, notice that it is shaped by the abundance of different network motifs, as indicated by the colouring. I highlighted three different groups of motifs whenever a node is part of one[9], namely *leaves* (nodes of degree $d = 1$), *inner tree nodes* and *detours*. Inner tree nodes have been previously discovered to "undermine power grid stability" (Menck and Kurths 2012; Menck, Heitzig, Kurths, et al. 2014) in the sense that these particular nodes with $d > 1$, adjacent to or inside dead ends/trees, exhibit a significantly diminished single-node basin stability.

[8] The standard error is derived for T=1,000 initial conditions.

[9] Theses three are exclusive, each node is only participating in one type of motif or none.

Consequently, the majority of them falls into $\mathcal{V}^p$. Likewise, the same authors identified leaves as nodes with fair stability. These two motifs are found in tree-shaped appendices, which are discussed in great detail in the following Sec. 6.4.

Detours, the third motif, are triangles in which one node is only connected to its two neighbours. The neighbours, in turn, each are connected to the remaining nodes and detours often are bridges between different parts of a network. Each detour contains exactly one node k with degree $d_k = 2$ and local clustering coefficient $C_k = 1$, the so-called *detour node* (indicated in the inset of Fig. 6.3). Fig. 6.1 reveals that the single-node basin stability estimate for detour nodes is fair or even high, notably they do not fall into the poor stability class $\mathcal{V}^p$.

The imprint of larger motifs on the single-node basin stability estimates, however, seems to be less pronounced in the sense that there is no clear relationship to network characteristics.

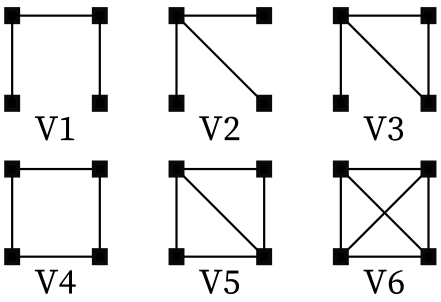

Figure 6.2. – **The six four-node motifs V1-V6 in undirected networks.** The figure has been previously published in [P1].

There are six different four-node motifs in undirected networks, with an edge count varying from three to six (Fig. 6.2). The ensemble results indicate that the number of poor nodes decreases with the number of edges in the motif, i.e. local redundancy of paths between nodes is beneficial for the stability of inherent nodes [P1]. The four-node motifs $V4$, $V5$ and $V6$ were also analysed as isolated networks with regard to basin stability in the context of power grids (Ji and Kurths 2014). The consecutive addition of edges to $V4$ leads to a shrinking multistable regime in favour of globally stable synchronisation. Remarkably, the asymptotic stability of the synchronous state, measured by the largest transverse Lyapunov exponent, is insensitive to these edge additions, showing again that basin stability yields complementary information about a multistable dynamical system.

6.3.2. Prediction of Poor Stability

The detrimental effect of inner tree nodes has been discovered through distinctive patterns in the shortest-path betweenness, where these nodes take up specific values. Fig. 6.3 underlines that for low values of the vertex current-flow betweenness b_k^w of a node k, upward peaks of increased $\hat{\mu}_{\mathcal{B}}^k$ dominate the stability spectrum. The colour code respectively marker size highlights that these are almost solely due to detour nodes. The dashed vertical lines in Fig. 6.3 indicate current-flow betweenness values b_k^w for which the expected single-node basin stability is significantly lowered. Notably, the results regarding the detrimental effect of dead trees (Menck, Heitzig, Kurths, et al. 2014) are retained, as b_k^w coincides with b_k due to the absence of alternative shortest paths in tree-shaped appendices.

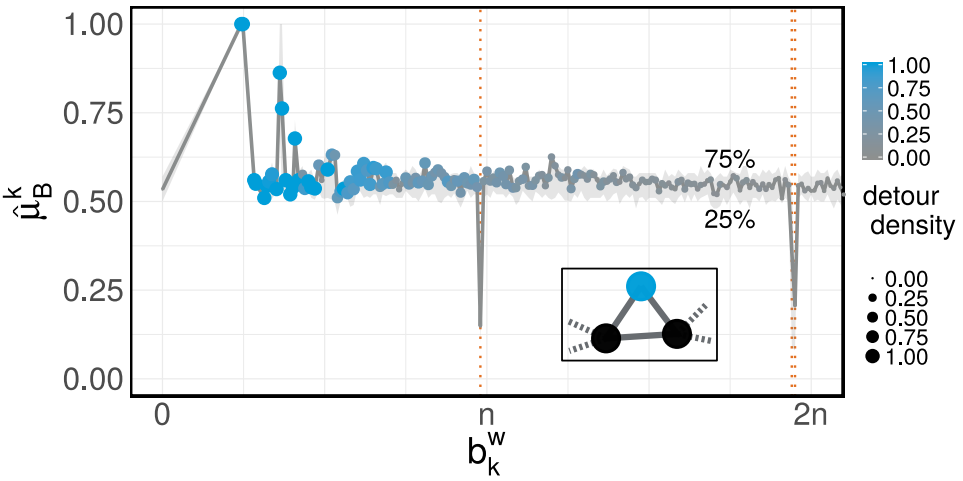

Figure 6.3. – **Vertex current-flow betweenness**: The markers indicate the fraction of detour nodes (inset) with the respective betweenness value, i.e. the detour density. The shading illustrates the first and third quartile of the $\hat{\mu}_B^k$ distribution at a given value of ${b_k}^w$. The vertical dashed lines are located at minima of ${b_k}^w$, realised at nodes in dead trees. Adapted from [P1].

This result illustrates that small motifs like detours[10] link specific stability properties to mesoscale network measures. Hence, when a node is identified as a detour node, it can almost surely be predicted to fall into the class of fair or high stability. More formally, I define a binary variable χ which is one when a node k falls into $\mathcal{V}^p$ and zero otherwise. The idea is, that the prediction of a discrete variable like χ reduces the complexity of predicting continuous basin stability estimates, given also that the classes are separated quite well in Fig. 6.1. The result of the prediction will be a probability p_k for each node k to have poor stability $\chi = 1$.

A pre-classification of the node set yields three possible cases:

(o) detour nodes,

(i) nodes being neither detour nodes nor inner tree nodes,

(ii) inner tree nodes.

For detour nodes (o), $p_k \equiv 0$ can be estimated directly from the ensemble results. Contrarily, for inner tree nodes (ii) one expects $p_k \gg 0$, however more information is needed. For the remaining nodes (i), the situation is a priori unclear.

In the following, I outline a prediction scheme for cases (i) and (ii), using logistic regression. This is a suitable regression method here, because the dependent variable is binary and because a nonlinear relation between χ and explanatory variables can be expected. The regression estimates for each node k the probability p_k of a categorical dependent variable – in our case it is χ – given a set Q_k of values of q explanatory variables. The method assumes

[10] Note that detour nodes are a prime example for a situation where b_k vanishes and b_k^w yields significantly different information (cf. Fig. 3.2).

$$p_k = P(\chi = 1|Q_k) = \frac{1}{1 + \mathrm{e}^{-f(Q_k)}} \,, \qquad \text{with } f(Q_k) = c_0 + \sum_{j=1}^{q} c_j Q_{k,j} + \epsilon_k \,. \tag{6.2}$$

The resulting regression model Eqn. 6.2 includes linear coefficients of the explanatory variables, an intercept c_0 and an error term ϵ_k accounting for uncertainty. Consequently, a regression then yields $q + 1$ constants estimated over all nodes in case (i) respectively (ii), using for instance a maximum likelihood procedure (Agresti 2002). The logistic function in Eqn. 6.2 ensures that the real-valued outcome of f is transformed into a probability between 0 and 1.

Besides the information whether a node is an inner tree node or a detour node, different network characteristics (cf. Sec. 3.3) contribute to Q_k. In particular, the explanatory variables yielding the best prediction[11] turn out to be local network characteristics like the strength s_k, average neighbour strength $s_k^N := \frac{1}{k_k} \sum_{j=1}^{n} \Theta(A_{jk}) s_j$ and weighted local clustering coefficient C_k^w of a node k. Furthermore, two mesoscale characteristics, the vertex current-flow betweenness b_k^w and the current-flow closeness c_k^w are used.

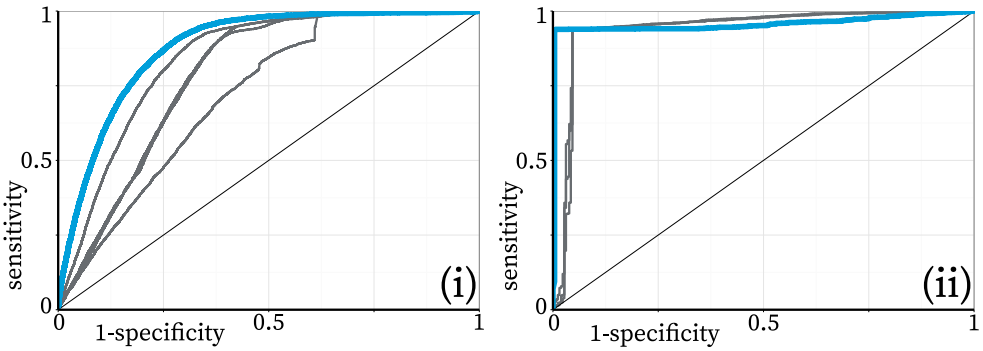

Figure 6.4. – **Prediction of poor single-node basin stability**: Receiver operating characteristics for **left** (i) nodes being neither detour nodes nor inner tree nodes, **right** (ii) inner tree nodes. The blue curves highlight the best prediction in terms of their AUC (see text). Adapted from [P1].

An established method to compare the predictive performance of statistical models from various combinations of explanatory variables is the so-called *receiver operating characteristic* ROC. It is the relation between the *sensitivity* (true positive rate) and *specificity* (true negative rate) of a prediction[12]. When p_k exceeds a given threshold, the prediction of poor single-node basin stability is accepted and the range of thresholds $\tau \in [0;1]$ yields a curve in the ROC plot. There are four possibilities for true/false predictions at a node k, given a threshold τ:

[11] The predictive performance using weighted characteristics generally exceeds that of using their unweighted counterparts for this specific problem.

[12] sensitivity: $\frac{\sum \text{true positive}}{\sum \text{condition positive}}$ and specificity: $\frac{\sum \text{true negative}}{\sum \text{condition negative}}$

- true positive: $p_k > \tau$ and $k \in \mathcal{V}^p$
- false positive: $p_k > \tau$ and $k \notin \mathcal{V}^p$
- true negative: $p_k < \tau$ and $k \notin \mathcal{V}^p$
- false negative: $p_k < \tau$ and $k \in \mathcal{V}^p$

Ideally, a statistical model approaches the top left corner of a ROC with both high sensitivity and specificity, minimising the risk of false predictions. Otherwise, pure guessing would result in a diagonal, i.e. the chance to get false positives or negatives is equal. This can be quantified using the *area under curve* (Metz 1978; Hanley et al. 1982; LeDell et al. 2012) (AUC) measure, which gives $AUC = 1$ for a perfect prediction and $AUC = 0.5$ for random guessing.

The AUC value and its variance are estimated in a cross-validation procedure (LeDell et al. 2012). The basic idea is that the ensemble is randomly divided into a training set, on which the regression is performed, and a test set on which the prediction is made. The sample variance of AUC values for different separations is then a good estimate for the robustness of the ROC result.

Fig. 6.4 pictures ROC curves for regression models based on different explanatory variables Q_k for case (i) and (ii). For brevity, here I present only the best-performing regression models. Their regression coefficients and a discussion of alternative models (corresponding to the remaining ROC curves in Fig. 6.4) is contained in [P1].

Let us first consider case (ii), the inner tree nodes. It turns out that the model with the best performance in terms of its AUC is achieved by considering only the vertex current-flow betweenness $Q_k = \{b_k^w\}$ (right panel of Fig. 6.4). This model reaches a sensitivity and specificity of 94% respectively 99% and has an $AUC = 0.959 \pm 0.005$. The inner tree nodes are generally identified via particular betweenness values, however, using b_k^w, one can further tell apart critical nodes with poor stability estimates. The regression yields a negative coefficient for b_k^w such that nodes with a low betweenness are more likely to have high p_k.

Concerning case (i), the best-performing model uses all five explanatory variables, i.e $Q_k = \{s_k, s_k^N, C_k^w, b_k^w, c_k^w\}$. This model reaches a sensitivity and specificity of 84% respectively 77% and has an $AUC = 0.915 \pm 0.002$ (left panel of Fig. 6.4). The largest coefficients again are negative and belong to C_k^w, the weighted local clustering coefficient, and c_k^w, the current-flow closeness centrality. Notably, a high value of C_k^w corresponds to the abundance of short local cycles in the neighbourhood of a node k, i.e. local redundancy. Hence, centrality and local clustering seem to promote basin stability, as the resulting p_k is rather low.

In summary, the ensemble analysis yields statistical models to predict whether single-node basin stability $\mu_{\mathcal{B}}^k$ will be low, based solely on network characteristics. In particular, a node has a high probability to be in $\mathcal{V}^p$ if it

(o) is **not** a detour node.

(i) has certain values of $Q_k = \{s_k, s_k^N, C_k^w, b_k^w, c_k^w\}$, foremost a **low** clustering coefficient C_k^w or **low** centrality c_k^w.

(ii) is an inner tree node with **low** current-flow betweenness b_k^w.

6.4. Stability Maps of Tree-Shaped Appendices

This section refers to research originally published in [P5].

Abstract I introduce a novel classification scheme targeted at nodes in tree-shaped appendices, illustrate how a joined analysis of probabilistic measures reveals novel states and discuss the role of hubs for survivability.

6.4.1. Node Classification of Tree-Shaped Appendices

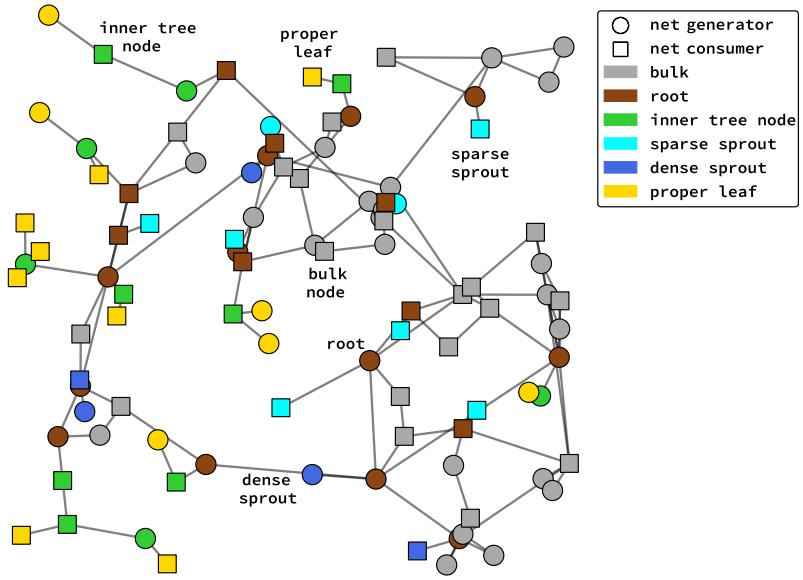

Figure 6.5. – **Topological node classification**: In this example network, the nodes are coloured according to their topological classification, as defined in this section. It contains 20 tree-shaped appendices. The network is a spatially-embedded synthetic power grid topology (Sec. 3.4.3) with 100 nodes of which one half are net generators (circles) and another half are net consumers (squares). The figure has been previously published in [P5].

Asymptotic stability analysis provides indication that trees are less synchronisable (Yook et al. 2006). As discussed in the introduction to this chapter, tree-shaped appendices, called dead ends/trees, are also prone to instability with respect to large perturbations (Menck, Heitzig, Kurths, et al. 2014). As we will see, these statements are not universal for all nodes in trees, but it is possible to discern their roles in more detail. Particularly, the following topological classification of nodes happens to separate them precisely according to their stability class.

Definition 15 (Tree-shaped appendix, root)**.** *Consider an undirected connected network* $\mathcal{G} = (\mathcal{V}, \mathcal{E}, w)$ *that is not a tree itself. Then, a* tree-shaped appendix *is defined as an*

induced subgraph $\mathcal{G}' = \mathcal{G}[\mathcal{V}']$ *which is a tree, i.e. it is connected and contains no cycle, that is maximal in the sense that there is no subgraph* $\mathcal{G}'' = \mathcal{G}[\mathcal{V}'' \supset \mathcal{V}']$ *with the same properties.* $\mathcal{G}'$ *contains exactly one node having neighbours in the remaining network* $\mathcal{G} - \mathcal{G}'$*, the so-called* root $r \in \mathcal{V}'$*. It follows directly that a root node has a degree* d *of at least* $k \geq 3$*.*

The union of all tree-shaped appendices is referred to as the *forest part* $\mathcal{F}$ of $\mathcal{G}$. To distinguish whether a node belongs to the forest or to the *bulk* (i.e. all non-tree nodes $\mathcal{G} - \mathcal{F}$) is still quite coarse and a more detailed classification is needed to tell apart the different roles of nodes inside $\mathcal{F}$. With the root nodes, one distinguished class has already been introduced. All nodes in a tree are further characterised by two numbers, i.e. their depth and height.

Definition 16 (Depth, height)**.** *Given a tree-shaped appendix* $\mathcal{T}$ *defined as above, the* depth $\delta(k)$ *associated to a node* $k \in \mathcal{T}$ *is the length of the shortest path from* k *to the root* r*. The root itself has depth* $\delta(r) = 0$*. Equivalently, the* height $\eta(k)$ *of a node* $k \in \mathcal{T}$ *is the length of the longest path between* k *and a leaf* $l \in \mathcal{T}$ *. Leaves have a height of* $\eta(l) = 0$[13]*.*

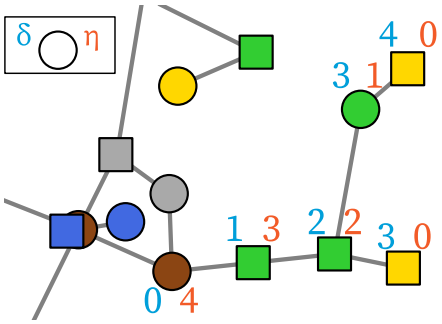

Figure 6.6. – **Depth and height:** δ and η according to Def. 16 are given to the left respectively right of the nodes in a tree-shaped appendix. Node shapes and colours are the same as in Fig. 6.5.

Fig. 6.6 illuminates how the definitions of depth δ and height η apply to an example. All nodes are uniquely identified according to their position and further node categories can be defined. For instance, leaf nodes ($\eta = 0$) can be easily divided into *proper leaves* with $\delta > 1$ and *sprouts* with $\delta = 1$. As we see later, it can be useful to further distinguish *dense sprouts* that connect to a root of high degree ($d_{root} > 5$) and the otherwise *sparse sprouts*. Besides this division, many other are possible, depending on the research question. For the sake of simplicity, all nodes in the forest that are neither leaves nor sprouts or roots are referred to as *inner tree nodes* in the following. The node classification at this level of detail is visualised in Fig. 6.5 for an example network.

The identification of tree-shaped appendices of a graph $\mathcal{G}$ along with the height and depth values can be efficiently performed using the algorithm given in Appendix A.2. Here and in the following, I use a different naming convention than established previously by Menck, Heitzig, Kurths, et al. (ibid.). Tree-shaped appendices correspond to dead ends/trees, nodes in dead trees are inner tree nodes and the roots correspond to nodes adjacent to dead ends/trees.

[13] This somehow counter-intuitive definition of depth and height follows the standard graph-theoretical convention that trees grow downwards.

6.4.2. The Stability Map: Exotic Solitary Oscillations

To HIGHLIGHT how this approach can be useful for analysing dynamical systems, probabilistic stability estimates are compared for different groups in the node classification. In particular, the SCONE model Eqn. 4.30 again is used to estimate single-node basin stability $\mu_{\mathcal{B}}^k$ and single-node survivability $\mu_{\mathcal{S}}^k$. This is performed for an ensemble of 50 synthetic power grid topologies[14] with $n = 100$ nodes. Within this model ensemble, almost half of the nodes belong to the forest [P5]. The model setup is analogous to Sec. 6.3, i.e. Kuramoto oscillators with inertia are considered in a lossless transmission grid, except for using homogeneous line capacities here. Although this is less realistic, using transmission capacities that do not depend on the line lengths allows to delineate dynamical effects attributable to the underlying topology of the network from its spatial embedding. As a next step in future research, this simplification should be dropped. Given the phase space as X, the desirable regime is chosen depending on the maximal tolerated frequency deviation ω^+ as

$$X^+\left(\omega^+\right) := \{(\phi,\omega) \in X \ : \ |\omega_k| \leq \omega^+ \ \forall_k\} \ . \tag{6.3}$$

For both $\mu_{\mathcal{B}}^k$ and $\mu_{\mathcal{S}}^k$, initial conditions are drawn uniformly at random from the sets

$$R_k = \{(\phi,\omega) \in X \ : \ |\phi_k| \leq \pi \wedge |\omega_k| \leq \omega^+ \wedge \ (\phi_i,\omega_i) = (\phi_i^*,\omega_i^*) \ \forall_{i\neq k}\} \tag{6.4}$$

at every node k, where $x^\star = (\phi^*,\omega^*)$ is the synchronous operating state of the power grid.

Single-node basin stability and survivability are estimated using a sample size of $T = 200$ trajectories (cf. Eqn. 5.45) simulated up to a time interval of $t = 100$ time units. According to Eqn. 2.25, the absolute standard error of the sampling is than at most 4%.

The four panels in Fig. 6.7 depict so-called *stability maps* for increasing values of ω^+. First of all, the low correlation between the measures is confirmed, i.e. transient and asymptotic stability analyses yield significantly different information about a dynamical system. To estimate only one quantity is generally not sufficient to infer the second[15]. Hence, it is meaningful to complementary consider $\hat{\mu}_{\mathcal{B}}^k$ and $\hat{\mu}_{\mathcal{S}}^k$ simultaneously in the stability map. Notably, the node classes defined above are mutually separated in the stability maps, i.e. they feature typical characteristics regarding asymptotic and transient stability at different tolerances ω^+.

As discussed in Sec. 5.5, basin stability is an upper bound to survivability under certain conditions. Particularly, both measures have to be estimated from an identical set R_k of initial conditions and the only attractor in X^+ should be the synchronous operating state. As soon as there are different attractors in X^+, this relation does not hold anymore as we shall see now.

[14] The model parameters are $\{n_0, s, p, q, r, u\} = \{1, 0.2, 0.3, 0.1, 1, 0\}$, cf. Sec. 3.4.3.

[15] Certain node categories tend to be correlated, though. This is the case e.g. for inner tree nodes and proper leaves at intermediate values of ω^+ (cf. Fig. 6.7).

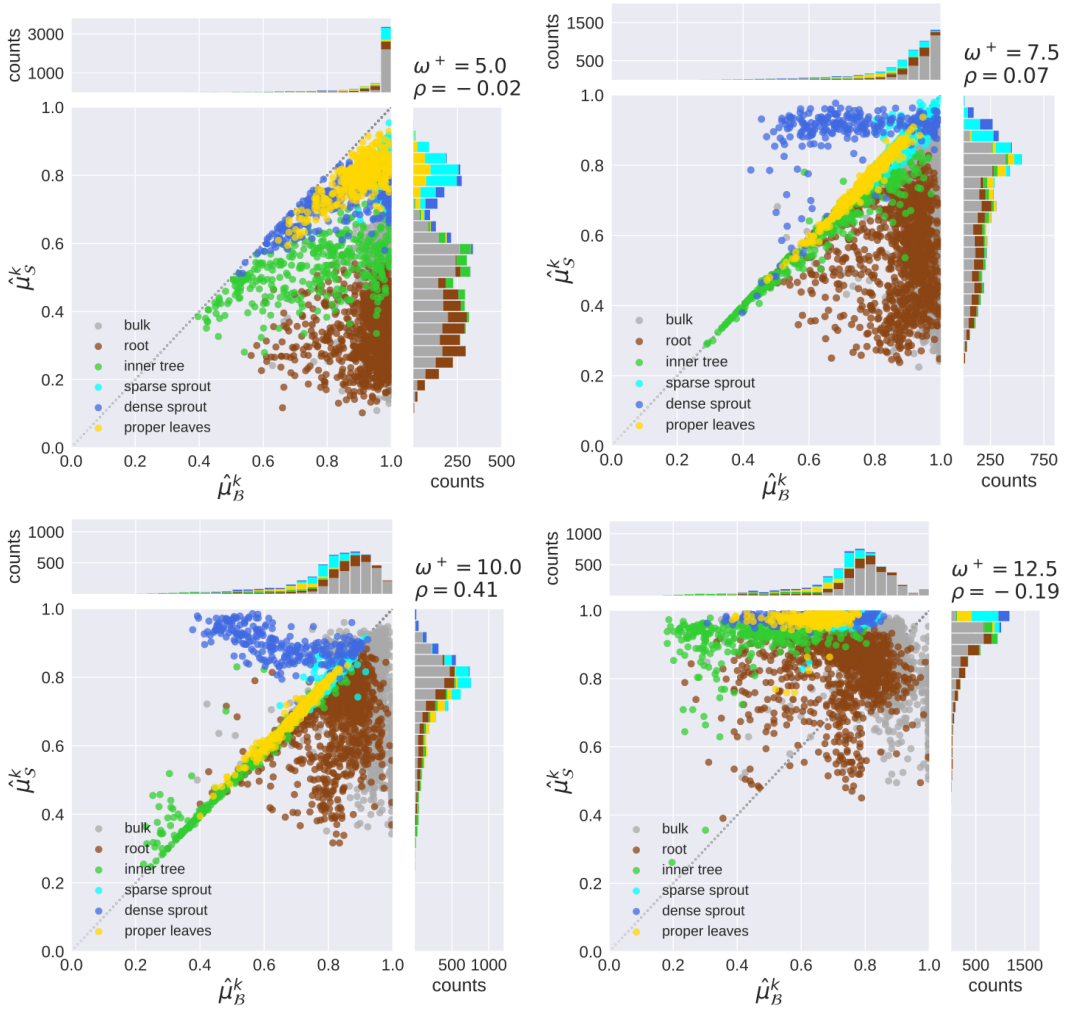

Figure 6.7. – **Stability maps of single-node basin stability vs. survivability:** Scatter plots and distributions of all $N \times M = 5,000$ nodes for different perturbations levels $\Delta\omega$. The data points and bins are coloured according to the topological classification scheme illustrated in Figure 6.5. ρ denotes the Pearson correlation coefficient. The figure has been previously published in [P5].

In the upper left panel ($\omega^+ = 5$), single-node basin stability is an upper bound across all nodes. The highly skewed distribution of $\hat{\mu}_B^k$ towards 1 indicates that the desirable regime is almost entirely contained in the basin of attraction of $x^\star$, about 73% of all nodes have $\hat{\mu}_B^k \geq 0.95$. As discussed in the previous section, a multi-modal distribution is achieved for higher perturbation levels, e.g. for high tolerances $\omega^+ = 100$. The $\hat{\mu}_S^k$ distribution is bi-modal and reveals, that proper leaves and sprouts have the highest single-node survivability values[16]. Otherwise, sparse sprouts also score higher than dense sprouts, indicating further that a low

[16]The observation that low-degree nodes tend to have a higher survivability re-engages us in the next section Sec. 6.4.3.

nearest-neighbour degree is beneficial as well. In turn, the root nodes tend to be the most critical. Although $\hat{\mu}^k_{\mathcal{B}}$ is close to 1 in this group, $\hat{\mu}^k_{\mathcal{S}} < 0.5$ indicates that for half of the network-local perturbations at root nodes the overall system experiences large transient frequency deviations.

In the lower right panel ($\omega^+ = 12.5$), most nodes are above the diagonal, i.e. $\hat{\mu}^k_{\mathcal{B}} < \hat{\mu}^k_{\mathcal{S}}$. This indicates the appearance of an undesirable attractor (or more) inside the desirable regime X^+. Consequently, trajectories that do not return to the synchronous state still survive. This is expected, as the system is multistable with co-existing stable limit cycles (cf. Sec. 4.2.3), corresponding to frequency oscillations. The frequency oscillations are located close to the natural frequencies $|\gamma_k P_k| = 10$ which are smaller than ω^+. Hence, the limit cycle is contained in X^+ and non-synchronous solutions are likely to remain within the desirable regime.

An interesting phenomenon can be observed for intermediate values of $\omega^+ = 7.5$ (upper right panel) and $\omega^+ = 10$ (lower left panel). While the majority of nodes behaves as if there was no undesirable attractor in X^+, a particular class of nodes behaves differently – dense sprouts. Irrespective of their high survivability $\hat{\mu}^k_{\mathcal{S}} \approx 0.9$, a considerable amount of perturbations at dense sprouts leads to a desynchronisation of single nodes. An analysis of the respective time series reveals that this behaviour corresponds to *exotic solitary states*. Single nodes are desynchronised and do not oscillate close to their natural frequency (which is outside X^+) but around fractional values thereof. This oscillation is overlayed with high harmonics, i.e. high-frequency oscillations of the frequency variable with low amplitude. The fact that the average frequency deviation is not related to the node's natural frequency distinguishes this state from previously described solitary states (Jaros et al. 2017; Maistrenko et al. 2017). An example is shown in Fig. 6.8.

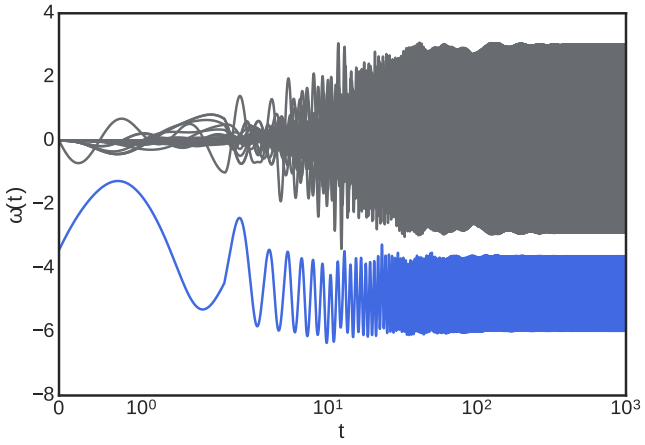

Figure 6.8. – **Exotic solitary state:** Shown are the frequency time series $\omega(t)$ of a particular simulation with an initial perturbation causing a node into an exotic solitary state (blue curve). The figure has been previously published in [P5].

While the remaining network is still rather coherent, a single node oscillates in a limit cycle around $\omega = 4.8$, which is less than half the natural frequency. The deviation between the time-average of an exotic solitary's frequency and the synchronous

regime might become comparatively small, such that operational bounds are not violated. This apparent attractor is a novel observation in networks of power grids – modelled as Kuramoto oscillators with inertia – especially in conjunction with the role of dense sprouts. The state can only exist in a network, i.e. it cannot be understood by considering the isolated node dynamics or the infinite-busbar model Eqn. 4.17. It remains an interesting question for future research to develop a theoretical understanding of the appearance and exact position of exotic solitary states. Proper leaves and sparse sprouts, however, do not show this behaviour. In fact, $\hat{\mu}^k_{\mathcal{B}}$ and $\hat{\mu}^k_{\mathcal{S}}$ are correlated, as for inner tree nodes.

Another observation for intermediate perturbation levels is that while $\hat{\mu}^k_{\mathcal{S}}$ tends to increase with larger ω^+, this is not the case for dense sprouts. The average single-node survivability for this class actually decreases. It is still subject to future research to reveal the underlying mechanism.

In summary, stability maps are *discovery tools*. They are efficient to estimate from high-dimensional complex systems[17] and – together with the classification – facilitate the identification of critical motifs. It is, however, expectable that a statistical regression similar to Sec. 6.3 or sophisticated data clustering algorithms further improve upon these results in the future.

6.4.3. Further Insights on Survivability

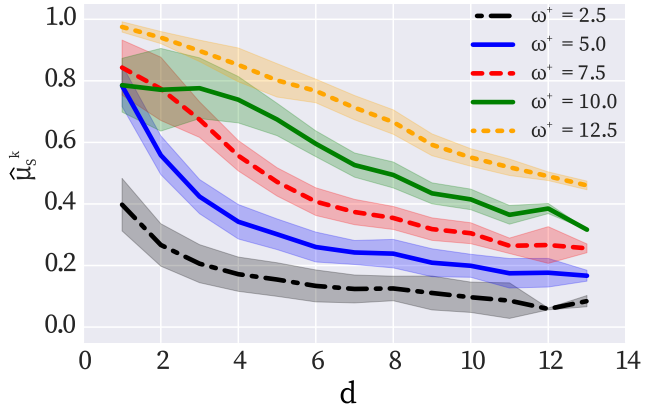

Figure 6.9. – **Survivability-degree relationship**: The curves depict $\hat{\mu}^k_{\mathcal{S}}$ averaged over nodes with the same degree $d_k = d$. The shading indicates one standard deviation. The figure has been previously published in [P5].

Another important result of the ensemble analysis is that the single-node survivability $\mu^k_{\mathcal{S}}$ shows a significant negative correlation with the degree for all sizes ω^+ of the desirable region X^+, irrespective of the node type. This result is summarised in Fig. 6.9. At $\omega^+ = 12.5$, for instance, the power grid survives almost surely a perturbation at a leave node with degree $d = 1$, while the probability decreases to $\mu^k_{\mathcal{S}} < 0.5$ for large-degree nodes. Interestingly, from $\omega^+ = 5$ to 7.5 and $\omega^+ = 7.5$ to

[17] Note that Fig. 6.7 can be derived for all ω^+ at once by sampling from the largest desirable region and conditioning the measures on subsets afterwards.

10, nodes with degree $d = 1$ increase considerably less then the general trend in μ_S^k. A comparison with Fig. 6.7 reveals that this effect can mainly be attributed to proper leaves and dense sprouts, for which the average survivability decreases strongly.

A consequence of this survivability-degree relationship is that high-degree nodes (hubs) should be avoided in the design of power grids. As a side effect, this would also decrease the number of dense sprouts and hence the likelihood of the exotic solitary oscillations discovered above. This is an indication that rather homogeneous network topologies like distributed networks (cf. Fig. 3.1) do not only have a better synchronisability (Nishikawa, Motter, et al. 2003) but also are more likely to remain within bounds after large perturbations. Still, it is important to validate these results with more realistic models and parameters.

6.5. The Spectral Gap and the Role of Cycles

This section refers to research originally published in [P4].

Abstract In this section, I focus on the relationship between synchronisability and cycles, discuss the special role of four-cycles and use a probabilistic approach to sample network alterations.

6.5.1. Balanced Trees

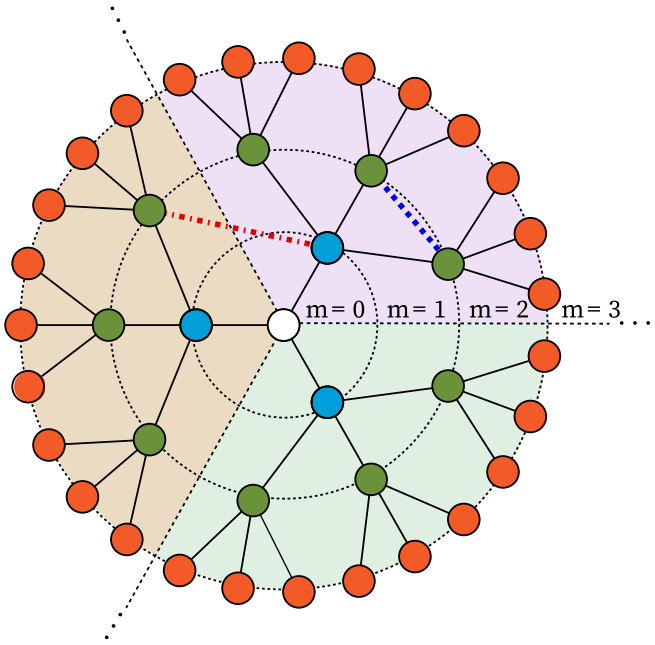

Figure 6.10. – **Illustration of a balanced tree** $G(m,3)$: The node colour indicates the depth level m (first 3 levels are shown). The background colour highlights the $l = 3$ principal branches of the tree. Edge addition creates a cycle which either includes the central node (red, dash-dotted) or not (blue, dashed). The figure has been previously published in [P4].

Complementing the discussion of trees and probabilistic stability in the preceding section, I return to an asymptotic stability analysis with master stability functions (cf. Sec. 2.3.3). Irrespective of the dynamics on a network, this framework allows to draw conclusions about the asymptotic stability of synchronisation from the eigenvalue spectrum of their Laplacian matrix.

Consider a network given by a finite balanced tree $G(m,l)$[18] which is highly symmetric. It is characterised by the branching number l and the number of depth (cf. Sec. 6.4) levels m, i.e. each node except the central one has degree $d = l + 1$.

[18] A balanced tree $G(m,l)$ contains $n = \frac{l^{m+1}-1}{l-1}$ nodes and $n-1$ edges. Hence, the mean degree approaches 2 from below for large m.

Whenever an edge is added to the tree, it inevitably creates a cycle. Now, there are two distinct cases. If (a) a new edge ij connects two nodes from the same principal branch (dashed blue line in Fig. 6.10), the cycle contains the central node and (b) otherwise not. The nodes' depth δ, as defined in the previously section, determines the length of the cycles as

$$l_{ij} = \delta(i) + \delta(j) - 2\delta(p) + 1 \,, \tag{6.5}$$

where p is the closest common predecessor of i and j. In case (a), p is the central node and $\delta(p) = 0$, hence the longest possible cycle has a length of $l_{ij} = 2m + 1$, connecting two leaf nodes.

6.5.2. How Does Adding a Cycle Affect Stability?

By systematically investigating the change in the Laplacian eigenvalue spectrum for all possible additional edges, the aim is to uncover the dependence of synchronisability on different kinds of cycles. As the first Laplacian eigenvalue (assume they are sorted) is $\lambda_1 = 0$, we are mostly interested in the largest one λ_{max} and the smallest non-zero λ_2, also known as the *Fiedler eigenvalue* or *spectral gap*. It is known from early results by Fiedler (Merris 1994) that, by adding an edge, the Laplacian spectrum of the tree interlaces the one of the new graph. That is, adding an edge cannot decrease an eigenvalue of the Laplacian. In the context of synchronisation, the key observable is the synchronisability (cf. Sec. 2.3.3):

$$R = \frac{\lambda_{max}}{\lambda_2} \,. \tag{6.6}$$

Earlier studies observed that trees have a particularly low synchronisability (Yook et al. 2006), indicating that a pure tree can be difficult to synchronise.

Fig. 6.11 pictures the distribution of ΔR, i.e. the relative improvement of the synchronisability, as a function of the length of the new cycle. Since λ_2 does not change within numerical accuracy, ΔR is directly proportional to $\Delta\lambda_{max}$. Several aspects can be observed here. First of all, in terms of ΔR, the cases (a) and (b) yield analogous results. Concerning asymptotic stability, the apparent symmetry of the network with three principal branches, which is broken in case (b), does not seem to be important. An exception are 3-cycles, for which the distributions differ significantly. In particular, the 3-cycle with the highest ΔR is created by connecting two nodes with $m = 1$ (cf. Fig. 6.10). For a fixed cycle length, ΔR decreases with the distance of the connected nodes from the central node, i.e. cycles between leaves of the tree have almost no impact on the Laplacian spectrum. This is pictured in Fig. 6.11b for four-cycles but is also visible in Fig. 6.11, as for 11-cycles – which are created by edges connecting leaf nodes – the synchronisability is left unchanged. Intriguingly, the largest average as well as maximal (about 8%) ΔR is observed for four-cycles, irrespective of whether they contain the central node or not. This dominance of four-cycles pertains over several orders of system size [P3]. However, as Fig. 6.11c highlights, the probability of observing a four-cycle is comparatively low. In general, their stronger effect on the eigenvalue spectrum does not influence

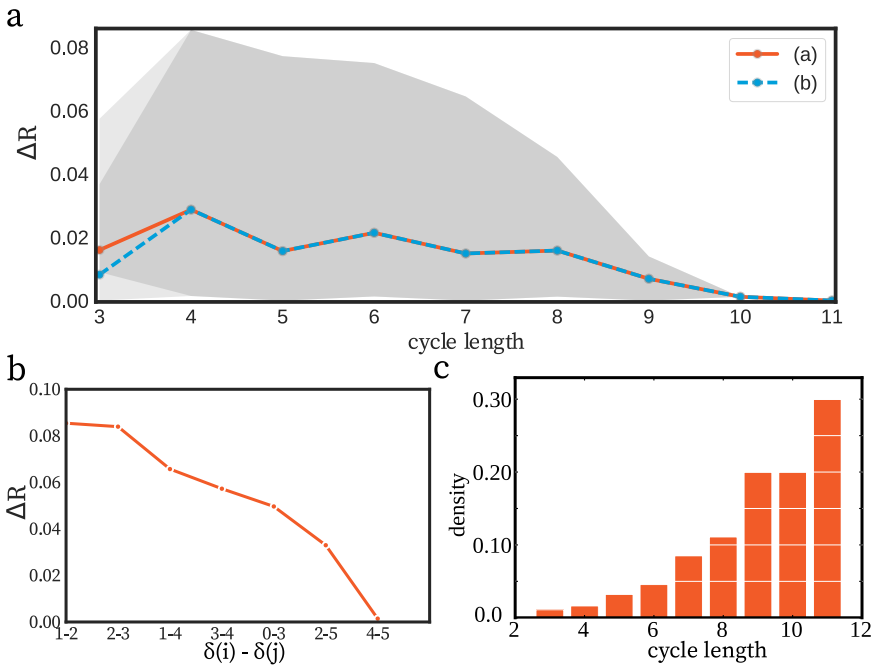

Figure 6.11. – **Synchronisability depending on cycle lengths**: **a** Pictured is the average relative improvement ΔR of the synchronisability R varying with the length of the added cycle (cases (a) and (b)). The shading indicates the spread between the minimum and maximum possible. **b** For edges ij connecting nodes with $\delta(i) \neq \delta(j)$, this shows the expected ΔR when ij creates a four-cycle. **c** Histogram of cycle lengths in $G(5,3)$. Adapted from [P3].

the expected ΔR when randomly placing an edge.

Concerning the consequences for the stability of synchronisation in power grids, the master stability function corresponding to the swing equation has a root at 0 and is otherwise negative [F2]. Hence, a network of Kuramoto oscillators with inertia is synchronisable for any positive coupling strength under the assumption of identical inertia and damping. In general, a more complex behaviour is possible (cf. Sec. 2.3.3), for instance for alternative inverter models including time delay or higher-order synchronous machine models. There, the master stability function can have more roots, determining stability intervals. For a fixed coupling constant, all Laplacian eigenvalues have to fit in this interval; the smaller R, the better. Any increase in R or λ_{max} due to the addition of an edge may lead to a transgression of the stability interval (cf. Fig. 2.6), especially in the case of four-cycles. Consequently, the coupling constant needs to be adjusted accordingly, if possible.

6.5.3. Probabilistic Synchronisability Study

Generalising the model from the previous section, the synchronisability of trees with multiple added cycles is considered. Real-world infrastructure networks, for instance, are rarely trees but have a number of redundant edges. They are typically essential for a proper functioning of the dynamics on the network, as the loss of a

redundant edge leaves the network intact. Otherwise, the sparse power grids are rather tree-like and the heuristic assumption that such networks are characterised by an underlying minimum spanning tree[19], is so far consistent with actual network data. In the following, I present results of a probabilistic approach to assess the variation of synchronisability by sampling random edge additions to $G(m,l)$

A balanced tree $G(m,l)$ of n nodes has $n-1$ edges, hence the number r of yet unconnected node pairs is given by

$$r = \frac{n(n-1)}{2} - (n-1) = \frac{(n-2)(n-1)}{2} . \tag{6.7}$$

We can introduce a parameter $p \in [0;1]$, i.e. the probability of making a new connection. The expected graph density ρ of $G(m,l)$ is then simply

$$\rho = 2\frac{pr+n-1}{n(n-1)} = p\left(1-\frac{2}{n}\right)+\frac{2}{n} \sim p \text{ (as } n \to \infty) . \tag{6.8}$$

Not only does ρ increase with p but it also interpolates between a cycle-free network ($p=0$) and a network with the maximum number of cycles ($p=1$).

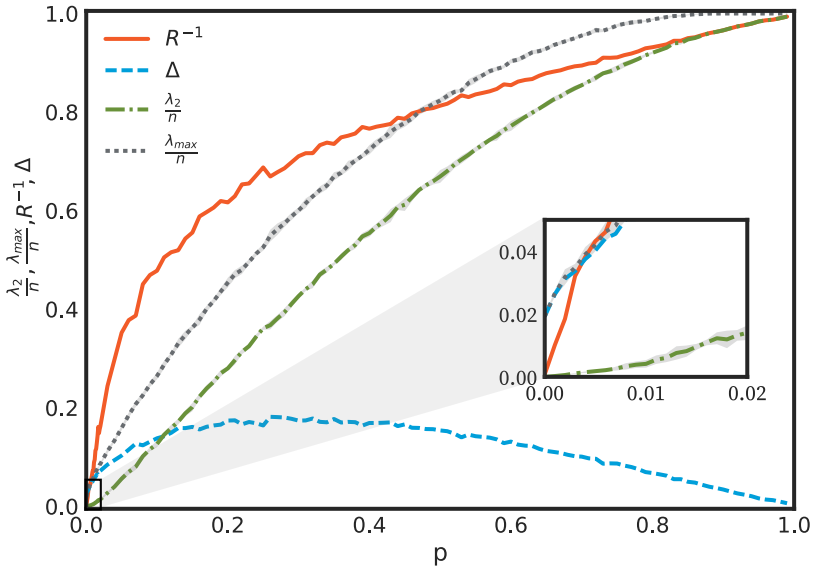

Figure 6.12. – **Synchronisability of random edge addition**: Pictured are the Fiedler λ_2/n and maximal λ_{max}/n Laplacian eigenvalue, the inverse synchronisability R^{-1} and the spread Δ, varying with the parameter p controlling how many edges are randomly added. The edges are added to $G(5,3)$ with a fixed number of nodes n. The shading indicates one standard deviation. Adapted from [P3].

Numerically determined bounds on the nonzero Laplacian eigenvalues, λ_2 and λ_{max} are shown in Fig. 6.12 for varying p. As highlighted in the inset, for a few edges added (e.g. a single one), the synchronisability is mainly determined by

[19]This is also a central assumption of the growth model in Sec. 3.4.3.

changes in λ_{max} (inset of Fig. 6.12). The algebraic connectivity measured by the Fiedler eigenvector λ_2 is not affected. The reverse is true for the limit of $p \approx 1$, i.e. R approaches one from above (Fig. 6.12 depicts R^{-1}) and the eigenvalue spectrum becomes extremely narrow. Consequently, the synchronisability R improves with p, i.e. for networks with higher density. This agrees with the known low synchronisability of trees (Yook et al. 2006).

For a fixed coupling strength, the synchronous solution loses stability as soon as the global shift of the spectrum towards higher eigenvalues transgresses a root of the master stability function, as illustrated in Fig. 2.6. The spread $\Delta = (\lambda_{max} - \lambda_2)/n$ of the spectrum, however, depends non-monotonically on p, i.e. it is maximal for intermediate graph densities. Hence, although R is high in the low-density regime, the spread Δ remains small enough such that the network is likely to be synchronisable by a small adjustment of the coupling constant. Typical power grids, whose density scales as $\rho \approx 2.7/(n-1)$ with the mean degree of $\bar{d} = 2.7$, are exactly in this low-density regime.

In summary, there is an intermediate regime of graph density respectively number of cycles for which a stable synchronous state is more difficult to maintain, especially if the coupling structure cannot be altered. The extent of this regime depend on the dynamical system in question. It remains an interesting task for future research to expand the analysis to to basin stability, which is known to complement the results for synchronisability (Menck, Heitzig, Marwan, et al. 2013).

6.6. Summary and Key Results

In this chapter, I present my research regarding relationships between probabilistic or asymptotic stability and network characteristics. The starting point is a discussion of findings related to small network motifs in Sec. 6.3, i.e. four-node patterns and *detours*, within a large ensemble of synthetic power grid topologies. The latter, a special triangular motif, correlates to medium to high single-node basin stability. In particular, I demonstrate that the multi-modal distribution of single-node basin stability $\hat{\mu}_{\mathcal{B}}^k$ across nodes k is determined by the abundance of different network motifs.

The rather well-separated group of nodes with poor stability ($\hat{\mu}_{\mathcal{B}}^k < 1/3$) corresponds to critical elements in a power grid, as a perturbation there likely desynchronises the system. Consequently, I derive an approach for the identification and prediction of critical nodes by purely topological means using a nonlinear statistical regression method. The explanatory observables for the best-performing models are whether a node is a detour respectively in a dead end/tree, its (average neighbour) strength, weighted local clustering, current-flow closeness and betweenness.

These network characteristics are sufficient to predict about 80% of the nodes correctly to be critical or not. In particular, a node has a high probability of being critical if it

(a) is not a detour node.

(b) is a node in a tree-shaped appendix (excluding leaf nodes) with low betweenness b_k^w.

(c) is neither in (a) or (b) and has a low clustering coefficient C_k^w or low centrality c_k^w.

These findings significantly extend previous results on the influence of dead trees by Menck, Heitzig, Kurths, et al. (2014) and illustrate that a more fine-grained discrimination of nodes is needed.

Consequently, Sec. 6.4 generalises dead ends/trees to tree-shaped appendices of complex networks as an important class of motifs, yielding a novel classification scheme for nodes in such appendices. A computationally efficient algorithm, applicable to any undirected network, is given in Appendix A.2. The different roles, which nodes in tree-shaped appendices assume, are outlined in a complementary analysis of single-node basin stability and survivability in a so-called *stability map*. In contrast to deriving an integrated measure, the advantage of considering different stability measures in parallel lies in the accentuation of the different node classes. They have clearly distinct implications on stability, visible as separated groups in the stability map.

In particular, analysing stability maps for a large ensemble of synthetic power grids reveals the existence of exotic solitary states. These states correspond to single nodes in a limit cycle around a fraction of their natural frequency, by which they are different from conventional solitary oscillations. They are solely observable at "dense sprout" nodes, i.e. leaves connected to nodes with at least five further neighbours. This is a pure network effect, not appearing for isolated units. As these frequency oscillations seem to be stable and can occur close to the stable operating state, they can pose a severe risk for power grids[20]. Furthermore, a significant negative correlation between single-node survivability (cf. Sec. 5.5) and the degree of a node implies that hubs with large degrees facilitate the transient growth of disturbances. At the same time, tree-shaped appendices tend to contain nodes with low single-node basin stability. The key learning for an optimal network design – beneficial for both notions of stability – is to avoid both hubs and appendices. This is, for instance, achieved by distributed networks with rather homogeneous degree distribution (cf. Fig. 3.1).

In Sec. 6.5, I add a remark on the influence of cycles on the linear synchronisability of complex systems using the framework of master stability functions. Starting with a tree, cycles are added in a controlled way to isolate their effects on the asymptotic stability of synchronisation, which is determined by the eigenvalue spectrum of the Laplacian matrix. The main finding is that the addition of a single edge can cause the largest improvement of synchronisability when it adds a four-cycle, in particular in proximity of the most central node. The change of synchronisability for adding a random fraction p of edges is studied using a probabilistic approach, interpolating between a cycle-free ($p = 0$) and complete network ($p = 1$). This reveals an interesting trade-off. On the one hand, the addition of an increasing number of edges to

[20] This phenomenon is similar to other effects like inter-area oscillations in large-scale power grids (Jan-E-Alam 2009), which are expected to be more prominent in future power grids with low inertia (Quitmann et al. 2009).

the tree improves the synchronisability. The spread of the Laplacian spectrum, on the other hand is changing non-monotonously, being maximal for an intermediate regime of graph density. In this regime, the eigenvalue spectrum is broad, such that adding another edge likely leads to a transgression of the stability interval's boundary. As power grids typically have a low density and are characterised by an underlying spanning tree, they are less likely to lose asymptotic stability of synchronisation via edge additions. Compared to nonlinear effects of adding cycles, i.e. Braess' paradox, the spread of the Laplacian spectrum might also be less important to consider in practice. This can change however, when more complex dynamical models are considered.

7. Synopsis

Contents of this Chapter

7.1. Summary

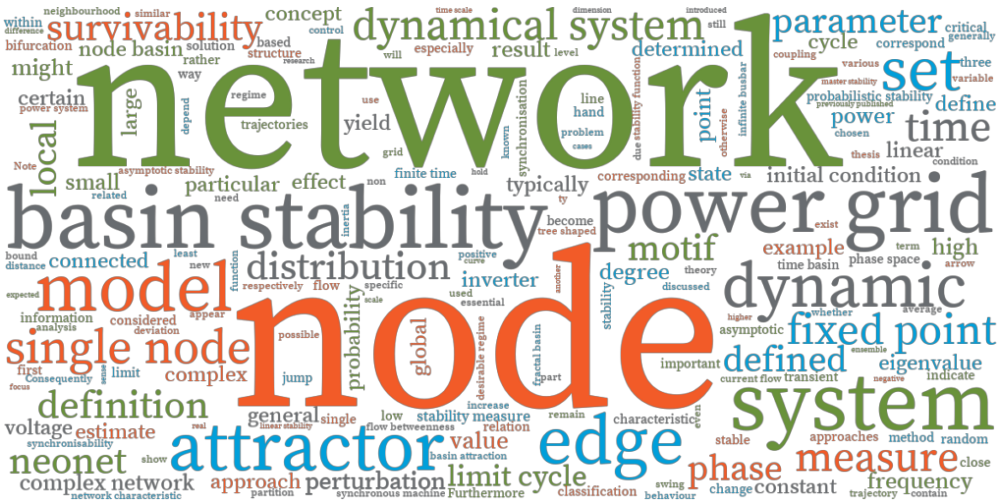

Figure 7.1. – **Wordcloud of this thesis**: Shown are the non-trivial words with the most frequent occurrence in this thesis. The font size is related to the word count, i.e. frequently-used words are larger than rare ones.

What is this thesis all about? In the following, I attempt to summarise the main aspects of each chapter. First, however, have a look at Fig. 7.1 which visualises the subjects discussed most frequently on the previous pages. The font size corresponds to the relative number of appearances of a word. Apparently, the most prominent terms are "node", "network", "system" and "power grid", followed by "basin stability", "attractor", "survivability" and "single node". Hence, the essential building blocks of the physical system under study are reflected via their importance in the meta-structure of this thesis. The power grid as a dynamical system is determined by processes at its nodes, which interact through a network topology in a complex way. Both network structure and node dynamics need to be compatible, not only facilitating the emergence of synchronisation, but also rendering it as stable as possible. Developing suitable stability concepts as well as uncovering their relationships to the network structure is the central motivation for this thesis and the research presented herein.

I am going to recapitulate the essential aspects of the previous chapters, following the tripartite structure given by the theoretical foundations, the model setup and the research results on probabilistic stability measures.

Qualitatively, *dynamical systems* show a rich variety of behaviour which can be best understood by considering their so-called *phase space*. Typically, the main interest lies in the *time-asymptotic behaviour* of solutions to the equations that specify the evolution of a system. This leads to the concept of attractors, which can be defined in different ways. Here, I consider *measure attractors* in the sense of Milnor. These are asymptotic states which are not necessarily stable against small perturbations,

but randomly chosen solutions converge to them with a positive probability. The total catchment area of an attractor is termed *basin of attraction*.

Complex dynamical systems exhibit macroscopic phenomena like synchronisation. *Phase synchronisation*, in particular, is an emergent effect related to the proper functioning of power grids. In this context, phase synchronised dynamical units are described as oscillators whose frequencies are entrained to the power grid's rated frequency and whose phases are locked to each other such that pairwise differences are constant.

Established approaches to assessing the stability of synchronisation, or attractors in general, are based on the pioneering ideas of Lyapunov. An attractor is considered to be stable if a small (infinitesimal) perturbation causes only a small response of the system and a return to the initial attractor. This leads to the *asymptotic stability* framework, where stability is discussed qualitatively based on a linear representation of a dynamical system close to an attractor. New attractors emerge or loose stability when system parameters are varied. This is termed a *bifurcation* and I discuss several basic examples. Power grids are typically operated in a regime where the system is multistable, i.e. several attractors coexist. Consequently, switching to an alternative attractor alters the state of a system qualitatively. For complex networks, so-called *master stability functions* frame the linear stability analysis in a particularly insightful way, disentangling the local processes at the nodes from network effects.

When it comes to large (finite) perturbations, different methods are needed. So-called *direct methods* are based on Lyapunov functions, which are potential-like functions with local minima on attractors whose existence ensures asymptotic stability. Lyapunov functions are, however, difficult to determine, especially in high dimensions, and yield conservative bounds for the extent of basins that are not easily correlated with parameter changes. Alternatively, *basin stability* is a probabilistic approach for quantifying stability based on the basin volume. It corresponds to the probability that a system returns to an attractor after an even finite random perturbation. In practice, basin stability is estimated using a Monte Carlo scheme, which is especially effective for high-dimensional systems and might incorporate network-local perturbations at single nodes in a network. Basin stability is not subject to the curse of dimensionality due to the fact that the precise geometry of the basin is not considered. Prominent examples for *fractal basin geometries* are fractal basin boundaries and riddled basins. While, in the former case only the boundaries are intertwined in a fractal way, in the latter the basin has no open interior at all. This can pose a problem to simulating the long-term behaviour of single trajectories correctly and is again discussed in Sec. 5.3 concerning the Monte Carlo estimation of basin stability.

Power grids are characterised by their *complex network* structure. A complex network is neither regular nor completely random but occupies a space inbetween. There are various characteristics which can be used to distinguish different kinds of complex networks, for both its nodes and edges. I discuss *node characteristics* in more detail, whereof there are *local*, *mesoscale* and *global* variants. While local network characteristics only consider a node and its immediate neighbourhood, global characteristics need information about the whole network. An example for a mesoscale measure is Newman's current-flow betweenness, which I here generalise

to arbitrarily weighted networks. It relates to a node's average share in flows on the network. In some research contexts, it can be insightful to regard a network not as a monolithic entity but as a *network of networks*. It is reflected in the partition of a network in interacting sub-parts. Particular models are multiplex or, more general, multilayer networks. I define a novel variant termed *neonet*, complementary to the existing concepts. It is a model where there is no one-to-one relation between nodes in different sub-networks, not assuming the layered structure of multilayer networks. To differentiate this concept from other approaches, the sub-networks are termed patches and the edges between them constitute the so-called seam. Neonets appear, of course not exclusively, in the context of spatially-embedded infrastructure networks. While, on the one hand, empirical data on real-world networks is rare and, on the other hand, network ensembles are needed to test statistical hypotheses, synthetic network topologies are needed. I introduce a novel *concurrent-growth algorithm* for spatially-embedded neonets as a generalisation of a previous model for isolated networks[1]. It assumes that different patches appear in different development phases. Each patch is initiated as a minimum spanning tree which subsequently extends over time, adding redundant edges according to a heuristic trade-off function.

The considerations of the previous chapters culminate in a model of power grid dynamics which I here refer to as the *SCONE model* (SeCond Order NEonet model). It combines a specific dynamical system representation with the network model discussed above. There are two important classes of *node dynamics*, namely *synchronous generators* as well as *grid-forming inverters* through which renewables connect to the grid. I derive their governing equations from basic assumptions and show how they can be described as *Kuramoto oscillators with inertia*. This opens the possibility to treat both classes in an identical mathematical fashion with separate parameter sets. These oscillators exhibit phase synchronisation and are non-identical due to their diverse input power respectively attached consumption. Besides that, desynchronised solutions corresponding to frequency oscillations exist and can be determined approximately. The second ingredient to the SCONE model is its *network structure*. Empirically, power grids are separated in a hierarchy of *voltage levels*, ranging from extra-high and high to medium and low voltage. The extra-high and sometimes also high levels are commonly summarised as transmission grids, responsible for balancing production and demand in power grids over long distances. Large-scale power producers connect directly to the transmission grid. The remaining voltage levels are distribution grids, designed to distribute power locally, down to the consumer level. Distribution grids are undergoing a major transformation as they comprise the majority of renewable energy sources, connected via inverters. From a *complex network* perspective, power grids are sparse networks where a node has less than three neighbours on average, independent of the network size. This and further characteristics are generally not reproduced by standard network models, especially when they neglect the spatial embedding. Moreover, the partition into voltage levels naturally induces a *description as a neonet*. Hence, the dynamic units in the SCONE model are interconnected by synthetic neonet topologies derived

[1] This research contribution is published in [P3].

from the growth model introduced in the previous chapter. The complete SCONE model is summarised in compact form at the end of the chapter for later reference.

After assembling the underlying theory and defining a basic model, the remainder of the thesis is dedicated to probabilistic stability measures and their relationship to network characteristics.

The increasing use of basin stability in research highlights the advantages of probabilistic stability measures for high-dimensional systems, especially complex networks. They are typically based on classifying single solutions of a dynamical system in a Monte Carlo sampling, wherefore numerical integration is necessary. Consequently, I systematically investigate possible limitations for probabilistic methods – in particular basin stability – in systems with *fractal basin geometries* where the long-term prediction of trajectories can be obstructed. This is known as *final-state sensitivity* and particularly manifested in significant rounding errors dominating the overall estimation error. My results are twofold[2]. On the one hand, fractal basin boundaries still allow for a meaningful basin stability estimation. The final-state sensitivity does not significantly influence the estimation error. This result is especially important for the application of basin stability to power grids, where fractal boundaries can be observed in the second-order model (Hasegawa et al. 1999). On the other hand, riddled basins do not allow a meaningful Monte Carlo estimation at all. A systematic relation of the estimation error to an increase in numerical precision cannot be observed. Consequently, I suggest to use an estimate of the rounding error's contribution, given by comparing stability estimates at different numerical precision, as a (rough) performance indicator in practice.

Besides final-state sensitivity, another problem are *subsequent perturbations* building up a critical state even if they are small. So far, this is not captured by established probabilistic stability measures, which are based on a distribution of singular perturbations. Here, I introduce a new concept termed *finite-time basin stability*[3]. The reasoning is the following. Consider a genuine dynamical system subject to possibly large perturbations, appearing less often than a certain time interval. This could be, for instance, an approximation to stochastic processes dominated by jumps and approximately deterministic behaviour inbetween. If the time interval is sufficiently long for a perturbed trajectory to return sufficiently close to an attractor inbetween perturbations, subsequent jumps are almost statistically independent events. Otherwise, the effect of a perturbation depends on the previous one. These conditions are precisely quantified by defining a measure of *approximate independence*. Then, finite-time basin stability corresponds to the probability that a system returns sufficiently close to an attractor within a given finite time. Asymptotically, when perturbations become rare enough, it coincides with the conventional basin stability. Hence, the critical time scale where both measures become approximately equal determines the so-called *independence time*. Furthermore, an important result is the derivation of a lower bound on the cumulative *probability to remain* within the basin.

In practice, however, the asymptotic behaviour might be less important when

[2]The results of this section are published in [P7].
[3]The results of this section are published in [P6].

there are constraints to the transients of a system. Power grids, for instance, are operated within strict bounds on deviations from the rated grid frequency and any violation activates various countermeasures. Generally, such bounds partition the phase space in a *desirable* and *undesirable regime*. In this context, I present a novel probabilistic stability measure termed *survivability*[4]. It corresponds to the probability that a system remains within the desirable regime at least for a finite time, given a random finite-size perturbation. The set of initial conditions, from which emanating trajectories never transgress the boundary of the desirable regime, is termed *infinite-time basin of survival*. Approximating the dynamics by a linear systems, it is possible to derive *semi-analytic lower bounds* on the volume of the basin of survival, i.e. the infinite-time survivability. Furthermore, survivability can be estimated efficiently by using a Monte Carlo scheme. Numerical experiments indicate firstly a good performance of the approximation even in a nonlinear system and secondly that basin stability and survivability are indeed uncorrelated. In comparison, survivability has the further advantage that it is not subject to the problems with fractal basins discussed above, as it is not based on asymptotic sets like the basin of attraction. In summary, survivability provides a novel measure of stability given transient bounds which is amenable to computationally fast semi-analytic approximations.

As probabilistic stability measures typically rely on time-consuming simulations of dynamical systems, it is necessary to reduce the complexity of the problem to make them applicable to practical situations. In power grids, for instance, transmission grid operators assess the stability of the current operating point at least every 15 minutes. In the case of survivability, it is possible to use bounds that do not rely on time-domain simulations. Alternatively, the problem might be simplified by taking the structure of complex networks into account. More general, it is still an open task to derive an explicit dependence of stability measures on a specific network's topology. In this chapter, however, I present some indications for *motifs* (small substructures of a network) with particular influences on the stability, e.g. of synchronisation.

An analysis of a large ensemble of synthetic power grids using the SCONE model revealed that single-node basin stability is distributed in three classes of nodes with poor, fair and high stability. Poor nodes are *critical* in the sense that a perturbation there likely desynchronises the system. I reveal that nodes in *tree-shaped appendices*, which have been identified as destabilising structures called dead ends in previous studies, need to be finer distinguished[5]. In particular, nodes with high current-flow betweenness are not critical opposed to low-betweenness nodes. Moreover, there is a triangular motif that is generally beneficial for stability as it does not contain critical nodes. I refer to them as *detour nodes*, because they are on a detour between different parts of the network and hence have vanishing shortest-path betweenness. Several of these relationships are assembled in a *statistical predictor* for poor single-node basin stability. The information whether a node is on a detour or in an appendix, together with five selected network characteristics is sufficient to derive a statistical regression model able to predict critical nodes correctly in about 80% of

[4]The results of this section are published in [P2].
[5]The results of this section are published in [P1].

cases. Apparently, the network structure is the main influence determining basin stability. Such fast estimators are essential for real-time applications, at least for a pre-selection of the most critical nodes.

Adding survivability to the picture sharpens the image. I first introduce a novel classification scheme of nodes in *tree-shaped appendices*[6]. These are all trees connected to the remaining network via a single node, the *root*. The special case of a single node attached to the root is called a *sprout*, if the root has a high degree it is a *dense sprout*. A combined plot of single-node basin stability and survivability resembles a so-called *stability map*. They reveal that different classes of nodes have clearly distinct implications on stability, visible as separated groups in the stability map. Furthermore, there is a novel dynamic state appearing exclusively at dense sprouts. When a perturbation at such a node does not resynchronise, the system approaches an *exotic solitary oscillation* of the sprout's frequency while the remaining network is almost synchronised. It is different from previously described solitary states in that the average frequency deviation has no obvious relationship to the natural frequency of the single oscillator. Both the discovery of unexpected phenomena as well as the differentiation of node classes highlight the advantage of complementary considering different probabilistic measures in a stability map instead of combining them into an integrated quantity. Furthermore, single-node survivability exhibits a pronounced negative correlation to the degree of a node. Hence, while hubs tend to have a particularly low survivability, the opposite is true for leaves. Together with the potential of tree-shaped appendices to contain critical nodes with low single-node basin stability, an optimal network design is to avoid both hubs and appendices. This is, for instance, achieved by distributed networks with rather homogeneous degree distribution.

Power grids are typically sparse networks with only few redundant connections along *cycles*. As a simple model, I consider a tree. When an edge is added to a tree, it creates a cycle of a specific length. I use this approach to systematically study the impact of cycles on the stability of synchronisation in a controlled way[7]. In contrast to probabilistic stability measures discussed so far, which are based on sampling the phase space, I here follow a different approach. In particular, an asymptotic stability analysis using *master stability functions* is combined with a probabilistic approach of sampling changes to the network topology. In this framework, the synchronisability is determined by the spectrum of the graph Laplacian, characterised by its spread between the minimal and maximal eigenvalue. It turns out that four-cycles have the largest effect on the eigenvalues when they are added, especially so the closer they are to the most central node. In a second step, a random amount of edges is added to the tree to investigate how the synchronisability is affected. This model interpolates between the cycle-free tree and a fully-connected network with a monotonically increasing graph density. While the synchronisability decreases (improves) with an increasing density, the eigenvalue spread is not monotonic, being maximal for an intermediate regime of graph density. A large spread of the spectrum might be compensated for by an adjustment of the coupling constant, to avoid transgressing

[6] The results of this section are published in [P5].
[7] The results of this section are published in [P4].

the boundary of the stability interval. For low densities, i.e. the regime of typical power grid topologies, however, adding another edge is not likely to destabilise the synchronous state.

7.2. Research Contributions and Outlook

Graph Theory: Analysis and Modelling of Complex Networks

Regarding the modelling of spatially-embedded networks of networks, I contributed a consistent framework of definitions including a growth model (Sec. 3.4.2). The notion of a neonet extends the concept of multilayer networks, which are predominantly used in the previous literature, to arbitrary interdependent networks. In particular, it does not assume identical sets of nodes in each subnetwork and does not imply a layered hierarchy. Note that I introduced an alternative naming convention in this thesis to avoid a confusion with the other approaches. The network growth model is the first of its kind for spatially-embedded neonets, generalising a previous model for single networks [F3]. As spatially-embedded neonets appear not only in the context of power grids but in infrastructure networks in general, this framework and model may contribute to different research fields and opens a way for hypotheses-testing when empirical network data is rare. Given the modular structure of the model, it is straight-forward to replace the heuristic assumptions on the growth process with empirical knowledge, for instance by incorporating geographic distributions of producers and consumers. Worthwhile future extensions include a generalisation to directed networks or the inclusion of node types (producer, consumer, etc.). Furthermore, the tree classification in Sec. 6.4 resembles a novel formalisation of tree-shaped appendices, together with a computationally efficient algorithmic realisation. Such appendices are a particularly prominent feature of infrastructure networks with an important dynamical signature when it comes to the stability of synchronisation. Hence, Sec. 6.4 is also a showcase for a possible application of this classification scheme to differentiate dynamical effects of different node groups in complex networks. Again, it is left for future research to generalise the topological classification to directed networks.

Related publications: [P3] and [P5].

Nonlinear Dynamics: Probabilistic Stability Measures

A large part of the work presented here is of a methodological nature, concentrating on probabilistic approaches to assessing stability in complex systems. Recently, this field has gained increased attention by the introduction of basin stability. An integral ingredient is its identification of asymptotic states in a Monte Carlo estimation. The results on basin stability's applicability to fractal basin geometries (Sec. 5.3) demonstrate possible limitations of the approach. Although final-state sensitivity due to fractal basins is well-known and occasionally observed in experiments, there seems to be no systematic study on its role in Monte Carlo schemes yet. Further on, finite-time basin stability generalises basin stability to take the return time to an attractor into account (Sec. 5.4). By this, it is a novel probabilistic stability measure.

Applying it to systems where large perturbations are expected to occur repeatedly, finite-time basin stability determines the critical time scale for the system to return close enough to an attractor such that perturbations are approximately independent events. This approach includes the timing of transients into a stability measure and furthermore allows to determine the regime of applicability of the original basin stability. Besides the definition of a new probabilistic stability measure, the derivation of the bound to the cumulative exit probability from the basin may find broader application, as the bound is efficient to determine. The derivation of finite-time basin stability is so far restricted to fixed points, such that it is a potential aim for future research to generalise this approach to more complicated attractors. Furthermore, the bound on the remain probability is derived from rather conservative assumptions and may be improved. The most important next step, however, should be the application to networks. Subsequently, survivability (Sec. 5.5) as a novel stability measure is introduced. The main contributions of this concept are given in its ability to incorporate almost arbitrary constraints on transients in the stability assessment, as well as in its independence from knowledge about attractors and identification of final states. This renders survivability an ideal stability measure for dynamical systems, where the transient behaviour is more important than asymptotic stability. Remarkably, it is the first probabilistic stability measure which can be approximated analytically, at least for linear(-ised) systems, and hence computed without time-domain simulations. I see the main potential for future research in this field in improving this analytic approximation. Furthermore, it is still open to explore the limitations of survivability applicability.

Related publications: [P2], [P7] and [P6].

Nonlinear Dynamics: Stability of Synchronisation on Complex Networks

Above, different probabilistic stability measures are developed, mainly within the framework of synchronisation on oscillator networks. An important advantage of these methods is, that it is straight-forward to consider network-local perturbations, i.e. a distribution of perturbations occurring at a single node of a network. This leads to the single-node variants of basin stability and survivability. While previous approaches combined different aspects of stability in integrated measures, a complementary consideration of the single measures in what I termed a stability map (Sec. 6.4) is an alternative approach. It turns out to be particularly useful in distinguishing node groups with coherent stability implications. Here, the classification of tree-shaped appendices is particularly insightful. As an example, this approach allowed for the discovery of exotic solitary states in the power grid model. To the best of the author's knowledge, this is described and linked to the appearance of dense sprouts for the first time. In the future, stability maps as a discovery tool may be significantly enhanced by considering more and different stability indicators, as well as by extended classification schemes. On the analytic side, it is yet open to fully understand the appearance of exotic solitary states at dense sprouts and to explain their precise average frequency deviation. Another important insight is the apparent relationship between the new measure of survivability and the node degree, such that hubs with many neighbours exhibit a particularly low survivability,

or conversely have a high probability to exceed desirable bounds. It is an open problem to develop the analytic approach described in Sec. 5.5 towards an explanation of this effect. Similarly, the observations for (i) detour nodes as well as (ii) nodes in appendices with different current-flow betweenness (Sec. 6.3) or (iii) the addition of cycles (Sec. 6.5) are yet purely phenomenological and lack a deeper understanding. Still, these results enable a statistical prediction that discovers critical nodes correctly in about 80% of all cases. The important practical implications here are, that a computationally fast approximate estimation of probabilistic stability measures seems within reach. Also, the effect of adding cycles is studied in terms of synchronisability, which is a linear approach. Future research should apply probabilistic stability approaches to the tree model, in order to find a relationship to cycles as a fundamental motif.

As a general remark, the considerations above are still conceptual on many levels, especially by considering a symmetric bimodal distribution of net producers and net consumers. Here, more heterogeneous, i.e. realistic, distributions should be considered, for instance to investigate the role of decentral power supply. Besides, all results should be validated with detailed real network dynamics, be it from actual data or industry-standard simulations.

Related publications: [P1] [P4] and [P5].

Modelling Power Grids

For developing new methods, it is a common approach to use test cases of low complexity. Hence, in this thesis, the underlying power grid model SCONE (Sec. 4.4) is far from being application-ready but more conceptual, both in its parametrisation and assumptions. It is restricted to modelling synchronous machines and grid-forming inverters on short time scales. This is permitted by phase synchronisation being one of the fastest dynamical phenomena in power grids, while the long-term behaviour is dominated by other aspects, e.g. voltage magnitude dynamics. While the second-order dynamics is sufficient to estimate survivability, which focuses on transients, asymptotic basin stability estimations are less reliable. This shows of course that higher-order dynamics generally have to be included in a power grid model, but also that it might be sufficient to reduce the model complexity, depending on the research question.

In conclusion, the SCONE model can be further used in the future to investigate the synchronisation of Kuramoto oscillators with inertia on networks of networks. Moreover, as a pair of network model and node dynamics, it is modular such that the second-order dynamics can easily be extended or the network topology replaced by actual data. To increase the relevance of this work for power grid modelling, several immediate improvements can be suggested. They range from (i) considering realistic fluctuations of intermittent feed-in as discussed in Sec. 4.2, (ii) describing the dynamical system via differential algebraic equations (DAE) for algebraic constraints at passive nodes to (iii) modelling time delays arising from inverters.

Related publications: [P1] and [P5].

A. Algorithms

Contents of this Chapter

A.1. Concurrent-Growth Model for Spatially Embedded Infrastructure Neonets

The following algorithm is reproduced from [P3] with minor adjustments of notation.

To perform the algorithm, the following parameters need to be specified:

- $L \geq 1$: Number of patches.
- $n_0^\ell = \mathcal{V}^\ell \geq 1$: Number of initial nodes of level ℓ at its introduction.
- $n_\phi^\ell \geq 0$: Number of additional nodes of level ℓ grown in phase $\phi \geq \ell$.
- $\alpha^\ell, \beta^\ell, \gamma^\ell$: Node location distribution parameters governing the amount of spatial clustering. Alternative choices, e.g. uniform distributions, are possible as well.
- p^ℓ: Expected number of redundant edges each new node gets immediately.
- q^ℓ: Expected number of additional redundant edges added to random nodes at each growth step.
- $r^\ell, u^\ell \geq 0$: Importance of redundant edge benefits.
- s^ℓ: Rate of edge splittings.

For each phase $\phi = 1...L$, the algorithm performs the following steps I and G:

I Introduction and initialisation of a new patch labelled $\ell = \phi$.

I1 Add n_0^ℓ many nodes v_i^ℓ to $\mathcal{V}^\ell$ at random locations $x\left(v_i^\ell\right)$ as follows.

I1.1 Draw $x(v_1^\ell)$ uniformly at random from R.

I1.2 For $i = 2 \ldots n_0^\ell$, determine $x\left(v_i^\ell\right)$ according to Eqn. 3.25.

I2 Find the minimum spanning tree (w.r.t. Euclidean distance) of these n_0^ℓ many locations and add all its edges to $\mathcal{E}^\ell$.

I3 Add m (cf. Eqn. 3.22) redundant edges to $\mathcal{G}^\ell$ as follows. For $a = 1 \ldots m$, draw a $v \in \mathcal{V}^\ell$ uniformly at random, find that $v' \in V^\ell \setminus \{v\}$ that has no edge to v yet for which $f^\ell(v, v')$ is maximal and add a new edge vv' to $\mathcal{E}^\ell$.

I4 If $\ell > 1$, connect $v_1 \in \mathcal{V}^\ell$ to the previous patch by finding the node $v \in \mathcal{V}^{\ell-1}$ that minimises $d_2(v_1, v)$ and add a new edge $v_1 v$ to $\mathcal{E}^{\ell-1}$. (This ensures a connected neonet.)

G Simultaneous growth of all already existing patches, i.e. $\ell = 1 \ldots \phi$. For each $\ell = 1 \ldots \phi$, let U^ℓ be a set of n_ϕ^ℓ many new nodes to be added to $\mathcal{V}^\ell$ in phase ϕ and let U be the union of all these U^ℓ. For each $v \in U$, drawn uniformly at random without replacement, being assigned to $\mathcal{G}^\ell$, do the following:

G0 Add v to $\mathcal{V}^\ell$. With probabilities $1 - s^\ell$ and s^ℓ, perform either steps G1–G4 or step G5 below, respectively.

G1 Determine $x(v)$ according to Eqn. 3.25.

G2 Find that node $v' \in \mathcal{V}_c^\ell \setminus \{v\}$ for which $d_2(v, v')$ is minimal, add a new edge vv' to $\mathcal{E}^\ell$.

G3 Draw a number $k \geq 0$ from the geometric distribution with mean p^ℓ and repeat the following k times: find that node $v' \in \mathcal{V}_c^\ell \setminus \{v\}$ that has no edge to v yet for which $f^\ell(v, v')$ is maximal and add a new edge vv' to $\mathcal{E}^\ell$.

G4 Draw a number $k \geq 0$ from the geometric distribution with mean q^ℓ and repeat the following k times: draw a node $v'' \in \mathcal{V}^\ell$ uniformly at random, find that node $v' \in \mathcal{V}_c^\ell \setminus \{v''\}$ that has no edge to v'' yet for which $f^\ell(v'', v')$ is maximal and add a new edge $v''v'$ to $\mathcal{E}^\ell$.

G5 Select an edge $v'v'' \in \mathcal{E}^\ell$ uniformly at random, draw $a \in [0, 1]$ uniformly at random, let $x(v) = ax(v') + (1 - a)x(v'')$, remove $v'v''$ from $\mathcal{E}^\ell$ and add two new edges $v'v$ and vv'' to $\mathcal{E}^\ell$.

Note that, after performing the algorithm, no edges belong to the seam $\mathcal{E}_{seam}$ yet. Some nodes are adjacent to edges from different patches, however, the algorithm accounted these nodes to the hierarchically "higher" patch. To add the seam, the following steps are performed to obtain a neonet according to Def. 10:

Do the following for all nodes $u \in \mathcal{V}^\ell$ where different edges meet.

F1 For all neighbours $v \in \mathcal{V}^k$, add a node u' to $\mathcal{V}^k$ with $x(u') = x(u)$.

F2 Remove the edge uv from $\mathcal{E}$. Add a new edge $u'v$ to $\mathcal{E}^k$.

F3 Add an edge uu' to $\mathcal{E}_{seam}$.

A.2. Identification of Tree-Shaped Appendices

The identification of tree-shaped appendices (cf. Sec. 6.4) of a graph $\mathcal{G} = (\mathcal{V}, \mathcal{E}, w)$ along with the height and depth values can be efficiently performed using the algorithm proposed in Nitzbon et al. (2017) (reproduced from there):

In the first part, we iteratively define

- a decreasing sequence of node sets $V_0 \supset V_1 \supset V_2 \ldots$,
- the respective induced subgraphs $G_i = G[V_i]$,
- a sequence of disjoint height level sets H_i,
- parents $\pi(x)$,
- sets of children $C(x)$,
- branches $B(x)$,
- and height labellings $\eta(x)$,

by successively removing leaves from the remaining graph as follows.

Put $V_0 := V$ and initially $C(x) := \emptyset$ for all $x \in V$.

Given V_i and G_i, let $H_i := \{x \in V_i : d_{G_i}(x) = 1\}$ be the set of leaves of G_i[1]. For each $x \in H_i$, let the *parent* of x, $\pi(x)$, be the unique neighbour of x in G_i; add x to its set of *children*, $C(\pi(x))$. Note that $\pi(x) \in V_i - H_i$. The *branch* of x is $B(x) := \{x\} \cup \bigcup_{y \in C(x)} B(y)$, and the height is $\eta(x) = i$. As long as $H_i \neq \emptyset$, put $V_{i+1} := V_i - H_i$ and repeat.

To finish the first part after these iterations, let $N := \bigcup_i H_i$ be the set of all thus identified non-root nodes, let $R := \{\pi(x) : x \in N\} - N$, and call each $r \in R$ a *root*. Put $B(r) := \{r\} \cup \bigcup_{y \in C(r)} B(y)$ and $\eta(r) := 1 + \max\{\eta(x) : x \in N, \pi(x) = r\}$ for all $r \in R$. The tree-shaped parts T of G are now exactly the subgraphs $T = G[B(r)]$ induced by the branches of any roots $r \in R$.

In the second part, we define a *depth* $\delta(x)$ for each $x \in N \cup R$, counted outwards starting from the roots, in addition to the height, which is counted inwards starting from the leaves. This is again done iteratively by defining a sequence of disjoint depth level sets D_i. Put $D_0 := W_0 := R$, and put $\eta(x) := 0$ for each $x \in D_0$. Having defined D_{i-1} and W_{i-1}, define $D_i := \bigcup_{x \in D_{i-1}} C(x) - W_{i-1}$ and $W_i := D_{i-1} \cup D_i$, and put $\delta(x) := i$ for each $x \in D_i$, iterating this until $D_i = \emptyset$. Note that $\delta(x)$ is the distance from x to the root of its tree-shaped part.

Finally, we put $S := \{x \in N \,|\, \eta(x) = 0 \wedge \delta(x) = 1\} = \{x \in L \,|\, \delta(x) = 1\}$ (sprouts), $S_d := \{x \in S \,|\, \bar{d}_{\mathcal{N}} > 5\}$ (dense sprouts), $S_s := \{x \in S \,|\, \bar{d}_{\mathcal{N}} < 6\}$ (sparse sprouts), $P := \{x \in N \,|\, \eta(x) = 0 \wedge \delta(x) > 1\} = \{x \in L \,|\, \delta(x) > 1\}$ (proper leaves).

---

[1] For any (sub-)graph $G' = (V', E', w)$ and node $x \in V'$, $k_{G'}(x)$ denotes the degree of x in G'. A node with $k_{G'}(x) = 1$ is called a leaf of G'.

Bibliography

Abarbanel, H. D. I., N. F. Rulkov, and M. M. Sushchik (1996). „Generalized synchronization of chaos: The auxiliary system approach“. In: *Phys. Rev. E* 53.5, pp. 4528–4535. DOI: 10.1103/PhysRevE.53.4528 (cit. on p. 17).

Abrams, D. M. and S. H. Strogatz (2004). „Chimera states for coupled oscillators“. In: *Phys. Rev. Lett.* 93.17, p. 174102. DOI: 10.1103/PhysRevLett.93.174102 (cit. on p. 18).

Acebrón, J. A., L. L. Bonilla, C. J. Pérez Vicente, F. Ritort, and R. Spigler (2005). „The Kuramoto model: A simple paradigm for synchronization phenomena“. In: *Rev. Mod. Phys.* 77.1, pp. 137–185. DOI: 10.1103/RevModPhys.77.137 (cit. on p. 17).

Agresti, A. (2002). *Categorical Data Analysis*. 2nd. New Jersey: John Wiley & Sons, Inc. (cit. on p. 124).

Agresti, A. and B. A. Coull (1998). „Approximate is better than "exact" for interval estimation of binomial proportions“. In: *Am. Stat.* 52.2, pp. 119–126. DOI: 10.2307/2685469 (cit. on p. 29).

Alexander, J. C., J. A. Yorke, Z. You, and I. Kan (1992). „Riddled Basins“. In: *Int. J. Bifurc. Chaos* 02.04, pp. 795–813. DOI: 10.1142/S0218127492000446 (cit. on pp. 34, 86 sq., 89).

Amato, F., M. Ariola, C. Cosentino, C. T. Abdallah, and P. Dorato (2003). „Necessary and sufficient conditions for finite-time stability of linear systems“. In: *Proc. 2003 Am. Control Conf. 2003*. Vol. 5. IEEE, pp. 4452–4456. DOI: 10.1109/ACC.2003.1240541 (cit. on p. 110).

Amato, F., M. Ariola, and P. Dorato (2001). „Finite-time control of linear systems subject to parametric uncertainties and disturbances“. In: *Automatica* 37.9, pp. 1459–1463. DOI: 10.1016/S0005-1098(01)00087-5 (cit. on p. 110).

Anderson, P. M., A. A. Fouad, and H. H. Happ (1979). *Power System Control and Stability*. 2, illustr. Vol. 9. 2. Wiley-IEEE Press, p. 672. DOI: 10.1109/TSMC.1979.4310158 (cit. on pp. 58 sq., 61 sq., 81).

Anishchenko, V., V. Astakhov, A. Neiman, T. Vadivasova, and L. Schimansky-Geier (2006). *Dynamics of Chaotic and Stochastic Systems*. Berlin: Springer (cit. on p. 110).

Anvari, M., G. Lohmann, M. Wächter, P. Milan, E. Lorenz, D. Heinemann, M. R. R. Tabar, and J. Peinke (2016). „Short term fluctuations of wind and solar power systems“. In: *New J. Phys.* 18.6, p. 063027. DOI: 10.1088/1367-2630/18/6/063027 (cit. on p. 58).

Anvari, M., M. R. R. Tabar, J. Peinke, and K. Lehnertz (2016). „Disentangling the stochastic behavior of complex time series“. In: *Sci. Rep.* 6.1, p. 35435. DOI: 10.1038/srep35435 (cit. on p. 58).

Arenas, A., A. Cabrales, A. Díaz-Guilera, R. Guimerà, and F. Vega-Redondo (2003). „Search and Congestion in Complex Networks“. In: *Stat. Mech. Complex Networks*. Ed. by R. Pastor-Satorras, M. Rubi, and A. Díaz-Guilera. Lecture No. Springer. Chap. 11, pp. 175–194 (cit. on p. 44).

Arenas, A., A. Díaz-Guilera, J. Kurths, Y. Moreno, and C. Zhou (2008). „Synchronization in complex networks“. In: *Phys. Rep.* 469.3, pp. 93–153. DOI: 10.1016/j.physrep.2008.09.002 (cit. on pp. 16, 24).

Arrillaga, J. (1998). *High voltage direct current transmission*. 2nd. London: The Institution of Electrical Engineers (cit. on p. 3).

Ashwin, P. and M. Timme (2005). „Unstable attractors: existence and robustness in networks of oscillators with delayed pulse coupling“. In: *Nonlinearity* 18.5, pp. 2035–2060. DOI: 10.1088/0951-7715/18/5/009 (cit. on p. 34).

Aubin, J.-P. (2001). „Viability Kernels and Capture Basins of Sets Under Differential Inclusions“. In: *SIAM J. Control Optim.* 40.3, pp. 853–881. DOI: 10.1137/S036301290036968X (cit. on p. 110).

Aubin, J.-P., A. Bayen, and P. Saint-Pierre (2011). *Viability Theory - New Directions* (cit. on p. 110).

Auer, S., F. Hellmann, M. Krause, and J. Kurths (2017). „Stability of Synchrony against Local Intermittent Fluctuations in Tree-like Power Grids“. In: *arXiv:1702.08707* (cit. on p. 58).

Aylett, P. (1958). „The energy-integral criterion of transient stability limits of power systems“. In: *Proc. IEE Part C Monogr.* 105.8, p. 527. DOI: 10.1049/pi-c.1958.0070 (cit. on p. 62).

Barabanov, N., J. Schiffer, R. Ortega, and D. Efimov (2017). „Conditions for Almost Global Attractivity of a Synchronous Generator Connected to an Infinite Bus“. In: *IEEE Trans. Automat. Contr.* 62.10, pp. 4905–4916. DOI: 10.1109/TAC.2017.2671026 (cit. on p. 65).

Barabási, A.-L. (1999). „Emergence of Scaling in Random Networks“. In: *Science (80-.).* 286.5439, pp. 509–512. DOI: 10.1126/science.286.5439.509 (cit. on p. 51).

Barahona, M. and L. M. Pecora (2002). „Synchronization in Small-World Systems“. In: *Phys. Rev. Lett.* 89.5, p. 054101. DOI: 10.1103/PhysRevLett.89.054101 (cit. on p. 24).

Barrat, A., M. Barthélemy, R. Pastor-Satorras, and A. Vespignani (2004). „The architecture of complex weighted networks“. In: *Proc. Natl. Acad. Sci.* 101.11, pp. 3747–3752. DOI: 10.1073/pnas.0400087101 (cit. on pp. 38, 46).

Barthélemy, M. (2011). „Spatial networks“. In: *Phys. Rep.* 499.1-3, pp. 1–101. DOI: 10.1016/j.physrep.2010.11.002 (cit. on pp. 38, 50, 72).

Battelino, P. M., C. Grebogi, E. Ott, J. A. Yorke, and E. D. Yorke (1988). „Multiple coexisting attractors, Basin boundaries and basic sets“. In: *Phys. D Nonlinear Phenom.* 32.2, pp. 296–305. DOI: 10.1016/0167-2789(88)90057-7 (cit. on pp. 32 sq.).

Boccaletti, S., G. Bianconi, R. Criado, C. del Genio, J. Gómez-Gardeñes, M. Romance, I. Sendiña-Nadal, Z. Wang, and M. Zanin (2014). „The structure and dynamics of multilayer networks“. In: *Phys. Rep.* 544.1, pp. 1–122. DOI: 10.1016/j.physrep.2014.07.001 (cit. on p. 48).

Boccaletti, S., J. Kurths, G. Osipov, D. Valladares, and C. Zhou (2002). „The synchronization of chaotic systems“. In: *Phys. Rep.* 366.1-2, pp. 1–101. DOI: 10.1016/S0370-1573(02)00137-0 (cit. on p. 16).

Boccaletti, S., V. Latora, Y. Moreno, M. Chavez, and D.-U. U. Hwang (2006). „Complex networks: Structure and dynamics“. In: *Phys. Rep.* 424.4-5, pp. 175–308. DOI: 10.1016/j.physrep.2005.10.009 (cit. on pp. 38, 50).

Bonneuil, N. (2006). „Computing the viability kernel in large state dimension“. In: *J. Math. Anal. Appl.* 323.2, pp. 1444–1454. DOI: 10.1016/j.jmaa.2005.11.076 (cit. on p. 110).

Borůvka, O. (1926a). „O jistém problému minimálním“. In: *Práce Morav. přírodovědecké společnosti* 3, pp. 37–58 (cit. on p. 7).

— (1926b). „Příspěvek k otázce ekonomické stavby elektrovodných sítí“. In: *Elektrotechnický Obz.* Pp. 153–154 (cit. on p. 7).

Braess, D. (1968). „Über ein Paradoxon aus der Verkehrsplanung“. In: *Unternehmensforsch. Oper. Res. - Rech. Opérationnelle* 12.1, pp. 258–268. DOI: 10.1007/BF01918335 (cit. on p. 118).

Brandes, U. (2001). „A faster algorithm for betweenness centrality*“. In: *J. Math. Sociol.* 25.2, pp. 163–177. DOI: 10.1080/0022250X.2001.9990249 (cit. on p. 42).

Brechtel, A., P. Gramlich, D. Ritterskamp, B. Drossel, and T. Gross (2016). „Master stability functions reveal diffusion-driven instabilities in multi-layer networks“. In: 1, pp. 1–7 (cit. on p. 25).

Brummitt, C. D., R. M. D'Souza, and E. A. Leicht (2012). „Suppressing cascades of load in interdependent networks“. In: *Proc. Natl. Acad. Sci. U. S. A.* 109.12, E680–9. DOI: 10.1073/pnas.1110586109 (cit. on p. 47).

Brzeski, P., M. Lazarek, T. Kapitaniak, J. Kurths, and P. Perlikowski (2016). „Basin stability approach for quantifying responses of multistable systems with parameters mismatch“. In: *arXiv:1602.03751* February, pp. 1–15 (cit. on pp. 84, 117).

Brzeski, P., J. Wojewoda, T. Kapitaniak, J. Kurths, and P. Perlikowski (2017). „Sample-based approach can outperform the classical dynamical analysis - experimental confirmation of the basin stability method“. In: *Sci. Rep.* 7.1, p. 6121. DOI: 10.1038/s41598-017-05015-7 (cit. on pp. 31, 84).

Buldyrev, S. V., R. Parshani, G. Paul, H. E. Stanley, and S. Havlin (2010). „Catastrophic cascade of failures in interdependent networks.“ In: *Nature* 464.7291, pp. 1025–1028. DOI: 10.1038/nature08932 (cit. on p. 47).

Bullmore, E. and O. Sporns (2009). „Complex brain networks: graph theoretical analysis of structural and functional systems“. In: *Nat. Rev. Neurosci.* 10.3, pp. 186–198. DOI: 10.1038/nrn2575 (cit. on p. 38).

Camilli, F., L. Grüne, and F. Wirth (2001). „A generalization of Zubov's method to perturbed systems“. In: *SIAM J. Control Optim.* 40, pp. 496–515 (cit. on p. 28).

Carroll, C. (2006). „Canonical correlation analysis: Assessing links between multiplex networks“. In: *Soc. Networks* 28.4, pp. 310–330. DOI: 10.1016/j.socnet.2005.07.004 (cit. on p. 48).

Chaudhuri, U. and A. Prasad (2014). „Complicated basins and the phenomenon of amplitude death in coupled hidden attractors“. In: *Phys. Lett. A* 378.9, pp. 713–718. DOI: 10.1016/j.physleta.2014.01.003 (cit. on p. 34).

Clauset, A., C. R. Shalizi, and M. E. J. Newman (2009). „Power-Law Distributions in Empirical Data“. In: *SIAM Rev.* 51.4, pp. 661–703. DOI: 10.1137/070710111 (cit. on p. 50).

„Coal Consumption Affecting Climate“ (1912). In: *Rod. Otamatea Times, Wait. Kaipara Gaz.* P. 7 (cit. on p. 3).

Cobb, C. and P. Douglas (1928). „A Theory of Production“. In: *Am. Econ. Rev.* 18.1, pp. 139–165. DOI: 10.1515/humr.1998.11.2.161 (cit. on p. 52).

Coelho, E., P. Cortizo, and P. Garcia (2002). „Small-signal stability for parallel-connected inverters in stand-alone AC supply systems“. In: *IEEE Trans. Ind. Appl.* 38.2, pp. 533–542. DOI: 10.1109/28.993176 (cit. on pp. 64 sq.).

Coletta, T., R. Delabays, I. Adagideli, and P. Jacquod (2016). „Topologically protected loop flows in high voltage AC power grids“. In: *New J. Phys.* 18.10, p. 103042. DOI: 10.1088/1367-2630/18/10/103042 (cit. on p. 67).

Coletta, T. and P. Jacquod (2016). „Linear stability and the Braess paradox in coupled-oscillator networks and electric power grids“. In: *Phys. Rev. E* 93.3, p. 032222. DOI: 10.1103/PhysRevE.93.032222 (cit. on p. 118).

Costa, L. D. F., F. A. Rodrigues, G. Travieso, and P. R. Villas Boas (2007). „Characterization of complex networks: A survey of measurements“. In: *Adv. Phys.* 56.1, pp. 167–242. DOI: 10.1080/00018730601170527 (cit. on p. 38).

Coullet, P., J. M. Gilli, M. Monticelli, and N. Vandenberghe (2005). „A damped pendulum forced with a constant torque“. In: *Am. J. Phys.* 73.12, p. 1122. DOI: 10.1119/1.2074027 (cit. on p. 66).

Cozzo, E., M. Kivelä, M. D. Domenico, A. Solé-Ribalta, A. Arenas, S. Gómez, M. A. Porter, and Y. Moreno (2015). „Structure of triadic relations in multiplex networks“. In: *New J. Phys.* 17.7, p. 073029. DOI: 10.1088/1367-2630/17/7/073029 (cit. on p. 48).

Criado, R., J. Flores, A. García del Amo, J. Gómez-Gardeñes, and M. Romance (2012). „A mathematical model for networks with structures in the mesoscale“. In: *Int. J. Comput. Math.* 89.3, pp. 291–309. DOI: 10.1080/00207160.2011.577212 (cit. on pp. 48, 51).

Dahms, T., J. Lehnert, and E. Schöll (2012). „Cluster and group synchronization in delay-coupled networks“. In: *Phys. Rev. E* 86.1, p. 016202. DOI: 10.1103/PhysRevE.86.016202 (cit. on p. 25).

Daza, A., A. Wagemakers, B. Georgeot, D. Guéry-Odelin, and M. A. F. Sanjuán (2016). „Basin entropy: a new tool to analyze uncertainty in dynamical systems“. In: *Sci. Rep.* 6.1, p. 31416. DOI: 10.1038/srep31416 (cit. on pp. 33, 84).

Daza, A., A. Wagemakers, M. A. F. Sanjuán, and J. A. Yorke (2015). „Testing for Basins of Wada“. In: *Sci. Rep.* 5, p. 16579. DOI: 10.1038/srep16579 (cit. on pp. 32, 34).

De Domenico, M., C. Granell, M. A. Porter, and A. Arenas (2016). „The physics of multilayer networks“. In: *Nat. Phys.* 12.10, pp. 901–906. DOI: 10.1038/nphys3865 (cit. on p. 47).

De Domenico, M., A. Solé-Ribalta, E. Cozzo, M. Kivelä, Y. Moreno, M. a. Porter, S. Gómez, and A. Arenas (2013). „Mathematical Formulation of Multilayer Networks“. In: *Phys. Rev. X* 3.4, p. 041022. DOI: 10.1103/PhysRevX.3.041022 (cit. on p. 48).

De Montis, A., M. Barthélemy, A. Chessa, and A. Vespignani (2005). „The structure of Inter-Urban traffic: A weighted network analysis“. In: *Geographical*, pp. 1–12 (cit. on p. 41).

Delabays, R., T. Coletta, and P. Jacquod (2017). „Multistability of phase-locking in equal-frequency Kuramoto models on planar graphs“. In: *J. Math. Phys.* 58.3, p. 032703. DOI: 10.1063/1.4978697 (cit. on p. 67).

Dena (2012). „Ausbau- und Innovationsbedarf der Stromverteilnetze in Deutschland bis 2030.“ In: p. 410 (cit. on p. 4).

Dewenter, T. and A. K. Hartmann (2015). „Large-deviation properties of resilience of power grids“. In: *New J. Phys.* 17.1, p. 015005. DOI: 10.1088/1367-2630/17/1/015005 (cit. on p. 119).

Donges, J. F. (2012). „Functional network macroscopes for probing past and present Earth system dynamics“. PhD thesis. Humboldt-Universität zu Berlin (cit. on p. 42).

Donges, J. F., I. Petrova, A. Loew, N. Marwan, and J. Kurths (2015). „How complex climate networks complement eigen techniques for the statistical analysis of climatological data“. In: *Clim. Dyn.* P. 16. DOI: 10.1007/s00382-015-2479-3 (cit. on p. 38).

Donges, J. F., H. C. H. Schultz, N. Marwan, Y. Zou, and J. Kurths (2011). „Investigating the topology of interacting networks: Theory and application to coupled climate subnetworks“. In: *Eur. Phys. J. B* 84.4, pp. 635–651. DOI: 10.1140/epjb/e2011-10795-8 (cit. on pp. 47 sq.).

Dörfler, F. and F. Bullo (2011). „Kron Reduction of Graphs with Applications to Electrical Networks“. In: *IEEE Trans. Circuits Syst. Fundam. Theory Appl.* Pp. 1–14 (cit. on p. 73).

— (2014). „Synchronization in complex networks of phase oscillators: A survey“. In: *Automatica* 50.6, pp. 1539–1564. DOI: 10.1016/j.automatica.2014.04.012 (cit. on p. 83).

Dörfler, F., M. Chertkov, and F. Bullo (2013). „Synchronization in complex oscillator networks and smart grids.“ In: *Proc. Natl. Acad. Sci. U. S. A.* 110.6, pp. 2005–10. DOI: 10.1073/pnas.1212134110 (cit. on p. 83).

Dörfler, F., J. W. Simpson-Porco, and F. Bullo (2016). „Breaking the Hierarchy: Distributed Control and Economic Optimality in Microgrids“. In: *IEEE*

Trans. Control Netw. Syst. 3.3, pp. 241–253. DOI: 10.1109/TCNS.2015.2459391 (cit. on pp. 68, 83).

Dorogovtsev, S. N. and J. F. F. Mendes (2001). „Evolution of networks“. In: *Adv. Phys.* P. 67. DOI: 10.1080/00018730110112519 (cit. on p. 50).

Dueñas-Osorio, L., J. I. Craig, and B. J. Goodno (2004). „Probabilistic response of interdependent infrastructure networks“. In: *Network*, pp. 28–30 (cit. on pp. 47, 51).

Ebeling, W. and I. M. Sokolov (2005). *Statistical Thermodynamics and Stochastic Theory of Nonequilibrium Systems*. Singapore: World Scientific (cit. on p. 110).

ENTSO-E (2013). *Network Code on Operational Security*. Tech. rep. ENTSO-E, p. 55 (cit. on p. 83).

— (2016). *Frequency Stability Evaluation Criteria for the Synchronous Zone of Continental Europe*. Tech. rep., p. 25 (cit. on p. 101).

Erdős, P. and A. Rényi (1960). „On the evolution of random graphs“. In: *Publ. Math. Inst. Hungar. Acad. Sci*, pp. 1–45 (cit. on pp. 37, 73).

Ergun, H., J. Beerten, and D. Van Hertem (2012). „Building a new overlay grid for Europe“. In: *IEEE Power Energy Soc. Gen. Meet.* DOI: 10.1109/PESGM.2012.6344805 (cit. on p. 72).

Evans, M. and T. Swartz (2000). *Approximating integrals via Monte Carlo and deterministic methods*. Oxford: OUP (cit. on pp. 29, 85).

Filatrella, G., A. H. Nielsen, and N. F. Pedersen (2008). „Analysis of a power grid using a Kuramoto-like model“. In: *Eur. Phys. J. B* 61.4, pp. 485–491. DOI: 10.1140/epjb/e2008-00098-8 (cit. on p. 62).

Fortunato, S. (2010). „Community detection in graphs“. In: *Phys. Rep.* 486.3-5, pp. 75–174. DOI: 10.1016/j.physrep.2009.11.002 (cit. on pp. 42, 47).

Freeman, L. C. (1977). *A Set of Measures of Centrality Based on Betweenness*. DOI: 10.2307/3033543 (cit. on pp. 42, 44).

— (1978). „Centrality in social networks conceptual clarification“. In: *Soc. Networks* 1.3, pp. 215–239. DOI: 10.1016/0378-8733(78)90021-7 (cit. on p. 44).

Freidlin, M. I. and A. D. Wentzell (2012). *Random Perturbations of Dynamical Systems*. Vol. 260. Grundlehren der mathematischen Wissenschaften. Berlin, Heidelberg: Springer Berlin Heidelberg, p. 488. DOI: 10.1007/978-3-642-25847-3 (cit. on p. 110).

Fujiwara, N. and J. Kurths (2009). „Spectral universality of phase synchronization in non-identical oscillator networks“. In: *Eur. Phys. J. B* 69.1, pp. 45–49. DOI: 10.1140/epjb/e2009-00078-6 (cit. on p. 25).

Gajduk, A., M. Todorovski, and L. Kocarev (2014). „Stability of power grids: An overview“. In: *Eur. Phys. J. Spec. Top.* 223.12, pp. 2387–2409. DOI: 10.1140/epjst/e2014-02212-1 (cit. on p. 28).

Gale, D. M. and S. Kariv (2014). *Networks of Networks: The Last Frontier of Complexity*. Ed. by G. D'Agostino and A. Scala. Vol. 97. Understanding Complex Systems 2. Cham: Springer International Publishing, pp. 99–103. DOI: 10.1007/978-3-319-03518-5 (cit. on p. 47).

Gambuzza, L. V. and M. Frasca (2015). „Intra-layer synchronization in multiplex networks“. In: *EPL (Europhysics Lett.* 110.2, pp. 1–5. DOI: 10.1209/0295-5075/110/20010 (cit. on p. 47).

Garas, A. (2016). *Interconnected Networks*. Ed. by A. Garas. Understanding Complex Systems. Cham: Springer International Publishing. DOI: 10.1007/978-3-319-23947-7 (cit. on p. 47).

Gastner, M. T. and M. E. J. Newman (2006). „Optimal design of spatial distribution networks“. In: *Phys. Rev. E* 74.1, pp. 016117–016123. DOI: 10.1103/PhysRevE.74.016117 (cit. on p. 52).

German Advisory Council On Global Change (2011). *World in transition. A social contract for sustainability*. Berlin (cit. on p. 3).

Giesl, P. and S. Hafstein (2015). „Review on computational methods for {Lyapunov} functions“. In: *Discret. Contin. Dyn. Syst. Ser. B* 20, pp. 2291–2331 (cit. on pp. 27 sq.).

Giesl, P., B. Hamzi, M. Rasmussen, and K. N. Webster (2016). „Approximation of Lyapunov Functions from Noisy Data“. In: *arXiv Prepr.* Pp. 1–24 (cit. on p. 28).

Gilbert, E. N. (1959). „Random Graphs“. In: *Ann. Math. Stat.* 30.4, pp. 1141–1144. DOI: 10.1214/aoms/1177706098 (cit. on pp. 73, 121).

Gitterman, M. (2008). *The Noisy Pendulum*, p. 120 (cit. on p. 71).

Glass, L. and M. C. Mackey (1988). *From clocks to chaos: the rhythms of life*. Princeton University Press (cit. on p. 16).

Glover, J. D., M. S.Sarma, and T. J.Overbye (2012). *Power system analysis and design*. Cengage Learning (cit. on pp. 63, 74).

Graham, R., A. Hamm, and T. Tél (1991). „Nonequilibrium potentials for dynamical systems with fractal attractors or repellers“. In: *Phys. Rev. Lett.* 66.24, pp. 3089–3092. DOI: 10.1103/PhysRevLett.66.3089 (cit. on pp. 27 sq.).

Graham, R. and T. Tél (1984). „Existence of a Potential for Dissipative Dynamical Systems“. In: *Phys. Rev. Lett.* 52.1, pp. 9–12. DOI: 10.1103/PhysRevLett.52.9 (cit. on pp. 27, 110).

Grebogi, C., E. Kostelich, E. Ott, and J. A. Yorke (1986). „Multi-dimensioned intertwined basin boundaries and the kicked double rotor“. In: *Phys. Lett. A* 118.9, pp. 448–452. DOI: 10.1016/0375-9601(86)90749-8 (cit. on p. 33).

Grebogi, C., H. E. Nusse, E. Ott, and J. A. Yorke (1988). „Basic Sets: Sets that Determine the Dimension of Basin Boundaries“. In: *Lect. Notes Math.* Vol. 1342, pp. 220–250 (cit. on p. 33).

Grebogi, C., E. Ott, and J. A. Yorke (1983). „Fractal Basin Boundaries, Long-Lived Chaotic Transients, and Unstable-Unstable Pair Bifurcation“. In: *Phys. Rev. Lett.* 50.13, pp. 935–938. DOI: 10.1103/PhysRevLett.50.935 (cit. on pp. 32 sq.).

— (1987). „Chaos, Strange Attractors, and Fractal Basin Boundaries in Nonlinear Dynamics“. In: *Science (80-.).* 238.4827, pp. 632–638. DOI: 10.1126/science.238.4827.632 (cit. on p. 33).

Guarino, B. (2016). *Monkey stumbles into hydroelectric power plant and triggers 4-hour blackout across Kenya - The Washington Post* (cit. on p. 4).

Guckenheimer, J. and P. J. Holmes (2002). *Nonlinear Oscillations, Dynamical Systems, and Bifurcations of Vector Fields (Applied Mathematical Sciences)*. 1st ed. 19. New York: Springer-Verlag (cit. on pp. 13 sq., 20, 22).

Gurvich, V. (2010). *Metric and ultrametric spaces of resistances*. Tech. rep. 14, pp. 1496–1505. DOI: 10.1016/j.dam.2010.05.007 (cit. on p. 40).

Hafstein, S. (2004). „A constructive converse {Lyapunov} theorem on exponential stability“. In: *Discret. Contin. Dyn. Syst.* 10, pp. 657–678 (cit. on p. 28).

Hahn, W. (1958). „Über die Anwendung der Methode von Ljapunov auf Differenzengleichungen“. In: *Math. Ann.* 136.5, pp. 430–441. DOI: 10.1007/BF01347793 (cit. on p. 27).

Halappanavar, M., E. Cotilla-Sanchez, E. Hogan, D. Duncan, Zhenyu, Huang, and P. D. H. Hines (2015). „A Network-of-Networks Model for Electrical Infrastructure Networks“. In: *arXiv Prepr.* Pp. 1–13 (cit. on p. 50).

Hanley, J. A. and B. J. McNeil (1982). „The meaning and use of the area under a receiver operating characteristic (ROC) curve.“ In: *Radiology* 143.1, pp. 29–36. DOI: 10.1148/radiology.143.1.7063747 (cit. on p. 125).

Hasegawa, Y. and Y. Ueda (1999). „Global basin structure of attraction of two degrees of freedom swing equation system“. In: *Int. J. Bifurc. Chaos* 09.08, pp. 1549–1569. DOI: 10.1142/S0218127499001085 (cit. on pp. 86, 146).

Heitzig, J., J. F. Donges, Y. Zou, N. Marwan, and J. Kurths (2012). „Node-weighted measures for complex networks with spatially embedded, sampled, or differently sized nodes“. In: *Eur. Phys. J. B* 85.1, p. 38. DOI: 10.1140/epjb/e2011-20678-7 (cit. on p. 40).

Heitzig, J., T. Kittel, J. F. Donges, and N. Molkenthin (2016). „Topology of sustainable management of dynamical systems with desirable states: from defining planetary boundaries to safe operating spaces in the Earth system“. In: *Earth Syst. Dyn.* 7.1, pp. 21–50. DOI: 10.5194/esd-7-21-2016 (cit. on p. 109).

Herrmann, C., M. Barthélemy, and P. Provero (2003). „Connectivity distribution of spatial networks“. In: *Phys. Rev. E* 68.2, p. 026128. DOI: 10.1103/PhysRevE.68.026128 (cit. on p. 73).

Hilborn, R. C. (2000). „Chaos and Nonlinear Dynamics: An Introduction for Scientists and Engineers“. In: p. 650 (cit. on p. 21).

Hill, D. and Guanrong Chen (2006). „Power Systems as Dynamic Networks“. In: *2006 IEEE Int. Symp. Circuits Syst.* IEEE, pp. 722–725. DOI: 10.1109/ISCAS.2006.1692687 (cit. on pp. 4, 31).

Hofmann, A. (2015). *In the Eye of the Storm: Peak Squirrel Activity - Public Power Chat* (cit. on p. 4).

Holling, C. S. (1973). „Resilience and Stability of Ecological Systems“. In: *Annu. Rev. Ecol. Syst.* 4.1, pp. 1–23. DOI: 10.1146/annurev.es.04.110173.000245 (cit. on p. 31).

Holme, P. and J. Saramäki (2012). „Temporal networks“. In: *Phys. Rep.* 519.3, pp. 97–125. DOI: 10.1016/j.physrep.2012.03.001 (cit. on p. 24).

Hsiao-Dong Chang, Chia-Chi Chu, and G. Cauley (1995). „Direct stability analysis of electric power systems using energy functions: theory, applications, and perspective“. In: *Proc. IEEE* 83.11, pp. 1497–1529. DOI: 10.1109/5.481632 (cit. on p. 28).

Huang, L., Q. Chen, Y.-C. Lai, and L. M. Pecora (2009). „Generic behavior of master-stability functions in coupled nonlinear dynamical systems“. In: *Phys. Rev. E* 80.3, p. 036204. DOI: 10.1103/PhysRevE.80.036204 (cit. on p. 27).

Hunt, B. R. and E. Ott (2015). „Defining Chaos“. In: *Chaos An Interdiscip. J. Nonlinear Sci.* 25.9, p. 097618. DOI: 10.1063/1.4922973 (cit. on p. 16).

Hurley, M. (1982). „Attractors: persistence, and density of their basins“. In: *Trans. Am. Math. Soc.* 269.1, pp. 247–247. DOI: 10.1090/S0002-9947-1982-0637037-7 (cit. on p. 15).

Iooss, G. and D. D. Joseph (1990). „Stability and Bifurcation in Conservative Systems“. In: *Elem. Stab. Bifurc. Theory*. New York, NY: Springer New York, pp. 303–318. DOI: 10.1007/978-1-4612-0997-3_12 (cit. on p. 15).

Jan-E-Alam, M. (2009). „A Study on the Presence of Inter-Area Oscillation Mode in Bangladesh Power System Network“. In: *J. Electr. Eng.* 36.Ii (cit. on p. 138).

Jaros, P., S. Brezetsky, R. Levchenko, D. Dudkowski, T. Kapitaniak, and Y. Maistrenko (2017). „Solitary states for coupled oscillators“. In: 1, pp. 1–6 (cit. on p. 130).

Ji, P. and J. Kurths (2014). „Basin stability of the Kuramoto-like model in small networks“. In: *Eur. Phys. J. Spec. Top.* 223.12, pp. 2483–2491. DOI: 10.1140/epjst/e2014-02213-0 (cit. on pp. 84, 122).

Ji, P., T. K. D. Peron, P. J. Menck, F. A. Rodrigues, and J. Kurths (2013). „Cluster Explosive Synchronization in Complex Networks“. In: *Phys. Rev. Lett.* 110.21, p. 218701. DOI: 10.1103/PhysRevLett.110.218701 (cit. on pp. 17, 66 sq.).

Jiang, Y. (2000). „Globally coupled maps with time delay interactions“. In: *Phys. Lett. A* 267.5-6, pp. 342–349. DOI: 10.1016/S0375-9601(00)00135-3 (cit. on p. 34).

Johnson, J. (2016). „Hypernetworks: Multidimensional relationships in multilevel systems“. In: *Eur. Phys. J. Spec. Top.* 225.6-7, pp. 1037–1052. DOI: 10.1140/epjst/e2016-02653-4 (cit. on p. 38).

Kaluza, P., A. Kolzsch, M. T. Gastner, and B. Blasius (2010). „The complex network of global cargo ship movements“. In: *J. R. Soc. Interface* 7.48, pp. 1093–1103. DOI: 10.1098/rsif.2009.0495 (cit. on p. 38).

Kan, A. van, J. Jegminat, J. F. Donges, and J. Kurths (2016). „Constrained basin stability for studying transient phenomena in dynamical systems“. In: *Phys. Rev. E* 93.4, p. 042205. DOI: 10.1103/PhysRevE.93.042205 (cit. on p. 84).

Kan, I. (1994). „Open sets of diffeomorphisms having two attractors, each with an everywhere dense basin“. In: *Bull. Am. Math. Soc.* 31.1, pp. 68–74 (cit. on p. 34).

Kautz, R. L. and R. Monaco (1985). „Survey of chaos in the rf-biased Josephson junction“. In: *J. Appl. Phys.* 57.3, pp. 875–889. DOI: 10.1063/1.334687 (cit. on p. 71).

Keener, J. P. (1980). „Infinite Period Bifurcation and Global Bifurcation Branches“. In: *SIAM J. Appl. Math.* 41.1, pp. 127–144. DOI: 10.1137/0141010 (cit. on p. 24).

Kemeth, F. P., S. W. Haugland, L. Schmidt, I. G. Kevrekidis, and K. Krischer (2016). „A classification scheme for chimera states“. In: *Chaos An Interdiscip. J. Nonlinear Sci.* 26.9, p. 094815. DOI: 10.1063/1.4959804 (cit. on p. 18).

Kenett, D. Y., M. Perc, and S. Boccaletti (2015). „Networks of networks – An introduction“. In: *Chaos, Solitons & Fractals* 80, pp. 1–6. DOI: 10.1016/j.chaos.2015.03.016 (cit. on p. 47).

Kennedy, J. and J. A. Yorke (1991). „Basins of Wada“. In: *Phys. D Nonlinear Phenom.* 51.1-3, pp. 213–225. DOI: 10.1016/0167-2789(91)90234-Z (cit. on pp. 32 sq.).

Kettemann, S. (2016). „Delocalization of disturbances and the stability of ac electricity grids“. In: *Phys. Rev. E* 94.6, p. 062311. DOI: 10.1103/PhysRevE.94.062311 (cit. on p. 84).

Kim, H., S. H. Lee, and P. Holme (2015). „Community consistency determines the stability transition window of power-grid nodes“. In: *New J. Phys.* 17.11, p. 113005. DOI: 10.1088/1367-2630/17/11/113005 (cit. on pp. 84, 118).

— (2016). „Building blocks of the basin stability of power grids“. In: *Phys. Rev. E* 93.6, p. 062318. DOI: 10.1103/PhysRevE.93.062318 (cit. on pp. 31, 84, 118).

Kittel, T., J. Heitzig, K. Webster, and J. Kurths (2017). „Timing of transients: quantifying reaching times and transient behavior in complex systems“. In: *New J. Phys.* 19.8, p. 083005. DOI: 10.1088/1367-2630/aa7b61 (cit. on pp. 84, 98).

Kivelä, M., A. Arenas, M. Barthélemy, J. P. Gleeson, Y. Moreno, and M. a. Porter (2014). „Multilayer networks“. In: *J. Complex Networks* 2.3, pp. 203–271. DOI: 10.1093/comnet/cnu016 (cit. on p. 48).

Klein, D. J. and M. Randić (1993). „Resistance distance“. In: *J. Math. Chem.* 12.1, pp. 81–95. DOI: 10.1007/BF01164627 (cit. on pp. 7, 39 sq.).

Klein, M., G. Rogers, and P. Kundur (1991). „A fundamental study of inter-area oscillations in power systems“. In: *IEEE Trans. Power Syst.* 6.3, pp. 914–921. DOI: 10.1109/59.119229 (cit. on p. 84).

Klemm, K. and S. Bornholdt (2005). „Topology of biological networks and reliability of information processing“. In: *Proc. Natl. Acad. Sci.* 102.51, pp. 18414–18419. DOI: 10.1073/pnas.0509132102 (cit. on p. 116).

Klotz, S. (2017). *Ringschluss bewahrte Potsdam vor längerem Stromausfall*. Tech. rep. Stadtwerke Potsdam (cit. on p. 4).

Kolmogorov, A. (1998). „On tables of random numbers“. In: *Theor. Comput. Sci.* 207.2, pp. 387–395. DOI: 10.1016/S0304-3975(98)00075-9 (cit. on p. 38).

Kopell, N. and R. Washburn (1982). „Chaotic motions in the two-degree-of-freedom swing equations“. In: *IEEE Trans. Circuits Syst.* 29.11, pp. 738–746. DOI: 10.1109/TCS.1982.1085094 (cit. on p. 71).

Kraut, S. and U. Feudel (2003). „Enhancement of noise-induced escape through the existence of a chaotic saddle“. In: *Phys. Rev. E* 67.1, p. 015204. DOI: 10.1103/PhysRevE.67.015204 (cit. on p. 110).

Kriener, B., L. Anand, and M. Timme (2012). „Complex networks: when random walk dynamics equals synchronization“. In: *New J. Phys.* 14.9, p. 093002. DOI: 10.1088/1367-2630/14/9/093002 (cit. on p. 39).

Kundur, P. S., J. Paserba, V. Ajjarapu, et al. (2003). „Overview on definition and classification of power system stability“. In: *Electr. Power Deliv. Syst.* Pp. 1–15 (cit. on pp. 31, 81 sqq.).

Kuramoto, Y. (1975). „Self-entrainment of a population of coupled non-linear oscillators“. In: *Int. Symp. Math. Probl. Theor. Phys.* Berlin/Heidelberg: Springer-Verlag, pp. 420–422. DOI: 10.1007/BFb0013365 (cit. on p. 17).

— (1984). „Cooperative Dynamics of Oscillator Community“. In: *Prog. Theor. Phys. Suppl.* 79, pp. 223–240. DOI: 10.1143/PTPS.79.223 (cit. on p. 17).

Kuramoto, Y. and D. Battogtokh (2002). „Coexistence of Coherence and Incoherence in Nonlocally Coupled Phase Oscillators“. In: February 2008 (cit. on p. 18).

Kurant, M. and P. Thiran (2006). „Layered Complex Networks“. In: *Phys. Rev. Lett.* 96.13, p. 138701. DOI: 10.1103/PhysRevLett.96.138701 (cit. on p. 48).

Kuznetsov, Y. A. (1998). *Elements of Applied Bifurcation Theory*. 2nd. Springer, p. 614 (cit. on p. 21).

Lai, Y.-C. and C. Grebogi (1995). „Intermingled basins and two-state on-off intermittency“. In: *Phys. Rev. E* 52.4, R3313–R3316. DOI: 10.1103/PhysRevE.52.R3313 (cit. on p. 34).

— (1996a). „Characterizing riddled fractal sets“. In: *Phys. Rev. E* 53.2, pp. 1371–1374 (cit. on p. 34).

Lai, Y.-C. and C. Grebogi (1996b). „Noise-Induced Riddling in Chaotic Systems“. In: *Phys. Rev. Lett.* 77.25, pp. 5047–5050. DOI: 10.1103/PhysRevLett.77.5047 (cit. on p. 34).

Lai, Y.-C., C. Grebogi, J. A. Yorke, and S. C. Venkataramani (1996). „Riddling Bifurcation in Chaotic Dynamical Systems“. In: *Phys. Rev. Lett.* 77.1, pp. 55–58. DOI: 10.1103/PhysRevLett.77.55 (cit. on p. 34).

Lai, Y.-C. and T. Tél (2011). *Transient Chaos*. Vol. 173. Applied Mathematical Sciences 1983. New York, NY: Springer New York, p. 499. DOI: 10.1007/978-1-4419-6987-3 (cit. on p. 34).

Lakervi, E. and E. J. Holmes (1995). *Electricity distribution network design*. 2nd. IEEE Power Series 21. IET (cit. on p. 72).

LeDell, E., M. L. Petersen, and M. J. V. D. Laan (2012). „Computationally Efficient Confidence Intervals for Cross-validated Area Under the ROC Curve Estimates“. In: *U.C. Berkeley Div. Biostat. Pap. Ser.* (Cit. on p. 125).

Leng, S., W. Lin, and J. Kurths (2016). „Basin stability in delayed dynamics“. In: *Sci. Rep.* 6.1, p. 21449. DOI: 10.1038/srep21449 (cit. on pp. 31, 84).

Li, B. and K. Y. M. Wong (2017). „Optimizing synchronization stability of the Kuramoto model in complex networks and power grids“. In: *Phys. Rev. E* 95.1, p. 012207. DOI: 10.1103/PhysRevE.95.012207 (cit. on p. 117).

Li, T.-Y. and J. A. Yorke (1975). „Period Three Implies Chaos“. In: *Am. Math. Mon.* 82.10, p. 985. DOI: 10.2307/2318254 (cit. on p. 16).

Lodato, I., S. Boccaletti, and V. Latora (2007). „Synchronization properties of network motifs“. In: *EPL* 78, p. 28001. DOI: 10.1209/0295-5075/78/28001 (cit. on p. 116).

Lopes, A. O. (1992). „On the Dynamics of Real Polynomials on the Plane“. In: *Comput. Graph.* 16.1, pp. 15–23 (cit. on p. 86).

Lorenz, E. N. (1963). „Deterministic Nonperiodic Flow“. In: *J. Atmos. Sci.* 20.2, pp. 130–141. DOI: 10.1175/1520-0469(1963)020<0130:DNF>2.0.CO;2 (cit. on p. 16).

Lundström, N. L. P. (2017). „How to find simple nonlocal stability and resilience measures“. In: pp. 1–25 (cit. on p. 84).

Lundström, N. L. P. and J. O. Aidanpää (2007). „Dynamic consequences of electromagnetic pull due to deviations in generator shape“. In: *J. Sound Vib.* 301.1-2, pp. 207–225. DOI: 10.1016/j.jsv.2006.09.030 (cit. on p. 31).

Lyapunov, A. M. (1907). „Problème général de la stabilité du mouvement“. In: *Ann. la Fac. des Sci. Toulouse Mathématiques* 9.9, pp. 203–474. DOI: 10.5802/afst.246 (cit. on p. 27).

Maas, G., M. Bial, and J. Fijalkowski (2007). „Final report—System disturbance on 4 November 2006“. In: *Union Coord. Transm. Electr.* November, p. 84 (cit. on p. 4).

Machowski, J., J. Bialek, and J. Bumby (2011). *Power system dynamics: stability and control*. John Wiley \& Sons, Ltd. (cit. on pp. 58, 61 sqq., 74, 76 sq., 81).

MacMahon, M. and D. Garlaschelli (2015). „Community Detection for Correlation Matrices“. In: *Phys. Rev. X* 5.2, p. 021006. DOI: 10.1103/PhysRevX.5.021006 (cit. on pp. 42, 47).

Maidens, J. N., S. Kaynama, I. M. Mitchell, M. M. K. Oishi, and G. A. Dumont (2013). „Lagrangian methods for approximating the viability kernel in high-dimensional systems“. In: *Automatica* 49.7, pp. 2017–2029. DOI: 10.1016/j.automatica.2013.03.020 (cit. on p. 110).

Maistrenko, Y., S. Brezetsky, P. Jaros, R. Levchenko, and T. Kapitaniak (2017). „Smallest chimera states“. In: *Phys. Rev. E* 95.1, p. 010203. DOI: 10.1103/PhysRevE.95.010203 (cit. on pp. 18, 130).

Malisoff, M. and F. Mazenc (2009). *Constructions of Strict Lyapunov Functions*. 1st ed. Communications and Control Engineering. London: Springer London, pp. XVI, 386. DOI: 10.1007/978-1-84882-535-2 (cit. on p. 27).

Maluck, J. and R. V. Donner (2017). „Distributions of positive correlations in sectoral value added growth in the global economic network“. In: *Eur. Phys. J. B* 90.2, p. 26. DOI: 10.1140/epjb/e2016-70485-7 (cit. on p. 38).

Manik, D., M. Rohden, H. Ronellenfitsch, X. Zhang, S. Hallerberg, D. Witthaut, and M. Timme (2017). „Network susceptibilities: Theory and applications“. In: *Phys. Rev. E* 95.1, p. 012319. DOI: 10.1103/PhysRevE.95.012319 (cit. on p. 117).

Manik, D., M. Timme, and D. Witthaut (2016). „Cycle flows and multistabilty in oscillatory networks: an overview“. In: pp. 1–44 (cit. on p. 67).

Manik, D., D. Witthaut, B. Schäfer, M. Matthiae, A. Sorge, M. Rohden, E. Katifori, and M. Timme (2014). „Supply networks: Instabilities without overload“. In: *Eur. Phys. J. Spec. Top.* 223.12, pp. 2527–2547. DOI: 10.1140/epjst/e2014-02274-y (cit. on pp. 66, 73).

Marris, E. (2008). „Energy: Upgrading the grid“. In: *Nature* 454.7204, pp. 570–573. DOI: 10.1038/454570a (cit. on p. 4).

Martens, E. A., E. Barreto, S. H. Strogatz, E. Ott, P. So, and T. M. Antonsen (2009). „Exact results for the Kuramoto model with a bimodal frequency distribution“. In: *Phys. Rev. E* 79.2, p. 026204. DOI: 10.1103/PhysRevE.79.026204 (cit. on p. 18).

Martens, E. A., C. Bick, and M. J. Panaggio (2016). „Chimera states in two populations with heterogeneous phase-lag“. In: *Chaos An Interdiscip. J. Nonlinear Sci.* 26.9, p. 094819. DOI: 10.1063/1.4958930 (cit. on p. 31).

Martens, E. A., M. J. Panaggio, and D. M. Abrams (2016). „Basins of attraction for chimera states“. In: *New J. Phys.* 18.2, p. 022002. DOI: 10.1088/1367-2630/18/2/022002 (cit. on p. 84).

Maslennikov, O. V., V. I. Nekorkin, and J. Kurths (2015). „Basin stability for burst synchronization in small-world networks of chaotic slow-fast oscillators“. In: *Phys. Rev. E* 92.4, p. 042803. DOI: 10.1103/PhysRevE.92.042803 (cit. on p. 84).

McDonald, S. W., C. Grebogi, E. Ott, and J. A. Yorke (1985). „Factal Basin Boundaries“. In: *Phys. 17D* 17.2, pp. 125–153 (cit. on pp. 32 sq.).

Medjroubi, W., U. Philipp, M. Scharf, and C. Matke (2017). „Open Data in Power Grid Modelling : New Approaches Towards Transparent Grid Models“. In: *Energy Reports* 3, pp. 14–21. DOI: 10.1016/j.egyr.2016.12.001 (cit. on p. 50).

Menck, P. J. (2014). „How wires shape volumes – on the relation between network topology and nonlocal power grid stability“. Dissertation. Humboldt-Universität zu Berlin (cit. on pp. 29, 116).

Menck, P. J., J. Heitzig, J. Kurths, and H. Joachim Schellnhuber (2014). „How dead ends undermine power grid stability“. In: *Nat. Commun.* 5, p. 3969. DOI: 10.1038/ncomms4969 (cit. on pp. 29, 31, 77, 84, 106, 109, 116, 118, 121 sq., 126 sq., 138).

Menck, P. J., J. Heitzig, N. Marwan, and J. Kurths (2013). „How basin stability complements the linear-stability paradigm“. In: *Nat. Phys.* 9.2, pp. 89–92. DOI: 10.1038/nphys2516 (cit. on pp. 25, 28–31, 90, 119, 121, 137).

Menck, P. J. and J. Kurths (2012). „Topological Identification of Weak Points in Power Grids“. In: *Nonlinear Dyn. Electron. Syst. Proc. NDES 2012*. VDE. VDE, pp. 144–147 (cit. on pp. 29 sq., 84, 116, 121).

Merris, R. (1994). „Laplacian matrices of graphs: a survey“. In: *Linear Algebra Appl.* 197-198.C, pp. 143–176. DOI: 10.1016/0024-3795(94)90486-3 (cit. on p. 134).

Metz, C. E. (1978). „Basic principles of ROC analysis“. In: *Semin. Nucl. Med.* 8.4, pp. 283–298. DOI: 10.1016/S0001-2998(78)80014-2 (cit. on p. 125).

Milan, P., M. Wächter, J. Peinke, M. W??chter, and J. Peinke (2013). „Turbulent character of wind energy“. In: *Phys. Rev. Lett.* 110.13, p. 138701. DOI: 10.1103/PhysRevLett.110.138701 (cit. on p. 58).

Milgram, S. (1967). „The Small-World Problem“. In: *Psychol. Today* 1.1, pp. 61–67 (cit. on p. 37).

Milnor, J. (1985). „On the concept of attractor“. In: *Commun. Math. Phys.* 99.2, pp. 177–195. DOI: 10.1007/BF01212280 (cit. on pp. 15 sq., 32).

Milo, R., S. S. Shen-Orr, S. Itzkovitz, N. Kashtan, D. Chlovskii, and U. Alon (2002). „Network Motifs: Simple Building Blocks of Complex Networks“. In: *Science (80-.).* 298.5594, pp. 824–827. DOI: 10.1126/science.298.5594.824 (cit. on pp. 42, 116).

Mitra, C., A. Choudhary, S. Sinha, J. Kurths, and R. V. Donner (2017). „Multiple-node basin stability in complex dynamical networks“. In: *Phys. Rev. E* 95.3, p. 032317. DOI: 10.1103/PhysRevE.95.032317 (cit. on p. 84).

Mitra, C., T. Kittel, A. Choudhary, J. Kurths, and R. V. Donner (2017). „Recovery time after localized perturbations in complex dynamical networks“. In: pp. 1–21 (cit. on p. 84).

Mitra, C., J. Kurths, and R. V. Donner (2015). „An integrative quantifier of multistability in complex systems based on ecological resilience“. In: *Sci. Rep.* 5.1, p. 16196. DOI: 10.1038/srep16196 (cit. on pp. 31 sq., 84).

Molkenthin, N., K. Rehfeld, N. Marwan, and J. Kurths (2015). „Networks from Flows - From Dynamics to Topology“. In: *Sci. Rep.* 4.1, p. 4119. DOI: 10.1038/srep04119 (cit. on p. 38).

Molkenthin, N. and M. Timme (2016). „Scaling Laws in Spatial Network Formation“. In: *Phys. Rev. Lett.* 117.16, p. 168301. DOI: 10.1103/PhysRevLett.117.168301 (cit. on p. 73).

Momeni, N. and B. Fotouhi (2015). „Growing multiplex networks with arbitrary number of layers“. In: *Phys. Rev. E - Stat. Nonlinear, Soft Matter Phys.* 92.6, pp. 1–19. DOI: 10.1103/PhysRevE.92.062812 (cit. on p. 51).

Moreno, Y., M. Vázquez-Prada, and A. F. Pacheco (2004). „Fitness for synchronization of network motifs“. In: *Phys. A Stat. Mech. its Appl.* 343.4, pp. 279–287. DOI: 10.1016/j.physa.2004.05.033 (cit. on p. 116).

Motter, A. E., S. A. Myers, M. Anghel, and T. Nishikawa (2013). „Spontaneous synchrony in power-grid networks“. In: *Nat. Phys.* 9.3, pp. 191–197. DOI: 10.1038/nphys2535 (cit. on pp. 77, 83).

Mucha, P. J., T. Richardson, K. Macon, M. A. Porter, and J.-P. Onnela (2010). „Community Structure in Time-Dependent, Multiscale, and Multiplex Networks“. In: *Science (80-.).* 328.5980, pp. 876–878. DOI: 10.1126/science.1184819 (cit. on pp. 47 sq.).

Nagata, M., Y. Hirata, N. Fujiwara, G. Tanaka, H. Suzuki, and K. Aihara (2017). „Smoothing effect for spatially distributed renewable resources and its impact on power grid robustness“. In: *Chaos An Interdiscip. J. Nonlinear Sci.* 27.3, p. 033104. DOI: 10.1063/1.4977510 (cit. on p. 58).

Netzentwicklungsplan (2017). *Netzentwicklungsplan Strom 2030 - Version 2017, 1. Entwurf*. Tech. rep. 50Hertz Transmission GmbH, Amprion GmbH, TenneT TSO GmbH, TransnetBW GmbH (cit. on p. 3).

Newman, M. E. J. (2003). „The Structure and Function of Complex Networks“. In: *SIAM Rev.* 45.2, pp. 167–256. DOI: 10.1137/S003614450342480?journalCode=siread (cit. on p. 38).

— (2005). „A measure of betweenness centrality based on random walks“. In: *Soc. Networks* 27.1, pp. 39–54. DOI: 10.1016/j.socnet.2004.11.009 (cit. on pp. 7, 43 sq.).

— (2006). „Modularity and community structure in networks“. In: *Proc. Natl. Acad. Sci.* 103.23, pp. 8577–8582. DOI: 10.1073/pnas.0601602103 (cit. on pp. 42, 47).

— (2008). „The physics of networks“. In: *Phys. Today* 61.11, pp. 33–38. DOI: 10.1063/1.3027989 (cit. on p. 38).

Nicosia, V., G. Bianconi, V. Latora, and M. Barthélemy (2013). „Growing Multiplex Networks“. In: *Phys. Rev. Lett.* 111.5, p. 058701. DOI: 10.1103/PhysRevLett.111.058701 (cit. on pp. 48, 51).

Nishikawa, T., F. Molnar, and A. E. Motter (2015). „Stability Landscape of Power-Grid Synchronization“. In: *IFAC-PapersOnLine* 48.18, pp. 1–6. DOI: 10.1016/j.ifacol.2015.11.001 (cit. on p. 83).

Nishikawa, T. and A. E. Motter (2010). „Network synchronization landscape reveals compensatory structures, quantization, and the positive effect of negative interactions“. In: *Proc. Natl. Acad. Sci.* 107.23, pp. 10342–10347. DOI: 10.1073/pnas.0912444107 (cit. on p. 118).

Nishikawa, T. and A. E. Motter (2015). „Comparative analysis of existing models for power-grid synchronization“. In: *New J. Phys.* 17.1, p. 015012. DOI: 10.1088/1367-2630/17/1/015012 (cit. on pp. 60, 62 sq., 73).

Nishikawa, T., A. E. Motter, Y.-C. Lai, and F. C. Hoppensteadt (2003). „Heterogeneity in Oscillator Networks: Are Smaller Worlds Easier to Synchronize?“ In:

Phys. Rev. Lett. 91.1, p. 014101. DOI: 10.1103/PhysRevLett.91.014101 (cit. on p. 132).

Noh, J. D. and H. Rieger (2004). „Random Walks on Complex Networks“. In: *Phys. Rev. Lett.* 92.11, pp. 118701–1. DOI: 10.1103/PhysRevLett.92.118701 (cit. on p. 44).

Nusse, H. E. and J. A. Yorke (1996). „Wada basin boundaries and basin cells“. In: *Phys. D Nonlinear Phenom.* 90.3, pp. 242–261. DOI: 10.1016/0167-2789(95)00249-9 (cit. on p. 33).

— (2003). „Characterizing the basins with the most entangled boundaries“. In: *Ergod. Theory Dyn. Syst.* 23.3, pp. 895–906. DOI: 10.1017/S0143385702001360 (cit. on p. 33).

Opsahl, T. and P. Panzarasa (2009). „Clustering in weighted networks“. In: *Soc. Networks* 31.2, pp. 155–163. DOI: 10.1016/j.socnet.2009.02.002 (cit. on p. 46).

Osipov, G. V., J. Kurths, and C. Zhou (2009). *Complex Systems and Self-organization Modelling*. Ed. by C. Bertelle, G. H. Duchamp, and H. Kadri-Dahmani. Understanding Complex Systems. Berlin, Heidelberg: Springer Berlin Heidelberg, p. 370. DOI: 10.1007/978-3-540-88073-8 (cit. on p. 16).

Ott, E., J. C. Alexander, I. Kan, J. C. Sommerer, and J. A. Yorke (1994). „The transition to chaotic attractors with riddled basins“. In: *Phys. D Nonlinear Phenom.* 76.4, pp. 384–410. DOI: 10.1016/0167-2789(94)90047-7 (cit. on p. 34).

Ott, E. and T. M. Antonsen (2008). „Low dimensional behavior of large systems of globally coupled oscillators“. In: *Chaos An Interdiscip. J. Nonlinear Sci.* 18.3, p. 037113. DOI: 10.1063/1.2930766 (cit. on p. 17).

Ott, E., C. Grebogi, and J. A. Yorke (1990). „Controlling chaos“. In: *Phys. Rev. Lett.* 64.11, pp. 1196–1199. DOI: 10.1103/PhysRevLett.64.1196 (cit. on p. 16).

Pagani, G. A. and M. Aiello (2011). „Towards decentralization: A topological investigation of the medium and low voltage grids“. In: *IEEE Trans. Smart Grid* 2.3, pp. 538–547. DOI: 10.1109/TSG.2011.2147810 (cit. on p. 72).

— (2013). „The Power Grid as a complex network: A survey“. In: *Phys. A Stat. Mech. its Appl.* 392.11, pp. 2688–2700. DOI: 10.1016/j.physa.2013.01.023 (cit. on pp. 41, 72 sq.).

Panaggio, M. J. and D. M. Abrams (2015). „Chimera states: coexistence of coherence and incoherence in networks of coupled oscillators“. In: *Nonlinearity* 28.3, R67–R87. DOI: 10.1088/0951-7715/28/3/R67 (cit. on p. 18).

Parrilo, P. (2000). „Structured Semidefinite Programs and Semialgebraic Geometry Methods in Robustness and Optimiziation“. PhD thesis. California Institute of Technology, Pasadena, CA (cit. on p. 28).

Pavlyukevich, I. (2007a). „Cooling down Lévy flights“. In: *J. Phys. A Math. Theor.* 40.41, pp. 12299–12313. DOI: 10.1088/1751-8113/40/41/003 (cit. on pp. 91, 100).

— (2007b). „Lévy flights, non-local search and simulated annealing“. In: *J. Comput. Phys.* 226.2, pp. 1830–1844. DOI: 10.1016/j.jcp.2007.06.008 (cit. on pp. 91, 100).

Pecora, L. M. and T. L. Carroll (1998). „Master stability function for synchronized coupled systems“. In: *Phys. Rev. Lett.* 80.1, p. 2109. DOI: 10.1103PhysRevLett.80.2109 (cit. on pp. 24, 27).

— (2015). „Synchronization of chaotic systems“. In: *Chaos An Interdiscip. J. Nonlinear Sci.* 25.9, p. 097611. DOI: 10.1063/1.4917383 (cit. on p. 31).

Pelikan, S. (1985). „A Dynamical Meaning of Fractal Dimension“. In: *Trans. Am. Math. Soc.* 292.2, p. 695. DOI: 10.2307/2000239 (cit. on p. 33).

Pereira, T., J. Eldering, M. Rasmussen, and A. Veneziani (2014). „Towards a general theory for coupling functions allowing persistent synchronization“. In: *Nonlinearity* 27, pp. 501–525. DOI: 10.1088/0951-7715/27/3/501 (cit. on p. 25).

Perl, A. D. and A. R. Goetz (2014). „Corridors, hybrids and networks: three global development strategies for high speed rail“. In: *J. Transp. Geogr.* 42, pp. 134–144. DOI: 10.1016/j.jtrangeo.2014.07.006 (cit. on p. 41).

Pesch, T., H. J. Allelein, and J. F. Hake (2014). „Impacts of the transformation of the German energy system on the transmission grid“. In: *Eur. Phys. J. Spec. Top.* Resilient Power Grids and Extreme Events. DOI: 10.1140/epjst/e2014-02214-y (cit. on p. 3).

Pikovsky, A., M. Rosenblum, and J. Kurths (2001). *Synchronization: A universal concept in nonlinear sciences*. Vol. 12. Cambridge: Cambridge University Press, p. 3. DOI: 10.1017/CBO9780511755743 (cit. on pp. 16 sq.).

Pisarchik, A. N. and U. Feudel (2014). „Control of multistability“. In: *Phys. Rep.* 540.4, pp. 167–218. DOI: 10.1016/j.physrep.2014.02.007 (cit. on p. 28).

Porfiri, M. (2011). „A master stability function for stochastically coupled chaotic maps“. In: *EPL (Europhysics Lett.* 96.4, p. 40014. DOI: 10.1209/0295-5075/96/40014 (cit. on p. 25).

Prill, R. J., P. a. Iglesias, and A. Levchenko (2005). „Dynamic Properties of Network Motifs Contribute to Biological Network Organization“. In: *PLoS Biol.*

3.11. Ed. by A. Lander, e343. DOI: 10.1371/journal.pbio.0030343 (cit. on p. 116).

Quitmann, E. and E. Erdmann (2009). *The Power System Will Need More! How Grid Codes Should Look Ahead*. Tech. rep. Enercon (cit. on pp. 83, 138).

Rakshit, S., B. K. Bera, S. Majhi, C. Hens, and D. Ghosh (2017). „Basin stability measure of different steady states in coupled oscillators". In: *Sci. Rep.* 7.February, p. 45909. DOI: 10.1038/srep45909 (cit. on p. 84).

Rakshit, S., B. K. Bera, M. Perc, and D. Ghosh (2017). „Basin stability for chimera states". In: *Sci. Rep.* 7.1, p. 2412. DOI: 10.1038/s41598-017-02409-5 (cit. on p. 84).

Redner, S. and J. R. Dorfman (2002). „A Guide to First-Passage Processes". In: *Am. J. Phys.* 70.11, pp. 1166–1166. DOI: 10.1119/1.1509421 (cit. on pp. 91, 110).

Rega, G. and S. Lenci (2005). „Identifying, evaluating, and controlling dynamical integrity measures in non-linear mechanical oscillators". In: *Nonlinear Anal. Theory, Methods Appl.* 63.5-7, pp. 902–914. DOI: 10.1016/j.na.2005.01.084 (cit. on p. 32).

Rockström, J., W. Steffen, K. Noone, et al. (2009). „Planetary boundaries: Exploring the safe operating space for humanity". In: *Ecol. Soc.* 14.2, pp. 472–475. DOI: 10.1038/461472a (cit. on p. 109).

Rodrigues, F. A., T. K. D. Peron, P. Ji, and J. Kurths (2016). „The Kuramoto model in complex networks". In: *Phys. Rep.* 610, pp. 1–98. DOI: 10.1016/j.physrep.2015.10.008 (cit. on pp. 17, 31, 62, 65).

Rohden, M., A. Sorge, M. Timme, and D. Witthaut (2012). „Self-Organized Synchronization in Decentralized Power Grids". In: *Phys. Rev. Lett.* 109.6, p. 064101. DOI: 10.1103/PhysRevLett.109.064101 (cit. on pp. 77, 117).

Rohden, M., A. Sorge, D. Witthaut, and M. Timme (2014). „Impact of network topology on synchrony of oscillatory power grids". In: *Chaos An Interdiscip. J. Nonlinear Sci.* 24.1, p. 013123. DOI: 10.1063/1.4865895 (cit. on p. 116).

Rohden, M., D. Witthaut, M. Timme, and H. Meyer-Ortmanns (2017). „Curing critical links in oscillator networks as power flow models". In: *New J. Phys.* 19.1, p. 013002. DOI: 10.1088/1367-2630/aa5597 (cit. on pp. 117 sq.).

Romeiras, F. J., C. Grebogi, E. Ott, and W. Dayawansa (1992). „Controlling chaotic dynamical systems". In: *Phys. D Nonlinear Phenom.* 58.1-4, pp. 165–192. DOI: 10.1016/0167-2789(92)90107-X (cit. on p. 16).

Rosas-Casals, M. (2009). „Topological complexity of the electricity transmission network. Implications in the sustainability paradigm“. PhD thesis. Universitat Politècnica de Catalunya, p. 134 (cit. on pp. 72 sq., 82, 119).

Rosas-Casals, M., S. Valverde, and R. V. Solé (2007). „Topological Vulnerability of the {Europe}an Power Grid Under Errors and Attacks“. In: *Int. J. Bifurc. Chaos* 17.07, pp. 2465–2475. DOI: 10.1142/S0218127407018531 (cit. on pp. 72 sq.).

Rosato, V., L. Issacharoff, F. Tiriticco, S. Meloni, S. De Porcellinis, and R. Setola (2008). „Modelling interdependent infrastructures using interacting dynamical models“. In: *Int. J. Crit. Infrastructures* 4.1, pp. 63–79 (cit. on p. 47).

Rössler, O. E. (1979). „An equation for hyperchaos“. In: *Phys. Lett. A* 71.2, pp. 155–157 (cit. on p. 21).

Rössler, O. E. (1976). „An equation for continuous chaos“. In: *Phys. Lett. A* 57.5, pp. 397–398. DOI: 10.1016/0375-9601(76)90101-8 (cit. on p. 16).

Rosvall, M., a. Trusina, P. Minnhagen, and K. Sneppen (2005). „Networks and cities: An information perspective“. In: *Phys. Rev. Lett.* 94.2, p. 28701. DOI: 10.1103/PhysRevLett.94.028701 (cit. on p. 50).

Roth, C., S. M. Kang, M. Batty, and M. Barthélemy (2011). „Structure of Urban Movements: Polycentric Activity and Entangled Hierarchical Flows“. In: *PLoS One* 6.1. Ed. by M. Perc, e15923. DOI: 10.1371/journal.pone.0015923 (cit. on p. 41).

Sakaguchi, H. and Y. Kuramoto (1986). „A Soluble Active Rotater Model Showing Phase Transitions via Mutual Entertainment“. In: *Prog. Theor. Phys.* 76.3, pp. 576–581. DOI: 10.1143/PTP.76.576 (cit. on p. 17).

Sauer, P. W. and M. A. Pai (1998). *Power System Dynamics and Stability*. Prentice-Hall, Inc., p. 368 (cit. on pp. 58, 61 sq., 65, 81).

Schäfer, B., C. Grabow, S. Auer, J. Kurths, D. Witthaut, and M. Timme (2016). „Taming instabilities in power grid networks by decentralized control“. In: *Eur. Phys. J. Spec. Top.* 225.3, pp. 569–582. DOI: 10.1140/epjst/e2015-50136-y (cit. on pp. 63, 83).

Schäfer, B., M. Matthiae, M. Timme, and D. Witthaut (2015). „Decentral Smart Grid Control“. In: *New J. Phys.* 17.1, p. 015002. DOI: 10.1088/1367-2630/17/1/015002 (cit. on pp. 31, 63, 83).

Schäfer, B., M. Matthiae, X. Zhang, M. Rohden, M. Timme, and D. Witthaut (2017). „Escape routes, weak links, and desynchronization in fluctuation-driven

networks". In: *Phys. Rev. E* 95.6, p. 060203. DOI: 10.1103/PhysRevE.95.060203 (cit. on p. 58).

Schaub, M. T., J.-C. Delvenne, S. N. Yaliraki, and M. Barahona (2012). „Markov Dynamics as a Zooming Lens for Multiscale Community Detection: Non Clique-Like Communities and the Field-of-View Limit". In: *PLoS One* 7.2. Ed. by O. Sporns, e32210. DOI: 10.1371/journal.pone.0032210 (cit. on p. 42).

Schaub, M. T., R. Lambiotte, and M. Barahona (2012). „Encoding dynamics for multiscale community detection: Markov time sweeping for the map equation". In: *Phys. Rev. E* 86.2, p. 026112. DOI: 10.1103/PhysRevE.86.026112 (cit. on p. 42).

Scheffer, M. (2009). *Critical Transitions in Nature and Society*. Princeton: Princeton University Press (cit. on p. 31).

Schellnhuber, H. J. (1999). „'Earth system' analysis and the second Copernican revolution". In: *Nature* 402.supp, pp. C19–C23. DOI: 10.1038/35011515 (cit. on p. 5).

Schiffer, J., E. Fridman, R. Ortega, and J. Raisch (2016). „Stability of a class of delayed port-Hamiltonian systems with application to microgrids with distributed rotational and electronic generation". In: *Automatica* 74, pp. 71–79. DOI: http://dx.doi.org/10.1016/j.automatica.2016.07.022 (cit. on p. 83).

Schiffer, J., F. Dörfler, and E. Fridman (2017). „Robustness of distributed averaging control in power systems: Time delays & dynamic communication topology". In: *Automatica* 80.February, pp. 261–271. DOI: 10.1016/j.automatica.2017.02.040 (cit. on p. 83).

Schiffer, J., D. Goldin, J. Raisch, and T. Sezi (2013). „Synchronization of droop-controlled microgrids with distributed rotational and electronic generation". In: *52nd IEEE Conf. Decis. Control*. IEEE, pp. 2334–2339. DOI: 10.1109/CDC.2013.6760229 (cit. on p. 64).

Schiffer, J., R. Ortega, A. Astolfi, J. Raisch, and T. Sezi (2014a). „Conditions for stability of droop-controlled inverter-based microgrids". In: *Automatica* 50.10, pp. 2457–2469. DOI: 10.1016/j.automatica.2014.08.009 (cit. on p. 64).

— (2014b). „Stability of Synchronized Motions of Inverter–Based Microgrids Under Droop Control". In: *IFAC Proc. Vol.* 47.3, pp. 6361–6367. DOI: 10.3182/20140824-6-ZA-1003.00863 (cit. on p. 4).

Schiffer, J., D. Zonetti, R. Ortega, A. M. Stanković, T. Sezi, and J. Raisch (2016). „A survey on modeling of microgrids—From fundamental physics to phasors

and voltage sources". In: *Automatica* 74, pp. 135–150. DOI: 10.1016/j.automatica.2016.07.036 (cit. on pp. 4, 63, 65).

Schmietendorf, K. (2012). „Synchronisation und Spannungsstabilität in einem Netzwerk von Synchronmaschinen". Diploma. Westfälische Wilhelms-Universität Münster, p. 107 (cit. on p. 62).

Schmietendorf, K., J. Peinke, R. Friedrich, and O. Kamps (2014). „Self-organized synchronization and voltage stability in networks of synchronous machines". In: *Eur. Phys. J. Spec. Top.* 223.12, pp. 2577–2592. DOI: 10.1140/epjst/e2014-02209-8 (cit. on pp. 31, 62, 65, 77).

Schmietendorf, K., J. Peinke, and O. Kamps (2016). „On the stability and quality of power grids subjected to intermittent feed-in". In: *arXiv:1611.08235*, pp. 1–5 (cit. on p. 58).

Schröder, M., S. Chakraborty, D. Witthaut, J. Nagler, and M. Timme (2016). „Interaction Control to Synchronize Non-synchronizable Networks". In: *Sci. Rep.* 6, p. 37142. DOI: 10.1038/srep37142 (cit. on p. 58).

Schröder, M., M. Timme, and D. Witthaut (2017). „A universal order parameter for synchrony in networks of limit cycle oscillators". In: *Chaos An Interdiscip. J. Nonlinear Sci.* 27.7, p. 073119. DOI: 10.1063/1.4995963 (cit. on p. 18).

Sen, P., S. Dasgupta, A. Chatterjee, P. A. Sreeram, G. Mukherjee, and S. S. Manna (2003). „Small-world properties of the Indian railway network". In: *Phys. Rev. E* 67.3, p. 036106. DOI: 10.1103/PhysRevE.67.036106 (cit. on p. 50).

Serdukova, L., Y. Zheng, J. Duan, and J. Kurths (2016). „Stochastic basins of attraction for metastable states". In: *Chaos An Interdiscip. J. Nonlinear Sci.* 26.7, p. 073117. DOI: 10.1063/1.4959146 (cit. on p. 100).

— (2017). „Metastability for discontinuous dynamical systems under Lévy noise: Case study on Amazonian Vegetation". In: *Sci. Rep.* 7.1, p. 9336. DOI: 10.1038/s41598-017-07686-8 (cit. on p. 100).

Shen, J.-l., H.-w. Yin, J.-h. Dai, and H.-j. Zhang (1996). „Riddled Basin of Laser Cooled-Ions in a Paul Trap". In: *Chinese Phys. Lett.* 13.2, pp. 81–84. DOI: 10.1088/0256-307X/13/2/001 (cit. on p. 34).

Shen-Orr, S. S., R. Milo, S. Mangan, and U. Alon (2002). „Network motifs in the transcriptional regulation network of Escherichia coli". In: *Nat. Genet.* 31.1, pp. 64–68. DOI: 10.1038/ng881 (cit. on p. 42).

Shrimali, M. D., A. Prasad, R. Ramaswamy, and U. Feudel (2008). „The nature of attractor basins in multistable systems". In: *Int. J. Bifurc. Chaos* 18.06, pp. 1675–1688. DOI: 10.1142/S0218127408021269 (cit. on p. 28).

Simpson-Porco, J. W., F. Dörfler, and F. Bullo (2016). „Voltage collapse in complex power grids - Supplementary Information“. In: *Nat. Commun.* 7.20, p. 10790. DOI: 10.1038/ncomms10790 (cit. on p. 82).

Skardal, P. S., D. Taylor, and J. Sun (2014). „Optimal Synchronization of Complex Networks“. In: *Phys. Rev. Lett.* 113.14, p. 144101. DOI: 10.1103/PhysRevLett.113.144101 (cit. on p. 117).

Solé, R. V., M. Rosas-Casals, B. Corominas-Murtra, and S. Valverde (2008). „Robustness of the European power grids under intentional attack“. In: *Phys. Rev. E* 77.2, p. 026102. DOI: 10.1103/PhysRevE.77.026102 (cit. on pp. 72, 82, 119).

Soliman, M. S. and J. M. T. Thompson (1989). „Integrity Measures Quantifying the Erosion of Smooth and Fractal Basins of Attraction“. In: *J. Sound Vib.* 135.3, pp. 453–475 (cit. on pp. 32, 84).

— (1990). „Stochastic penetration of smooth and fractal basin boundaries under noise excitation“. In: *Dyn. Stab. Syst.* 5.4, pp. 281–298. DOI: 10.1080/02681119008806101 (cit. on p. 32).

Soltan, S. and G. Zussman (2016). „Generation of synthetic spatially embedded power grid networks“. In: *2016 IEEE Power Energy Soc. Gen. Meet.* IEEE, pp. 1–5. DOI: 10.1109/PESGM.2016.7741383 (cit. on pp. 50, 52).

Sommerer, J. C. and E. Ott (1993). „A physical system with qualitatively uncertain dynamics“. In: *Nature* 365.6442, pp. 138–140. DOI: 10.1038/365138a0 (cit. on p. 34).

Sonnenschein, B., T. K. D. Peron, F. A. Rodrigues, J. Kurths, and L. Schimansky-Geier (2015). „Collective dynamics in two populations of noisy oscillators with asymmetric interactions“. In: *Phys. Rev. E* 91.6, p. 062910. DOI: 10.1103/PhysRevE.91.062910 (cit. on p. 47).

Spielman, D. A. and N. Srivastava (2011). „Graph Sparsification by Effective Resistances“. In: *SIAM J. Comput.* 40.6, pp. 1913–1926. DOI: 10.1137/080734029 (cit. on p. 40).

Steen, J. (1991). *"Eine neue Zeit ...!" : Die Internationale Elektrotechnische Ausstellung 1891*. Frankfurt am Main: Historisches Museum Frankfurt am Main, p. 711 (cit. on p. 3).

Stephenson, K. and M. Zelen (1989). „Rethinking centrality: Methods and examples“. In: *Soc. Networks* 11.1, pp. 1–37. DOI: 10.1016/0378-8733(89)90016-6 (cit. on p. 44).

Strano, E., V. Nicosia, V. Latora, S. Porta, and M. Barthélemy (2012). „Elementary processes governing the evolution of road networks“. In: *Sci. Rep.* 2, pp. 1–8. DOI: 10.1038/srep00296 (cit. on p. 72).

Strano, E., M. Zanin, E. Estrada, and F. Lillo (2013). „Spatially embedded socio-technical complex networks“. In: *Eur. Phys. J. Spec. Top.* 215.1, pp. 1–4. DOI: 10.1140/epjst/e2013-01710-x (cit. on p. 38).

Strenge, L., H. Kirchhoff, G. L. Ndow, and F. Hellmann (2017). „Stability of meshed DC microgrids using probabilistic analysis“. In: *IEEE Second Int. Conf. onDC Microgrids 2017*. IEEE, pp. 175–180 (cit. on p. 4).

Strogatz, S. H. (1994). *Nonlinear dynamics and chaos*. Reading, Massachusetts: Perseus Books Publishing (cit. on pp. 22, 67).

— (2000). „From Kuramoto to Crawford: exploring the onset of synchronization in populations of coupled oscillators“. In: *Phys. D Nonlinear Phenom.* 143.1-4, pp. 1–20. DOI: 10.1016/S0167-2789(00)00094-4 (cit. on p. 17).

— (2012). *Sync: How Order Emerges From Chaos In the Universe, Nature, and Daily Life*. New York: Hachette Books, p. 352 (cit. on pp. 16 sq.).

"Studie im Auftrag des Bundesministeriums für Wirtschaft und Energie (BMWi)" (2014). *„Moderne Verteilernetze für Deutschland“ (Verteilernetzstudie)*. Tech. rep., p. 209 (cit. on p. 76).

Stumpf, M. P. H. and M. A. Porter (2012). „Critical Truths About Power Laws“. In: *Science (80-.).* 335.6069, pp. 665–666. DOI: 10.1126/science.1216142 (cit. on p. 50).

Sun, J., E. M. Bollt, and T. Nishikawa (2009). „Master stability functions for coupled nearly identical dynamical systems“. In: *EPL (Europhysics Lett.* 85.6, p. 60011. DOI: 10.1209/0295-5075/85/60011 (cit. on p. 25).

Tabar, M. R. R., M. Anvari, G. Lohmann, D. Heinemann, M. Wächter, P. Milan, E. Lorenz, and J. Peinke (2014). „Kolmogorov spectrum of renewable wind and solar power fluctuations“. In: *Eur. Phys. J. Spec. Top.* 223.12, pp. 2637–2644. DOI: 10.1140/epjst/e2014-02217-8 (cit. on p. 58).

Tandon, A., M. Schröder, M. Mannattil, M. Timme, and S. Chakraborty (2016). „Synchronizing noisy nonidentical oscillators by transient uncoupling“. In: *Chaos An Interdiscip. J. Nonlinear Sci.* 26.9, p. 094817. DOI: 10.1063/1.4959141 (cit. on p. 58).

Tang, L., X. Wu, J. Lü, J.-a. Lu, and R. M. D'Souza (2016). „Master stability functions for multiplex networks“. In: *arXiv:1611.09110*, pp. 1–23 (cit. on p. 25).

Tél, T. (1990). „Transient Chaos“. In: *Dir. Chaos*. Ed. by B.-l. Hao. Vol. 3. World Scientific, Singapore, pp. 149–221. DOI: 10.1039/c2cc90008d (cit. on p. 16).

— (1991). „Controlling transient chaos“. In: *J. Phys. A. Math. Gen.* 24.23, pp. L1359–L1368. DOI: 10.1088/0305-4470/24/23/007 (cit. on p. 16).

Timme, M., F. Wolf, and T. Geisel (2002). „Prevalence of Unstable Attractors in Networks of Pulse-Coupled Oscillators“. In: *Phys. Rev. Lett.* 89.15, p. 154105. DOI: 10.1103/PhysRevLett.89.154105 (cit. on p. 19).

Travers, J. and S. Milgram (1969). „An Experimental Study of the Small World Problem“. In: *Sociometry* 32.4, pp. 425–443 (cit. on p. 37).

Tsonis, A. A. and P. J. Roebber (2004). „The architecture of the climate network“. In: 333, pp. 497–504. DOI: 10.1016/j.physa.2003.10.045 (cit. on p. 38).

UFE (2003). „Rapporto sul blackout italiano del 28 settembre 2003“. In: *Uff. Fed. Dell'Energia* (cit. on p. 4).

Ulbig, A., T. S. Borsche, and G. Andersson (2013). „Impact of Low Rotational Inertia on Power System Stability and Operation“. In: *arXiv*, pp. 1–12. DOI: 10.3182/20140824-6-ZA-1003.02615 (cit. on pp. 4, 83).

U.S.-Canada Power System Outage Task Force (2004). *Final Report on the August 14, 2003 Blackout in the United States and Canada: Causes and Recommendations* (cit. on pp. 4, 47).

Vespignani, A. (2010). „The fragility of interdependency“. In: *Nature* 464.April (cit. on p. 47).

Von Neumann, J. (1951). „Various techniques used in connection with random digits“. In: *J. Res. Nat. Bur. Stand.* 12, pp. 36–38 (cit. on p. 29).

Wang, P., G. Robins, P. Pattison, and E. Lazega (2013). „Exponential random graph models for multilevel networks“. In: *Soc. Networks* 35.1, pp. 96–115. DOI: 10.1016/j.socnet.2013.01.004 (cit. on p. 51).

Watts, D. J. and S. H. Strogatz (1998). „Collective dynamics of 'small-world' networks“. In: *Nature* 393.6684, pp. 440–442. DOI: 10.1038/30918 (cit. on pp. 37, 46, 73, 119).

Waxman, B. M. (1988). „Routing of multipoint connections.pdf“. In: *IEEE J. Sel. Areas Commun.* 6.9, pp. 1617–1622 (cit. on p. 73).

Weckesser, T., H. Johannsson, and J. Ostergaard (2013). „Impact of model detail of synchronous machines on real-time transient stability assessment“. In: *2013 IREP Symp. Bulk Power Syst. Dyn. Control - IX Optim. Secur. Control*

Emerg. Power Grid. IEEE, pp. 1–9. DOI: 10.1109/IREP.2013.6629364 (cit. on pp. 61 sqq., 65).

Wegner, A. E. (2014). „Subgraph covers – An information theoretic approach to motif analysis in networks“. In: *Phys. Rev. X* 4.4, p. 10. DOI: 10.1103/PhysRevX.4.041026 (cit. on p. 42).

Wiedermann, M., J. F. Donges, J. Heitzig, and J. Kurths (2013). „Node-weighted interacting network measures improve the representation of real-world complex systems“. In: *EPL (Europhysics Lett.* 102.2, p. 28007. DOI: 10.1209/0295-5075/102/28007 (cit. on pp. 40, 48).

Wiedermann, M., J. F. Donges, J. Kurths, and R. V. Donner (2016). „Spatial network surrogates for disentangling complex system structure from spatial embedding of nodes“. In: *Phys. Rev. E* 93.4, p. 042308. DOI: 10.1103/PhysRevE.93.042308 (cit. on p. 50).

Wiley, D. A., S. H. Strogatz, and M. Girvan (2006). „The size of the sync basin“. In: *Chaos An Interdiscip. J. Nonlinear Sci.* 16.1, p. 015103. DOI: 10.1063/1.2165594 (cit. on p. 31).

Winfree, A. T. (2001). *The geometry of biological time*. New York: Springer (cit. on p. 16).

Witthaut, D., M. Rohden, X. Zhang, S. Hallerberg, and M. Timme (2016). „Critical Links and Nonlocal Rerouting in Complex Supply Networks“. In: *Phys. Rev. Lett.* 116.13, p. 138701. DOI: 10.1103/PhysRevLett.116.138701 (cit. on p. 117).

Witthaut, D. and M. Timme (2012). „Braess's paradox in oscillator networks, desynchronization and power outage“. In: *New J. Phys.* 14.8, p. 083036. DOI: 10.1088/1367-2630/14/8/083036 (cit. on p. 118).

— (2013). „Nonlocal failures in complex supply networks by single link additions“. In: *Eur. Phys. J. B* 86.9. DOI: 10.1140/epjb/e2013-40469-4 (cit. on p. 118).

Wolfrum, M. and O. E. Omel'Chenko (2011). „Chimera states are chaotic transients“. In: *Phys. Rev. E* 84.1, p. 015201. DOI: 10.1103/PhysRevE.84.015201 (cit. on p. 18).

Wu, X., F. Dörfler, and M. R. Jovanovic (2016). „Input-Output Analysis and Decentralized Optimal Control of Inter-Area Oscillations in Power Systems“. In: *IEEE Trans. Power Syst.* 31.3, pp. 2434–2444. DOI: 10.1109/TPWRS.2015.2451592 (cit. on p. 84).

Yook, S.-H. and H. Meyer-Ortmanns (2006). „Synchronization of Rössler oscillators on scale-free topologies“. In: *Phys. A Stat. Mech. its Appl.* 371.2, pp. 781–789. DOI: 10.1016/j.physa.2006.04.116 (cit. on pp. 126, 134, 137).

Zakrzhevsky, M., A. Klokov, V. Yevstignejev, E. Shilvan, and A. Kragis (2010). „Bifurcation analysis and rare attractors in driven damped pendulum systems“. In: *J. Vibroengineering* 12.4, pp. 369–374 (cit. on p. 85).

Zamora-López, G., C. Zhou, and J. Kurths (2010). „Cortical hubs form a module for multisensory integration on top of the hierarchy of cortical networks.“ In: *Front. Neuroinform.* 4.March, p. 1. DOI: 10.3389/neuro.11.001.2010 (cit. on p. 47).

Zhang, X., S. Hallerberg, M. Matthiae, D. Witthaut, and M. Timme (2016). „Dynamic Network Response Patterns“. In: pp. 1–6 (cit. on p. 58).

Zhifang Wang, A. Scaglione, and R. J. Thomas (2010). „Generating Statistically Correct Random Topologies for Testing Smart Grid Communication and Control Networks“. In: *IEEE Trans. Smart Grid* 1.1, pp. 28–39. DOI: 10.1109/TSG.2010.2044814 (cit. on pp. 50, 72 sq.).

Zhou, C., A. E. Motter, and J. Kurths (2006). „Universality in the Synchronization of Weighted Random Networks“. In: *Phys. Rev. Lett.* 96.3, p. 034101. DOI: 10.1103/PhysRevLett.96.034101 (cit. on p. 47).

Zhou, C., L. Zemanová, G. Zamora-López, C. C. Hilgetag, and J. Kurths (2007). „Structure-function relationship in complex brain networks expressed by hierarchical synchronization“. In: *New J. Phys.* 9. DOI: 10.1088/1367-2630/9/6/178 (cit. on p. 47).

Zou, Y., T. Pereira, M. Small, Z. Liu, and J. Kurths (2014). „Basin of Attraction Determines Hysteresis in Explosive Synchronization“. In: *Phys. Rev. Lett.* 112.11, p. 114102. DOI: 10.1103/PhysRevLett.112.114102 (cit. on p. 31).

Selbständigkeitserklärung

Ich erkläre, dass ich die Dissertation selbständig und nur unter Verwendung der von mir gemäß §7 Abs. 3 der Promotionsordnung der Mathematisch-Naturwissenschaftlichen Fakultät, veröffentlicht im Amtlichen Mitteilungsblatt der Humboldt-Universität zu Berlin Nr. 126/2014 am 18.11.2014 angegebenen Hilfsmittel angefertigt habe.

Berlin, den 20.11.2017 Paul Schultz